Optimisation of Eicosapentaenoic Acid Production from a New Zealand Microalga in a Tubular Photobioreactor

A thesis submitted for the degree of Doctor of Philosophy in

Chemical and Process Engineering

by

Daniel Mark Hunter Smith

May 2020

Department of Chemical and Process Engineering

University of Canterbury

Christchurch, New Zealand

Abstract

This work focussed on the optimisation of the volumetric productivity (mg EPA L^{-1} d^{-1}) of eicosapentaenoic acid (EPA, 20:5 n-3) from a New Zealand strain of microalgae, *Trachydiscus* sp. LCR-Awa-9-2. EPA is a high value polyunsaturated omega-3 fatty acid which plays a beneficial role in the prevention and treatment of a variety of human health conditions such as arthritis and cardiovascular disease. *Trachydiscus* sp. LCR-Awa-9-2 was a recently isolated strain of microalgae and at the time of isolation the strain showed a high fraction of EPA in its fatty acids (42 g/100 g total fatty acids). Due to the high amount of EPA present in the cells the microalga was a promising contender for commercial production of EPA. Research was required to determine the optimal conditions for growth and EPA productivity of the microalga and to allow evaluation of whether EPA production would be commercially viable using this strain.

In this work, the growth of *Trachydiscus* sp. LCR-Awa-9-2 in a purpose-built 76 L tubular photobioreactor was investigated as a first milestone towards potential scale up of the culturing of this microalga. The influence of different culture conditions on growth and EPA content were investigated at small scale in shake flasks and airlift photobioreactors. Studies were also conducted into the lipidome of the microalga and the oxygen evolution rate was investigated under a variety of conditions as a proxy measure of photosynthesis rate. Conditions such as liquid velocity, light intensity, light wavelength, and semi-continuous culturing were investigated in the tubular photobioreactor. In shake flasks the effect of nutrients (NaCl, Co, B, lactose, galactose, CO_2, and Bold's Basal modified Awarua (BBMA) vs. Zehnder (Z) media) were investigated as well as the effect of diurnal light cycling (24:0, 12:12, 16:8, hours light : hours dark).

The highest maintainable EPA productivity in this study of 30 ± 2 mg L^{-1} d^{-1} was achieved with semi-continuous culturing in the tubular photobioreactor at a cell density of approximately 4.5×10^7 cells mL^{-1} and a dilution rate of 0.19 d^{-1}. The highest EPA productivity in batch cultures of 16 ± 2 mg L^{-1} d^{-1} was achieved in shake flasks with 10% CO_2. In both cases BBMA medium was used. The highest EPA fraction was 46 ± 1 g/100 g fatty acids and the highest content was 6.1 ± 0.1 g/100 g dry biomass, both achieved under the same conditions in the tubular photobioreactor (warm white light, 1500 µmol m^{-2} s^{-1}, late exponential phase, BBMA medium, 3% CO_2). The EPA fraction achieved was the highest that had been reported for this microalga. The maximum cell

density achieved was $1.0 \pm 0.1 \times 10^8$ cells mL^{-1} in shake flasks with 3% CO_2, BBMA medium and a light intensity of 500 µmol m^{-2} s^{-1}. Light availability was identified as the key limiting factor to the further improvement of EPA productivity of cultures. Diurnal cycles in shake flasks showed that cell densities and EPA productivity decreased with increasing dark time, but EPA content increased. The fraction of the photobioreactor volume illuminated influenced the growth of cultures in the tubular photobioreactor with decreasing illuminated volume negatively influencing both the growth rate and maximum cell density.

Increasing NaCl concentration negatively impacted both the EPA fraction and growth of cultures, with cultures unable to grow at a NaCl concentration of 35 g L^{-1}; however, EPA content was greatest at a NaCl concentration of 1 g L^{-1}. Cultures were able to grow at CO_2 concentrations up to 30% but growth was not observed at 100% CO_2. Air without supplemental CO_2 (0.04% CO_2) lead to carbon limitation of cultures and high pH (> pH 9) which inhibited growth. Oxygen evolution rates were roughly equal over a pH range of 3 to 7 but decreased outside this range. Cells were able to photosynthesise over a temperature range of 5 to 40 °C but the maximum rate was achieved at 20 to 25 °C with the rate decreasing above and below these temperatures. Warm white was found to be the most efficient light colour for oxygen evolution rate compared to red, blue, and green. Blue, warm white, and combined red-green-blue-warm white (RGBWW) light colours did not significantly impact EPA content of cells in the tubular photobioreactor but warm white was the most efficient for growth based on cells produced per quantity of photons supplied.

Lipidomic analysis of *Trachydiscus* sp. LCR-Awa-9-2 showed that the majority of EPA (50 ± 2 wt%) was located in the monogalactosyl diacylglycerides (MGDG), as had been reported for other species of microalgae. Significant degradation of lipid extracts occurred during extraction from freeze-dried biomass using a modified Bligh and Dyer method. Degradation of lipids was overcome by extraction from fresh biomass using a hot isopropanol extraction method to prevent degradation due to enzymatic activity. Results from thin layer chromatography (TLC) separations of lipid extracts indicated that an unconfirmed minor glycolipid class may be present and that this could potentially be monoglucosyl diacylglyceride (GlcDG); however, the class of the lipids was unable to be conclusively identified during this study. The potential GlcDG class of interest was not detected in similar analyses of lipids from *Chlorella vulgaris*. Presence of GlcDG would

indicate a gene transfer event from cyanobacteria as GlcDG is not typically produced by eukaryotic microalgae.

The results of this study showed that *Trachydiscus* sp. LCR-Awa-9-2 was able to be grown in a tubular photobioreactor and that the microalga was likely to be well-suited to large-scale culturing. The microalga tolerated a wide range of CO_2 concentrations, pH, temperature, and shear stress, and was able to be semi-continuously cultured; all of which are beneficial for large-scale culturing. Further small improvements in EPA productivity may be possible by reduction of dark volumes in future designs of tubular photobioreactors to improve growth rates, as well as increasing the EPA content of the cells. Photoautotrophic production of EPA from *Trachydiscus* sp. LCR-Awa-9-2 at the scale used in this study was unlikely to be commercially viable and so future work is required to improve the economics of culturing this microalga for EPA.

Acknowledgements

As usual, this thesis was not possible without the help of many people and organisations. Firstly, an enormous thank you must go to my supervisors Ken Morison and Gabriel Visnovsky for your guidance and support over my doctoral journey as well as your teaching during my years at the University of Canterbury. I am also grateful for my fellow algae students, Mehrnoush Tangestani and Alivia Alfiarty, for their advice, encouragement, and help in the lab. Thank you to Phil Novis (Manaaki Whenua - Landcare Research) for instigating the project with this microalga, organising funding, your algae advice, and organising equipment loans. I am also extremely grateful for the time and advice of the technical staff from across the University of Canterbury, namely Graham Mitchell, Graham Furniss, and Leigh Richardson for their work on construction of the tubular photobioreactor as well as the other Chemical and Process Engineering (CAPE) workshop staff who contributed to this. A thank you must also go to Rob McGregor (School of Physical and Chemical Sciences) for his glassblowing expertise as well as Glenn Wilson for fielding my many quote and order requests. Thank you also to Rayleen Fredericks and Michael Sandridge for your endless help in the lab sorting out numerous equipment failures and tracking down all manner of things that I required.

My time at the University of Almería in early 2017 proved invaluable during the design and construction of the tubular photobioreactor and I thank Emilio Molina Grima for welcoming me into his department during my brief time there. Thank you's must also be given for the guidance and help provided by Lorenzo Lopez Rosales, Francisco García Camacho, and Francisco Gabriel Acién Fernández. Thank you to the Biomolecular Interactions Centre (BIC) and CAPE for providing funding to make that trip possible. Thank you as well to Yusuf Chisti (Massey University) for your time showing me your tubular photobioreactor setup and advice. I also thank the many researchers who fielded queries that arose during this work for your time in replying and the advice you provided.

I would not have been able to pursue this work if it were not for the financial support supplied from the UC Doctoral Scholarship and CAPE. Likewise, the build of the tubular photobioreactor and various analyses would not have been possible without the support of funding supplied from Te Rūnanga o Ngāi Tahu and the Science for Technological Innovation National Science Challenge. I also gratefully acknowledge the opportunity to work with the microalga in this study that was granted by Te Rūnanga o Awarua, Te Rūnanga o Ngāi Tahu, and the Department of Conservation.

Of course, last but most certainly not least, thank you to my family, my partner, and her family for supporting me through my years of university study and encouraging me to pursue everything to the best of my ability.

Thank you, everyone.

Table of Contents

1 Introduction

1.1 Background and project motivation

Microalgae are a source of many biotechnologically and industrially interesting compounds. Microalgae have existed on Earth for millennia, but humans have only cultivated and researched microalgae on a large-scale for food and other industrial uses for around a century or so (Becker, 1994). Harnessing and optimising the growth of microalgae and production of their desired metabolites is of great interest for research and industry to make microalgae bioprocesses commercially viable. Microalgae contain an array of useful compounds from antioxidants to fatty acids and have also been used as a source of dietary protein (Becker, 1994; Cohen, 1999; Stoyneva-Gärtner *et al.*, 2019). Nutraceutical and pharmaceutical compounds produced from microalgae are commercially interesting high-value products and are the focus of most current companies growing microalgae (Borowitzka, 2013; Buono *et al.*, 2014; Cohen, 1999; Stoyneva-Gärtner *et al.*, 2019). Microalgae are a good source of lipids and have been touted as a biodiesel feedstock, although many barriers (primarily economic) currently lie in the way of commercialisation of these types of commodity products (Borowitzka, 2013; Chisti, 2007).

Microalgae are primarily photoautotrophic organisms, meaning they use light for their energy source and inorganic carbon for their carbon source (Reece *et al.*, 2010). Growing these organisms on large-scale thus requires culture vessels which allow a sufficient supply of these key resources. A photobioreactor is the general term used for enclosed reactors of various configurations and geometries used to grow microalgae photoautotrophically (Andersen, 2005; Tredici *et al.*, 2013). Optimisation of the design and culture conditions in photobioreactors is key to maximising the productivity of microalgae bioprocesses. Microalgae reach relatively low cell densities compared to other industrially applicable microorganisms such as bacteria or yeast (typically 5 g L^{-1} dry mass for microalgae versus >50 g L^{-1} for many bacteria (Andersen, 2005)). The limited cell density achievable places even greater importance on optimising conditions for the growth of microalgae to improve culture productivity.

Central to this research was a newly isolated strain of microalgae, *Trachydiscus* sp. LCR-Awa-9-2, which was collected from the Awarua-Waituna Wetlands in Southland, New Zealand (Tangestani, 2019). This microalga showed a high fraction of fatty acids (about 40% of total fatty acids) of the omega-3, polyunsaturated fatty acid,

eicosapentaenoic acid (EPA). EPA and other omega-3 fatty acids are high-value nutraceutical products (US$ 140 kg^{-1} for bulk oil (Borowitzka, 2013)) which may play an important role in cardiovascular and brain health as well as treating inflammation in humans, among other health benefits (Buono *et al.*, 2014; Kris-Etherton *et al.*, 2002; Simopoulos, 1991; Simopoulos, 2002). Currently, the majority of the world's supply of omega-3 fatty acids such as EPA are extracted from fish oil (Cohen, 1999; Stoyneva-Gärtner *et al.*, 2019; Tocher *et al.*, 2019). However, there has been great concern for many years around the over-fishing of the oceans (Botsford *et al.*, 1997) and so obtaining EPA from fish oil to meet the demand could be an unsustainable process (Tocher *et al.*, 2019). Fish obtain the majority of the EPA they accumulate in their oils from the microalgae they eat (Stoyneva-Gärtner *et al.*, 2019). Therefore, by producing EPA directly from microalgae it is possible to 'cut out the middle-fish' and produce EPA in a more sustainable and efficient manner (Adarme-Vega *et al.*, 2012).

1.2 Research problem, scope, and objectives

The motivation for this project was to maximise the biomass concentration and EPA content to optimise the volumetric EPA productivity of *Trachydiscus* sp. LCR-Awa-9-2 in a scalable culture system. Optimising the volumetric productivity (mass produced per unit volume of culture per unit time, henceforth referred to as productivity unless otherwise specified) of EPA from this microalga was key to investigating the feasibility of any future commercial process. Additionally, this microalga had not yet been grown beyond bench scale (approximately 1 L culture volume) and so the behaviour of this alga in a larger scale system needed to be investigated. The overarching research problem that was to be investigated in this research was "what are the optimal culture conditions for *Trachydiscus* sp. LCR-Awa-9-2 to maximise its EPA productivity in a scalable culture system?".

The scope of this research focussed on designing and building a culture system that would provide data on the behaviour of this microalga at large-scale and allow optimisation of the culture conditions in this system. This research also aimed to pursue further questions that arose from previous research that had been conducted investigating the effect of light, temperature and nutrients on the growth and EPA productivity of the microalga (Alfiarty, 2018; Tangestani, 2019). Work was also conducted on investigating the lipidome of the microalga and the role and location of EPA with the aim to provide insight to focus future efforts in optimising EPA productivity.

2 Literature Review

2.1 Microalgae: background and biology

2.1.1 Microalgae

The term "microalgae" encompasses a wide range of photosynthetic, eukaryotic and prokaryotic, uni- and multi-cellular microorganisms, which generally require a microscope to be observed (Cooper, 1996). In the context of this work, "microalgae" primarily refers to eukaryotic, photosynthetic microorganisms, as opposed to prokaryotic cyanobacteria or multicellular algae. Microalgae and cyanobacteria have been attributed to be one of the key influences in the development of life on Earth as we know it, contributing around 70% of the cumulative oxygen in Earth's atmosphere through production by photosynthesis over the course of millennia (Cooper, 1996).

Microalgae have been found to live in almost every environment on Earth; from the oceans and rivers to highland snow and soil (Cooper, 1996). More than 30,000 species of microalgae have been identified, and it is estimated that there are greater than 70,000 species present on Earth (Guiry, 2012). Despite the diversity and worldwide presence of microalgae, there are only a few dozen strains that have been extensively studied and exploited for industry. Some examples of microalgae that are cultured industrially are *Haematococcus pluvialis* (Gao *et al.*, 2017; López *et al.*, 2006), *Nannochloropsis gaditana* (Basso *et al.*, 2014; Camacho-Rodríguez *et al.*, 2015; Rocha *et al.*, 2003), and *Chlorella vulgaris* (Filali *et al.*, 2011; Fu *et al.*, 2012; Menon *et al.*, 2013; Yun & Park, 2003).

Microalgae have been cultured by humans at small scale for food for well over 100 years, and literature shows that interest in microalgae for industrial applications has been strong for more than 70 years (Becker, 1994; Burlew, 1953). The popularity of biotechnology in recent decades has reaffirmed the importance of the role microalgae in the field (Becker, 1994; Cohen, 1999). Particularly topical are the potential uses of microalgae for carbon sequestration, emissions and pollution mitigation, pharmaceutical and nutraceutical products, as a biofuel feedstock, and as an alternative to respiring microorganisms in traditional bioprocesses (Andersen, 2005; Chisti, 2006; Stoyneva-Gärtner *et al.*, 2019).

2.1.2 The microalgal cell

Eukaryotic cells are defined by having the features of a nucleus and other internal membraned organelles (Reece *et al.*, 2010). The microalgal cell differs from most other

eukaryotic cells by the presence of a chloroplast to conduct photosynthesis. While both plants and algae conduct photosynthesis, microalgae are differentiated due to their lack of distinct structures such as leaves or branches (Cooper, 1996). Microalgae can adopt a diverse range of morphologies, in both size and shape (Richmond, 2008). Typically, microalgae cells have a diameter in the region of tens of micrometres (approximately one-tenth of the width of a human hair) and they can range in shape from spherical to filamentous chains. A typical microalga cell consists of a cell wall, cell membrane, nucleus, pyrenoid, mitochondria, and a chloroplast, as shown in Figure 2.1. Other cellular features can also be present depending on the species, such as flagella and lipid or starch bodies (Richmond, 2008).

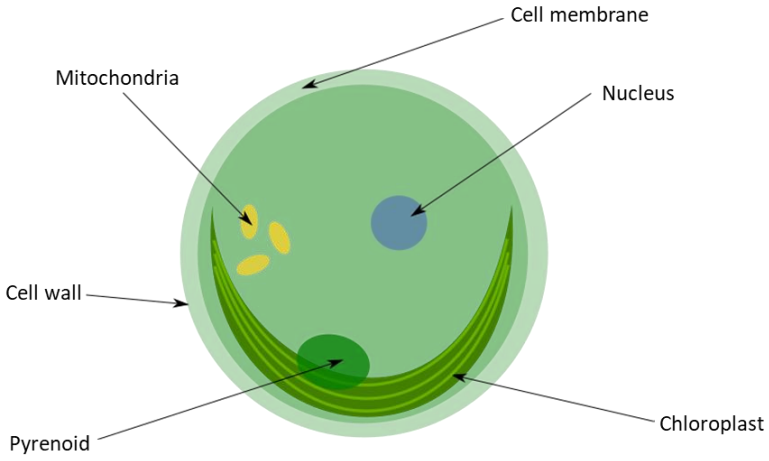

Figure 2.1 – Simplified schematic of a microalga cell and some of its key cellular structures. Based on Richmond (2008).

The cell wall provides mechanical strength to the cells and in algae it is generally composed of glycoproteins and polysaccharides (Reece *et al.*, 2010). The cell membrane allows the cell to control transport of compounds in and out of the cell and is formed by a lipid bilayer, generally consisting of phospholipids. DNA (deoxyribose nucleic acid) is contained in the nucleus of the cell. The nucleus allows control of protein synthesis and DNA replication through regulation by enzymes and controlled transport of genetic material. Energy for the cell is managed by the chloroplast, mitochondria and pyrenoid. The chloroplast harvests light for use in photosynthesis, while the pyrenoid contains apparatuses to concentrate and fix carbon dioxide (Richmond, 2008). Mitochondria are used to synthesise energy-carrying molecules without the use of photosynthesis for use in other cellular processes (Reece *et al.*, 2010).

The chloroplast and its associated membranes are of particular interest in this research due to their fatty acid composition, typically housing the majority of EPA in microalgae (Cohen, 1999; Siegenthaler & Murata, 1998; Wada & Murata, 2009). Thylakoid membranes make up the bulk of chloroplasts and are central to photosynthetic processes (Siegenthaler & Murata, 1998). The chloroplast consists of layers of thylakoid membranes stacked on top of one another and the spaces inside and between the membranes are used to induce concentration gradients and house the proteins and pigments involved in photosynthesis (Ke, 2001; Reece *et al.*, 2010; Siegenthaler & Murata, 1998). Photosynthesis is covered further in § 2.3.

2.1.3 Applications of microalgae

Perhaps the most topical and widely published application of microalgae is their potential use as a biofuel feedstock (Mata *et al.*, 2010). Production of biodiesel in particular requires a source of lipids which can be turned into fatty acid methyl esters. Microalgae have high lipid contents when compared to other feedstocks such as canola and are able to be grown on otherwise non-arable land (Chisti, 2007). However, the cost of culturing microalgae means that production of commodity products such as biofuels are not economically viable, at least while the price of petrochemical fuels remains relatively low (Borowitzka, 2013).

Microalgae are also useful for remediation of wastewater from a variety of sources (Posten & Walter, 2012). They can be utilised to reduce nutrient concentrations in waste streams such as farming effluent, as well as to remove trace metals and other contaminants from sources such as mining wastewater (Bwapwa *et al.*, 2017; Cai *et al.*, 2013). Microalgae are also a key component of the microbial consortium present in most municipal wastewater treatment plants (Richmond, 2008).

There are a variety of health products that can be produced from microalgae ranging from dietary supplements to pharmaceutical drugs (Cohen, 1999). These products can range from pigments and antioxidants to proteins and polyunsaturated fatty acids. Health-related products often garner high market prices as they are traditionally difficult to manufacture and can warrant the cost of microalgae processes to produce them (Borowitzka, 2013). Microalgae are also a source of many pigment compounds such as carotenoids which are used in the production of cosmetic products and health supplements (Spolaore *et al.*, 2006). One key pigment produced from microalgae is astaxanthin which, amongst other things, is the key component that gives the pink colour

of salmon flesh and so is an important ingredient in aquacultural feed formulations for this purpose (Stoyneva-Gärtner *et al.*, 2019).

One of the oldest uses of microalgae by humans is as a source of food (García *et al.*, 2017). Some species of microalgae and cyanobacteria can contain high proportions of protein (up to around 50 wt% of dry mass (Burlew, 1953)) and can also be grown in areas where traditional food crops may not be able to be grown. The cyanobacterium *Spirulina* is one of the most widely recognised species used for food due to its high protein content (García *et al.*, 2017).

2.2 *Trachydiscus* sp. LCR-Awa-9-2

Central to this research was the strain of microalgae *Trachydiscus* sp. LCR-Awa-9-2. This microalga showed a high proportion of EPA in its fatty acids when isolated (about 40% of total fatty acids) (Alfiarty, 2018; Tangestani, 2019; Thom, 2015). The microalga was isolated from the Awarua-Waituna Wetlands, a peatland in Southland, New Zealand. It is a eukaryotic, unicellular, freshwater microalga of the class eustigmatophyceae. *Trachydiscus* sp. LCR-Awa-9-2 fits into the evolutionary tree of life as shown in Figure 2.2.

The closest relatives to *Trachydiscus* sp. LCR-Awa-9-2 reported in published literature are a European strain, *Trachydiscus minutus* (Rezanka *et al.*, 2010), and a Chinese strain, *Trachydiscus guangdongensis* (Gao *et al.*, 2019). The marine microalga (apart from one freshwater strain) *Nannochloropsis* sp. is also a member of the eustigmatophytes and is the most widely researched species in this class (Andersen *et al.*, 1998; Cohen, 1999; Stoyneva-Gärtner *et al.*, 2019). Fellow eustigmatophytes also show a high fraction of EPA in their fatty acids, with the highest fractions typically in the region of 30–50% of total fatty acids (Stoyneva-Gärtner *et al.*, 2019).

Eustigmatophyceae are characterised by the presence of chlorophyll *a*, but not *b* or *c* and have violaxanthin as their major carotenoid (Heimann & Huerlimann, 2015; Larkum *et al.*, 2003). Their cell walls are made from cellulose and they use laminarin (a polysaccharide) as a carbohydrate energy store (Larkum *et al.*, 2003). This class of alga can be found in marine, freshwater, and terrestrial environments. Eustigmatophyceae are nonmotile, unicellular, oval to round shape, and generally less than 5 μm in diameter (Heimann & Huerlimann, 2015).

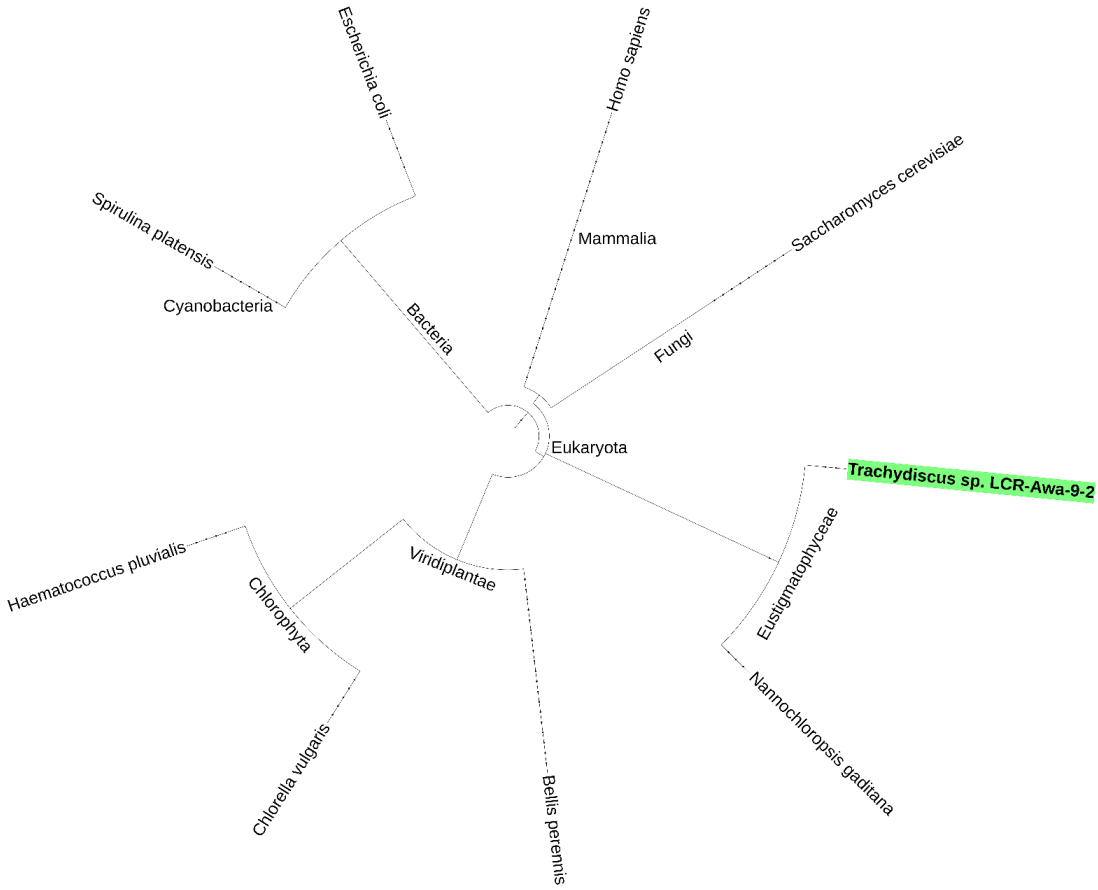

Figure 2.2 – Simplified phylogenetic tree showing the position of Trachydiscus sp. LCR-Awa-9-2 in relation to some other common organisms. Diagram generated with phyloT tree generator and Interactive Tree of Life (iTOL) online software (Letunic & Bork, 2019).

The characteristics of *Trachydiscus* sp. LCR-Awa-9-2 are consistent with this class with it being a spherical, unicellular microalga with a typical cell diameter of 5–10 µm. The cell is non-motile and has the tendency to produce lipid storage bodies which are seen as red-orange globules under a light microscope. Examples of typical light microscopy images of *Trachydiscus* sp. LCR-Awa-9-2 cells are shown in Figure 2.3.

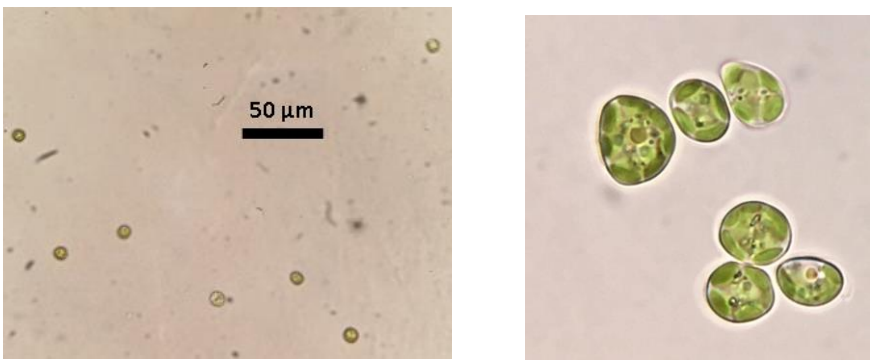

Figure 2.3 – Optical microscope images of Trachydiscus sp. LCR-Awa-9-2 cells.

2.2.1 Previous research on *Trachydiscus* sp. LCR-Awa-9-2

Previous research has focussed on cultivation of *Trachydiscus* sp. LCR-Awa-9-2 on solid media agar plates, shake flask cultures, and cultivation in bench-scale airlift photobioreactors (Alfiarty, 2018; Tangestani, 2019; Thom, 2015). An improved growth medium (Bold's Basal modified Awarua medium, BBMA) was developed as reported by Alfiarty (2018) allowing the maximum cell density to reach up to approximately 9×10^7 cells mL^{-1} in shake flasks. Tangestani (2019) investigated the influence of light wavelength and intensity, temperature, mixotrophic and heterotrophic growth on biomass production and EPA content on agar plates, in shake flasks, and in airlift photobioreactors. The microalga was shown to be able to grow consistently under a 24-hour light regime with air enriched with 3% CO_2. The maximum cell density achieved in laboratory scale airlift photobioreactors was approximately 3.9×10^7 cells mL^{-1} using Z media at a light intensity of 130 µmol m^{-2} s^{-1} (white LED light). All studies were conducted as batch cultures.

Work by Alfiarty (2018) showed that the improved BBMA medium increased the maximum biomass concentration 100% from that achieved with the original Bold's Basal medium (BBM). Trace nutrients such as cobalt and boron were shown to not be essential for growth of the microalga and high concentrations (six times that in BBM) of zinc, boron and sulphate were suspected to poison the cells. Nitrate and phosphate starvation were shown to increase the fatty acid content of the cells but stimulated an increase of oleic acid (18:1 n-9) more than EPA. Cultures were shown to be light limited at a light intensity of 250 µmol m^{-2} s^{-1} and an increase to an intensity of 500 µmol m^{-2} s^{-1} improved the growth of cultures.

Results from Tangestani (2019) showed that the highest EPA fraction of 35.2 g/100 g total fatty acids was achieved under photoautotrophic growth in airlift photobioreactors, followed by a dark treatment at 40 °C. The highest EPA content of 9.6 g/100 g dry biomass was achieved with a dark treatment at 30 °C for 72 hours. EPA productivity was greatest under blue light with Z media in airlift photobioreactors at 25 °C, reaching a maximum productivity of 15.6 mg L^{-1} d^{-1}. Heterotrophy and mixotrophy studies showed that the cells could grow on a range of organic carbon sources, with the best growth results obtained from mixotrophic cultivation using lactose and galactose.

25 °C was the best temperature for growth rate and EPA content, while the growth rate was similar at 20 °C but a higher cell density was achieved. Growth and cell densities

were lower at 15 °C than 20 °C or 25 °C and growth was significantly hindered at temperatures above 28 °C. Although cultures did not grow above 28 °C, the microalga was able to tolerate temperatures up to 35 °C where the cultures were able to maintain a constant cell density and did not collapse. Cultures were shown to grow over a pH range of 4.0 to 8.5, with optimal growth at pH 7.0 in Z medium in shake flasks.

Key areas that had not yet been investigated in the above studies was the growth of *Trachydiscus* sp. LCR-Awa-9-2 in a scalable culture system, investigation of its lipidome, and continuous culturing. This study aimed to investigate these key areas as well as further research of culture conditions that had not yet been investigated or fully explored.

2.3 Light, photosynthesis, and photoautotrophic growth

2.3.1 The nature of light, its measurement, and photosynthetically active radiation

The physics and properties of light

Light is fundamentally electromagnetic radiation. Depending on the wavelength of the radiation, light can be broadly categorised as radio waves, gamma rays, x-rays, and visible light to name a few. Light exhibits wave-particle duality (i.e. it behaves as both a particle and a wave) and a packet of light energy or 'particle' is referred to as a photon. The energy of photons of different wavelengths of light can be determined by Equation (2.1) where the energy at a given wavelength, E_λ, is inversely proportional to the wavelength, λ, and the constants h and c are the Planck constant and the speed of light in a vacuum, respectively (Serway & Jewett, 2007).

$$E_\lambda = \frac{h\,c}{\lambda} \qquad (2.1)$$

The range of the light spectrum visible to humans is roughly the wavelengths from 380 nm to 740 nm, with shorter wavelength light appearing blue and longer wavelength light appearing red. Outside the extremes of the visible range, shorter wavelengths are termed ultraviolet (UV) and longer wavelength are termed infrared (IR). Wavelengths of light may be absorbed or transmitted by different materials and absorbed light energy can be transformed into other forms such as heat or electrical energy (Serway & Jewett, 2007). The process of absorbing light and transforming it into other energy forms is the basis for providing energy for photosynthesis as discussed further below. The absorbance of different materials can vary depending on the wavelength and so not all wavelengths of

light will be absorbed in equal amounts (Shannon & Wyant, 1979), this affects the usability of different wavelengths of light for photosynthesis and materials used in photobioreactor construction as discussed below and in § 4.

Measurement of light

Measurement of light is required for a range of subjects such as solar power design and photography, and the measurements used vary depending on the field in question. Measurement of light is broadly divided into categories of photometry (perceived brightness to the human eye), luminance (amount of light emitted or reflected in a given area as perceived by human eye), radiometry (non-subjective or perceptive measurement of electromagnetic radiation), and brightness (subjective perception of luminance) (Johnsen, 2011). In the context of culturing microalgae, radiometry is the category of greatest importance.

There are many units used to measure the intensity of light. The most common light measurement is luminous intensity, which is weighted by the response of human eyes to light. The SI unit for luminous intensity is the candela (cd). Other units that are often used to measure light are lumens, lux and candle power, with lumens most widely used for rating light bulbs, lux for photography and candle power an imperial unit for measuring brightness of lights such as torches or spotlights. The measurement of energy provided by light is widely used in solar power or global warming contexts. For these purposes light is typically measured in W m^{-2} to give the total power flux (Johnsen, 2011).

When considering light for microalgae cultures it is most commonly measured in µmol m^{-2} s^{-1}, also referred to as photon flux density[i] (Andersen, 2005). This is a direct measure of how many micromoles of photons pass through a one square metre area per second, irrespective of their wavelength. The wavelength range that the photons are measured over for microalgae is normally 400–700 nm (as discussed further below in context to photosynthesis) and so photons outside this range are not measured (Johnsen, 2011).

[i] Alternative units previously used in some studies are the micro-Einstein, µE, (e.g. Acién Fernández *et al.* (2000)) where 1 µE is equivalent to 1 µmol of photons; or quanta (e.g. Molina Grima *et al.* (1995)) where one quanta is the equivalent of one photon.

In the context of microalgal cultures, the incident light intensity, I_0, (i.e. the light intensity at the surface of the culture) is often reported in terms of the photon flux density (Andersen, 2005; Becker, 1994) However, as a variety of different photobioreactor geometries can be used to grow microalgae (as discussed in § 2.6), the area that light passes through for a given culture system can vary considerably. Due to this, a given photon flux density applied to one style of cultivation system does not provide the same quantity of photons to the culture as it would for another system with a different geometry. Another measure can be defined as the total photon flux, I_{total}, which is a measure of the quantity of photons supplied per unit volume of culture per unit time. This measurement allows direct comparison of the amount of light, and thus energy, truly supplied to a given culture irrespective of photobioreactor geometry. Each cell in a culture will 'see' a proportion of the total light supplied, referred to here as the cell specific photon flux, I_{cell}, which is the quantity of photons supplied per cell per unit time. As the cell density changes over the course of a culture the cells share the quantity of photons supplied, and so for a constant light intensity the cell specific photon flux decreases as cell density increases.

Light is attenuated as it penetrates microalgal cultures and the cells absorb the light and thus the light intensity varies with the position within the culture (Acién Fernández *et al.*, 2013). Additionally, as the concentration of cells or pigments changes, so does the extent of attenuation of light over a given distance in the culture. Due to this, light gradients are present in cultures and the light intensity varies with position as well as time. As cells are normally constantly moving in photobioreactors, they are exposed to a varying light intensity (Takache *et al.*, 2015). A variety of models have been applied to account for these effects which are covered in § 2.7.3. These models generally focus on determining the average light intensity that cells are exposed to, among other methods.

Light sources

The wavelength composition of light depends on the source from which it is produced. Natural sunlight has a broad distribution of wavelengths as it is produced primarily by black body radiation (Serway & Jewett, 2007). Shorter wavelengths of light (below around 400 nm) are largely filtered out by the Earth's atmosphere; however, the distribution of light intensities over the transmitted wavelengths in the visible and infrared range is relatively consistent with roughly equal intensities for the wavelengths in this range (Chen & Blankenship, 2011).

In comparison, the composition of light produced from artificial sources can vary considerably (Andersen, 2005). There are four main forms of artificial light sources used in microalgae culturing: incandescent, fluorescent, vapour discharge, and light emitting diodes (LEDs) (Becker, 1994; Burlew, 1953; Glemser *et al.*, 2016; van Oorschot, 1955). Incandescent bulbs produce light similarly to sunlight by black body radiation and produce a continuous distribution of wavelengths (with a greater intensity at the infrared end of the spectrum when compared to sunlight). They produce more heat that other light sources and are generally no longer recommended for microalgal culturing (Glemser *et al.*, 2016). Vapour discharge lamps produce a few selected wavelengths of light depending on the atomic species of the vapour and produce light more efficiently than incandescent bulbs. Fluorescent lamps also produce a few select wavelengths of light depending on the fluorescent phosphor coating used on the tubes (Schulze *et al.*, 2014). An example of a fluorescent tube light spectrum is shown in Figure 2.4.

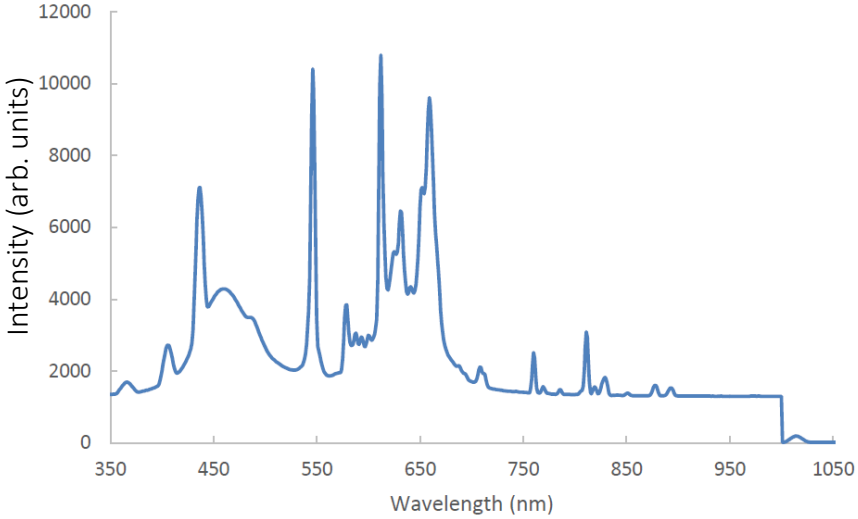

Figure 2.4 – Emission spectrum of a fluorescent tube light. Reprinted with permission from Alfiarty (2018).

Single colour LEDs (i.e. red, green and blue) produce narrow wavelength ranges of light, while white LEDs produce a broad spectrum with a strong peak in the blue wavelengths and a distribution over the 500 to 800 nm range, normally peaking in intensity in the 600 nm range (Schubert, 2006). The distribution of wavelengths produced by white LEDs is due to a phosphor coating being excited by use of a blue or violet LED chip. The exact blend of phosphor coating that is chosen will alter the 'temperature' of the light colour produced by the LED (e.g. cool or warm white); however, in all cases a strong blue or violet peak is seen in the spectra from the underlying LED chip used to excite the

phosphor coating (Schubert, 2006). LEDs are widely used for microalgal culturing as they produce light more efficiently than other sources and their cost has dramatically decreased in recent years (Schulze *et al.*, 2014; Wishkerman & Wishkerman, 2017).

Controlling the intensity of light sources

Light intensity can be controlled in three ways, either by using shading to absorb some of the light emitted, by decreasing the amount of light produced by the source, or by increasing the distance from the light source. Shading can be achieved by using materials to absorb a proportion of the light passing through (e.g. using partially opaque plastic) or by reducing the area through which light can pass through (e.g. using a woven cloth) (Andersen, 2005). As discussed earlier, materials do not all absorb light of all wavelengths equally and so this must be taken into consideration when using this approach to ensure that the desired wavelengths are not filtered out. However, this approach can also be of benefit when certain wavelengths of light are desired or not desired (Mohsenpour *et al.*, 2012), such as UV light from sunlight. Shading by the use of woven cloths does not normally result in particular wavelengths being filtered out; however, as the dimensions of the gap between fibres approach that of the wavelength of the light diffraction may occur to the light passing through the cloth which may be undesirable (Serway & Jewett, 2007).

The method for controlling of the intensity of artificial light sources depends on the light source itself, but the approaches that are used for common light sources such as LEDs are the control of current, or pulse width modulation (PWM). Increasing or decreasing the current flow through an LED results in an almost proportional increase or decrease in light intensity (Schubert, 2006). PWM involves switching LEDs on and off rapidly (on the order of kHz) so that the average light intensity 'seen' is lower (Schulze *et al.*, 2014). The duty cycle (time on to time off ratio) determines the brightness, where a 0% duty cycle is off, 50% is half brightness, and 100% is full brightness and so the LED is, on average, 'on' 0%, 50%, and 100% of the time respectively. PWM control of LEDs is what was used in this study.

Light and photosynthesis

Radiation can only be utilised by cells for photosynthesis if they can absorb it. Due to this, only some of the electromagnetic spectrum is useful for photosynthesis (Ke, 2001; Reece *et al.*, 2010). Photosynthetically active radiation (commonly abbreviated to PAR) is defined as light with a wavelength in the region of 400 to 700 nm (Andersen, 2005). This

definition arises from the region in which common photosynthetic pigments such as chlorophyll *a* strongly absorb. However, pigments can absorb light outside of this PAR range and so the true 'active' radiation range is not limited to 400–700 nm. Additionally, light is not absorbed evenly throughout the PAR range, with red and blue wavelengths typically being more strongly absorbed than green wavelengths (Reece *et al.*, 2010). An example of the *in vitro* absorption spectra of chlorophyll *a* and *b* are shown in Figure 2.5.

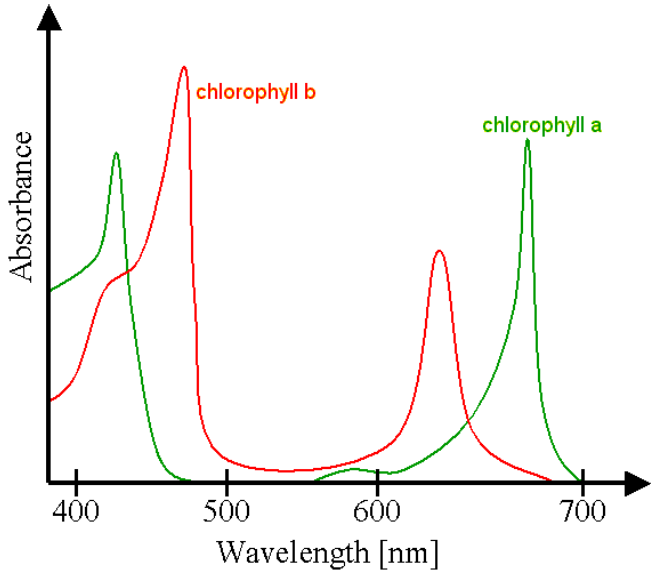

Figure 2.5 – Typical in vitro absorption spectra of chlorophyll a and b. Adapted from "Chlorophyll ab spectra" by Daniele Pugliesi under the Creative Commons Attribution-Share Alike 3.0 Unported license.

It is normally recommended to match the supplied light wavelengths with the absorption profile of pigments in microalgae to allow maximum utilisation of the supplied photons. This approach is commonly seen in LED 'grow lights' tailored for indoor growing of plants which focus on supplying red and blue light wavelengths which align with the peak absorbance wavelength ranges of pigments such as chlorophyll (Schulze *et al.*, 2014).

Green light normally has wavelengths in the 500–600 nm range where chlorophyll pigments do not strongly absorb. This is the reason that plants and algae appear green to the human eye as the red and blue ends of the spectrum are absorbed. However, as green light is not strongly absorbed it is not as useful for photosynthesis (Reece *et al.*, 2010). Despite this, other pigments that can be present in microalgae can absorb light in the 'green' region and allow utilisation of these wavelengths. Work by Tangestani (2019) showed that *Trachydiscus* sp. LCR-Awa-9-2 could grow under green light and so green

light can still be absorbed and used by this microalga. One explanation of this observation could be due to the variation of the quantum yield of photosynthesis at different wavelengths of light. Quantum yield is the ratio of the amount of carbon that is fixed (or oxygen evolved) for a quantity of photons absorbed. While green light is not typically strongly absorbed, its quantum yield can be similar to that of other PAR wavelengths and so any absorbed photons are still able to be utilised similarly for photosynthesis (Skillman, 2008; Taiz & Zeiger, 1991).

As photons of a shorter wavelength have greater energy, light at the blue end of the spectrum provides more energy for photosynthesis for a given quantity of photons than light at the red end. However, short wavelength light in the ultra-violet (UV) region can damage cells by causing damage to DNA and other cellular components (Reece *et al.*, 2010). As the wavelength increases beyond 700 nm a phenomenon referred to as the "red drop" occurs (Emerson & Rabinowitch, 1960), where the energy of the photons is too low to be utilised for photosynthesis. Therefore, light wavelengths beyond 700 nm are not useful for photosynthetic growth in most microorganisms.

2.3.2 Photosynthesis and photoautotrophic growth of microalgae

Photosynthesis was defined by Charles Barnes in 1893 as *"the biological process for synthesis of complex carbon compounds out of carbonic acid, in the presence of chlorophyll, under the influence of light"* (Gest, 2002). Since then, the definition of photosynthesis has been updated and shaped by new discoveries of photosynthetic organisms and so a more recent definition proposed by Gest (1993) is: "*Photosynthesis is a series of processes in which electromagnetic energy is converted to chemical energy used for biosynthesis of organic cell materials; a photosynthetic organism is one in which a major fraction of the energy required for cellular syntheses is supplied by light.*"

Photoautotrophic growth occurs when an organism uses light as its main energy source and inorganic carbon for its carbon source (Reece *et al.*, 2010). Microalgae are photoautotrophic organisms; however, some strains can conduct heterotrophic or mixotrophic growth and can utilise organic carbon (e.g. sugars) for their energy and carbon sources (Andersen, 2005; Chen & Chen, 2006). Photoautotrophic growth is fundamentally limited by light and carbon dioxide supply (Andersen, 2005).

At the simplest level, photosynthesis is described by Equation (2.2) where carbon dioxide and water are converted to oxygen and the general carbohydrate [CH_2O] with the use of light energy (Reece *et al.*, 2010).

$$CO_2 + H_2O + \text{photons} \longrightarrow O_2 + [CH_2O] \qquad (2.2)$$

The carbohydrates produced from photosynthesis are further utilised in the cells to synthesise cellular metabolites. The overall reaction of photosynthesis occurs in a series of steps which are broadly categorised into the light-dependent and light-independent (or Calvin cycle) reactions (Reece *et al.*, 2010). Figure 2.6 shows a diagrammatic representation of the overall process of photosynthesis.

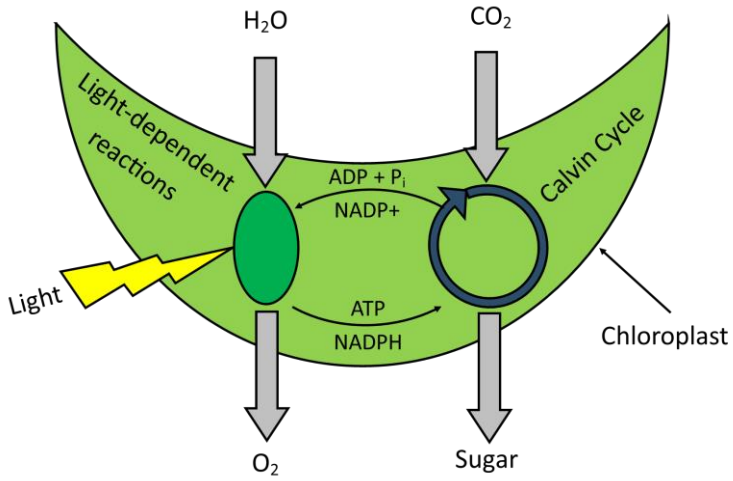

Figure 2.6 – Simplified overview of the relationship between light-dependent reactions and the Calvin cycle in the chloroplast during photosynthesis. Based on Reece et al. (2010, p. 234). ATP: Adenosine triphosphate; ADP: adenosine diphosphate; P_i: inorganic phosphate; NADP+: nicotinamide adenine dinucleotide phosphate; NADPH: reduced form of NADP+.

Light-dependent reactions of photosynthesis

The light-dependent reactions of photosynthesis utilise light energy to produce chemical energy carriers for use in the light-independent reactions. Briefly, light is absorbed by pigment complexes in the cells which use the energy to excite electrons which are harvested from the splitting of water into oxygen and free protons. The excited electrons are passed along the electron transport chain where proteins in the thylakoid membranes convert $NADP^+$ to NADPH and ADP to ATP. This overall process is illustrated in Figure 2.7. These chemical energy carriers are oxidised in the light-independent reactions and then returned to the light-dependent reactions to be reduced again (Reece *et al.*, 2010).

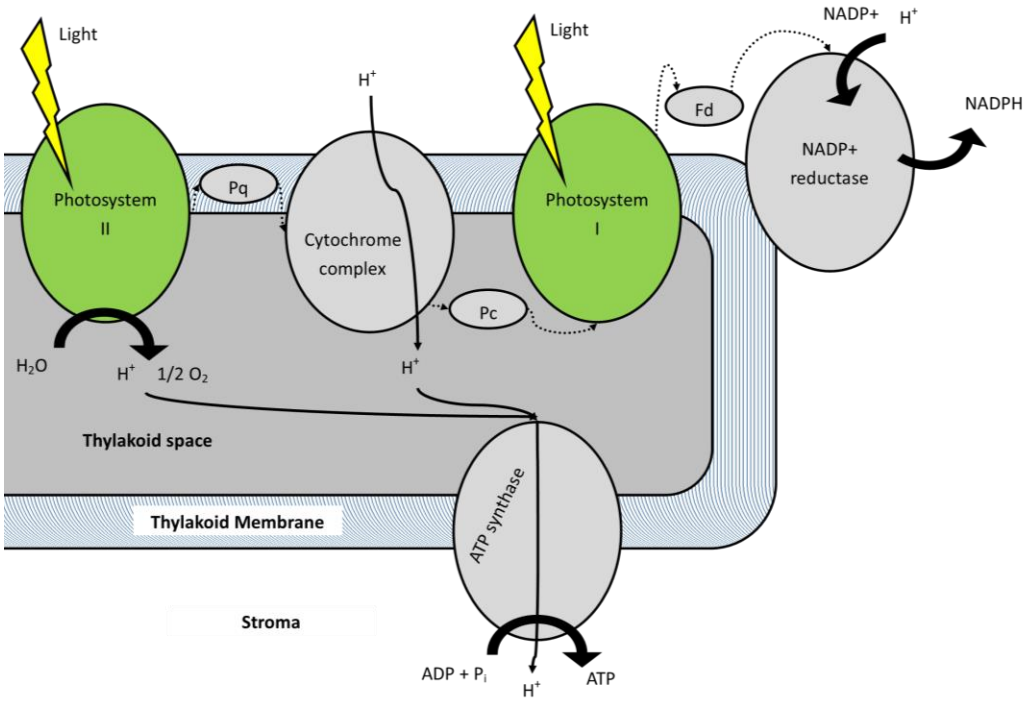

Figure 2.7 – Simplified schematic of the components of the light dependent reactions of photosynthesis and their relative locations in the thylakoid membranes. Based on Reece et al. (2010, p. 243). Pq: plastoquinone; Pc: plastocyanin; Fd: ferredoxin; NADP+: nicotinamide adenine dinucleotide phosphate; NADPH: reduced form of NADP+; ATP: adenosine triphosphate; ADP: adenosine diphosphate; P_i: inorganic phosphate.

The light-dependent reactions occur rapidly, of the order of milliseconds, while the rate of light-independent reactions are slower and thus limit the overall rate of photosynthesis (Ellis, 2010; Simionato *et al.*, 2013; Takache *et al.*, 2015). Additionally, excessive light can damage the apparatus associated with the light-dependent reactions through photooxidative and other photodamage processes (Raven, 2011). Once damaged, the apparatus can take considerable time to repair, on the order of tens of minutes (Raven, 2011).

Light-independent reactions of photosynthesis

The light-independent reactions of photosynthesis are commonly referred to as the Calvin cycle (also called the Calvin-Benson cycle or the 'dark' reactions; although these reactions do not require darkness to proceed). In these reactions, carbon dioxide is fixed into organic molecules in the Calvin cycle and sugars are produced for further use by the cell as illustrated in Figure 2.8. The energy required to carry out the reactions is supplied from NADPH and ATP produced from the light-dependent reactions (Reece *et al.*, 2010). CO_2 is fixed by ribulose-1,5-bisphosphate carboxylase/oxygenase (RuBisCO) and this is the committed and rate-limited step of the Calvin cycle.

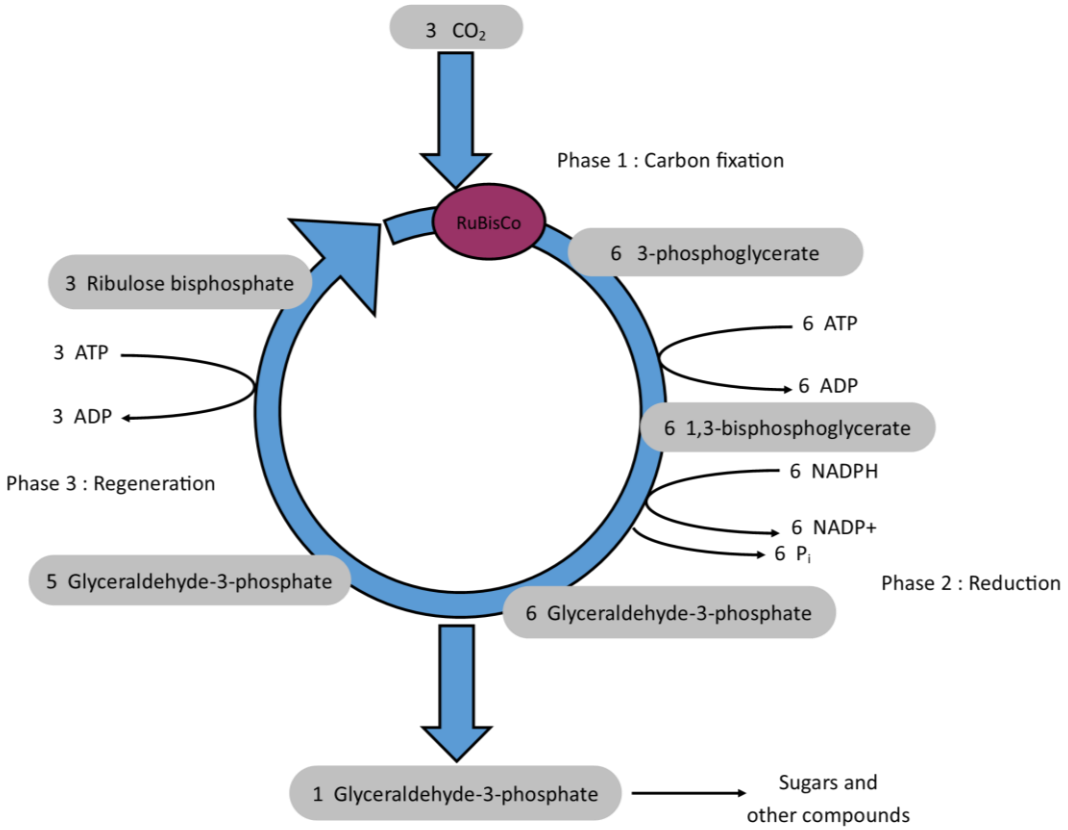

Figure 2.8 – Simplified diagram of the Calvin cycle. Based on Reece et al. (2010, p. 244). NADP+: nicotinamide adenine dinucleotide phosphate; NADPH: reduced form of NADP+; ATP: adenosine triphosphate; ADP: adenosine diphosphate; P_i: inorganic phosphate.

As mentioned previously, the rate of the light-independent reactions is slower than the light-dependent reactions. The overall rate of light-independent reactions, and thus photosynthesis, is limited by RuBisCO which is only able to fix approximately three molecules of carbon dioxide per second per enzyme (Ellis, 2010).

2.4 Microalgal lipids and eicosapentaenoic acid

2.4.1 Lipids

The meaning of the term 'lipid' is broad and can encompass a range of organic compounds produced by an organism that are soluble in organic solvents, but insoluble in water (Hine & Martin, 2016). Lipids are of particular interest with microalgae as they produce large quantities of lipids when compared to most other organisms such as bacteria. Lipids can be classified and defined more narrowly as discussed below, and different classes and components of lipids have applications to a range of products (Cohen, 1999).

Lipid classes

Due to the broad nature of the term lipid, there are many different classes of lipids. Lipids can be categorised into two main groups: saponifiable (fatty acid containing) and non-saponifiable (non-fatty acid containing) lipids (Prasad, 1996). Non-saponifiable lipids can include compounds such as waxes and sterols and can often be signalling molecules such as some hormones (Gurr & Harwood, 1991). Saponifiable lipids can be further categorised as neutral lipids and polar lipids. As the names suggest, neutral lipids are normally overall neutrally charged and non-polar, while polar lipids are polar molecules and are often charged but also include non-charged species. The head group present on the lipid species determines its categorisation. Each of these lipid categories can be split further into many more classes. Neutral lipids can include classes such as triacylglycerides while polar lipids include mainly classes such as phospholipids and glycolipids (Cohen, 1999).

Triacylglycerides are overall neutral and non-polar molecules and are typically used as energy storage by cells (Becker, 1994; Gurr & Harwood, 1991). They are also what are often referred to as fats and make up the majority of oils such as canola oil (Kates, 1986). Triacylglycerides consist of a glycerol head group to which three fatty acids are bonded via ester bonds (Gurr & Harwood, 1991). Phospholipids have a charged head group which consists of a glycerol moiety bonded to a phosphate group via an oxygen atom and then two fatty acids bonded via ester bonds. The phosphate group may then bond to a variety of other residues, such as choline, which determines the sub-class of the phospholipid as discussed further below. Glycolipids are similar in structure to phospholipids but instead contain a sugar group in place of the phosphate group. The sugar bonded to the glycerol determines the sub-class of the glycolipid with the most common sugar being galactose in photosynthetic organisms (Gurr & Harwood, 1991). Glycolipids are discussed further later in this section. The overall structure of these classes of saponifiable lipids are shown diagrammatically in Figure 2.9 and the typical chemical structures of the head groups of these lipid classes are shown in Figure 2.10.

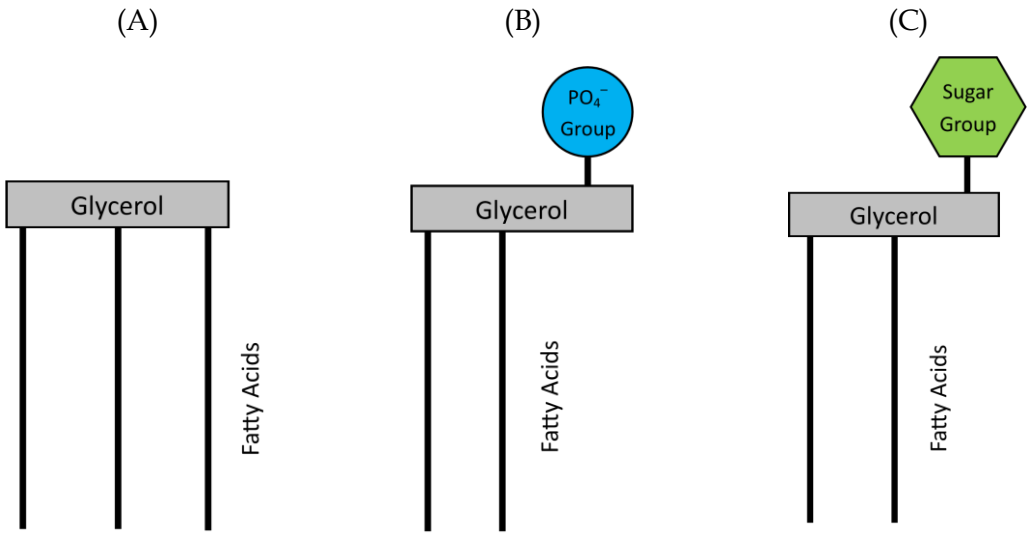

Figure 2.9 – Diagrammatic representation of the structures of common saponifiable lipid classes. A) triacylglycerides, B) phospholipids, C) glycolipids. Based on Gurr and Harwood (1991) and Prasad (1996).

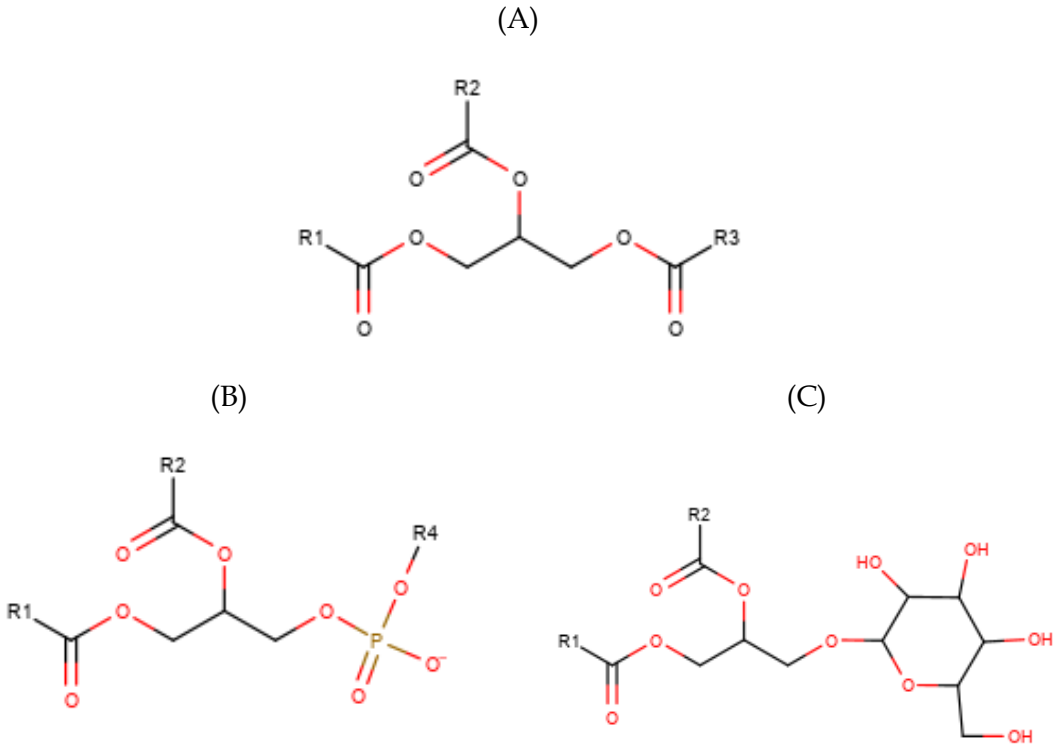

Figure 2.10 – Typical structures of head groups for A) triacylglycerides, B) phospholipids, and C) galactolipids. R1, R2, R3 are fatty acid tails, R4 are other phospholipid specific residues. Based on Gurr and Harwood (1991) and Prasad (1996).

Polar lipids are primarily associated with membranes in cells and are able to form lipid bilayers. These bilayers form due to hydrophobic fatty acid tails forming the inside region of the bilayer and the hydrophilic head groups forming the outside of the bilayer. Nearly all organisms use phospholipid bilayers to form their cell membranes (Gurr & Harwood, 1991).

While the head group of lipids denotes their classification, the fatty acid tails attached to the head group also play a role in the use and behaviour of different lipid species (Gurr & Harwood, 1991; Prasad, 1996).

Fatty acids

Free fatty acids consist of a hydrophobic tail and charged carboxylic acid head as shown in Figure 2.11 (Prasad, 1996). The carboxylic acid end is normally bonded through an ester bond to a head group such as glycerol, as described above; however, fatty acids can also exist in other forms such as free fatty acids or as other esterified species (Gurr & Harwood, 1991). Fatty acids are classified and named based on the length of their hydrophobic tail and degree of unsaturation, as well as the position of carbon-carbon double bonds (Prasad, 1996). If a fatty acid does not contain any carbon-carbon double bonds in its tail, it is classed as a saturated fatty acid. Saturated fatty acids are normally associated with energy storage in cells (Gurr & Harwood, 1991) but are also important components of cell membranes.

(A)

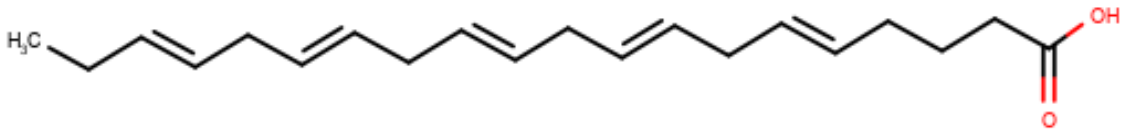

(B)

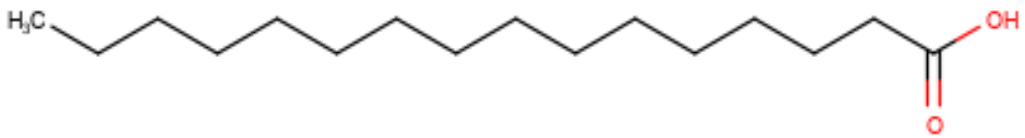

Figure 2.11 – Typical structures of fatty acids. A) polyunsaturated, eicosapentaenoic acid. B) saturated, palmitic acid.

If the tail of a fatty acid contains one or more carbon-carbon double bonds it is classed as an unsaturated fatty acid. These unsaturated fatty acids are then further classified depending on the location of the first double bond relative to the end of the tail. Fatty acids containing more than one carbon-carbon double bond are referred to as poly-unsaturated fatty acids (PUFAs) (Gurr & Harwood, 1991).

Fatty acids are often referred to by their lipid number which takes the form of "x:y" where x is the number of carbons in the carbon chain and y is the number of carbon-carbon double bonds present. A further extension of this is "x:y n-z" for unsaturated fatty acids where z is the location of the first double bond in the chain from the ω end of the fatty acid chain. The ω carbon is defined as the carbon located furthest from the carboxylic head group (which is referred to as the α carbon). For example, 16:0 refers to a fatty acid with 16 carbon atoms and zero double bonds (i.e. a saturated fatty acid, Figure 2.11 B); while 20:5 n-3 refers to a fatty acid with 20 carbon atoms and 5 double bonds, with the first double bond located at the ω 3-carbon position in the chain (Figure 2.11 A). An alternative nomenclature for double bond location is the 'Δ' denotation which is often used in the naming of enzymes involved in fatty acid synthesis which counts from the α carbon in the fatty acid. For example, an n-3 double bond in EPA is the equivalent of Δ17 (IUPAC-IUB Commission on Biochemical Nomenclature, 1977).

Two classes of unsaturated fatty acids that are important for human health are omega-3 and omega-6 polyunsaturated fatty acids (Ward & Singh, 2005). These classes of fatty acids derive their name from the position of the first carbon-carbon double bond in the fatty acid tail as described above (Gurr & Harwood, 1991). Omega-3 fatty acids contain their first double bond at the 3-carbon position, as seen for EPA in Figure 2.11 A. Similarly, omega-6 fatty acids contain their first double bond at the 6-carbon position in the fatty acid tail. These classes of fatty acids are important as humans and other animals are unable to synthesise the quantities that they require and so are primarily obtained through their diet (Tocher *et al.*, 2019). Omega-3 and -6 fatty acids may play a role in the prevention of a variety of health conditions and thus there is interest in their production for use for human health applications (Adarme-Vega *et al.*, 2012; Ward & Singh, 2005).

Fatty acids from natural sources normally contain even numbered carbon chains due to the biosynthesis pathways used to produce them (Gurr & Harwood, 1991). The typical pathways present in microorganisms add 2-carbon units to the fatty acid to increase its length resulting in chains increasing in length in multiples of two carbons. Odd

numbered fatty acids, e.g. 13:0, are uncommon in microalgae and most other natural sources but some other microorganisms are able to synthesise them (Christie, 1989).

Saturated or longer fatty acids have higher melting points than unsaturated or shorter fatty acids, for example, 16:0 has a melting point of 61 °C while 16:1 has a melting point of 1 °C and 18:1 has a melting point of 16 °C (Gurr & Harwood, 1991). The difference in melting point between saturated and unsaturated fatty acids is largely due to their conformation, with saturated fatty acids typically forming straight chains while unsaturated fatty acids are 'kinked' due to their double bonds. Their shape determines how closely fatty acids can pack together and interact. Longer fatty acids have higher melting points due to their increased intermolecular forces (Gurr & Harwood, 1991).

2.4.2 Microalgal lipids

Major lipid classes present in microalgae

In microalgae, lipids are typically divided into three main categories: neutral lipids, phospholipids, and glycolipids (Cohen, 1999). These lipids are constituents of many parts of the cell, namely as part of cellular membranes and as energy storage (Becker, 1994; Prasad, 1996; Ratledge, 1997). While these are the three main lipid classes that are normally referred to, there are also a variety of other lipid classes that can be present, as expanded on below.

Triacylglycerides are the normally the major component of neutral lipids in microalgae, but the neutral lipid class also includes species such as waxes, sterols, hydrocarbons, and free fatty acids as mentioned earlier. Triacylglycerides are mainly used as an energy store by microalgae and are the class of greatest interest in strains used for biodiesel production (Cohen, 1999). For microalga species such as *Chlorella*, triacylglycerides can account for around 80% by mass of the lipids in the cells (Burlew, 1953).

As mentioned earlier, phospholipids and glycolipids are typically found as constituents of cell membranes through forming lipid bilayers (Prasad, 1996). These two classes of lipids are often grouped together as polar lipids, so-called due to their head group causing a dipole on the molecule and thus are polar when compared to triacylglycerides (Cohen, 1999). Phospholipids are the main component of the cell membrane in microalgae as well as most other organisms. There are many sub-classes of phospholipids depending on the moiety attached to the phosphate group on the head

group (R4 in Figure 2.10 B). The most common phospholipid class is most organisms is phosphatidylcholine (PC). Other phospholipid classes are phosphatidylethanolamine (PE), phosphatidylserine (PS), phosphatidylinositol (PI), phosphatidylglycerol (PG), and diphosphatidylglycerol (DPG) (Prasad, 1996). Structures of these headgroup residues are shown in Figure 2.12.

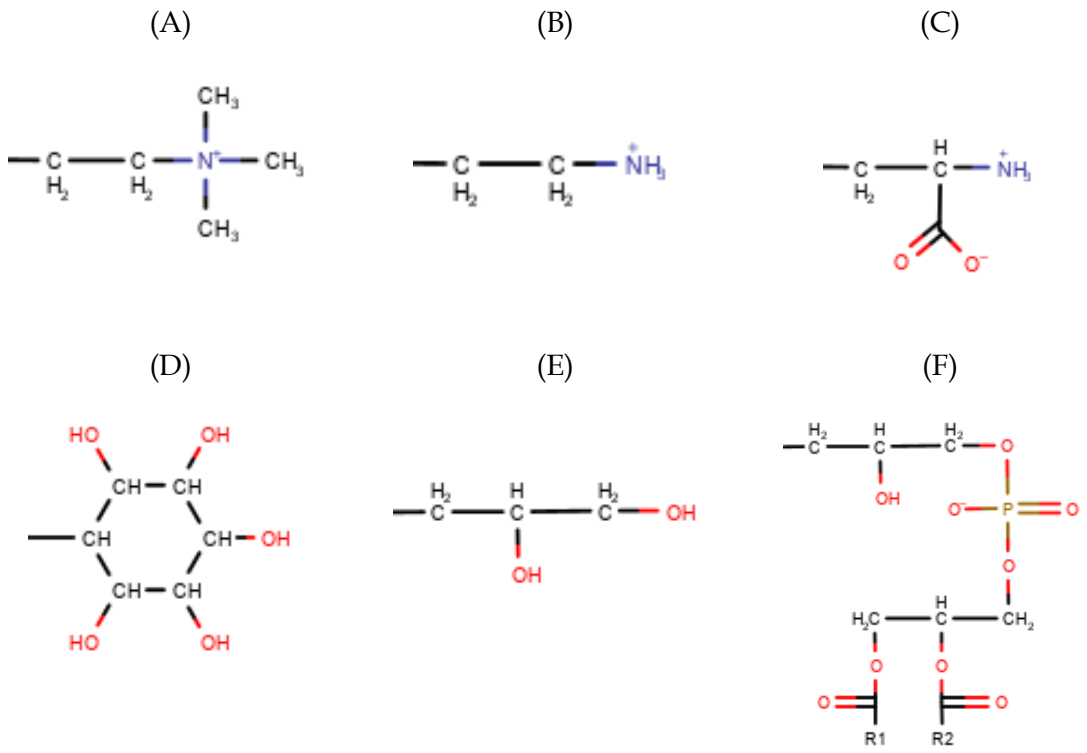

Figure 2.12 – Structures of headgroups of phospholipid classes, R4 residues from Figure 2.10 B. A) phosphatidylcholine; B) phosphatidylethanolamine; C) phosphatidylserine; D) phosphatidylinositol; E) phosphatidylglycerol; F) diphosphatidylglycerol. R1 and R2 are fatty acid tails. Based on Prasad (1996, p. 9).

Glycolipids found in microalgae are typically galactolipids. These lipids make up the majority of the lipids present in the thylakoid membranes of the chloroplast (Siegenthaler & Murata, 1998). The most common galactolipid class are the monogalactosyl diacylglycerides (MGDG) which contain a single galactose moiety attached to the glycerol head group. Another common galactolipid are the digalactosyl diacylglycerides (DGDG) which consists of two galactose sugars attached to each other and the glycerol headgroup. Structures of these galactolipids are shown in Figure 2.13.

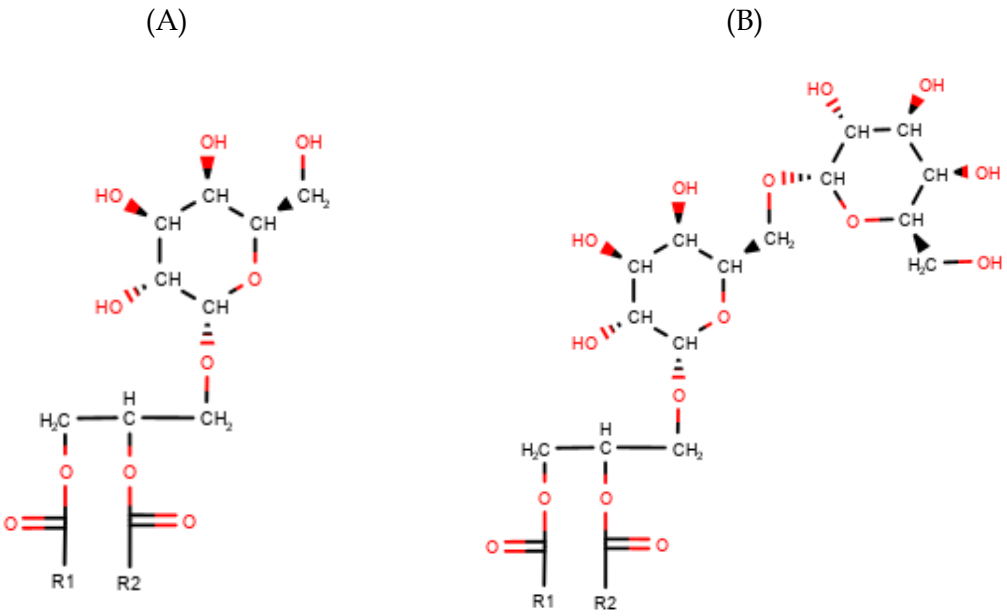

Figure 2.13 – Structures of galactolipid head groups. A) monogalactosyl diacylglyceride, B) digalactosyl diacylglyceride. R1 and R2 are fatty acid tails. Based on Prasad (1996, p. 12).

Other glycolipids containing other sugars can be also present in microalgae and cyanobacteria. For example, monoglucosyl diacylglycerides (i.e. MGDG but with glucose instead of galactose) can be present in cyanobacteria, such as *Synechocystis* sp., as it is a precursor in the production of MGDG (Tiago Toscano *et al.*, 2014).

A less common class of lipids, but one that is often also found in thylakoid membranes, are the sulphoquinovosyl diacylglycerides (SQDG) which are sulphur-containing (Siegenthaler & Murata, 1998). These lipids are often closely associated with membrane proteins. The structure of the headgroup of these lipids is shown in Figure 2.14.

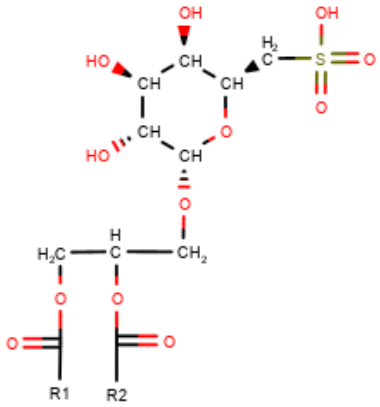

Figure 2.14 – Structure of a sulphoquinovosyl diacylglyceride headgroup. R1 and R2 are fatty acid tails. Based on Prasad (1996, p. 12).

A class of lipids that is often found only in microalgae are betaine lipids. They can be used by cells as a substitute for phospholipids under phosphate starved conditions. The most common class of betaine lipid in eustigmatophytes such as *Nannochloropsis* is diacylgyceryl-N-trimethylhomoserine (DGTS) (Cañavate *et al.*, 2016). Other classes of betaine lipids found in other microalgae are diacylglyceryl-hydroxymethyl-N,N,N-trimethyl-beta-alanine (DGTA) and diacylglyceryl-carboxyhydroxymethylcholine (DGCC). All of these classes contain a charged nitrogen as part of a quaternary amine moiety (Cañavate *et al.*, 2016; Dembitsky, 1996; Kato *et al.*, 2003). Structures of these betaine lipids are shown in Figure 2.15.

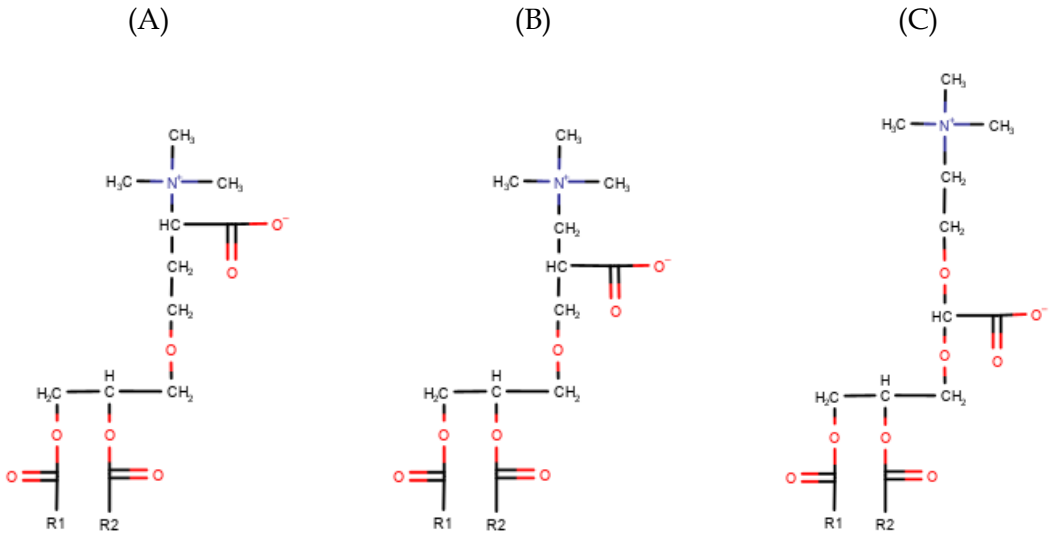

Figure 2.15 – Structures of the headgroups of betaine lipids. A) DGTS, B) DGTA, C) DGCC. R1 and R2 are fatty acid tails. Based on Dembitsky (1996).

Common fatty acid species present in microalgae

There are two main measures that can be used when reporting fatty acid content: either as a fraction of the total fatty acid content, or as a fraction of the total dry biomass. Henceforth for this thesis the terminology used is as follows; **fatty acid content** refers to the grams of a specific fatty acid, expressed as a free fatty acid, per 100 g of dry biomass. **Fatty acid fraction** refers to the grams a given fatty acid, expressed as a free fatty acid, per 100 g of total fatty acids expressed as free fatty acids. **Total fatty acid content** is the fraction of mass in grams of total fatty acids, expressed as free fatty acids, per 100 g of dry biomass. Therefore, the fatty acid content of a given fatty acid is the product of the total fatty acid content and the fatty acid fraction of that fatty acid.

Saturated fatty acids are commonly precursors to other metabolites in microalgae and can be used to store energy as they are more energy dense than unsaturated fatty acids (Gurr & Harwood, 1991). Some examples of typical saturated fatty acids present in microalgae are listed in Table 2.1. In eustigmatophytes, myristic (14:0) or palmitic acid (16:0) are often the most common saturated fatty acid present in the cells (Cohen, 1999; Volkman *et al.*, 1993).

Table 2.1- Common saturated fatty acids present in microalgae.

Short Name	Trivial Name
12:0	Lauric acid
14:0	Myristic acid
16:0	Palmitic acid
18:0	Stearic acid
20:0	Arachidic acid
22:0	Behenic acid

Unsaturated fatty acids are commonly of interest for health-related products, in particular the omega-3 polyunsaturated forms such as EPA and docosahexaenoic acid (DHA) (Tocher *et al.*, 2019). Common unsaturated fatty acids present in microalgae are summarised in Table 2.2. In eustigmatophytes the most prevalent unsaturated fatty acids are typically species such as EPA (20:5 n-3) or palmitoleic acid (16:1 n-7) (Cohen, 1999; Volkman *et al.*, 1993).

Table 2.2- Common unsaturated fatty acids present in microalgae.

Short Name	Trivial Name
14:1 n-5	Myristoleic acid
16:1 n-7	Palmitoleic acid
16:1 n-10	Sapienic acid
18:1 n-9	Oleic acid
18:2 n-6	Linoleic acid
18:3 n-3	α-linolenic acid (ALA)
18:3 n-6	γ-linolenic acid
18:4 n-3	Stearidonic acid
20:2 n-6	Eicosadienoic acid
20:3 n-3	Eicosatrienoic acid
20:3 n-6	Dihomo-γ-linolenic acid
20:4 n-3	Eicosatetraenoic acid
20:4 n-6	Arachidonic acid
20:5 n-3	**Eicosapentaenoic acid (EPA)**
22:1 n-9	Erucic acid
22:6 n-3	Docosahexaenoic acid (DHA)

The fatty acid composition of *Trachydiscus* sp. LCR-Awa-9-2 is similar to many other eustigmatophytes with EPA (20:5 n-3) and myristic acid (14:0) typically being the major constituents in its fatty acid profile. An example of a typical fatty acid composition of *Trachydiscus* sp. LCR-Awa-9-2 is shown in Table 2.3.

Table 2.3 – Example of a typical fatty acid profile of Trachydiscus sp. LCR-Awa-9-2 grown in BBMA medium. From Alfiarty (2018). FFA: free fatty acid; TFA: total free fatty acids.

Fatty Acid	Fatty Acid Fraction (g FFA / 100 g TFA)	Fatty Acid Content (g FFA / 100 g dry biomass)
14:0	16.50	1.98
14:1 n-5	0.63	0.08
16:0	7.62	0.91
16:1 n-7	10.10	1.21
16:2	0.48	0.06
18:0	1.23	0.15
18:1 n-9	3.64	0.44
18:1 n-7	0.18	0.02
18:2 n-6	6.69	0.80
18:3 n-3	2.17	0.26
20:0	0.54	0.07
20:3 n-6	0.55	0.07
20:4 n-6	3.44	0.41
20:5 n-3	**33.75**	**4.05**
22:0	7.22	0.87
Others	5.26	0.62

Biosynthesis of lipids in microalgae

As described earlier, fatty acids are generally biosynthesised by addition of 2-carbon units and desaturation of the fatty acid tail. Fatty acids are synthesised starting from the *de novo* fatty acid synthesis pathway which utilises acetyl-CoA (acetyl-coenzyme A) synthesised from products of the Calvin cycle. From the fatty acid synthesis pathway 16:0 and 18:0 free fatty acids are the major products formed which are then used to produce other fatty acids by elongation and desaturation processes. Fatty acid synthesis occurs in the plastid and the fatty acids produced are then transported to the endoplasmic reticulum to be utilised further by the eukaryotic lipid synthesis pathway. The alternative prokaryotic pathway of lipid synthesis occurs in the plastid. In the eukaryotic pathway, fatty acids are bound to CoA to form acyl-CoA species. Lysophosphatidic and phosphatidic acids are then made from the fatty acids from the acyl-CoA and glycerol-3-phosphate (Bellou *et al.*, 2014; Radakovits *et al.*, 2010). Phosphatidic acids themselves are found as components of cell membranes and are also

important signalling molecules (Gurr & Harwood, 1991). An overview of the general lipid synthesis pathways is shown in Figure 2.16.

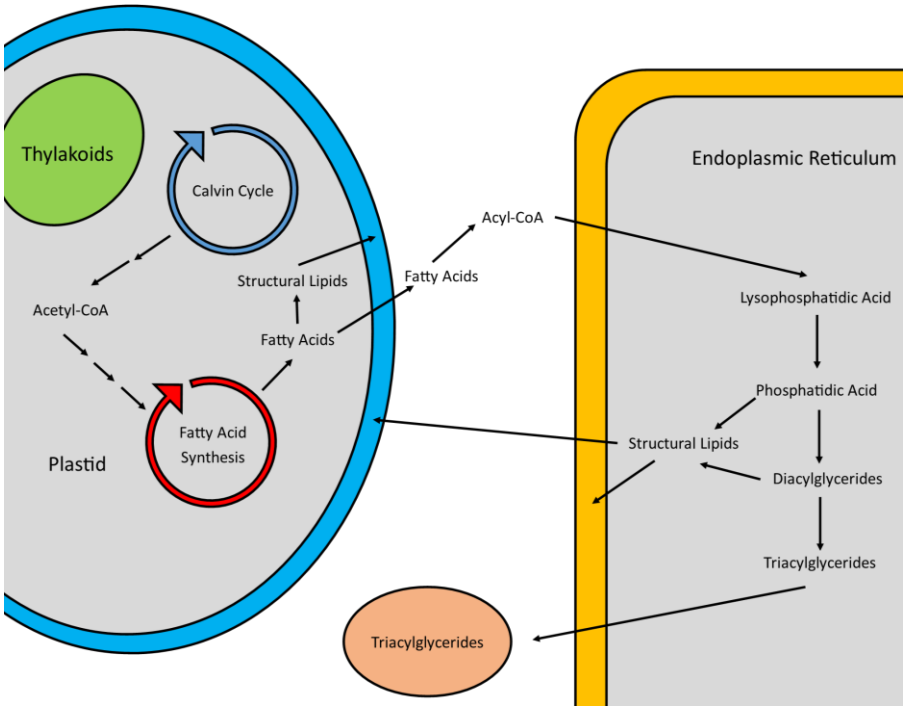

Figure 2.16 – Simplified overview of the synthesis of saponifiable lipids in microalgae. Based on Bellou et al. (2014) and Radakovits et al. (2010). CoA: Coenzyme A.

Triacylglycerides are synthesised from diacylglycerides in the eukaryotic pathway by addition of another fatty acid to the molecule. As the triacylglycerols accumulate they can form lipid bodies which are micelles formed from droplets of the triacylglycerides surrounded by a layer of phospholipids. These micelles form as the triacylglycerides accumulate in the membrane space of the endoplasmic reticulum and are eventually ejected as a micelle into the cytosol of the cell (Cagliari *et al.*, 2011).

Phospholipids are synthesised from phosphatidic acids through two main different pathways, either from diacylglycerides or cytidine diphosphate diacylglycerides. Phosphatidylcholine and phosphatidylethanolamine can be formed by either pathway, although phosphatidylethanolamine is a precursor to phosphatidylcholine in the latter pathway. Phosphatidylinositol and phosphatidylglycerol are formed through the cytidine diphosphate diacylglyceride pathway (Gurr & Harwood, 1991).

Galactolipids can be synthesised generally by two different pathways: one common to eukaryotic algae and plants, and the other common to cyanobacteria. In the eukaryotic pathway, diacylglycerides formed from phosphatidic acids are reacted with

uridine diphosphate-galactose to form MGDGs by MGDG synthase. DGDGs are formed by reacting the MGDG further with uridine diphosphate-galactose by DGDG synthase. Galactolipid synthesis typically occurs in, or in the region of, the chloroplast (Hölzl & Dörmann, 2019). The prokaryotic path of galactolipid synthesis present in cyanobacteria occurs by the reaction of diacylglycerides with uridine diphosphate-glucose to form monoglucosyl diacylglycerides (GlcDG). The glucose is then epimerised to form galactose on the lipids and form MGDGs. DGDGs are synthesised by reacting the MGDG with uridine diphosphate-galactose (Tiago Toscano *et al.*, 2014).

2.4.3 Eicosapentaenoic acid

Eicosapentaenoic acid (EPA) is a long-chain omega-3 polyunsaturated fatty acid (PUFA) (Cohen, 1999). Other fatty acids in the omega-3 family are docosahexaenoic acid (DHA) and α-linolenic acid (ALA). As mentioned earlier, these omega-3 fatty acids are important in the diet of humans as we are unable to synthesise omega-3 fatty acids in the quantities required (Tocher *et al.*, 2019). EPA in particular may play a beneficial role in infant brain function, arthritis, and preventing cardiovascular disease (Buono *et al.*, 2014; Kris-Etherton *et al.*, 2002; Simopoulos, 1991; Simopoulos, 2002). Fish oils are the most common source of EPA in human diets (Cohen, 1999; Tocher *et al.*, 2019). Due to issues such as overfishing and potential mercury contamination, obtaining EPA from fish oil has become less sustainable and less desirable. Additionally, EPA produced from fish oil is not vegan or vegetarian-friendly and other plant lipid sources do not typically contain EPA so there is potential for microalgae to fill this market niche that cannot be supplied by current sources (Pauly *et al.*, 2002; Tocher *et al.*, 2019).

Fish themselves do not produce large amounts of EPA, but instead acquire it primarily from their diet with the EPA originating from microalgae at the base of the food chain (Tocher *et al.*, 2019). As microalgae are a rich source of EPA, they are one of the most promising alternative sources for this fatty acid.

Biosynthesis of EPA and associated lipids

A number of possible biosynthetic pathways for the formation of EPA and other omega-3 fatty acids have been reported (Cao *et al.*, 2012; Cohen, 1999; Khozin-Goldberg *et al.*, 2002; Monroig *et al.*, 2013; Shiran *et al.*, 1996; Sukenik & Carmeli, 1990; Uttaro, 2006; Yap & Chen, 2001). The exact biosynthesis pathways of EPA in microalgae are unknown, but proposed pathways for microalgae such as *Monodus subterraneus* and *Phaeodactylum tricornutum,* among others, have been reported (Cohen, 1999; Mühlroth *et al.*, 2013). In

general, EPA is synthesised from 18:0 from desaturation and elongation of the fatty acid by elongase (Elo) and desaturase (Des) enzymes. Desaturation and elongation normally take place with the fatty acids bonded to a head group such as in MGDG or phosphatidylcholine (Cohen, 1999). The conventional pathway of EPA synthesis from 18:0 typically seen in microorganisms is shown in Figure 2.17. EPA can be formed through four different main pathways depending on the precursor fatty acid which are broadly characterised into the n-6 or n-3 pathways (Cao *et al.*, 2012).

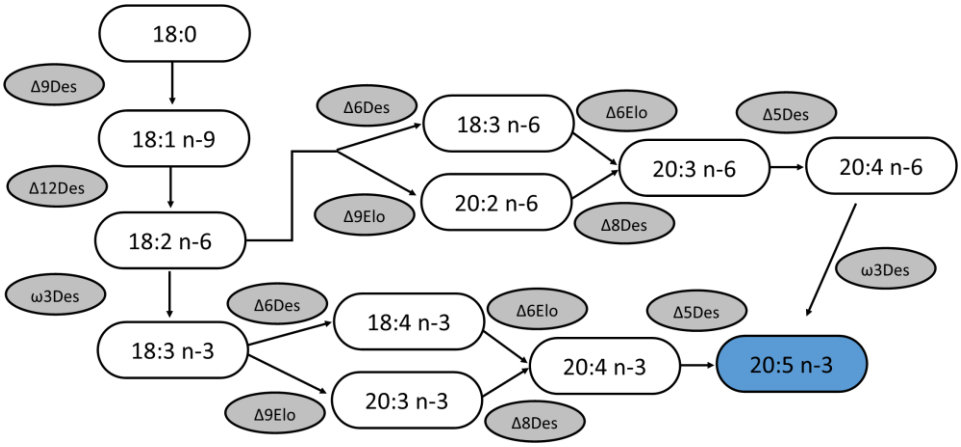

Figure 2.17 – Conventional pathways of EPA biosynthesis in microorganisms. Based on Cao et al. (2012).

EPA can be synthesised in either the cytoplasm (i.e. eukaryotic production) or chloroplast (i.e. prokaryotic production) of the cell depending on the pathway used. In the prokaryotic pathway, EPA is synthesised in MGDG-bound species. In the prokaryotic pathway, the precursor MGDG species typically contains a 20:4 fatty acid while the other fatty acid is typically a species such as 16:0 or 16:1 (e.g. MGDG 20:5/16:0). Due to this, when the 20:4 fatty acid undergoes desaturation to form 20:5 the resultant species lipid will only contain one EPA fatty acid moiety with the other being a different fatty acid. The eukaryotic pathway typically takes place with phospholipid-bound fatty acids with classes such as phosphatidylcholine (Mühlroth *et al.*, 2013). EPA produced from the eukaryotic pathway is also normally present with another fatty acid such as 14:0, 16:0 or 16:1 in the phospholipid species; however, when the EPA is transferred to the chloroplast it can be substituted for both fatty acids on the MGDG head group and thus produce EPA-only containing MGDG species (MGDG 20:5/20:5). These MGDG 20:5/20:5 species are only produced by eukaryotic synthesis of EPA, whereas either pathway can produce MGDG species with EPA associated with a 14:0, 16:0 or 16:1 fatty acid etc. An overview of a proposed pathway for *Monodus subterraneus* is shown in Figure 2.18.

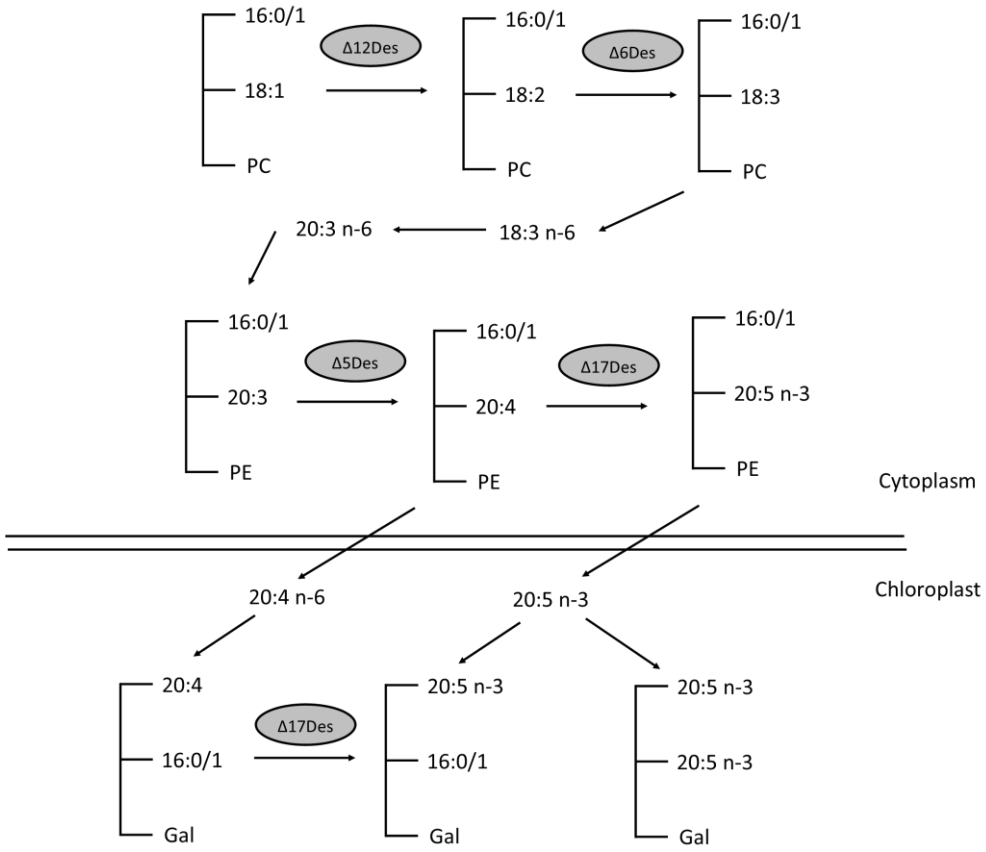

Figure 2.18 – Proposed biosynthesis pathway for EPA in Monodus subterraneus. Based on Cohen (1999, p. 37). PC: phosphatidylcholine; PE: phosphatidylethanolamine; Gal: galactose.

Increasing light levels can increase chloroplastic ω-3 desaturation (i.e. the prokaryotic pathway) which results in a greater proportion of MGDG 20:5/16:0 or 20:5/16:1 species in microalgae. Conversely, at lower light levels the eukaryotic pathway is preferred and results in a greater proportion of MGDG 20:5/20:5 species. In some microalgae, such as *Nannochloropsis oculata*, EPA synthesis only occurs by the eukaryotic pathway (Cohen, 1999).

EPA is normally concentrated in polar and structural lipids in microalgae. As seen in the biosynthetic pathways and discussed in above sections, EPA is mainly associated with MGDG lipids in the chloroplast for most microalgae (Cohen, 1999). Betaine lipids such as DGTS are also high in EPA in other eustigmatophytes (Cañavate *et al.*, 2016). EPA can be found in phospholipids such as phosphatidylcholine and phosphatidylethanolamine, but typically in lower amounts compared to MGDG (Cohen, 1999).

Applications of and market for EPA

While some animals can synthesise omega-3 fatty acids, they are not able to produce them at a rate high enough to supply quantity that is required (Tocher *et al.*, 2019). Due to this, microalgae are an important source of these fatty acids for human diets as they can synthesise far larger quantities of these fatty acids compared to other sources such as plants (Cohen, 1999). EPA is also a precursor to some pharmaceutical drugs such as eicosanoids and so high purity EPA is required in their manufacture (Cohen, 1999).

As mentioned earlier, in the health field EPA has been shown to play a role in preventing cardiovascular disease as well as controlling inflammation associated with arthritis (Becker, 1994; Kris-Etherton *et al.*, 2002; Stoyneva-Gärtner *et al.*, 2019). As EPA is not present in high amounts in most foods, supplementation of EPA from other sources such as fish oil has been shown to be important for good health. Microalgae with high omega-3 fatty acid contents are also ideal for aquaculture feeds to improve the nutritional value of farmed seafood (Stoyneva-Gärtner *et al.*, 2019). As oily fish such as salmon primarily accumulate EPA from their diet, commercially formulated fish feeds require a source of EPA to add to the formulation (Finco *et al.*, 2016).

It is recommended that an intake of 500 mg per day of omega-3 fatty acids such as EPA are required for good health in humans. This translates to a projected annual world demand for omega-3 fatty acids in this market of 1.27 million tonnes per year according to Tocher *et al.* (2019). It is projected that the global market for fish oils will increase to around US$ 5 billion by the year 2025 through demand in both the aquaculture and human health markets (Finco *et al.*, 2016). As the population of the world continues to increase the demand for these products will continue to grow and so alternative sources of omega-3 fatty acids such as microalgae are increasingly in demand (Tocher *et al.*, 2019).

2.4.4 Lipidomic analysis of microalgae

Lipidomics is the study of the lipid composition of organisms and the biosynthesis and metabolic pathways involved with lipids in cells (Wenk, 2005). As lipids are one of the major metabolites in microalgae, lipidomics is a particularly relevant field to this microorganism. A number of studies have been conducted into the lipidome of various microalgal strains (da Costa *et al.*, 2016) and advancements in analytical techniques in recent decades has accelerated work in this field (Cajka & Fiehn, 2014). A variety of techniques can be employed to analyse the lipidome of microalgae as discussed below.

They broadly cover two main areas: the separation of lipid mixtures by chromatography; and the detection and spectroscopic analysis of lipid species.

Chromatographic methods

Thin layer chromatography (TLC) is widely employed for lipid separations and a variety of methods exist for separation of desired lipid classes (Christie, 2019; Kates, 1986). TLC of lipids is normally performed with glass or aluminium plates covered with a thin layer of silica gel. Lipids are loaded onto the plate as a line along one edge, or in a spot in one corner. The plates are then dipped into a solvent which is wicked up the plate by capillary action. As the solvent rises it carries the lipids with it and the lipids are separated depending on their affinity for the silica and the solvent system used. TLC can be used to separate most lipid classes, either into general bulk classes (e.g. neutral lipids, phospholipids etc.) or further into individual subclasses (e.g. MGDG, phosphatidylcholine etc.). Bulk classes can generally be separated by one-dimensional TLC where the plate is eluted in one direction. Separation into lipid subclasses is normally achieved by two-dimensional TLC where the lipids are first separated in one direction into the major classes, then the plate is dried and a second solvent system is used to separate the lipid classes at 90 ° to the original elution direction (Kates, 1986). Examples of one- and two-dimensional TLC plates are shown in Figure 2.19.

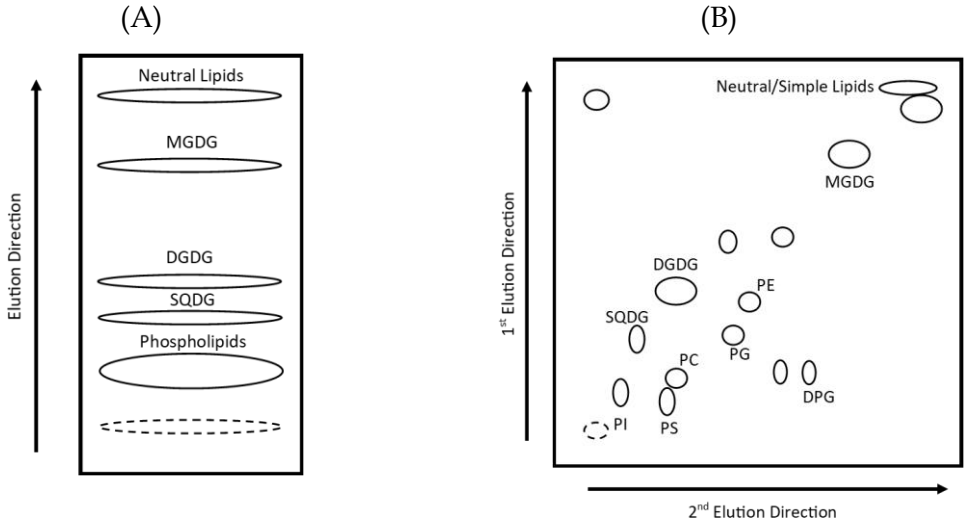

Figure 2.19 – Examples of the typical separation profiles of lipids by A) one-dimensional and B) two-dimensional TLC. Based on Christie (2019).

Liquid chromatography (LC) has been used extensively in lipidomic studies of recent times (Cajka & Fiehn, 2014; da Costa *et al.*, 2016; Zhao *et al.*, 2014). LC is divided into two classes, reverse-phase and normal phase (Burrows *et al.*, 2009) with reverse phase

being the most common method for lipid analyses (Cajka & Fiehn, 2014; da Costa *et al.*, 2016). For analysis, high performance LC (HPLC) or ultra-high performance LC (UHPLC, also called ultra-performance LC, UPLC) are most commonly used and allow quick and efficient separation of analytes (Cajka & Fiehn, 2014; Theodoridis *et al.*, 2012).

Reverse phase LC separation of fatty acids occurs based on chain length as well as the degree and type of unsaturation (Cohen, 1999). Retention times are increased with increasing length of the carbon chain and a decrease in the degree of unsaturation (Cohen, 1999). Typical columns employed for reverse-phase LC for lipid analysis are C_8 (octylsilyl) and C_{18} (octadecylsilyl) (Cajka & Fiehn, 2014; da Costa *et al.*, 2016). Flowrates are generally in the range of 0.1 to 0.5 mL min^{-1} and the columns operated at 40 to 55 ˚C (Cajka & Fiehn, 2014).

Mobile phases are divided into two categories, weak and strong (Burrows *et al.*, 2009). Typical weak and strong mobile phases for reverse phase LC are summarised in Table 2.4. Additives are also included in the mobile phases in low concentrations (5–10 mM, 0.05–0.1%) to improve separation and detection, typically these are ammonium acetate, ammonium formate, acetic acid, or formic acid (Cajka & Fiehn, 2014). A summary of a selection of LC methods reported in the literature for lipidomic studies of microalgae are reported in Appendix B.

Table 2.4 – Typical examples of weak and strong mobile phases for reverse phase LC for lipid analysis (Cajka & Fiehn, 2014).

Weak		**Strong**	
Solvents	**Ratio (v/v)**	**Solvents**	**Ratio (v/v)**
Water/methanol	50:50	Isopropyl alcohol/ acetonitrile	95:5 – 70:30
Water/acetonitrile	40:60 – 60:40	Isopropyl alcohol/ methanol/water	High % isopropyl alcohol
Water/methanol/acetonitrile	n.d.	Tetrahydrofuran/methanol/ water	75:20:5
Water/isopropyl alcohol	95:5		
Water/methanol/ tetrahydrofuran	50:30:20		

The solvent mixture which the samples for separation and analysis are dissolved in is of importance and must be compatible with the mobile phases used, able to dissolve the lipids from the extract, and prevent degradation of the extracts for analysis (Cajka & Fiehn, 2014). Examples of suitable solvent mixtures are reported by Cajka and Fiehn (2014) consisting of mixtures of methanol, chloroform, water, acetonitrile, butanol, isopropyl alcohol, and/or hexane, in various ratios.

Gas chromatography (GC) is used to separate volatile analytes and so is often employed for fatty acid analyses or for volatile low molecular weight lipid species. In order to analyse fatty acids, they must first be derivatised to form methyl esters. Normally wax columns are used for fatty acid analyses and separated fatty acid methyl esters based on chain length and degree of unsaturation. Gas chromatography is not suitable to analyse glycerolipids directly as they are not volatile enough and so only the fatty acid profile derived from these classes are able to be determined using this method. While it is not as useful as liquid chromatographic techniques for lipidomic studies, it is useful for determination of fatty acid composition of biomass and is widely used for this purpose (Christie, 1989).

Spectroscopic methods

One of the most common methods used in lipidomic studies is mass spectrometry (MS) (Wenk, 2005). Mass spectrometry allows the detection of molecules by their mass to charge ratio (m/z) and is a powerful technique for determination of lipid species. Electrospray ionisation (ESI) is a 'soft' ionisation method and one of the most common ionisation methods used in lipidomics. It typically results in limited fragmentation of lipid species allowing the full lipid molecule to be detected. However, lipid classes normally show distinctive fragmentation patterns of their head groups and constituent fatty acids which can be used to deduce the lipid species present. Mass spectrometry is often used in conjunction with HPLC or other chromatographic methods to reduce the complexity of the mixture being analysed by allowing spectroscopy of individual lipid species that have been separated (da Costa *et al.*, 2016).

Another common spectroscopic technique in lipidomics is nuclear magnetic resonance (NMR) (Wenk, 2005). NMR can be used to deduce the structure of lipid species but typically requires higher concentrations than MS analyses. Additionally, NMR requires reasonably pure lipid samples to avoid spurious signals from multiple lipid species when deducing structures of individual lipids. NMR can also be used to

investigate the structure of membranes and lipid-protein interactions. ^{1}H and ^{13}C NMR can be used for analysis of all lipid species, while ^{31}P NMR can be used for phospholipid species (Sarpal *et al.*, 2016; Wenk, 2005).

2.5 Effect of culture conditions on growth and EPA productivity of microalgae

Many factors influence the growth and cellular composition of microalgae. The key factors that can be controlled in cultures are the light intensity and quality, temperature, pH, nutrients, and culture strategy used (Andersen, 2005; Becker, 1994; Cohen, 1999). The response of microalgae to the conditions they are exposed to is often strain-specific; although there are some general trends seen across different strains to these conditions as discussed further below. Of key interest in this study was to determine the conditions that maximised the EPA productivity of *Trachydiscus* sp. LCR-Awa-9-2. EPA productivities of many other strains of microalgae have been reported for a variety of culture systems and conditions and these are summarised in Table 2.5. The EPA productivity of different species and conditions varied by three orders of magnitude in the studies compared. The effect of individual factors is expanded on further in the following sections.

Table 2.5 – EPA productivities reported in literature for various culture conditions, reactor geometries, and microalgae strains. The highest productivity achieved from previous work with Trachydiscus sp. LCR-Awa-9-2 has been highlighted.
I: light intensity; T: temperature; D: dilution rate; I_{av}: average light intensity; I_{max}: maximum light intensity.

Strain	**EPA Productivity (mg L^{-1} d^{-1})**	**Conditions**	**Reference**
Porphyridium cruentum	0.5	Open pond, winter	Ratledge (1997) as reported in Rezanka *et al.* (2010)
Nannochloropsis sp.	3.6	Glass column, 5 cm ID, batch	Sukenik *et al.* (1991) as reported by Cohen (1999)
Porphyridium cruentum	3.6	Flasks, batch	Akimoto *et al.* (1998) as reported in Rezanka *et al.* (2010)
Isochrysis galbana	4.6	Glass tubes, semi continuous	Otero *et al.* (1997a) as reported in Rezanka *et al.* (2010)
Phaeodactylum tricornutum	5.2	Glass tubes, semi continuous	Otero *et al.* (1997b) as reported in Rezanka *et al.* (2010)
Nannochloropsis oculata	5.5	Batch	Sukenik *et al.* (1989) as reported in Rezanka *et al.* (2010)
Isochrysis galbana	7.2	Fermenters, continuous	Grima *et al.* (1993) as reported in Rezanka *et al.* (2010)
Porphyridium cruentum	8.0	Open pond, ideal weather	Ratledge (1997) as reported in Rezanka *et al.* (2010)
Phaeodactylum tricornutum UTEX 640	13	Net generation rate, linear phase Outdoor tubular photobioreactor $T = 21 \pm 2$ ℃ pH = 7.6 $I_{max} = 3300$ µmol m^{-2} s^{-1} End of batch	Molina Grima *et al.* (1995)
Nannochloropsis oceanica CY2	14.4	Semi batch $I_0 = 150$ µmol m^{-2} s^{-1} $T = 28$ ℃ Blue-Red LEDs	Chen *et al.* (2015)
Isochrysis galbana	15.3	Fermenters, continuous	Molina Grima *et al.* (1994b) as reported in Rezanka *et al.* (2010)

Table 2.5 cont.– EPA productivities reported in literature for various culture conditions, reactor geometries, and microalgae strains. The highest productivity achieved from previous work with Trachydiscus sp. LCR-Awa-9-2 has been highlighted.
I: light intensity; T: temperature; D: dilution rate; I_{av}: average light intensity; I_{max}: maximum light intensity.

Strain	**EPA Productivity ($\mathbf{mg\ L^{-1}\ day^{-1}}$)**	**Conditions**	**Reference**
Nannochloropsis gaditana	15.6	Flat panel photobioreactor, outdoors $I_0 = 12 - 22$ MJ m^{-2} day^{-1} $D = 0.3$ day^{-1} pH = 7.8 $T = 18$ ℃	Camacho-Rodríguez *et al.* (2014)
Trachydiscus sp. LCR-Awa-9-2	15.6	Airlift photobioreactors Batch Blue LED light $I_0 = 130$ µmol m^{-2} s^{-1} $T = 25$ °C Z medium	Tangestani (2019)
Phaeodactylum tricornutum	19.0	Glass tubes, batch	Yongmanitchai and Ward (1991) as reported in Rezanka *et al.* (2010)
Phaeodactylum tricornutum UTEX 640	21	Net generation rate, linear phase Outdoor tubular photobioreactor $T = 21 \pm 2$ ℃ pH = 7.6 $I_{max} = 3300$ µmol m^{-2} s^{-1}	Molina Grima *et al.* (1995)
Isochrysis galbana	23.8	Cylindrical fermenters, continuous	Fernández Sevilla *et al.* (1998) as reported in Rezanka *et al.* (2010)
Phaeodactylum tricornutum	25.1	Glass tank, continuous	Yongmanitchai and Ward (1992) as reported by Cohen (1999)
Monodus subterraneus	25.7	Erlenmeyer, semi-continuous	Cohen (1994) as reported by Cohen (1999)

Table 2.5 cont.– EPA productivities reported in literature for various culture conditions, reactor geometries, and microalgae strains. The highest productivity achieved from previous work with Trachydiscus sp. LCR-Awa-9-2 has been highlighted. I: light intensity; T: temperature; D: dilution rate; I_{av}: average light intensity; I_{max}: maximum light intensity.

Strain	**EPA Productivity ($\mathbf{mg\ L^{-1}\ day^{-1}}$)**	**Conditions**	**Reference**
Nannochloropsis gaditana	30	Theoretical (model) $T = 17$ ℃ for $I_{av} = > 100$ µmol $m^{-2}s^{-1}$ OR $T = 23 - 25$ ℃ for $I_{av} = 60 - 70$ µmol $m^{-2}s^{-1}$	Camacho-Rodríguez *et al.* (2014)
Phaeodactylum tricornutum UTEX 640	30	Outdoor tubular photobioreactor 0.06 m tube diameter $T = 20 \pm 2$ ℃ pH = 7.7 $D = 0.04\ h^{-1}$ Spring/autumn	Acién Fernández *et al.* (2000)
Trachydiscus minutus	30	$T = 28$ ℃ Bubble column $I_0 = 470$ µmol $m^{-2}\ s^{-1}$	Cepák *et al.* (2014)
Nannochloropsis sp.	32	Outdoor tubular photobioreactor $T = 25$ ℃	Chini Zittelli *et al.* (1999)
Phaeodactylum tricornutum	33.5	Glass vessels, mixotrophic, batch	Cerón García *et al.* (2000) as reported in Rezanka *et al.* (2010)
Phaeodactylum tricornutum	47.8	Tubular reactor, continuous	Molina Grima *et al.* (1995) as reported by Cohen (1999)
Phaeodactylum tricornutum UTEX 640	50	Outdoor tubular photobioreactor 0.03 m tube diameter $T = 20 \pm 2$ ℃ pH = 7.7 $D = 0.04\ h^{-1}$ Spring/autumn	Acién Fernández *et al.* (2000)

Table 2.5 cont.– EPA productivities reported in literature for various culture conditions, reactor geometries, and microalgae strains. The highest productivity achieved from previous work with Trachydiscus sp. LCR-Awa-9-2 has been highlighted.
I: light intensity; T: temperature; D: dilution rate; I_{av}: average light intensity; I_{max}: maximum light intensity.

Strain	**EPA Productivity ($mg\ L^{-1}\ day^{-1}$)**	**Conditions**	**Reference**
Monodus subterraneus	56	Indoor, helical photobioreactor $I_0 = 82\ \mu mol\ m^{-2}s^{-1}$ $T = 26 \pm 2\ ℃$ $pH = 7.2$	Lu *et al.* (2001)
Monodus subterraneus	58.9	Flat plate reactor, semi-continuous Outdoors $T = 32\ ℃$ $pH = 7.5$	Hu *et al.* (1997)
Trachydiscus minutus	88	$I_0 = 450\ \mu mol\ m^{-2}s^{-1}$ $T = 28\ ℃$	Rezanka *et al.* (2010)
Phaeodactylum tricornutum UTEX 640	118	Batch culture, 24 h light per day $pH = 7.4$ $T = 20℃$	Meiser *et al.* (2004)
Nitzschia laevis	175	Fermenters, heterotrophic, perfusion-cell bleeding	Wen and Chen (2001) as reported in Rezanka *et al.* (2010)

2.5.1 Light intensity and quality

Both the intensity and quality (wavelength or distribution of wavelengths) of light used for microalgae cultures can impact the growth and cellular composition of microalgae. Light is one of the most important factors to optimise for photoautotrophic cultures of microalgae and is often the limiting factor when attempting to achieve high cell densities (Borowitzka & Vonshak, 2017).

The required light intensity for growth is strain specific, although most strains of microalgae show a similar trend in growth and photosynthesis response to light intensity. Light is one of the key limiting factors for microalgal growth and as the cell density increases, so does the attenuation of light in the culture and the culture can become light limited (Richmond, 2008; van Oorschot, 1955). The light intensity for microalgae cultures must be high enough that the cells are saturated with light while not causing photoinhibition from light that is too intense (Molina Grima *et al.*, 2009). Typically, a photosynthesis-irradiance curve for microalgae looks like that in Figure 2.20.

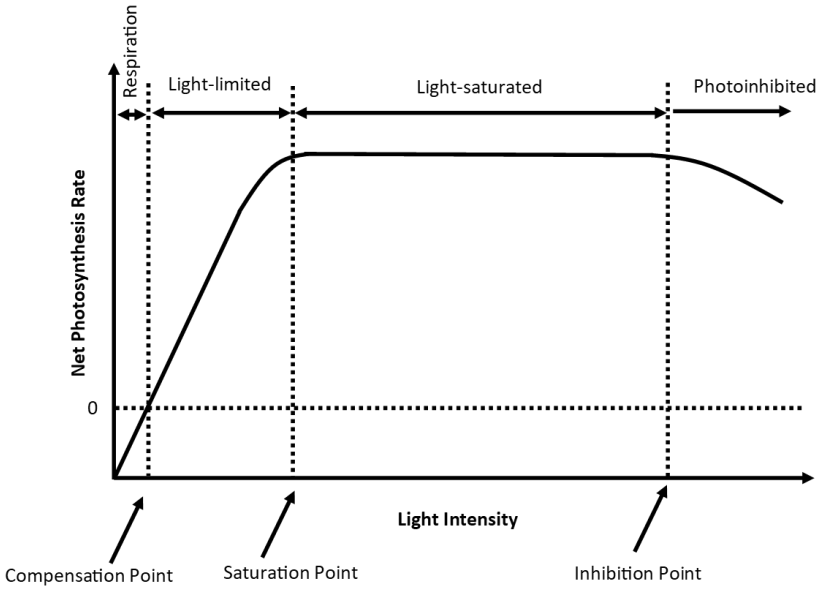

Figure 2.20 – Typical form of a photosynthesis irradiance curve for microalgae. Based on Acién Fernández et al. (2013).

With no light supplied the culture undergoes respiration with a net consumption of oxygen which continues until enough light is supplied to have a net zero oxygen production rate (the compensation point). At low irradiances the culture is light-limited, and the rate of photosynthesis increases proportionally with increasing light. This continues until the culture becomes saturated, at which point an increase in light intensity

does not produce an increase in photosynthesis rate. At high irradiances the rate of photosynthesis can decrease as photoinhibition takes place (Acién Fernández *et al.*, 2013). Photoinhibition occurs when the cells become damaged by the intense light and must spend time and energy to repair their photosynthetic apparatuses (Han, 2002; Raven, 2011).

At low light intensities, microalgae cells tend to produce more chlorophyll and other pigments in order to harvest all the available light. As the light intensity is increased, cells can produce less chlorophyll and more protective pigments to limit the quantity of photons they are absorbing so they do not become over-saturated (Deblois *et al.*, 2013; García-Camacho *et al.*, 2012). Typical reported incident irradiance values for the compensation point are 10–20 μmol m^{-2} s^{-1}, saturation occurs in the region of 100–500 μmol m^{-2} s^{-1}, and photoinhibition occurs at irradiance levels greater than 1000 μmol m^{-2} s^{-1} (Acién Fernández *et al.*, 2013; Acién Fernández *et al.*, 2010). Light tolerance is strain-specific and light adaption or acclimation can occur in cultures which effects the values for these points (Deblois *et al.*, 2013; MacIntyre *et al.*, 2002; Raven & Geider, 2003).

As mentioned above, light should ideally be supplied at intensities between the saturation and inhibition levels. However, as light is nearly completely attenuated at shallow depths of approximately 1–2 cm as cell densities increase (Chisti, 2016), cultures are often non-homogeneously illuminated. This results in cells at the surface potentially being photoinhibited while cells deeper in the culture are simultaneously photolimited (Carvalho *et al.*, 2011; Grima *et al.*, 1996).

The spectral composition of the light supplied to microalgae can also impact the maximum growth rate and cell density that can be achieved. For example, *Chlorella vulgaris* obtained a cell density >20% higher when grown under violet light than with red light (Mohsenpour *et al.*, 2012).

There have been many studies investigating the effect of irradiance on EPA content and productivity under various conditions. The two main considerations of most studies were light intensity and quality. Camacho-Rodríguez *et al.* (2014) found that decreasing the width of flat panel photobioreactors from 10 cm to 5 cm to reduce the light path increased EPA productivity in *Nannochloropsis gaditana* two-fold. It was also found that

EPA productivity in both flat panel and tubular photobioreactors was at its maximum in winter and decreased as temperature and irradiance increased.

It is also suggested that low irradiance levels, but high growth rates increase the dry weight percentage of lipids, fatty acids and pigments for *Phaeodactylum tricornutum* (Acién Fernández *et al.*, 2000). This has been summarised in Figure 2.21.

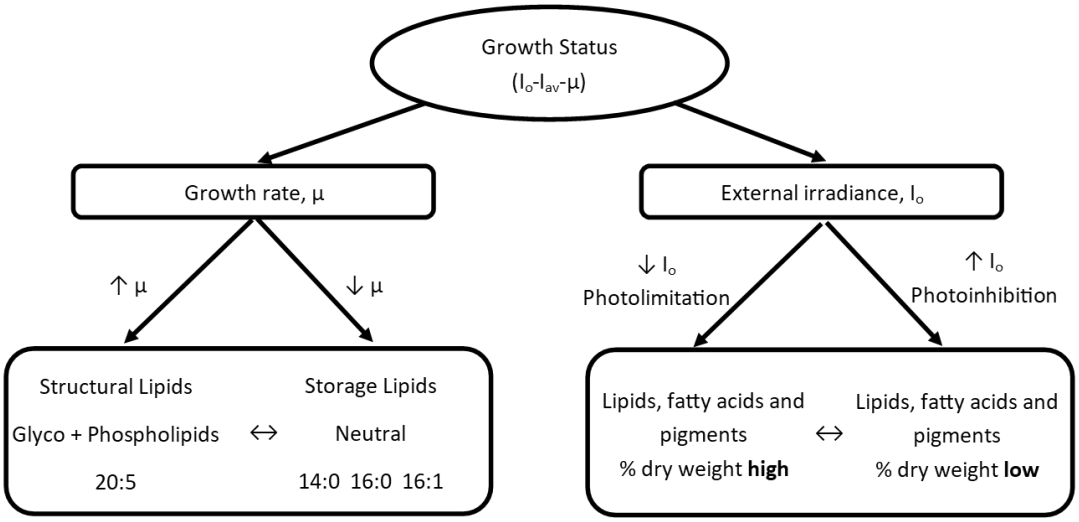

Figure 2.21 – Influence of irradiance and growth rate on EPA content of Phaeodactylum tricornutum. Based on Acién Fernández et al. (2000).

Chen *et al.* (2015) reported, for *Nannochloropsis oceanica* CY2, that EPA productivity was maximised by combining blue and red LEDs. Again for *Nannochloropsis oceanica* CY2, illumination with red LED light resulted in an EPA content of dry mass of 5.5%, with a content of 5.0% being able to be maintained under blue LED illumination and semi-batch operation (Chen *et al.*, 2013). For *Nannochloropsis gaditana*, the EPA fraction was found to be best under white light when compared to red or blue light (Kim *et al.*, 2014). *Tetraselmis suecica* showed an increase in EPA content when grown under red light compared to white blue and green, but produced smaller cells compared to white light (Abiusi *et al.*, 2014).

For *Nannochloropsis* sp. grown in a tubular photobioreactor, EPA productivity was found to reflect the culture's biomass productivity. The overall fatty acid composition of the biomass was found to vary greatly with outdoor conditions, light-dark cycles, and salinity, but EPA content remained stable at approximately 4% of dry mass (Chini Zittelli *et al.*, 1999). For *Trachydiscus minutus* an irradiance level of 100 μmol m^{-2} s^{-1} was best for EPA content of the biomass, but higher irradiance (470 to 1070 μmol m^{-2} s^{-1})

was best for EPA productivity (Cepák *et al.*, 2014). Light limitation has also been reported to increase EPA content for *Nannochloropsis* (Olofsson *et al.*, 2012).

Biomass and EPA productivity of *Phaeodactylum tricornutum* was enhanced at cell densities which support the fastest growth rate irrespective of irradiance. The greatest EPA productivity was achieved at the highest irradiance (Chrismadha & Borowitzka, 1994). Acién Fernández *et al.* (2000) found a decrease in the fatty acid content of *Phaeodactylum tricornutum* grown in tubular photobioreactors under high irradiances that caused photoinhibition at the reactor surface. As average irradiance increased so did the proportion of EPA as the content of saturated and monounsaturated fatty acids decreased. EPA content and biomass productivity were found to be at odds and so an optimum had to be found by achieving photolimitation while maintaining high growth rates.

Cohen (1994) found that cultivating *Monodus subterraneus* under low light or high biomass concentration increased the fatty acid proportion of EPA. The greatest EPA productivity was reached at a biomass concentration that also gave the best biomass productivity. Similarly, Hu *et al.* (1997) reported that the highest EPA content and productivity of *Monodus subterraneus* occurred with maintaining cell densities that also resulted in maximum biomass productivity. Lu *et al.* (2001) has also reported similar results for *Monodus subterraneus*, and that EPA and fatty acid content can be manipulated by manipulating the cell density and light intensity.

Short exposure of *Nannochloropsis* sp. BR2 to short-wave ultraviolet light (UV-C) by Sharma and Schenk (2015) resulted in a two-fold increase of EPA content. Exposure to UV-C also produced a significant increase in total lipids.

Results from the reported experiments suggest that light quality and intensity has an impact on the EPA content and productivity of microalgae. While there is no clear consensus across different strains, it is likely that light limited cultures that are growing strongly could produce higher EPA productivities. Modulation of the spectral composition of the light supplied may also have an impact on the EPA productivity, either by short exposure to UV-C or growth under a particular light colour. Overall, EPA productivities are likely to be greatest under conditions that promote the greatest biomass productivity.

2.5.2 Temperature

The optimal temperature for growth of microalgae is strain specific and related to the environment the microalgae evolved in. There is typically an optimal temperature for growth, above and below which the rate of growth decreases. Some microalgae grow optimally at 37–40 °C such as *Micractinium* sp. (Abu-Ghosh *et al.*, 2018), whereas the optimal temperature for other strains such as *Chlorella vulgaris* is 25 °C (Serra-Maia *et al.*, 2016). Increasing temperature tends to increase the rate of growth in most strains of microalgae but excessively high temperatures can decrease the rate of growth or kill the cells (Serra-Maia *et al.*, 2016). Temperature can also influence the cellular composition of microalgae, in particular the fatty acid composition.

One key cellular property that can be influenced by temperature is membrane fluidity (Gurr & Harwood, 1991). The fluidity of a membrane is a measure of its 'viscosity' and the ease at which substances such as membrane proteins are able to move within the membrane (Siegenthaler & Murata, 1998). Generally, membranes which contain unsaturated or shorter chain fatty acids are more fluid than those which contain longer-chain or saturated fatty acids (Gurr & Harwood, 1991). Cells are normally required to maintain a constant membrane fluidity (homeoviscous) for operation of membrane processes such as transport processes and so cells may alter their membrane composition in response to temperature changes (Siegenthaler & Murata, 1998). As temperature decreases so does the fluidity of membranes and vice versa so cells may respond by altering the composition of fatty acids in the membranes to counter this effect. This response can be achieved from an alteration in the expression of enzymes related to synthesis of different fatty acids in response to temperature change, such as increasing the synthesis of unsaturated fatty acids at low temperatures. Alternatively, organisms may alter their membrane fluidity by the adjustment of protein:lipid ratios in membranes (Gurr & Harwood, 1991; Siegenthaler & Murata, 1998). Membrane fluidity is important in photosynthetic processes for diffusion of lipophilic substances across and within cellular membranes, for example plastoquinone (PQ, Figure 2.7) in the thylakoid membranes (Ke, 2001; Wada & Murata, 2009).

The thylakoid membranes comprise primarily of glycolipids which typically contain a high proportion of EPA in cells (Ke, 2001). Therefore, there is potential that a decrease in temperature could increase the unsaturated fatty acid content, and thus EPA content, of the glycolipids to maintain membrane fluidity. As shuttling of lipophilic

compounds is central to the electron transport chain in photosynthesis this could justify the high proportion of unsaturated fatty acids in these membranes.

Cepák *et al.* (2014) found that EPA content of *Trachydiscus minutus* was highest at 20 °C but productivity was best at 28 °C, which was also best for growth. Camacho-Rodríguez *et al.* (2014) found that EPA productivity was best in winter for *Nannochloropsis gaditana*, due to lower temperatures and irradiance. Increasing temperature lowered the EPA content of *Phaeodactylum tricornutum* (Qiao *et al.*, 2016). Rousch *et al.* (2003) reported that increased temperature caused a rapid change in fatty acid content of *Phaeodactylum tricornutum* and *Chaetoceros muelleri*. The effects on each strain varied with a decrease in EPA content of *Phaeodactylum tricornutum* with increased temperature but little change was observed in the EPA content of *Chaetoceros muelleri* with increased temperature. They also reported that temperature changes exhibited a faster response than nutrient effects and that the extent of temperature change, rather than duration of exposure, was the important effect.

The results of studies considering the effect of temperature on microalgae showed that temperature can affect the EPA content and productivity. However, temperature appears to have a greater impact on the cellular growth which may in turn have the major impact on overall EPA productivity due to biomass productivity. Also, although membrane fluidity is regarded as important for cellular functions there is little quantitative data regarding membrane fluidity maintenance and the importance of EPA relative to other unsaturated fatty acids to adapt to temperature changes.

2.5.3 pH

pH influences the availability of different forms of inorganic carbon present in the medium. In an isolated system at low pH, free carbon dioxide and carbonic acid dominate the molar fraction. As the pH approaches the neutral range the major component becomes bicarbonate (hydrogen carbonate). At high pH carbonate becomes the dominant form. This is covered in further detail in § 2.5.4 below.

pH is a logarithmic measure of H^+ activity and so changes in pH will affect the proton concentration gradients across the cells (Burrows *et al.*, 2009; Reece *et al.*, 2010). Proton gradients are a common feature of many membrane transport processes as well as playing an important role in the reaction steps of photosynthesis during photophosphorylation (Reece *et al.*, 2010). Cells are able to control their internal pH by

control of H^+ flux across membranes. pH also has a strong effect on enzyme kinetics by affecting the conformation of enzymes (Atkinson & Mavituna, 1991; Cornish-Bowden, 2014; Reece *et al.*, 2010). Most microorganisms (except for extremophiles) tend to grow optimally at relatively neutral pH values (Reece *et al.*, 2010). As an example, for *Isochrysis galbana*, there is an optimum pH of approximately 7.5 for photosynthesis rate with sharp decreases outside the optimum pH to approximately half the rate at pH 5 and 9 (Ippoliti *et al.*, 2016).

2.5.4 Carbon dioxide

As discussed earlier, CO_2 is essential for photosynthesis as it is the source of carbon for the process. For microalgae the heuristic for the CO_2 requirement is that approximately 1.83 g of CO_2 is required per 1 g of dry biomass produced (Chisti, 2008). CO_2 is supplied to microalgae cultures by dissolution of the gas into the culture medium from the gas phase. CO_2 was present in atmospheric air at approximately 400 ppm at the time of this study (National Institute of Water and Atmospheric Research (NIWA), 2020a).

Carbon dioxide concentration in the supply air must be high enough that the culture is not carbon limited. However, the concentration must not be so high that it poisons the cells or acidifies the culture beyond the tolerance of the microalgae (Salih, 2011). The tolerance of microalgae to CO_2 concentration is strain specific. Some strains can tolerate up to 100% CO_2 (Salih, 2011) while others show strong inhibition at concentrations of 10% or lower (Hsueh *et al.*, 2009).

Carbon dioxide gas in contact with water (or culture media) dissolves to produce aqueous CO_2 and this can react with water to produce carbonic acid. From here, the carbonic acid can react to form bicarbonate and then onwards to form carbonate ions (Burrows *et al.*, 2009). This equilibrium scheme is illustrated in Figure 2.22. The equilibrium between the inorganic carbon species in the media produces a buffer system which helps to resist pH changes to the culture. Conversely, adjustments to the pH of a culture will affect the molar ratios of the inorganic carbon species present as previously described.

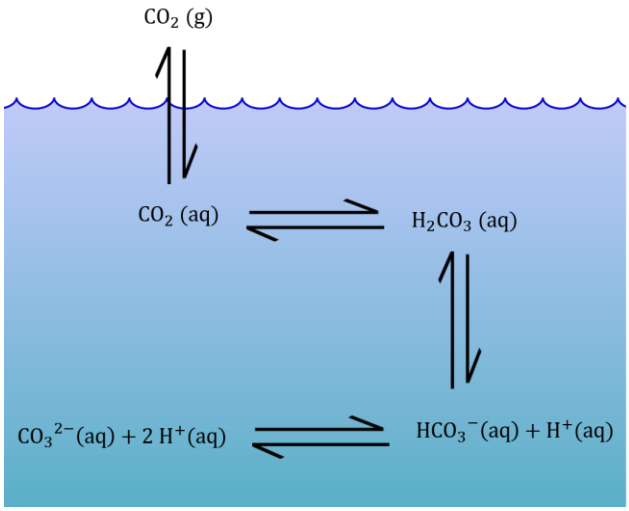

Figure 2.22 – Equilibrium between inorganic carbon species in water with interaction with CO_2 gas.

The equilibrium between CO_2, HCO_3^- and CO_3^{2-} can be modelled by Bjerrum plots which are described by Equations (2.3) to (2.5), where $C^*_{CO_2}$ is the equilibrium concentration of dissolved CO_2, $C^*_{H^+}$ is the equilibrium concentration of H^+ ions, C_{DIC} is the total concentration of dissolved inorganic carbon, $C^*_{HCO_3^-}$ is the bicarbonate ion equilibrium concentration and $C^*_{CO_3^{2-}}$ is the carbonate ion equilibrium concentration. K_1 and K_2 are the equilibrium constants for the reaction of CO_2 to bicarbonate and bicarbonate to carbonate, respectively (Mook, 2000). For a sealed system of a given total dissolved inorganic carbon concentration the mole fractions of each of the carbon species vary with pH in water as seen in Figure 2.23.

$$C^*_{CO_2} = \frac{{C^*_{H^+}}^2}{{C^*_{H^+}}^2 + K_1 C^*_{H^+} + K_1 K_2} C_{DIC} \qquad (2.3)$$

$$C^*_{HCO_3^-} = \frac{K_1 C^*_{H^+}}{{C^*_{H^+}}^2 + K_1 C^*_{H^+} + K_1 K_2} C_{DIC} \qquad (2.4)$$

$$C^*_{CO_3^{2-}} = \frac{K_1 K_2}{{C^*_{H^+}}^2 + K_1 C^*_{H^+} + K_1 K_2} C_{DIC} \qquad (2.5)$$

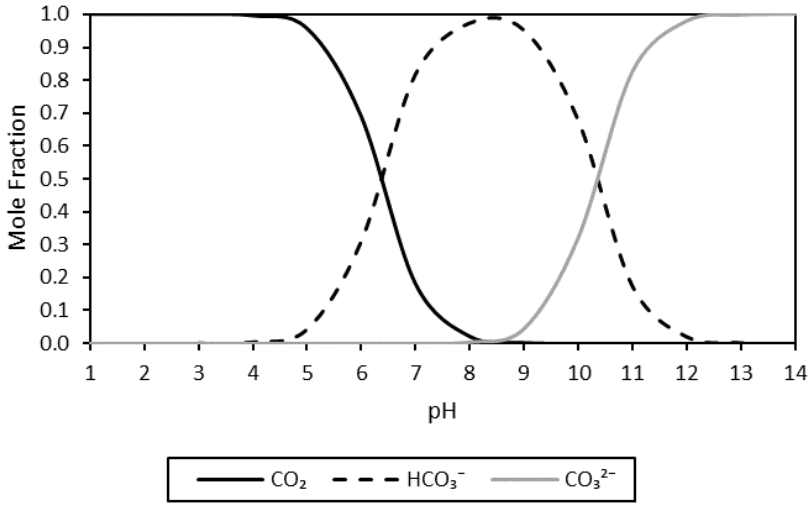

Figure 2.23 – Bjerrum plot of CO_2, HCO_3^- and CO_3^{2-} molar fractions with respect to total CO_2 species at different pH values for an isolated water system. $K_1 = 4.47 \times 10^{-7}\ mol\ L^{-1}$; $K_2 = 4.69 \times 10^{-11}\ mol\ L^{-1}$.

If CO_2 is continually supplied to the system, as in the case of microalgal culturing, the concentration of dissolved CO_2 as H_2CO_3 depends on the concentration of CO_2 in the gas phase. As the pH is increased the concentration of HCO_3^- and CO_3^{2-} increases; however, the concentration of H_2CO_3 remains relatively constant. Concentrations of these inorganic carbon species have been modelled by Noeparvar (2018) based on dairy liquid systems containing various ionic species such as phosphate and calcium ions in equilibrium with CO_2 in the atmosphere. A simplified model based on this work considering the effect of phosphate ions in solutions such as culture media was used to model the concentration of inorganic carbon species at different pH values with continually supplied CO_2 in the gas phase as seen in Figure 2.24 (K. Morison, 24th August 2019, personal communication).

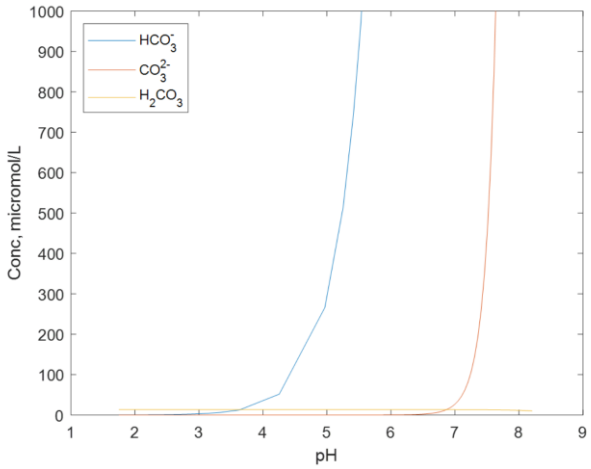

Figure 2.24 – Concentrations of H_2CO_3, HCO_3^- and CO_3^{2-} at different pH values for a system supplied with 30% CO_2 containing 0.003 mol L^{-1} Na_2HPO_4 .

Dissolved CO_2 is able to passively diffuse across cell membranes and does not require active transport. However, HCO_3^- and CO_3^{2-} require active membrane transport to be absorbed by cells. All microalgae strains can utilise dissolved CO_2 but not all are able to utilise HCO_3^- or CO_3^{2-} (Birmingham *et al.*, 1982; Saifuddin *et al.*, 2015). Within the cell, CO_2 can be concentrated by the pyrenoid around the chloroplast for use by RuBisCO. This allows the CO_2 concentration in the vicinity of where it is used to be higher than the bulk CO_2 concentration in the rest of the cell or media (Wei *et al.*, 2019).

Different CO_2 concentrations can affect the lipid composition of microalgae. For *Chlorella vulgaris*, the proportion of unsaturated fatty acids was higher when cultures were grown with air compared to 2% CO_2 (Tsuzuki *et al.*, 1990). The lipid content of *Scenedesmus bajacalifornicus* increased with increasing CO_2 concentration, reaching a maximum of 25.81 g/100 g dry biomass at 25% CO_2 (Patil & Kaliwal, 2017). Lipid productivity for *Nannochloropsis* sp. was highest at 15% CO_2 and the productivity decreased with CO_2 concentrations above and below this point (Saifuddin *et al.*, 2015). Hoshida *et al.* (2005) found that supplying cultures of *Nannochloropsis* sp. with CO_2 in concentrations above that already present in the atmosphere increased accumulation of EPA. The manner that CO_2 is supplied can also have an impact on EPA content, with intermittent CO_2 injection without pH control producing the best results for *Nannochloropsis oculata* (Shene *et al.*, 2016). Previous studies with *Trachydiscus* sp. LCR-Awa-9-2 showed that growth was improved with 3% CO_2 compared to air (Tangestani, 2019). Further investigation into the effect of CO_2 concentration had not yet been conducted with this microalga.

2.5.5 Culture media and nutrients

Other than CO_2, the key macro nutrients required by most microalgae are nitrogen and phosphorus. These two nutrients are key components of proteins and lipids among other cellular components. Other important nutrients such as sulphur and various metals are also required for growth. Metals such as iron, magnesium, potassium, and sodium are typically key nutrients required for microalgal growth, with magnesium in particular being important as it is a component of chlorophyll. Beyond these main nutrients a variety of trace nutrients can also be required such as vitamins or trace elements such as molybdenum or cobalt. Nutrient requirements are highly strain specific and some nutrients which are vital for growth of one strain of microalgae can be toxic to others. Due to this, a variety of different media recipes have been optimised for a range of microalgae (Andersen, 2005; Richmond, 2008).

As discussed earlier, previous work by Alfiarty (2018) developed an improved culture medium for *Trachydiscus* sp. LCR-Awa-9-2 as well as investigated the effects of nutrients on the growth and fatty acid composition of the microalga. Key results from this study showed that nitrate was the preferable form of nitrogen compared to urea and ammonia, and at the concentration supplied in BBMA medium it was unlikely to be a limiting nutrient. Trace elements such as cobalt and boron were not essential for growth and were likely slightly toxic to the microalga. Different iron sources did not appear to affect the growth of cultures significantly, although chelated sources were preferred. Vitamins such as biotin, vitamin B12, and thiamine were not shown to improve growth compared to vitamin-free media. Overall, nitrate was shown to be the limiting nutrient in the original media and so an increase in the amount of this nutrient showed the greatest impact on improved growth.

Nitrogen starvation is a common technique used to increase the total lipid content of many strains of microalgae (Bekirogullari *et al.*, 2017; Olofsson *et al.*, 2014; Pal *et al.*, 2011; Řezanka *et al.*, 2011; Rodolfi *et al.*, 2009). However, nitrogen starvation induces energy storage in the cells, most commonly in the form of saturated triacylglycerols (Kates, 1986; Ratledge, 1997). As EPA is typically mainly located in the polar lipids, an increase in triacylglycerols can result in a reduction in EPA content as a function of the total fatty acid content. In *Trachydiscus* sp. LCR-Awa-9-2 nitrogen and phosphorus starvation increased the fatty acid content of the cells but increased the oleic acid fraction more than the EPA fraction (Alfiarty, 2018).

Yongmanitchai and Ward (1991) found that increasing nitrate and urea concentrations increased the EPA content of *Phaeodactylum tricornutum*. EPA yield was also improved by the addition of vitamin B12. Nitrogen replete conditions produced the best EPA productivity for *Nannochloropsis oceanica* IMET1 (Meng *et al.*, 2015). A similar result was also found for *Phaeodactylum tricornutum* UTEX 640 with the best EPA productivity occurring in nitrogen replete conditions, while nitrogen starvation increased overall fatty acid productivity (Rodolfi *et al.*, 2017). San Pedro *et al.* (2015) reported that a decrease in nitrate concentration resulted in a lower EPA content of fatty acids in *Nannochloropsis gaditana*.

Rezanka *et al.* (2010) found a decrease in EPA productivity under nitrogen and sulphur starvation for *Trachydiscus minutus*. Similar results were reported for other strains (*Monodus subterraneus* and *Nannochloropsis* sp.) with low nitrogen resulting in decreased EPA content but increased total fatty acid content (Cohen, 1994; Rezanka *et al.*, 2010). Chen *et al.* (2013) also found that optimal supply of nitrogen doubled the EPA content of *Nannochloropsis oceanica* CY2.

The nitrogen source also has an impact of EPA production. Cepák *et al.* (2014) reported that for *Trachydiscus minutus* urea was as suitable as nitrates for the nitrogen source with regards to EPA production, but ammonium carbonate was not. Sodium nitrate was the optimal source for *Nannochloropsis oceanica* CY2 (Chen *et al.*, 2013).

Dunstan *et al.* (1993) observed that in nitrogen limited cultures of *Nannochloropsis oculata* the decrease in EPA content could be due to a reduction in the production of protein-rich chloroplasts due to reduced amino acid synthesis. They reasoned that the reduction in chloroplast production reduced the need for the associated thylakoid membrane lipids where EPA is mainly located.

The results of the surveyed studies showed that nutrient effects have a marked effect on the EPA content of cells. For most strains of microalgae nitrogen limitation results in an accumulation of triacylglycerols, resulting in a lower EPA content. The best EPA productivities tend to be achieved under nutrient replete conditions for most strains of microalgae.

Heterotrophy and mixotrophy

Heterotrophy involves the growth of microalgae on organic carbon sources such as sugars as their energy and carbon source. Similarly, mixotrophy also utilises organic

carbon sources while also supplying light and carbon dioxide to cultures (Richmond, 2008). Heterotrophic and mixotrophic growth of microalgae allows the elimination of growth limitation due to light attenuation in dense cultures. However, this approach can come at the cost of increased consequences of contamination from bacteria or fungi. Heterotrophic growth allows simpler cultivation systems to be used as the supply of light is not a critical factor and so this can simplify the design and geometry (and thus cost) of bioreactors. As not all microalgae can grow heterotrophically this approach is not applicable to all species (Perez-Garcia *et al.*, 2011).

Different heterotrophic nutrient sources can have an effect on the EPA content and productivity as well as the growth of microalgae (Chen & Chen, 2006). Common organic carbon sources are sugars such as glucose or compounds such as acetate or citrate; however, not all carbon sources can be utilised by all strains of microalgae (Perez-Garcia *et al.*, 2011). Cell densities achieved with heterotrophic cultures are typically far higher than photoautotrophic, for example *Nitzschia laevis* reached cell densities of 40 g L^{-1} during heterotrophic growth (Chen & Chen, 2006). Heterotrophic growth typically favours the production of saturated fatty acids; however, diatoms have shown increased production of polyunsaturated fatty acids such as EPA under heterotrophic conditions compared to photoautotrophic conditions (Perez-Garcia *et al.*, 2011).

Tangestani (2019) found that *Trachydiscus* sp. LCR-Awa-9-2 was capable of heterotrophic and mixotrophic growth using sugars, such as lactose and galactose. The potential for heterotrophic or mixotrophic production of EPA with this microalga could eliminate the requirement for sufficient light, which is generally the limiting factor for maximising productivity. In Table 2.5 the maximum productivity of the reviewed values of 175 mg L^{-1} d^{-1} was achieved with heterotrophic growth of *Nitzschia laevis* (Rezanka *et al.*, 2010) and so this could be a promising approach to maximise EPA productivity.

2.5.6 Culture strategy

Batch, fed-batch, and continuous culture strategies have all been investigated in the production of EPA from microalgae. Continuous culture strategies for EPA production have been used by Zou *et al.* (2000), Reis *et al.* (1996), and Meiser *et al.* (2004), among others, to varying success. Dilution rate has a key impact on the EPA productivity of continuous cultures, particularly in response to light availability (Fernandes *et al.*, 2015). Continuous cultures also allow control over nutrient stresses which can impact EPA content and productivity.

Batch cultures have also been used to produce EPA (Hoshida *et al.*, 2005; Meiser *et al.*, 2004; Yongmanitchai & Ward, 1992). In the case of the study by Meiser *et al.* (2004), the EPA productivity was higher for batch cultures than continuous cultures for *Phaeodactylum tricornutum*, albeit under different light regimes. However, Molina Grima *et al.* (1995) suggested that EPA productivity for *Phaeodactylum tricornutum* could be improved with continuous or semi-continuous cultures.

Two-stage culture strategies are an additional technique commonly use to trigger production of metabolites in microorganisms. The benefit of two-stage strategies allows an initial stage to promote growth of the culture and a secondary stage with optimal conditions for metabolite production (Fábregas *et al.*, 2001). Mitra *et al.* (2015) applied a two-stage strategy with *Nannochloropsis* sp. by growing the culture to exponential phase and then subjecting it to low light and temperature. This two-stage approach increased EPA content by 3.4-fold. In contrast, a two-stage cultivation of *Nannochloropsis oculata* to induce lipid production by alteration of salinity and irradiance resulted in a decrease in EPA content (Su *et al.*, 2011).

EPA content can also vary depending on the harvest time of cultures. Qiao *et al.* (2016) found that the DHA to EPA ratio of *Phaeodactylum tricornutum* fell with increasing growth time, possibly in response to unfavourable culture conditions. In *Nannochloropsis oculata*, the EPA fraction decreased with culture time (Su *et al.*, 2011). Dunstan *et al.* (1993) reported that during the stationary phase of growth the fraction of EPA decreased for *Nannochloropsis oculata* and *Pavlova lutheri* compared to during the exponential phase.

A study of three microalgal species (*Phaeodactylum tricornutum*, *Isochrysis galbana* and *Porphyridium cruentum*) found that the optimal culture strategy for PUFA production depended on the strain (Otero *et al.*, 1997a). This aligns with the research reviewed that there is no clear consensus on the best culture approach to use for all strains of microalgae.

Overall, culture strategies that promote the greatest growth rate of microalgae tend to result in the greatest EPA productivities. To this end, continuous culture strategies that maintain the culture in the exponential growth phase are normally desired. However, light limitation has also been found to increase EPA content and so the cell density should be maintained high enough to limit the light availability of the culture. Any optimal culture strategy is likely to be strain specific.

2.5.7 Shear stress

Mechanical stresses on cells are important to consider in biological reactors as excessive shear on cells can cause cell lysis and affect the performance of the culture (van't Riet & Tramper, 1991). As microalgae have cell walls they are more robust than cells which only have a cell membrane, such as animal cells. Due to this, minimising shear is not as critical in microalgae systems as in plant or animal cell cultures (Wu & Merchuk, 2002).

In bioreactors, shear forces can be imparted by mechanical equipment such as stirrers and pumps, microeddies formed from turbulent flow, bubble formation and collapse, and direct contact of the cells with the walls or other components of the bioreactor (Molina Grima *et al.*, 2001; van't Riet & Tramper, 1991).

Shear can be quantified using Equation (2.6), where τ is the shear stress, η_l is the dynamic viscosity of the liquid, $\dot{\gamma}$ is the shear rate, and $\frac{dv}{dx}$ is the velocity gradient (van't Riet & Tramper, 1991). Shear stresses can be quantified easily in laminar flow from the velocity gradients. However, in turbulent flow shear stress is difficult to determine (van't Riet & Tramper, 1991).

$$\tau = -\eta_l \frac{dv}{dx} = \eta_l \dot{\gamma} \qquad (2.6)$$

Quantification of the shear tolerance of microalgal cells has not been widely reported in literature (Michels *et al.*, 2010). Couette devices are commonly used for shear stress experiments on microorganisms (Dinsdale & Moore, 1962; Mitsuhashi *et al.*, 1995; O'Connor *et al.*, 2002). However, these devices are limited in the shear rates they can achieve without the addition of viscosity-increasing substances such as locust bean gum (Michels *et al.*, 2010). It is possible that these substances can influence cell viability under shear stress. One example is the use of carboxymethyl cellulose to improve the shear tolerance of *Phaeodactylum tricornutum* in sparged cultures, as reported by Camacho *et al.* (2001). A selection of some shear stress tolerances of microalgae that have been reported are summarised in Table 2.6.

Table 2.6 – Shear stress tolerances of different microalgae.

Strain	Shear stress tolerance (N m^{-2})	Reference
Protoceratium reticulatum [a]	$< 1.6 \times 10^{-2}$	Rodríguez *et al.* (2009)
Chaetoceros muelleri	$1 - 1.3$	Michels *et al.* (2010)
Isochrysis galbana	5.4	Michels *et al.* (2016)
Tetraselmis suecica	> 88	Michels *et al.* (2016)

[a] shear sensitive dinoflagellate

Other studies have grown microalgae in high shear environments such as photobioreactors with pumps (Scarsella *et al.*, 2012; Vandanjon *et al.*, 1999) and stirred tanks (Leupold *et al.*, 2013) to determine the cells' tolerance. However, there is little separation of variables, such as turbulent microeddy formation versus shear due to pump impellers. Due to the difficulty in quantifying shear in these turbulent systems the results are not deemed reliable. Shear stresses can also be imparted by contact between the cells and the walls of reactors (Molina Grima *et al.*, 2000) as well as aeration of the culture (Acién Fernández *et al.*, 2013). Microeddies are also a source of shear force in bioreactors and are more damaging as turbulence increases and microeddy lengths approach the size of cells (Batchelor, 1947; Brindley Alías *et al.*, 2004).

2.6 Cultivation systems for microalgae

Microalgae are cultivated on a vast range of scales from agar slants to cubic-metre-scale reactors. For photoautotrophic growth of microalgae all cultivation systems share some common core requirements (Andersen, 2005; Burlew, 1953) which are:

- Sufficient light supply
- Carbon dioxide supply
- Nutrient supply
- Oxygen and metabolite removal

2.6.1 Laboratory scale culture systems

Laboratory scale systems are mainly used for research and isolation of microalgal strains as well as culture maintenance. Laboratory scale cultivation of microalgae can be achieved in both solid and liquid media with common methods being agar plates or slants, shake flasks and bench scale photobioreactors (Burlew, 1953). Figure 2.25 shows an example of microalgae grown in shake flasks in an incubator.

Figure 2.25 – Shake flask cultures of Trachydiscus sp. LCR-Awa-9-2 in a modified shaking incubator.

These systems are limited mainly by the amount of biomass that can be produced in a given system. Solid media typically allows up production of up to hundreds of milligrams of dry biomass, while liquid media systems can produce a maximum concentration of approximately 5 g L^{-1} dry biomass and are typically limited in volume to the order of 10 L (Andersen, 2005; Burlew, 1953).

In small scale systems control of environmental conditions is typically simple and achievable with minimal resource and energy requirements. These systems also allow simultaneous testing of many conditions on growth and metabolite production of microalgae strains. Laboratory scale systems also allow easier mitigation of potential contamination sources as, for example, they can be easily autoclaved due to their small size (Andersen, 2005; Burlew, 1953).

2.6.2 Large-scale cultivation of microalgae

Large-scale cultivation of microalgae can be conducted in two main types of systems; open and closed (Becker, 1994; Burlew, 1953). Open systems, as the name implies, are open to the environment with no, or a minimal, barrier between the culture and the surrounding environment. In contrast, closed systems are separated from the external environment and there is no direct contact between the culture and the environment. Large-scale cultivation is typically conducted on the scale of hundreds of litres to cubic meters and can produce biomass on the order of tonnes per hectare per year (Acién Fernández *et al.*, 2013; Burlew, 1953; Chisti, 2016).

2.6.3 Open systems

Open systems are one commonly used option for mass culture of microalgae, but they present a number of disadvantages for optimal microalgal growth. In general, open systems are simpler and cheaper to construct than closed systems. However, they commonly suffer from contamination issues and lack of control over culture conditions which can result in lower biomass productivities than closed systems (Acién Fernández *et al.*, 2013; Becker, 1994; Tredici *et al.*, 2013).

Raceway ponds

The most commonly employed open systems for growing microalgae are raceway ponds (Becker, 1994; Chisti, 2016). These cultivation systems are simple in construction and operation consisting at the most basic level of an oval-shaped pond with a central divider circulated by a paddle wheel. Carbon dioxide and air are typically sparged into the culture in one defined area, such as close to the paddle wheel to minimise complexity (Becker, 1994). Examples of some typical raceway ponds are shown in Figure 2.26.

(A)

(B) (C)

Figure 2.26 – Examples of typical raceway ponds at semi-commercial scale (A and B) and pilot scale (C). Photos taken at University of Almería and Cajamar Foundation facilities (Spain), July 2017.

Raceway ponds are normally operated with a culture depth of 20 to 30 cm and can be anywhere from a few square metres to one hectare in area (Chisti, 2016; Grobbelaar, 2012). Due to the ponds being open to the atmosphere there are often issues with both microbial and chemical contamination of cultures. The ponds are also poorly mixed and illuminated due to laminar flow in the majority of the reactor and long light paths due to the depth of the culture. Control of pH and temperature is also poor and so the culture is at the mercy of environmental conditions (Acién Fernández *et al.*, 2013; Becker, 1994; Chisti, 2016). Due to their high surface area the rate of evaporation is considerable and can be highly variable depending on the environmental conditions. In large-scale reactors, hundreds of litres of water can evaporate per day and thus requires constant replacement to maintain the culture volume (Chisti, 2016).

Thin-layer reactors

To reduce the effect of light attenuation limiting cell densities that is observed with raceway reactors, thin layer reactors can be used. These reactors can be operated with a liquid depth of less than 1 cm to mitigate issues with light attenuation (Apel *et al.*, 2017). This style of reactor can improve culture growth compared to that achieved with typical

raceways and can also improve mixing in the culture by use of weirs and recirculating pumps. An example of a pilot scale thin layer reactor is shown in Figure 2.27.

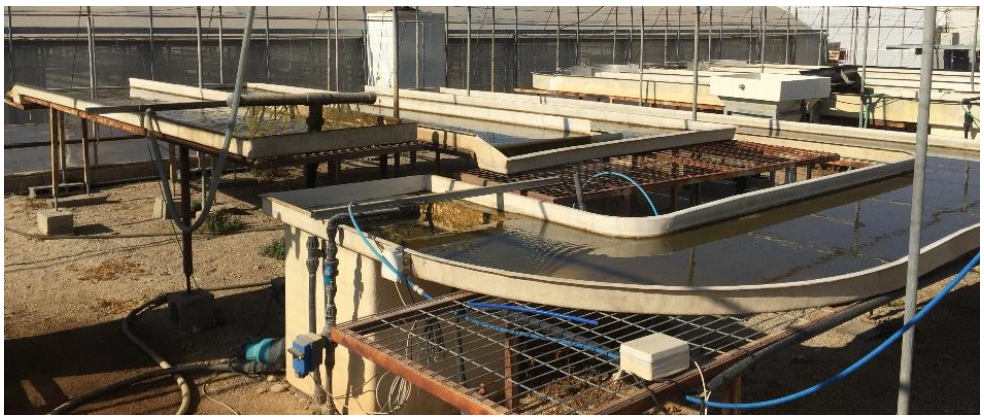

Figure 2.27 – Example of thin layer reactor. Photo taken at Cajamar Foundation facilities (Spain), July 2017.

While light attenuation is mitigated, the shallow culture depth results in a much lower volume being able to be cultured per unit area than comparable raceway reactors (Apel *et al.*, 2017; Doucha & Lívanský, 2014). Thin layer reactors also suffer from similar issues as raceway ponds with contamination and lack of control over culture conditions.

2.6.4 Closed systems

Closed systems are typically more expensive to construct and operate than open systems; however, they allow tighter control over culture conditions than open systems (Tredici *et al.*, 2013). The risk of contamination is also greatly reduced in closed systems as the culture is isolated from the outside environment. There are a variety of closed systems for microalgae, collectively these are referred to as photobioreactors. Each type of photobioreactor has benefits and disadvantages depending on the strain of microalgae to be grown and the desired product.

Bubble column photobioreactors

Bubble column photobioreactors are one of the simplest closed systems, consisting of a vertical column in which the culture is contained and bubbled with gas (Chisti, 1998). Due to their simplicity, bubble columns can be cheap to build, but they are limited in the volume that can be cultured using them. To increase the volume of the bubble column either the diameter or height must be increased. These dimensions are limited by light attenuation of the culture, mechanical strength of the construction material, and fluid dynamics to ensure adequate mixing (Acién Fernández *et al.*, 2013; Chisti, 1998; Kantarci

et al., 2005). Thus, in order to increase the production capacity of a culture facility using this style of reactor a large number of reactors of relatively small volume are required.

(A) (B)

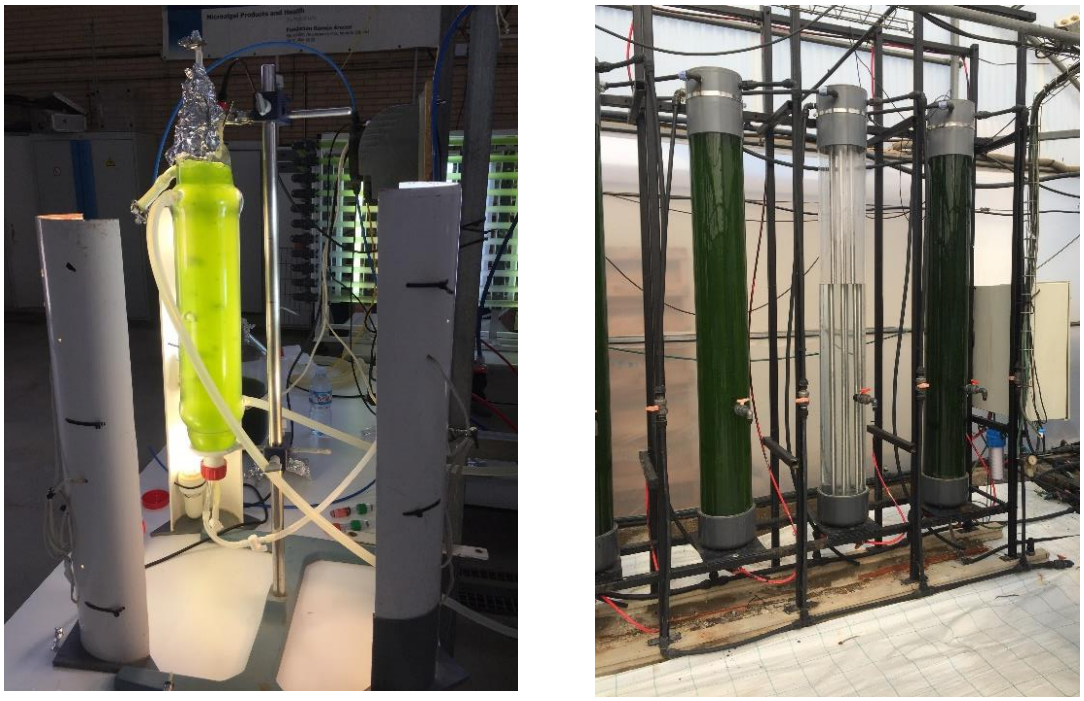

Figure 2.28 – Examples of bubble columns on A) bench scale and B) semi-commercial scale. Photos taken at University of Almería and Cajamar Foundation facilities (Spain), July 2017.

Airlift photobioreactors

Airlift photobioreactors are a form of modified bubble column. There are many configurations of airlift photobioreactors as shown in Figure 2.29. All airlift reactors share the common features of a riser and downcomer and use a sparged gas to induce liquid flow in the reactor (Chisti, 1998).

Airlift reactors have a better-defined flow profile than bubble columns and this can result in improved mixing of the culture. They are gentle on cells due to being pneumatically agitated and so can be used for shear-sensitive cultures (Chisti, 1998; García Camacho *et al.*, 1999). Scale up of airlift photobioreactors is limited similarly to bubble columns in that as the diameter of the reactor is increased so does the light attenuation and so large volumes of dense cultures cannot be achieved (Acién Fernández *et al.*, 2013). Again, in order to increase the production capacity a large number of reactors must be built with comparatively low volumes.

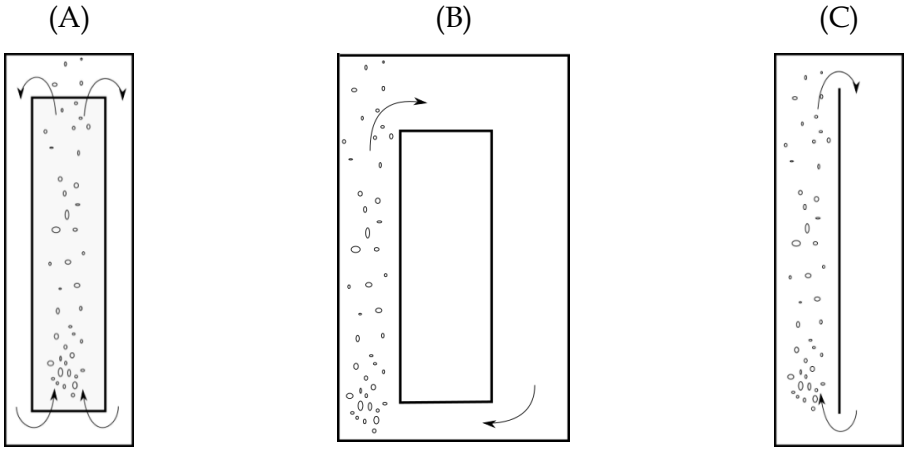

Figure 2.29 – Examples of common airlift bioreactor configurations. A) concentric tube, B) external draught and C) split-tube. Based on Chisti (1998).

Tubular photobioreactors

Tubular photobioreactors are touted as the most applicable closed photobioreactor for scale up of microalgae cultures (Burlew, 1953; Tredici *et al.*, 2013). These photobioreactors consist of three key components: a solar receiver; a bubble column; and a recirculating pump (Chisti, 2007). The general setup of a tubular photobioreactor is shown in Figure 2.30.

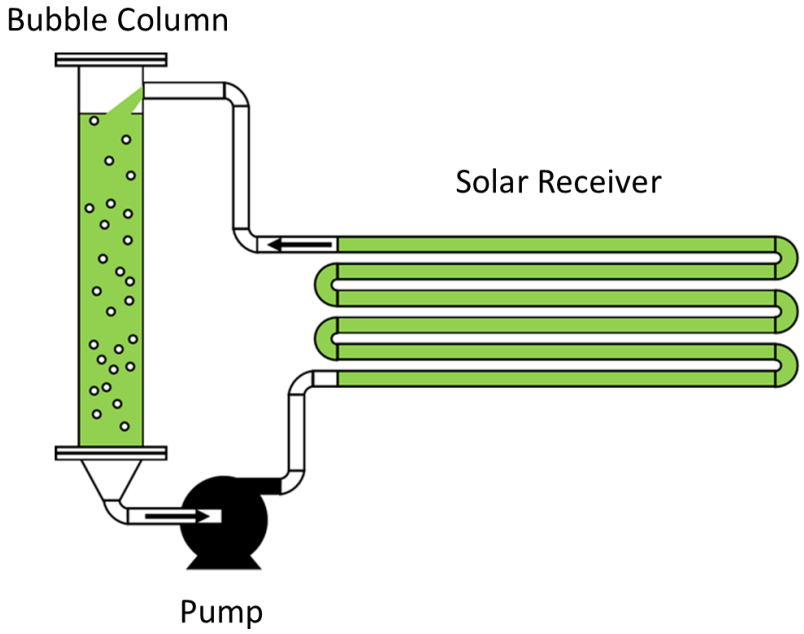

Figure 2.30 – Diagrammatic representation of the key tubular photobioreactor components. Based on Chisti (2007).

The culture is recirculated through the solar receiver where the culture is exposed to light and the bubble column where oxygen is stripped, and carbon dioxide is supplied. The solar receiver is typically constructed from relatively small diameter tubing (typically 20 mm to 100 mm) to minimise the light path in the culture so it is sufficiently illuminated (Tredici *et al.*, 2013). The bubble column is of larger diameter (>100 mm) to allow sufficient residence time to strip the oxygen in the culture and prevent bubble entrainment. Due to the small diameter of the solar receiver, sufficient light is able to be supplied to large culture volumes, hence their applicability to large-scale production as the volume can be increased without the light attenuation issues associated with bubble columns or airlift reactors (Acién Fernández *et al.*, 2013; Tredici *et al.*, 2013). Some examples of tubular photobioreactors constructed on different scales are shown in Figure 2.31.

(A) (B)

Figure 2.31 – Examples of tubular photobioreactors on A) bench scale and B) pilot scale. Photos taken at University of Almería (Spain), July 2017.

While tubular photobioreactors allow closed cultures on large-scale, they are much more complex than pneumatically agitated photobioreactors and thus are more costly to build and operate (Molina Grima *et al.*, 2009). Due to the culture being circulated by a mechanical pump, tubular photobioreactors are also unsuitable for shear-sensitive strains of microalgae, although pneumatically circulated tubular photobioreactors for shear-sensitive strains have been designed and used as reported by Acién Fernández *et al.* (2001). By stacking the solar receiver tubes vertically, the areal productivity (mass of biomass produced per unit area of land per unit time) of tubular photobioreactors can be increased. A greater volume of culture can be produced per square metre of land area without excessive light attenuation which would occur in a raceway pond with an equivalent areal volume (Molina Grima *et al.*, 2009; Tredici *et al.*, 2013).

Bag photobioreactors

One of the simplest and cheapest photobioreactors is a simple clear plastic bag. The plastic bag is sealed to form the desired shape, typically a long cylinder with a cone-shaped base, which is operated similarly to a bubble column (Acién Fernández *et al.*, 2013; Tredici *et al.*, 2013). Due to their ease of manufacture these reactors can be made quickly and cheaply but they are often only able to be used for one culture before being disposed of (Becker, 1994; Norsker *et al.*, 2011). The plastic bags are also prone to leaking and can have problems with contamination if not sealed correctly (Becker, 1994).

Flat plate photobioreactors

Flat plate photobioreactors are designed to minimise the light path through the reactor (Acién Fernández *et al.*, 2013; Tredici *et al.*, 2013). They are designed to have a large surface area to capture light are typically around 5–10 cm thick. An example of a flat plate photobioreactor is shown in Figure 2.32. The reactor can either be oriented standing vertically, angled towards the sun or lying horizontal. They are gentle on the algae growing in the reactor and so can be utilised for fragile strains where other reactors are not suitable (López-Rosales *et al.*, 2018). Due to their low thickness, the total volume that can be cultured in a reactor is limited when compared to other styles of reactor and so their areal productivity is comparatively low (Acién Fernández *et al.*, 2013; Becker, 1994; Tredici *et al.*, 2013). However, their simple design makes them a low-cost reactor option.

Figure 2.32 – Example of a flat-panel photobioreactor. Photo taken at University of Almería (Spain), July 2017.

2.6.5 Scale up of tubular photobioreactors for large-scale cultures

Scaling up microalgae cultures is of key importance in making microalgae bioprocesses commercially viable (Borowitzka & Vonshak, 2017). As described earlier, culture conditions are relatively easy to control in bench or laboratory scale systems; however, as the scale of the system increases it becomes increasingly difficult to economically control all culture conditions (Molina Grima *et al.*, 2009). Predicting the behaviour of cultures on large-scale can be difficult as stratification of the culture can occur, for example in large raceway ponds there is often thermal stratification over the depth of the pond (Chisti, 2016). In tubular photobioreactors stratification can occur in the solar receiver with dissolved oxygen levels increasing as residence time increases (Molina Grima *et al.*, 2001). Culture stratification is difficult to simulate in laboratory scale cultures due to the comparatively low culture volumes.

Scale up of tubular photobioreactors is not widely covered in literature as most large-scale facilities have retained methods as trade secrets. As a result, there is a lack of available data on large-scale tubular photobioreactors. There are several facilities using commercial scale tubular photobioreactors for production of high value products around the world. Two semi-commercial scale facilities are well documented in published literature: the Cajamar Foundation facilities and AlgaePARC.

The Cajamar Foundation facilities in Almería, Spain houses a collection of 10 fence-style tubular photobioreactors (Fernández *et al.*, 2014). Each reactor has a volume of 2.6 m^3 with a tube diameter of 0.09 m. The solar receiver length of each reactor is 400 m. AlgaePARC located in The Netherlands has both a large-scale horizontal and vertical tubular photobioreactor (Bosma *et al.*, 2014). These reactors have volumes of 0.56 m^3 (horizontal) and 1.06 m^3 (vertical). The tube diameter for both reactors was chosen to be 0.046 m as a balance between pressure drop and productivity. Liquid flow velocities were operated up to 0.6 m s^{-1} and the maximum tube length was approximately 80 m.

Two commercial scale facilities currently operating to produce high value products with tubular photobioreactors are Algomed and Algatechnologies. Algomed (Roquette Klötze GmbH & Co. KG), located in Klötze, Germany, has a large-scale tubular photobioreactor facility for production of *Chlorella*. They utilised 500 km of glass tubing to construct the solar receivers of their photobioreactors (Roquette Klötze GmbH & Co. KG, 2017). Algatechnologies Ltd. (Ketura, Israel), has a two-stage tubular photobioreactor system for commercial production of *Haematococcus pluvialis*. The tubular system is also

over 500 km in total length, covering 15 acres of land area (Algatechnologies Ltd., 2017). A combination of horizontal and vertical reactor geometries is used to induce astaxanthin production in the microalgae.

Molina Grima *et al.* (2000) have reported a method for scale up of airlift driven tubular photobioreactors. However, unless the microalgae strain to be grown is extremely shear sensitive, airlift tubular reactors are not as preferable as mechanically pumped reactors from a commercial standpoint. Due to effects such as varying relative light and dark volumes when increasing tube diameter, no comprehensive and reliable method has been reported for scaling up tubular photobioreactors (Molina Grima *et al.*, 1999).

The key constraints on scale up are the length of the solar receiver and maintaining a suitable light path (Bosma *et al.*, 2014; Molina Grima *et al.*, 2000; Molina Grima *et al.*, 1999). Maximum solar receiver length is limited to avoid excessive dissolved oxygen in the culture and carbon exhaustion. Supply of light limits the diameter of the solar receiver tubes. As production facilities increase in size they typically require the reactors to be located outdoors and as there is no control over the weather and seasons this can lead to variability in the culture performance for outdoor facilities (Becker, 1994; Burlew, 1953). Tight control of temperature in large-scale reactors can also prove uneconomic as reactor volumes increase which can limit the achievable culture conditions (Borowitzka & Vonshak, 2017; Grobbelaar, 2012). In order to obtain data for scaling up reactors there needs to be comparable dark and light volumes in the tubes of small-scale reactors. The influence of suboptimal culture conditions and dissolved oxygen tolerance also needs to be known.

2.7 Modelling of microalgal growth, metabolite production, and cultivation systems

2.7.1 Microalgae growth and photosynthesis rate models

Modelling the growth of microalgae is of strong interest to simulate processes and make sound decisions on the viability of scale up or implementation of a process. To date, there have been two reviews published on microalgae growth models which have identified approximately 40 reported models (Béchet *et al.*, 2013; Lee *et al.*, 2015). Models can consider a range of factors influencing growth, from nutrient concentrations to light and temperature. Typical models consider either the specific growth rate, μ, of the microalgae or the photosynthesis rate, P. As biomass is produced from photosynthesis

during photoautotrophic growth the photosynthesis rate is often assumed to be proportional to the growth rate.

Most models follow a typical format as seen in Equation (2.7), where the specific growth rate under a given set of conditions is a fraction of the maximum specific growth rate and various functions, each with values ranging from 0 to 1, are used to represent the effect of the desired environmental factor.

$$\mu = \mu_{max}\, f_1(I)\, f_2(T)\, f_3(\mathrm{pH})\, f_4(\mathrm{nutrients})\, f_5(\mathrm{CO_2}) \ldots f_n(n) \qquad (2.7)$$

Light is generally considered to be the limiting factor for growth for photoautotrophic microalgae (van Oorschot, 1955). Due to the influence of light on photoautotrophic growth there have been many models reported using light as the only factor such as those in Table 2.7. Early models such as Equation (2.8) treated light as a substrate for photosynthesis and thus applied a Monod-type model, which is discussed in later sections.

Table 2.7 – Growth kinetic models for light effects on photoautotrophic growth of microalgae.

Model	Reference	
$\mu = \mu_{max} \frac{I}{K_I + I}$	Burlew (1953)	*(2.8)*
$\mu = \mu_{max} \left(1 - \mathrm{e}^{-I/K_I}\right)$	van Oorschot (1955)	*(2.9)*
$\mu = \mu_{max} \frac{{I_{av}}^n}{K_I^n + {I_{av}}^n}$	Molina Grima *et al.* (1994a)	*(2.10)*
$\mu = \mu_{max} \frac{{I_{av}}^{\left(b+\frac{c}{I_0}\right)}}{K_I \cdot \left(1+\left(\frac{I_0}{I_i}\right)^a\right)^{b+\frac{c}{I_0}} + {I_{av}}^{\left(b+\frac{c}{I_0}\right)}}$	Molina Grima *et al.* (2009)	*(2.11)*

I, irradiance; K_I, irradiance saturation constant; I_{av}, average irradiance; I_i, inhibition light intensity; I_0, incident irradiance; a, b, c, n, experimentally determined parameters.

The models proposed in Table 2.7 are limited in the conditions that can be modelled. Namely they do not account for the light regime the cells are exposed to, and only Equation (2.11) accounts for photoinhibition. Rubio *et al.* (2003) proposed a series of models that account for the light regime that the cells are exposed to (such as intermittent or continuous illumination) and accounts for light limitation or inhibition. These models consider photosynthetic rate and so the growth kinetics are assumed to be proportional to the rate of photosynthesis.

A variety of other models have also been reported considering the impact of other conditions (Béchet *et al.*, 2013; Lee *et al.*, 2015). There are compromises to be made when choosing many of the models, typically between simplicity, accuracy, and the extent of experimental data required to fit the model parameters. The light factor models reported also do not account for the spectral composition of light. Wavelengths of light are utilised differently depending on how well they are absorbed and their energy and this will impact the rate of growth or photosynthesis as discussed earlier.

When all other factors such as nutrients, temperature and pH are optimal, light is the limiting factor for growth and so light-factor-only models could be suitable for modelling growth. However, in real systems and large-scale reactors conditions are rarely ideal and conditions for optimal production of desired metabolites may result in suboptimal growth conditions. In these cases, models which consider other growth conditions are beneficial as discussed in the following sections.

Nutrient consumption models are commonly used for all microorganisms. The most common model is the Monod model as in Equation (2.12) (Monod, 1949). This model accounts for the effect of the limiting substrate concentration, C_S, on growth and its saturation constant K_S.

$$\mu = \mu_{max} \frac{C_S}{K_S + C_S} \qquad (2.12)$$

The Monod model is an empirical equation based on the form of Michaelis–Menten kinetics (Reece *et al.*, 2010). For microalgae, generally this Monod model is added to light-factor models reported above, although it is also applied to only consider nutrients (Lee *et al.*, 2015). Carbon dioxide is commonly used as the limiting nutrient when photoautotrophic growth is considered; however, nitrogen and phosphorus are also often considered to be limiting.

Some examples of models which consider nutrient effects on growth are reported in Table 2.8. Typically, these models tend to follow a similar form as described above with each factor considered to have a multiplicative effect on the growth rate.

Table 2.8 – Growth models considering nutrient and light effects.

Model	Reference	
$\mu = \mu_{max}\left(\frac{C_N}{K_N+C_N}\right)\left(1-\frac{Q_{min}}{Q}\right)\frac{I}{I_{opt}}\ e^{\left(1-\frac{I}{I_{opt}}\right)}$	Wu *et al.* (2013)	(2.13)
$\mu = \mu_{max}\left(\frac{I_{av}}{K_I+I_{av}}\right)\left(\frac{C_{CO_2}}{K_{CO_2}+C_{CO_2}+\left(\frac{C_{CO_2}^2}{K_{CO_2}}\right)}\right)$	He *et al.* (2012)	(2.14)
$\mu = \mu_{max}\left(\frac{I_{av}}{K_I+I_{av}}\right)\left(\frac{C_{CO_2}}{K_{CO_2}+C_{CO_2}}\right)$	Filali *et al.* (2011)	(2.15)
$\mu = \mu_{max}\left(\frac{C_{CO_2}}{K_{CO_2}+C_{CO_2}}\right)\left(\frac{C_N}{K_N+C_N}\right)\frac{I_{av}}{I_{opt}}\ e^{\left(1-\frac{I}{I_{opt}}\right)}$	Yang (2011)	(2.16)

I_{opt}, optimal light intensity; C_S, concentration of substrate 's'; K_S, half saturation constant of substrate 's'; Q_{min}, minimum cell quota for algal existence of nutrient; Q nutrient cell quota.

As most nutrients are typically able to be supplied sufficiently by fed-batch culturing, nutrient-based models are mainly applicable to situations where nutrient concentrations are variable, such as when using wastewater for the culture media. They are also of use when considering nutrient starvation effects for triggering metabolite production. Nutrients such as nitrogen also have a direct impact on photosynthesis rates (van Oorschot, 1955) which are not considered in typical nutrient consumption models.

Few models account for the effects of all environmental conditions that effect microalgal growth such as temperature, pH, dissolved oxygen, nutrient concentrations, and irradiance. Many of these models make broad assumptions on the growth of microorganisms. They also apply inappropriate models to phenomena such as the Arrhenius equation to the effect of pH (Costache *et al.*, 2013). The issues raised above may serve to limit the universality of these types of models without thorough fitting to experimental data for specific strains.

For temperature, Roels (1983) proposed a model for growth assuming microorganisms have a similar response to temperature as enzymes. Equation (2.17) accounts for the increase in reaction rate, and thus growth, due to temperature and the denaturation of proteins at higher temperatures. Here E_a is the activation energy for photosynthesis, $E_a{}'$ is the activation energy for protein denaturation, k is the Boltzmann constant and K is a dimensionless constant (Béchet *et al.*, 2013).

$$f(T) = \frac{e^{\left(\frac{-E_a}{k\,T}\right)}}{1 + K\,\mathrm{e}^{\left(\frac{-E_a'}{k\,T}\right)}} \qquad (2.17)$$

Other temperature models include that proposed by Ketheesan and Nirmalakhandan (2013) in Equation (2.18) and Bernard and Rémond (2012) in Equation (2.19). Here T_{max} is the maximum temperature, T_{opt} is the optimum temperature and T_{min} is the minimum temperature for growth.

$$f(T) = 1.066^{T-20} \tag{2.18}$$

$$f(T) = \frac{\left((T-T_{max})(T-T_{min})^2\right)}{(T_{opt}-T_{min})[(T_{opt}-T_{min})(T-T_{opt})-(T_{opt}-T_{max})(T_{opt}-T_{min}-2T)]} \tag{2.19}$$

A model reported by Dermoun *et al.* (1992) considered the interaction of irradiance and temperature on growth. However, this required parameters to be determined from experiments for both light and temperature effects which is time intensive. This coupled model may provide accurate predictions of growth, but as commented by Béchet *et al.* (2013), this could be due to overfitting of the many experimentally determined parameters.

The proposed models covered here require considerable experimental data to determine the model parameters. However, prediction of culture performance under a variety of conditions is desirable for processes where there is little control over the environmental conditions, such as when reactors are located outdoors. As optimal metabolite content may be achieved under suboptimal growth conditions, a universal model would be a powerful tool to be able to predict productivity under a wide range of environmental conditions to optimise reactor operation.

2.7.2 EPA production models

There have been few models reported in literature on EPA production. As the production of EPA is strain specific, empirical models are normally used. However, as discussed previously, there can be the risk of overfitting models and they also do not describe the underlying phenomena and so are limited to their applicability. Extrapolation from these models should be approached with caution. As the impact of environmental factors on EPA production is also unclear, and strain specific, identification of appropriate models to apply is difficult.

Camacho-Rodríguez *et al.* (2014) based their model on the rate of product production, r_P, as a function of the concentration of biomass, C_b, and the rate of product formation in the biomass, q_p, as in Equation (2.20).

$$r_p = \frac{d[P]}{dt} = q_p\, C_b \tag{2.20}$$

The proportion of product in the biomass is given by the ratio of product formation to biomass formation, $Y_{P/x}$ ($g_P\ g_b^{-1}$), and the specific growth rate.

$$q_p = Y_{P/x}\, \mu \tag{2.21}$$

The ratio of product to biomass formation was deemed to be influenced by the temperature and average irradiance of the culture as in Equation (2.22), with the addition of fitting parameters a, b and c. For *Nannochloropsis gaditana,* a linear variation of EPA accumulation with temperature was proposed.

$$Y_{P/x} = (a + b\, T) + c\, I_{av} \tag{2.22}$$

Acién Fernández *et al.* (2000) remarked that EPA content in *Phaeodactylum tricornutum* depended mainly on the external and average irradiances on the culture and developed the empirical model in Equation (2.23) for EPA as g per 100 g of dry biomass.

$$\text{EPA content} = (6.29 - 0.0179\, I_{av}) + (-0.0021 + 7.57 \times 10^{-6}\, I_{av})\, I_{wm} \tag{2.23}$$

As lipid production is a common interest for microalgae, overall lipid production has been modelled by many researchers (Xu & Boeing, 2014). However, these models are mostly concerned with biofuel production and total lipid content rather than individual fatty acid species.

2.7.3 Modelling of photobioreactor systems

To analyse the performance of photobioreactors there have been many attempts to model the effects of various physical parameters associated with their operation. The key areas that are modelled are: light gradients, mass transfer, heat transfer, fluid mechanics, and their effects on growth kinetics.

Modelling of light in photobioreactors

As cell densities in cultures increase, as is required for commercial production, the light supplied to the photobioreactor will be attenuated at shallow depths in the culture. Light is often assumed to be attenuated according to the Beer-Lambert law (Equation (2.24)) (Acién Fernández *et al.*, 1997).

$$I(x) = I_0\, e^{(C_b\, K_a\, x)} \tag{2.24}$$

Here, I_0 is the incident irradiance at $x = 0$, x is the distance into the culture, C_b is the biomass concentration, and K_a is the extinction coefficient of the biomass in the broth.

However, the assumptions made to apply the Beer-Lambert law do not hold for microalga broths. Namely, the assumption that there is no light scattering is incorrect when the cells present in solution are considered. Additionally, different light wavelengths are absorbed to different extents due to pigment content of the cells which can vary under different conditions and over the course of a culture (Acién Fernández *et al.*, 1997).

While light scattering is not accounted for in the Beer-Lambert law it has been widely used in literature as an approximation for light attenuation (Acién Fernández *et al.*, 1997). Some empirical alternatives have been proposed, such as seen in Equation (2.25), that take into account light scattering (Yun & Park, 2003). In this equation, k_1 and k_2 are strain-specific parameters that must be determined through experiments.

$$I(x) = I_0 \, \mathrm{e}^{\left(\frac{-k_1 \, C_b \, x}{k_2 + C_b}\right)} \tag{2.25}$$

Another approach used for systems where light is scattered by particles in turbid systems is based more closely on the Beer-Lambert law (Equation (2.26)) where N_p is the number concentration of particles, L_I is the optical path length and A_{CS} is the light scattering cross-sectional area of the particle (Gregory, 2005).

$$I = I_0 \, \mathrm{e}^{(-N_p \, \mathrm{A}_{CS} \, L_I)} \tag{2.26}$$

This can be applied if all particles have the same cross-section. For a sphere of diameter d_p, A_{CS} is given by Equation (2.27). Q_{sc} is the scattering coefficient which can vary from close to 0 to >>1, for large particles $Q_{sc} \rightarrow 2$.

$$A_{CS} = \frac{Q_{sc} \, \pi \, d_p^2}{4} \tag{2.27}$$

Light modelling in photobioreactors is generally used in two main ways: calculation of average light intensity for situations where microalgae are rapidly cycled from light to dark conditions, and calculation of light profiles for depth-specific photosynthesis rates where microalgae are cycled slowly or negligibly from light to dark conditions (Chisti, 2016; Molina Grima *et al.*, 1999). Typically, the former situation is applied to closed photobioreactors with short light paths and good mixing and the latter to raceway ponds.

Average irradiance for tubular photobioreactors has been modelled as shown in Equation (2.28) (Acién Fernández *et al.*, 2013) where L_I is the length of the light path of the reactor.

$$I_{av} = \frac{I_0}{K_a\, C_b\, L_I}\left(1 - \mathrm{e}^{(-K_a\, C_b\, L_I)}\right) \tag{2.28}$$

Averaged irradiance does not consider the light history of cells and thus does not account for the potential increase in photosynthetic efficiency that can occur due to the flashing light effect (Burlew, 1953; Molina Grima *et al.*, 1999). Models that consider the light history of the cells are complicated and typically require computational fluid dynamics (CFD) modelling of the cells' positions over time in the reactor (Cheng *et al.*, 2016; Sato *et al.*, 2010). Simpler models consider a light limited and light saturated region in the reactor that cells are cycled in and out of (Molina Grima *et al.*, 2000). However, this considers a square-wave profile of light intensity which is not what the cells are subjected to in the real system where light intensity varies in a continuous fashion depending on the cells' positions (Brindley *et al.*, 2011).

Mass transfer in photobioreactors

Gas-liquid mass transfer is an important operation required in photobioreactors. Oxygen must be stripped from the culture to avoid excessive dissolved oxygen levels. Carbon dioxide must also be supplied as the carbon source for the microalgae. In gas-liquid mass transfer the liquid-side resistance is the limiting factor (van't Riet & Tramper, 1991). The rate of change of concentration of a desired gas in liquid, $\frac{dC_G}{dt}$, can be given by Equation (2.29).

$$\frac{dC_G}{dt} = k_L a\,(C_G - C_G^*) \tag{2.29}$$

k_L is the liquid-side mass transfer coefficient and C_G^* is the equilibrium gas concentration in the liquid. As specific interfacial area, a, is difficult to determine in gas-liquid systems, the overall mass transfer coefficient, $k_L a$, is commonly used (van't Riet & Tramper, 1991). There are a variety of correlations available to predict $k_L a$. The equilibrium concentration of a gas in water can be determined from Henry's law (Equation (2.30)) for dilute solutions (Henry, 1803; Sander, 2015).

$$C_G^* = H_G\, P_T\, y_G \tag{2.30}$$

The concentration changes depending on total pressure, P_T, gas mole fraction, y_G, and the Henry's constant, H_G, for the system.

Heat transfer in photobioreactors

Heat transfer in photobioreactors occurs from radiation, convection, or conduction with the outside environment as well as from deliberate heat exchange. The major contributors of heat are absorption of radiation, heat transfer to or from the environment by conduction and convection, and evaporation (Acién Fernández *et al.*, 2013).

The temperature of a culture, T, changes according to Equation (2.31) which can be used to determine the cooling or heating load (Acién Fernández *et al.*, 2013). The culture mass, m, with a heat capacity, c_p, undergoes a rate of temperature change $\frac{dT}{dt}$ depending on the amount of energy supplied or lost. Radiative energy is determined from the global radiation of the culture, G, the contact area of the radiation, A_{rad}, and the absorption of the culture, a. Heat transfer from the environment depends on the overall heat transfer coefficient, U, the area of heat transfer, $A_{transfer}$, and the temperature difference between the environment, T_{out}, and the culture. Heat loss due to evaporation is given by the rate of mass loss, $\dot{m}_{evaporated}$, and its enthalpy of vaporisation, $\Delta H_{vaporisation}$. Heat can also be supplied to the culture due to energy dissipation due to pumping and bubbling as well as through media or water supplied to replace the evaporated water which are not included here.

$$m_{culture}\, c_p \frac{dT}{dt} = G\, A_{rad}\, a + U\, A_{transfer}(T_{out} - T) + \dot{m}_{evaporated}\Delta H_{vaporisation} \qquad (2.31)$$

Fluid dynamics in photobioreactors

Turbulence is a key factor when considering mixing in bioreactors (van't Riet & Tramper, 1991). The Reynolds number, Re, is used to quantify turbulence (Equation (2.32)). In a pipe, Re_{pipe} depends on the pipe diameter, d_{pipe}, and the liquid velocity, u_L, viscosity, η_L, and density, ρ_L. Laminar flow occurs when $Re < 2000$ and turbulent flow occurs for $Re > 4000$ with a transition zone in the region $2000 < Re < 4000$ (de Nevers, 2005).

$$Re_{pipe} = \frac{\rho_L\, u_L\, d_{pipe}}{\eta_L} \qquad (2.32)$$

Superficial gas and liquid velocities are parameters commonly used for the design and operation of bioreactors (van't Riet & Tramper, 1991). Superficial velocity is defined as the volumetric flow rate of fluid, Q_F, divided by the cross-sectional area the fluid is flowing through, A_{cs} (Equation (2.33)).

$$u_{superficial} = \frac{Q_F}{A_{cs}} \tag{2.33}$$

Gas-liquid flow dynamics are also important for photobioreactors. Variables such as bubble size and rise velocity influence mass transfer which is particularly important for closed photobioreactors.

Fluid flow in reactors is governed by Bernoulli's equation (de Nevers, 2005) which is particularly important due to pressure drops in large-scale reactors to ensure sufficient flow (Acién Fernández *et al.*, 2013). The pressure drops for reactors can be used to estimate their pumping power consumption, P_{pump}, such as Equation (2.34) for tubular photobioreactors reported by Acién Fernández *et al.* (2013).

$$P_{pump} = \left(\frac{\pi}{8\,V}\right) d_{pipe}^2\, u_L^3 + \frac{0.0791\pi}{8\,V} \frac{L_{pipe}\,\eta_L^{0.25}}{\rho_L^{0.25}} d_{pipe}^{0.75} u_L^{2.75} \tag{2.34}$$

3 General Materials and Methods

3.1 Determination of cell and biomass concentrations

3.1.1 Haemocytometer counting method

The cell counting method used was based on that reported by Alfiarty (2018) and Andersen (2005). Cell counts were determined by counting using an improved Neubauer (0.1 mm deep) haemocytometer (Bright-Line; Hausser Scientific, U.S.A.). Samples were taken from the culture to be counted and diluted according to the expected cell concentration to achieve a diluted concentration of between approximately 2×10^5 cells mL^{-1} and 1×10^6 cells mL^{-1}. Samples were diluted with deionised water in an Eppendorf tube. The cells were counted in the four outside corner squares as in Figure 3.1. Cells on the top and left borders were counted and cells on the bottom and right borders were ignored. Each corner square represented a volume of 1×10^{-4} mL. Large groups of cells that were clumped were counted as a single cell, while small groups of cells (two or three) that were distinctly able to be counted were counted as individual cells.

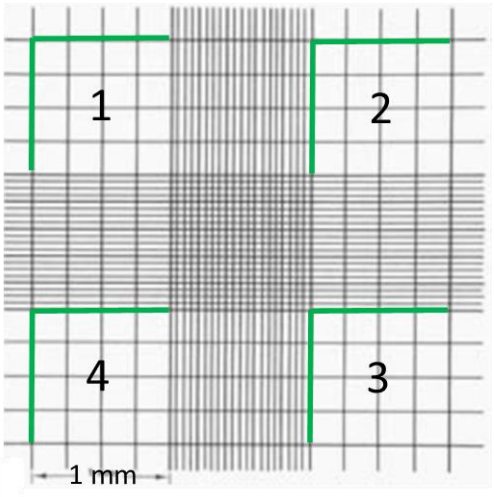

Figure 3.1 – Haemocytometer counting diagram. Based on Andersen (2005, p. 246).

Before loading the haemocytometer, the diluted samples were homogenised with a pipette by aspirating and expelling the sample 15 times in the Eppendorf tube. The coverslip was placed on the haemocytometer and 10 µL sample was then taken and loaded into one side of the counting chamber as described by Alfiarty (2018). A second sample was then taken to load the other side. After loading, the haemocytometer was allowed to sit for approximately one minute before counting to allow cells to settle so all cells were on the same focus plane. The cells were counted using an optical microscope (Olympus

BX60) at 200× magnification and a digital tally counter was used to reduce human error. The cell concentration, C_{cell}, in the culture was determined by using Equation (3.1).

$$C_{cell} = 2.5 \times 10^3 \, d_f \sum_{i=1,4} n_i \qquad (3.1)$$

Here, n_i is the number of cells counted in square i, and d_f is the dilution factor given by the total volume of the diluted sample divided by the volume of sample removed from the culture. The averages of the two sides of the haemocytometer were compared to ensure repeatability of each count and estimate uncertainties. If the cell counts from each side varied by greater than 20% a new cell count was taken.

The haemocytometer was cleaned between cell counts using 70% ethanol solution and lint-free tissue paper. Any residual ethanol solution was allowed to evaporate fully before adding samples to ensure there was no additional dilution from residual liquid in the counting chamber.

3.1.2 Biomass dry weight determination

Dry weight concentration was determined by two methods; freeze-drying of harvested samples, and filtration followed by oven drying. The freeze-drying process and apparatus used was based on that used by Alfiarty (2018) for consistency between studies. Culture samples of a known volume were centrifuged at 6,500 × rcf (relative centrifugal force) for 10 minutes in a pre-dried and weighed centrifuge tube and the supernatant decanted. The resulting biomass pellet was washed three times with deionised water to remove any remaining salts from the media. The tube containing the biomass pellet was flushed with argon to prevent oxidation and frozen at ≤−18 °C for at least 12 hours prior to loading into the freeze-dryer (FreeZone 2.5, Labconco, USA). The samples were typically kept in the freeze-dryer for two days or until a constant mass was reached, indicating all water had been removed.

Oven drying was conducted by filtering a known volume of culture sample through a Buchner filter funnel and flask under vacuum with a dried and pre-weighed Whatman GF/A glass microfibre filter. The collected biomass was washed three times with distilled water to remove any salts remaining from the culture media. The filter paper with collected biomass was carefully removed from the funnel and transferred to a watch glass or aluminium pan before being dried at 105 °C in an oven until a constant weight

was achieved (typically around five hours to overnight, depending on the quantity of biomass). Filter papers were cooled to room temperature in a desiccator prior to weighing.

3.2 Growth curve, maximum specific growth rate and productivity determination

Growth curves were plotted and analysed using Microsoft Excel. The specific growth rate for a given time of growth in a culture, μ,was determined using Equation (3.2). Here, $C_{cell,0}$ and $C_{cell,1}$ are the cell concentrations at the initial time, t_0, and time 1, t_1, respectively.

$$\mu = \frac{\ln(C_{cell,1}) - \ln(C_{cell,0})}{t_1 - t_0} \qquad (3.2)$$

Growth curves were modelled using the logistic equation (Equation (3.3)) where N_0 is the initial population density at time $t = 0$, N_t is the population density at time t. N_{max} is the maximum population density and μ_{max} is the maximum specific growth rate.

$$N_t = \frac{N_0\, N_{max}}{N_0 + (N_{max} - N_0)e^{-\mu_{max}\, t}} \qquad (3.3)$$

Growth curves were modelled by fitting the logistic equation to experimental data using the method of least squares in Microsoft Excel to determine μ_{max} using the inbuilt Solver function to minimise the sum of squared errors. The model was applied over the exponential range of the growth curves to avoid overfitting of the model to the stationary or lag phases of growth for determination of μ_{max}.

Biomass productivity for batch cultures was determined by the dry biomass concentration at harvest, divided by the number of days taken to reach that cell density. For example, a 76 L culture which required 14 days to reach a maximum density of 4.0 g L^{-1} would have a biomass productivity of 0.29 g L^{-1} d^{-1}. EPA productivity was calculated similarly using the EPA content of the biomass multiplied by the dry biomass concentration divided by the number of days required to reach the point of harvest. For example, if the above case had an EPA content of 5.0 g EPA/100 g dry biomass the EPA productivity would be 14 mg L^{-1} d^{-1}.

Productivity of semi-continuous cultures was determined by dividing the daily harvest volume by the total culture volume and multiplying by the biomass concentration. For example, a 76 L culture of which 20 L per day was harvested at a biomass

concentration of 2.0 g L^{-1} would have a biomass productivity of 0.53 g L^{-1} d^{-1}. If the biomass in this case had an EPA content of 5.0 g EPA/100 g dry biomass the EPA productivity would be 26 mg L^{-1} d^{-1}.

3.3 Statistical Analysis

Statistical analysis was conducted with Microsoft Excel using the inbuilt data analysis function. Cultures were considered to be statistically significantly different at 95 or 90% confidence levels ($p \leq 0.05$ or 0.10, respectively).

3.4 BBMA culture media preparation

Culture media were prepared according to the general methods reported by Andersen (2005). Ultra-pure deionised water (18.2 MΩ cm) was used for all small-scale medium preparations and reverse osmosis (RO) water (10 MΩ cm) for reactor-scale media. All stock solutions were prepared with glass labware. Stock solutions were autoclaved and then stored in the dark at 4 °C until needed. In particular, BBMA media was prepared as follows according to the recipe reported by Alfiarty (2018, p. 124):

Macronutrient stock solutions were prepared by dissolving the amounts in Table 3.1 in approximately 800 mL of water in a 1 L volumetric flask. Once fully dissolved, water was added to bring the volume to 1 L.

Table 3.1- Macronutrient stock solution compositions

Stock Solution	Component	Concentration (g L^{-1})
1	$NaNO_3$	100
2	$CaCl_2 \cdot 2\ H_2O$	5.00
3	$MgSO_4 \cdot 7\ H_2O$	15.0
4	KH_2PO_4	44.0
5	NaCl	5.00
6	Fe-Na-EDTA	12.0

The micronutrient stock solution (stock solution 7) was prepared by dissolving the components in Table 3.2 in approximately 800 mL of water in a 1 L volumetric flask. The volume was then taken up to 1 L with water once all components were dissolved.

Table 3.2 – Micronutrient stock solution (stock solution 7) composition

Component	Concentration (g L^{-1})
$ZnSO_4 \cdot 7\ H_2O$	8.82
$MnCl_2 \cdot 4\ H_2O$	1.44
MoO_3	0.71
$CuSO_4 \cdot 5\ H_2O$	1.57

To prepare the final medium, 10 mL of each of the above stock solutions 1–6 and 2 mL of stock solution 7 were added to 800 mL of deionised water in a volumetric flask and then diluted to 1 L with additional water. The prepared media was then transferred to a glass Schott bottle and autoclaved prior to use. The final concentration of the components in the prepared medium were as reported in Table 3.3.

Table 3.3 – Prepared BBMA medium final composition

Component	Mass Concentration (mg L^{-1})	Molar Concentration (mol L^{-1})
$NaNO_3$	1000	1.18×10^{-2}
$CaCl_2 \cdot 2\ H_2O$	50.0	3.40×10^{-4}
$MgSO_4 \cdot 7\ H_2O$	150	6.09×10^{-4}
KH_2PO_4	440	3.23×10^{-3}
NaCl	50.0	8.56×10^{-4}
Fe-Na-EDTA	120	3.27×10^{-4}
$ZnSO_4 \cdot 7\ H_2O$	17.6	6.13×10^{-5}
$MnCl_2 \cdot 4\ H_2O$	2.88	1.46×10^{-5}
MoO_3	1.42	9.86×10^{-6}
$CuSO_4 \cdot 5\ H_2O$	3.14	1.26×10^{-5}

3.5 Sterilisation and aseptic techniques

General aseptic techniques were carried out as described by Andersen (2005). Glassware and heat-stable culture media were sterilised by autoclaving at 121 °C and 103 kPa (15 psi) gauge. The time for autoclaving varied depending on the materials being sterilised; glassware was typically autoclaved for 20 minutes (larger pieces for 30 minutes), while culture media were autoclaved for anywhere from 20 to 60 minutes depending on the volume. Spent cultures, media, and contaminated glassware were autoclaved for 20 minutes or treated with 1 wt% sodium hypochlorite solution prior to disposal or re-use.

Manipulation of cultures was performed in a laminar flow biohood to avoid contamination from any airborne microorganisms. Materials that could not be autoclaved were disinfected by use of 70% (v/v) denatured ethanol in water. Disinfection of the tubular photobioreactor was performed using sodium hypochlorite solutions as described in § 3.11.

3.6 Measurement of light intensity and spectrum

Light intensities were measured using a spherical quantum sensor (Li-COR Spherical LI-193, Li-COR, U.S.A.) connected to a meter/datalogger (LI-1500 Light Sensor Logger, Li-COR, USA). The light intensity was measured over the range of 400–700 nm. Light intensity values were directly recorded in units of μmol m^{-2} s^{-1}. The light intensity of lighting systems was measured over a range of different PWM (pulse width modulation) values to determine the calibration curve for each light colour and system. The influence of external light sources was accounted for by measuring lighting systems in a darkened room and then again with external light sources switched on.

Spectra of light sources were recorded using a spectroradiometer (FS3 350–2500, ASD Inc., U.S.A.). Measurements were taken in a darkened room to avoid external light interference. The light spectra were recorded in 1 nm increments over a wavelength range of 350–750 nm, outside of which there was negligible light produced for the light sources used in this study.

3.7 Determination of nitrate concentration in culture media

Nitrate concentration was determined based on the ultraviolet spectrophotometric screening method reported by Eaton *et al.* (2005, pp. 4-87 - 88). Briefly, samples were treated with 1 mol L^{-1} HCl (analytical reagent grade) at a ratio of 1 mL per 50 mL of diluted sample. The absorbance of the treated samples were measured using a UV-Vis spectrophotometer (UV-1600PC, VWR, USA) at wavelengths of 220 nm and 275 nm using matched quartz cuvettes with a path length of 10 mm. Absorbance readings were corrected by subtracting twice the absorbance reading at 275 nm from that at 220 nm to account for organic matter (provided the correction value was <10% of $A_{220\,nm}$). To determine nitrate concentration in the culture media, raw culture samples were centrifuged at 6,500 × g for 10 minutes and the supernatant collected. A sample of the supernatant was then diluted with deionised water (typically a 100× dilution) and treated with 1 mol L^{-1} HCl to be analysed as above. The spectrophotometer was blanked with nitrate-free media prepared for analysis in the same fashion as the sample.

A calibration curve (Figure 3.2) was constructed by reading the absorbance at 220 nm and 275 nm of sodium nitrate stock solutions with nitrate concentrations between 0 and 8 mg L^{-1}. The resulting data was fitted to a linear line of best fit using LINEST in Microsoft Excel to determine the absorbance-to-concentration conversion factor. Samples, standards, and reagents were prepared using ultra-pure deionised water of >18.2 MΩ cm.

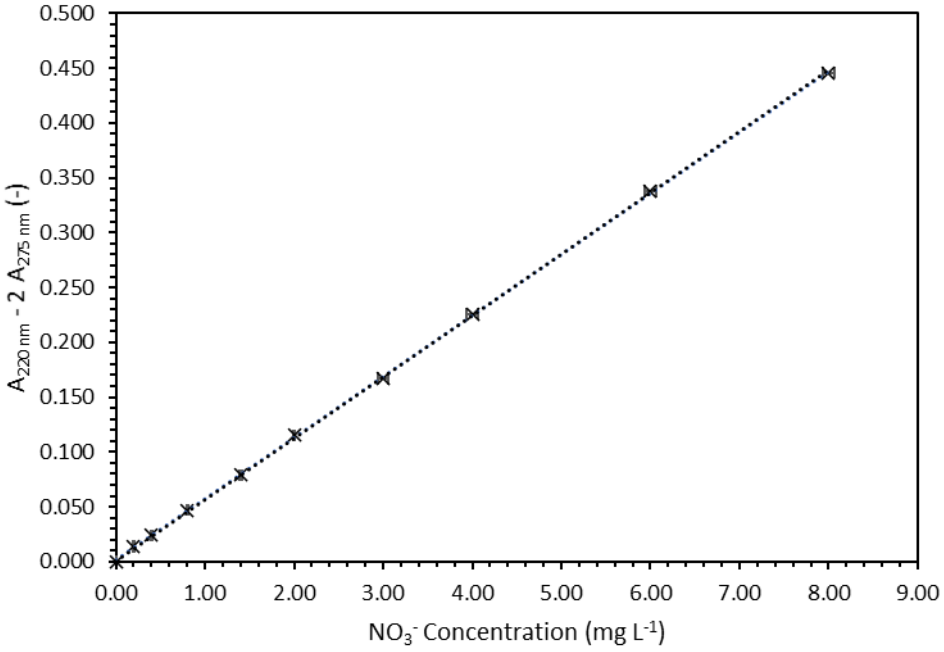

Figure 3.2 – Nitrate concentration calibration curve used for ultraviolet spectrophotometric method. Error bars represent measurement uncertainty in NO_3^- concentration.

The nitrate concentration in mg L^{-1} of the sample, $C_{NO_3^-}$, was calculated from the absorbance using Equation (3.4), where d_f is the dilution factor, $A_{220\,nm}$ is the absorbance of the sample at 220 nm and $A_{275\,nm}$ is the absorbance at 275 nm.

$$C_{NO_3^-} = 17.83\,(A_{220\,nm} - 2\,A_{275\,nm})\,d_f \qquad (3.4)$$

3.8 Incubator setup and general method for shake flask experiments

3.8.1 Apparatus

Shake flask cultures were grown in a modified MaxQ 6000 incubator (Thermo Fisher Scientific, USA) as used by Alfiarty (2018). The incubator was modified with LED lights and a gas supply system. Air and CO_2 flow rates were controlled with gas mass flow controllers (MCS series, Alicat Scientific, USA) and mixed in a 1 L Buchner flask before

being humidified in a second Buchner flask by bubbling the mixed gas through water. The humidified gas was sent to a manifold which split the gas up to 24 ways through individual stopcocks with Luer-lock fittings. The setup of the incubator is shown in Figure 3.3.

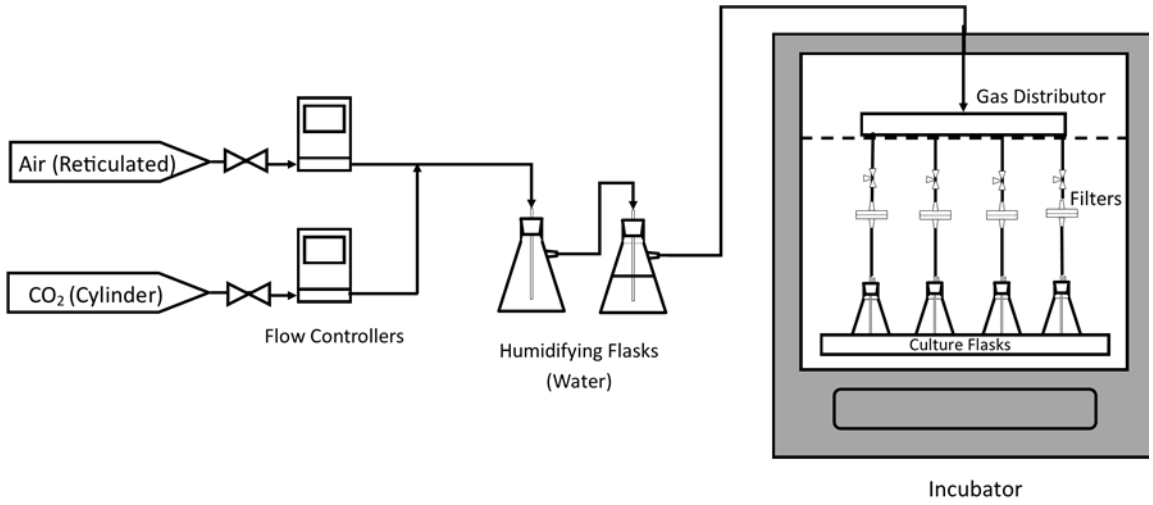

Figure 3.3 – Diagram of incubator setup for shake flask cultures.

Shake flask runs were conducted with 250 mL glass baffled flasks (KIMAX®, Kimble, USA) containing 100 mL of culture. The flasks were stoppered with a rubber stopper with two stainless-steel tubes to allow gas supply and a vent. The vent was plugged with cotton wool and covered with aluminium foil prior to sterilisation. A short section of silicon tubing was attached to the supply tube to allow connection to a filter and the gas supply manifold. 0.2 µm polytetrafluoroethylene (PTFE) syringe filters were installed in-line on each flask to sterilise the gas supply. The LED lights used were a mixture of warm white, cold white and violet which had a combined emission spectrum as shown in Figure 3.4. In all experiments the light intensity was set to its maximum value of 430–530 µmol m^{-2} s^{-1} depending on the flask position and shading from other culture flasks (typical average light intensity of 500 µmol m^{-2} s^{-1}).

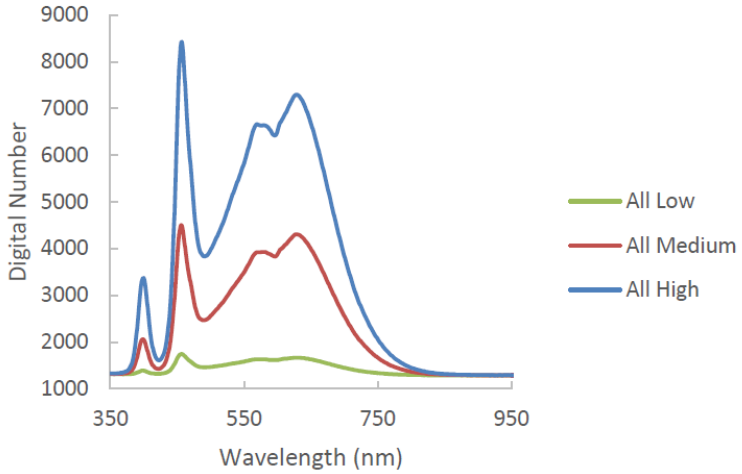

Figure 3.4 – Spectra of combination of warm white, cold white and violet LEDs used in the shaking incubator as reported by Alfiarty (2018) for low, medium and high intensity levels. Reprinted with permission.

3.8.2 Experimental methods

Manipulation and inoculation of shake flask cultures was carried out in a laminar flow biohood to avoid contamination as described in § 3.5. Shake flask cultures were conducted by inoculating cultures at an initial cell concentration of 2×10^5 cells mL^{-1} by first taking a cell count of the inoculum culture and then pipetting the required amount of inoculum into fresh media. Flasks were inoculated in duplicate for each experiment by inoculating 200 mL of fresh media to the desired cell concentration and then adding 100 mL of this inoculated media to each flask. Once inoculated, the flasks were placed in the incubator and attached to the gas supply. During experiments the flasks were rotated through different positions in the incubator tray each day to expose the flasks to a similar average light intensity over the experiment and avoid shading issues between flasks. For all experiments the shaking speed was set to 150 rpm and the temperature was 25.0 °C. The total gas flow rate was varied per experiment to ensure that all flasks were bubbled with gas; a minimum flow rate of 50 standard cm^3 min^{-1} (sccm) per flask was used.

3.9 Culture maintenance

Culture stocks were maintained in the incubator described in § 3.8. 100 mL of BBMA medium was used and the cultures were maintained in 500 mL baffled glass shake flasks (KIMAX®, Kimble, USA). CO_2 was supplied by diffusion from the atmosphere. The flasks were plugged with cotton wool and the neck and opening covered with aluminium foil. Culture stocks were typically inoculated every week and discarded after three weeks.

3.10 Airlift photobioreactor setup and general method for airlift reactor experiments

3.10.1 Apparatus

The airlift photobioreactors used in this study were those which have been previously described by Mazumda (2018) and Gopalakrishnan (2015). The airlift photobioreactors were of a concentric tube design and constructed from glass with a water jacket to allow temperature control. Temperature was maintained in the reactor by circulating water from a temperature controlled refrigerated water bath with a submersible pond pump through the water jacket on the reactor. A rubber stopper was located at the top of the reactor through which a sparger, vent, inoculum port and sampling port were located. Light was supplied from LED strips coiled around an acrylic tube located concentrically around the reactor. The spectra of the LEDs are shown in Figure 3.5 and the setup of the airlift photobioreactors is shown in Figure 3.6.

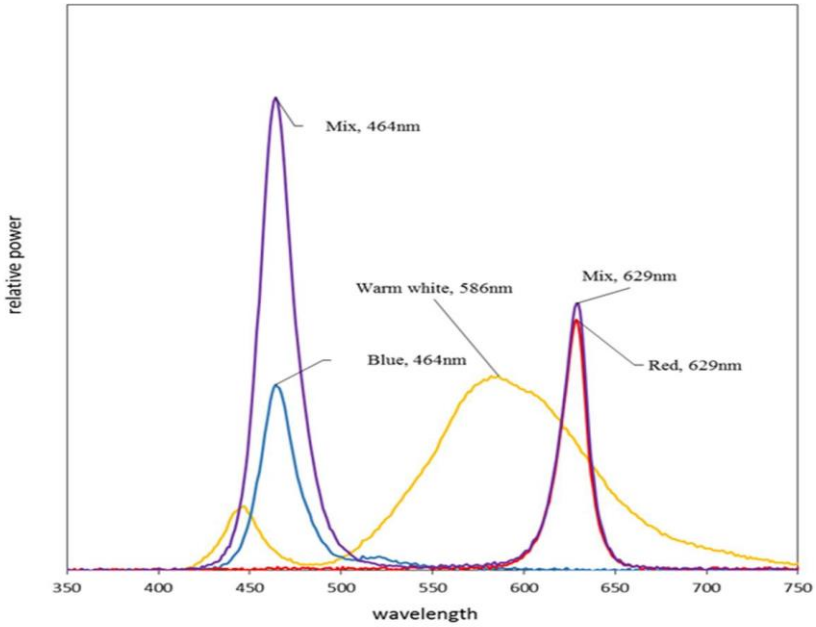

Figure 3.5 – Spectra of LEDs used in the airlift photobioreactor setup. As reported by Mazumda (2018). Reprinted with permission.

(A)

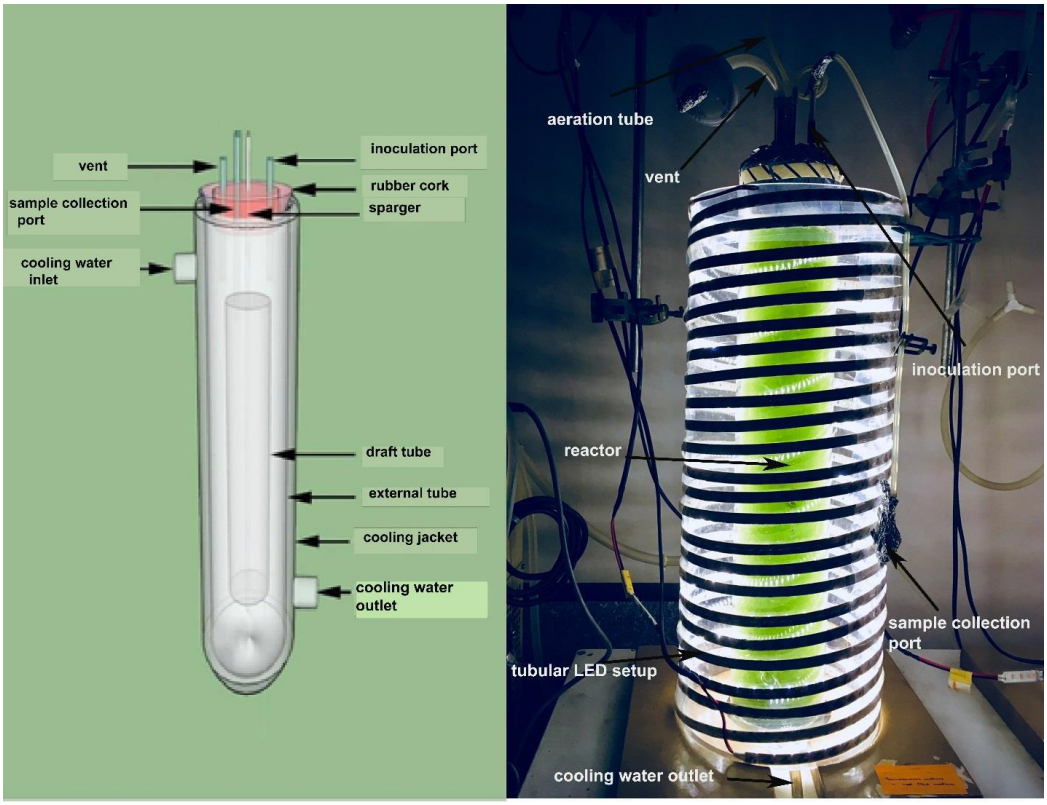

(B)

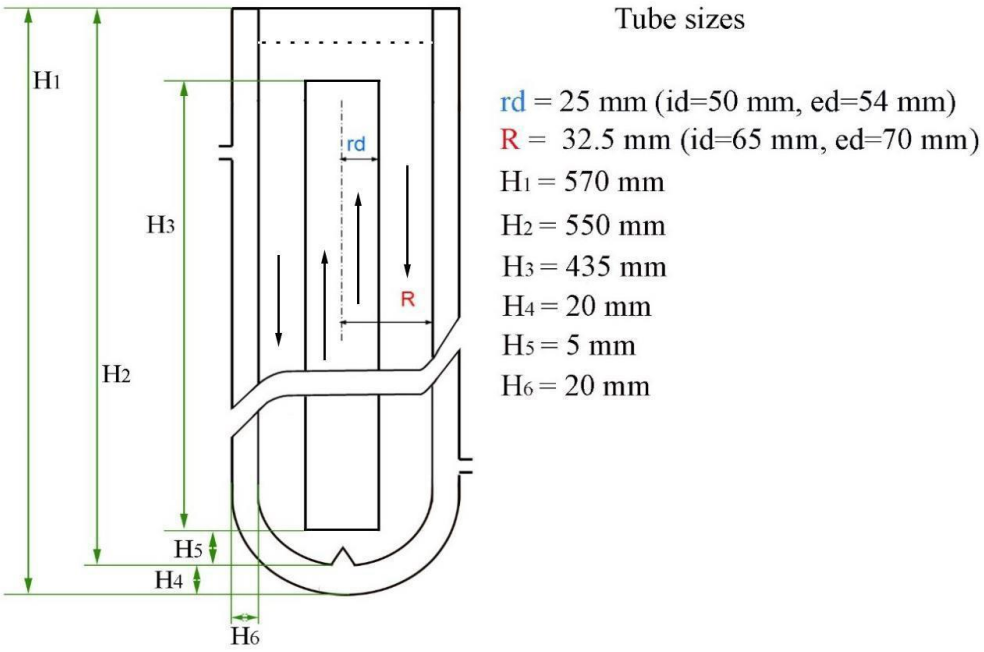

Figure 3.6 – A) Example of the setup of the airlift photobioreactors; B) Dimensions of the airlift photobioreactors. As reported by Gopalakrishnan (2015) and Mazumda (2018). Reprinted with permission.

Air and CO_2 were supplied via mass flow controllers (MCS series, Alicat Scientific, USA) and humidified by bubbling the gas mix through deionised water in a Buchner flask. A 0.2 µm inline filter was used between the humidifying Buchner flask and the reactor.

3.10.2 Experimental methods

Airlift photobioreactor cultures were conducted by inoculating 1500 mL of fresh sterile BBMA media in a biohood. The media was transferred to a modified Bucher flask to facilitate transfer of the culture to the airlift reactor. A short length of silicone tubing with a 0.2 µm filter was attached to the arm of the Buchner flask and a rubber stopper containing a stainless-steel tube connected to a length of silicone tubing was used to seal the top of the flask. The reactor was inoculated by attaching the tubing from the stopper to the inoculation port of the reactor and the 0.2 µm filter on the side arm to a compressed air supply. Compressed air was then used to pump the inoculated media from the Buchner flask into the reactor by positive pressure.

Air was supplemented with CO_2 at 3 vol% and a total flow rate of 750 standard mL min^{-1} (sccm) was used for the gas flow rate. The water bath temperature was maintained at 25.0 °C and warm white LED light was used at an intensity of 190 µmol m^{-2} s^{-1} (except for the wavelength experiment in § 6.4.3 where red and blue LED lights were as described further in that section).

3.11 General method for tubular photobioreactor experiments

The tubular photobioreactor that was used for these experiments was that which is described in detail in § 4. The following covers the general experimental methods used for the preparation and running of culture studies in the reactor.

3.11.1 Cleaning and sanitisation of tubular photobioreactor

Cleaning of the tubular photobioreactor was carried out in a series of stages. Immediately following the harvest of a completed run the reactor was filled with tap water and 2 L of 42 g L^{-1} sodium hypochlorite solution was added (final diluted concentration of approximately 1 g L^{-1}). The pump was run at a frequency of 30 Hz (liquid velocity of approximately 1.3 m s^{-1}) for at least one hour to circulate the bleach solution and kill any remaining microalgae in the reactor before it was drained. Following this, the reactor was rinsed twice with tap water, running the pump at a frequency of 30 Hz for around 15 minutes for each rinse cycle.

Once the reactor was rinsed, the glass elbows on the solar receiver section and rubber couplers were removed and washed with detergent and water. A soft brush was used to remove biofilm that had formed on the rubber coupler sleeves and a microfibre cloth was used to clean the inside of the glass elbows without causing scratches. All components were rinsed thoroughly with tap water to remove detergent residue.

The straight glass tubes were cleaned by spraying the inside surface with a 1 wt% sodium hypochlorite solution and a ball of dampened paper towels forced down the tube to mechanically remove any biofilm that remained. This process was repeated at least two times for each tube until no biofilm traces could be seen on visual inspection of the glass tubes. Once the tubes were clean the elbows and couplers were reinstalled following the recommended procedure from SCHOTT AG (2017b).

The bubble column was cleaned by removing it from the reactor frame and removing the internal heat exchanger and sparger. A microfibre cloth and detergent were used to remove biofilm from the walls of the bubble column without causing scratches. The heat exchanger and sparger were cleaned with detergent and a soft brush or microfibre cloth as appropriate to remove remaining biofilms. All components were washed thoroughly with tap water before reassembling. To clean the PVC pipes connecting the pump, bubble column and solar receiver, they were first removed from the reactor and then cleaned using a jet of water and detergent to remove any biofilm.

Once the components had been cleaned of any biofilm residues they were reassembled, and the reactor was filled with tap water. To the circulating tap water, 500 mL of concentrated hydrochloric acid was slowly added (to give a diluted concentration of approximately 0.1 mol L^{-1}). The acid solution was circulated for around one hour with the pump frequency set at 30 Hz to dissolve any adsorbed minerals from the reactor components. The reactor was then rinsed at least twice with tap water, or until testing with litmus paper showed the rinse water was neutral. During the rinse cycles the water was pumped around in a similar fashion to the previous rinsing cycles.

Prior to sanitisation of the reactor, the tubing used for inoculation and the 0.2 µm filter used to sterilise the culture media were autoclaved at 121 °C for 20 minutes. The pH probe was also calibrated prior to beginning the sanitisation process and the electrolyte in the dissolved oxygen probe replaced. To begin the sanitisation, the reactor was filled with tap water and sodium hypochlorite solution was added to achieve a concentration of

approximately 2 g L^{-1}. The inoculation and media supply tubes were rinsed with the solution by using a large syringe to suck the solution through the tubes. Once the tubes were rinsed with the solution, the sterilised filter and inoculation tubes were attached. The bleach solution was circulated through the reactor overnight (typically 12–18 hours) and then it was drained. The reactor was then rinsed twice with 0.2 µm filtered tap water, or until testing with litmus paper showed the rinse water was neutral. This was followed by a rinse with reverse osmosis water (>10 MΩ cm) which was also pumped in through the 0.2 µm filter.

3.11.2 Preparation of reactor and media, and inoculation of culture

The sanitised and rinsed reactor was filled with media prepared with reverse osmosis water (>10 MΩ cm) to which the required stock solutions for BBMA media, as described in § 3.4, were added (760 mL of each of the macronutrient stocks and 152 mL of the micronutrient stock). The media was pumped into the reactor through the 0.2 µm filter from 20 L plastic carboys.

Once the media was pumped into the reactor, it was circulated with the pump set at the speed desired for the experiment to be performed. Compressed air and CO_2 were also introduced at the flow rates to be used for the experiment (typically 7.37 standard L min^{-1} air and 0.23 standard cm^3 min^{-1} CO_2). The lights were turned on to the required setting and water bath turned on to bring the temperature of the media to 25 °C. The media was circulated for at least an hour with bubbling to ensure the media was well mixed, at the correct temperature, and to calibrate 100% air saturation for the dissolved oxygen probe.

A cell count was performed on the inoculum culture and the required volume of inoculum determined to give an initial cell density of 5×10^5 cells mL^{-1}. This volume of media was then drained from the tubular photobioreactor to maintain the working volume at 76 L. The airlift reactor was then disconnected from its setup and the inoculum tube from the tubular photobioreactor was attached to the sparger tube connection of the airlift reactor, the connection was sanitised with 70% ethanol solution during this process. The required volume of inoculum was then pumped into the reactor using a peristatic pump at a flow rate of around 50 mL min^{-1} until the total required volume had been added. Once the culture was inoculated it was allowed to mix for around one hour before a sample was taken to determine the initial cell count.

3.11.3 Sample harvesting

Samples of the culture were taken primarily from the drain ports located on the pump. For a typical cell count, around 20–50 mL of culture was collected into a beaker to flush the sampling port and then 20 mL of culture was collected into a separate beaker for analysis. Samples for the cell counts were taken immediately from the beaker before cells could settle out, then diluted and counted as described in § 3.1. The remaining culture sample was then used for other analyses, such as nitrate concentration analysis. Larger samples were taken in a similar fashion by, again, flowing a small volume of culture through the sampling port to flush it and then collecting the required volume of culture into the desired vessel. For biomass concentration and fatty acid analysis, typically 250 mL of culture was harvested then processed as described above and below for the desired analysis.

At conclusion of a culture run, the culture was harvested by the main drain valve below the bubble column. The first litre of culture harvested was disposed of to flush the drain line and then the rest of the culture was harvested into plastic 20 L carboys.

3.12 Oxygen evolution rate measurement

The apparatus and methods used to measure the oxygen evolution rate were based on that reported by Brindley *et al.* (2010) and Ippoliti *et al.* (2016) with adaptions made as outlined below.

3.12.1 Apparatus and characterisation

The apparatus consisted of a lighting array, culture vessel, magnetic stirrer, temperature-controlled water bath with inbuilt circulating pump, dissolved oxygen probe, and datalogger connected to a computer. The lighting array consisted of 4.5 m total length of SMD5050, 4-in-1 RGBWW LED strips (60 LED/m). The LEDs were dimmed by pulse width modulation (PWM) controlled by an Arduino Uno via IRF520N MOSFET modules, one for each colour channel. Light intensity was controlled by varying the PWM value outputted by the Arduino, where a PWM value of 0 was off and a PWM value of 255 was full brightness. The LED strips were attached to the inside of an aluminium cylinder, 150 mm high and 150 mm in diameter, with each section of LED strip spaced equally around the circumference.

The culture vessel was constructed from borosilicate glass and had a cylindrical culture chamber 40 mm in diameter and 100 mm in height. The base of the chamber was

slightly curved to aid cell dispersion and to centre the stirrer bar. The chamber was surrounded by a water jacket approximately 10 mm thick on the sides and base. The water jacket was connected to the water bath pump with silicon tubing. A PVC stopper, machined to hold the dissolved oxygen probe, was set loosely in the flask opening to reduce oxygen mass transfer from the surface of the culture while maintaining atmospheric pressure. The culture flask was placed on a magnetic stirrer and a Teflon-coated stirrer bar (size A15, olive shaped) was used to stir to the flask at 800 rpm. The temperature of the refrigerated water bath was regulated by a water bath controller to within ± 0.1 °C.

Dissolved oxygen levels were measured with a polarographic-style probe (Orion 083005MD, Thermo Fisher Scientific, USA) and datalogged on a computer with StarCom 1.0 software (Thermo Fisher Scientific, USA) via a dissolved oxygen meter/datalogger (Orion Star A223, Thermo Fisher Scientific, USA). The software also allowed logging of the temperature of the sample in the flask. The entire setup was arranged as in Figure 3.7 and Figure 3.8. Aluminium foil was used to cover the setup to exclude external light from entering the flask during the experiments.

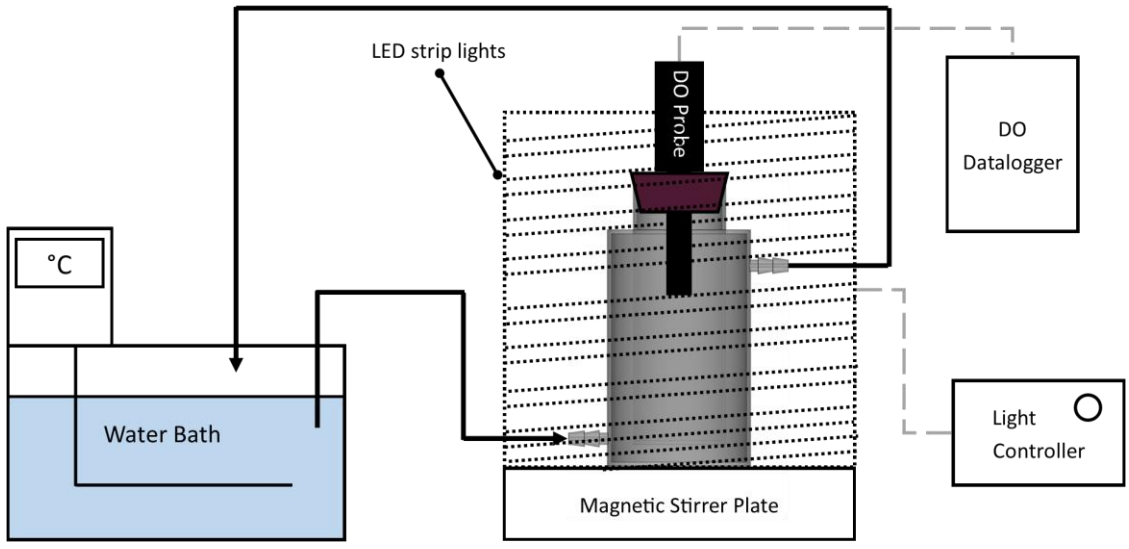

Figure 3.7 – Experimental setup of oxygen evolution apparatus. DO: dissolved oxygen.

(A)

(B)

(C)

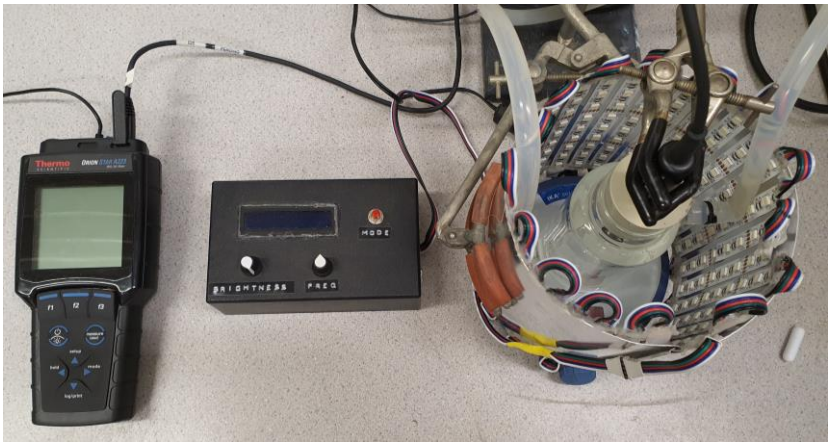

Figure 3.8 – Photos of experimental setup of oxygen evolution apparatus. A) flask; B) flask with lighting array; C) overall setup (aluminium foil covering on lighting array not present).

Light array characterisation

The light intensity of the lighting array was measured as described in § 3.6. Light intensities were measured for each light colour for a series of PWM values, V_{PWM}, as shown in the calibration curves in Figure 3.9. The non-linear response of the calibration curve for the combined colours was due to voltage drop from the power supply as the power demand increased. Light intensity was measured in absence of the culture flask. The light intensity in µmol m^{-2} s^{-1} was related to the PWM values according to Equations (3.5) to (3.9).

$$I_{all} = -0.00802\, {V_{PWM}}^2 + 9.87\, V_{PWM} \quad (3.5)$$

$$I_{red} = 1.28\, V_{PWM} \quad (3.6)$$

$$I_{green} = 1.77\, V_{PWM} \quad (3.7)$$

$$I_{blue} = 3.07\, V_{PWM} \quad (3.8)$$

$$I_{white} = 5.24\, V_{PWM} \quad (3.9)$$

The spectra of the LED strips used to illuminate the culture flask were measured as described in § 3.6 in a darkened room to avoid erroneous values from external light sources. Relative intensities were measured in 1 nm increments. The spectra of the LEDs in the 350–750 nm range can be seen in Figure 3.10, there was negligible light produced outside this range.

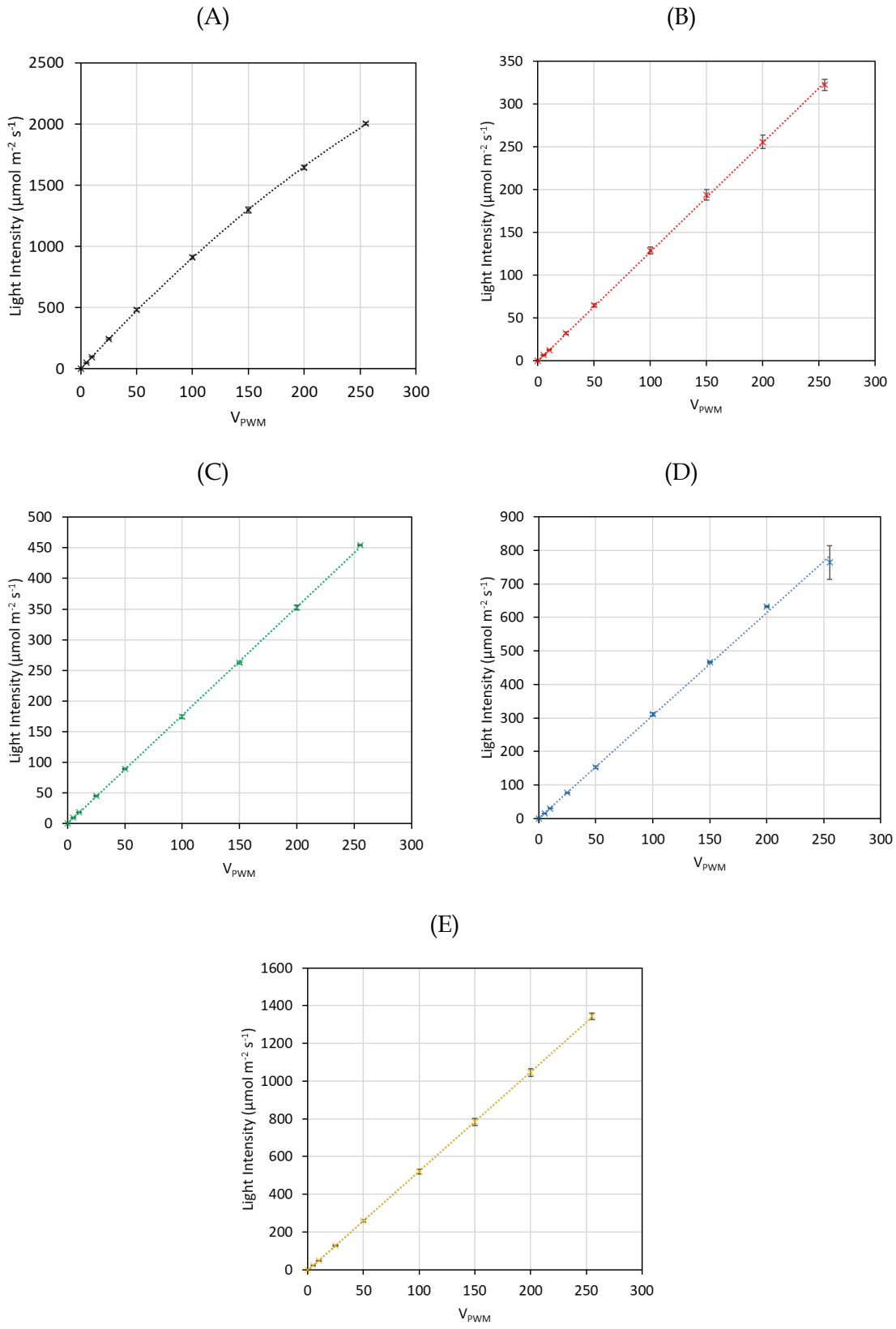

Figure 3.9 - Light intensity calibration curves for LED array of oxygen evolution apparatus. A) All colours; B) Red; C) Green; D) Blue; E) Warm white.

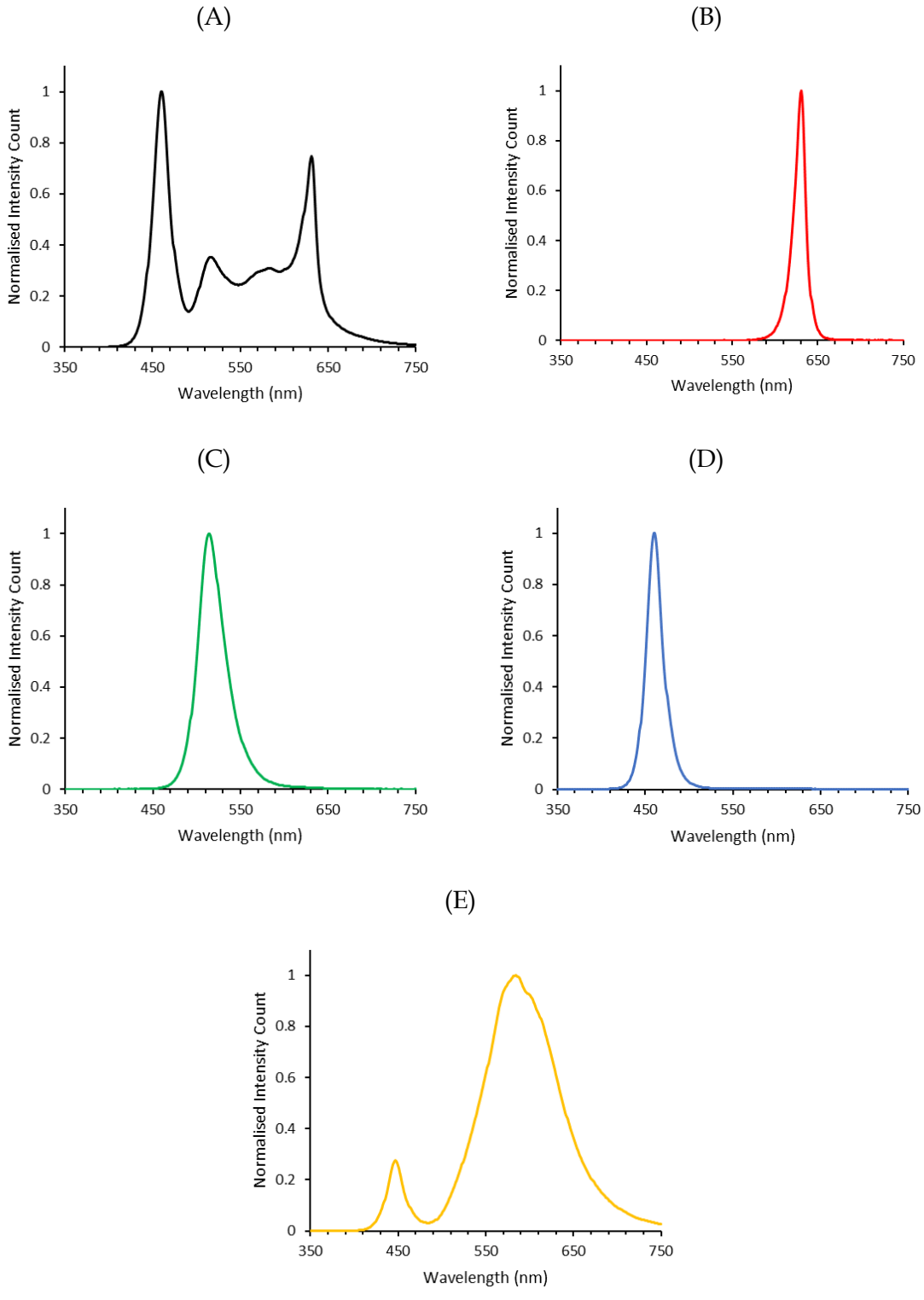

Figure 3.10 - Spectra of LEDs used in the lighting array for the oxygen evolution rate apparatus. A) All colours; B) Red; C) Green; D) Blue; E) Warm white.

3.12.2 General experimental method

Prior to each batch of experiments the dissolved oxygen probe was calibrated using the water-saturated air method as described in the user manual using the meter's built-in calibration method (Thermo Fisher Scientific Inc., 2007). The probe electrolyte solution was replaced daily to ensure consistent readings.

Fresh BBMA medium was used for all experiments. The medium was bubbled with air supplemented with 3 vol.% CO_2 for a minimum of one hour prior to experiments to maintain dissolved oxygen at 100% air saturation and saturate the media with dissolved CO_2 to avoid carbon limitation during the experiments. For a typical experiment, 100 mL of media was poured into the flask and the lights were turned on to the desired setting. The media was allowed to mix with the magnetic stirrer at 800 rpm until the temperature and dissolved oxygen levels were constant (typically up to 15 minutes). Once the media had equilibrated the inoculum culture was pipetted into the flask to reach the desired cell concentration for the experiment (typically between 1–2 × 10^6 cells mL^{-1}). Datalogging of temperature and dissolved oxygen concentration was started at this point and readings were taken every three seconds using the StarCom software.

Readings were taken for 15 to 30 minutes under the desired light conditions and then the lights were turned off to record the oxygen consumption rate for a further 15 to 30 minutes. At the conclusion of the experiment a cell count was taken on the experimental culture as described in § 3.1.1 to determine the cell density. Following the experiment, the culture was disposed of and fresh media and inoculum used to conduct the next experiment to avoid any cumulative effects from different treatments.

3.12.3 Data analysis

Data that was logged from each experiment was exported to Microsoft Excel where the LINEST function was used to determine the rate of increase or decrease of dissolved oxygen over the experiment. The function was applied over the linear region of dissolved oxygen rate of change (typically from 3 minutes to 13 minutes elapsed time of light and dark treatments). The rate of oxygen evolution measured in mg L^{-1} s^{-1} was then converted to fmol $cell^{-1}$ s^{-1} to allow comparison of the different conditions and account for variations in cell density. The net oxygen evolution rate was determined by the difference of the rate found under the light conditions and dark conditions.

3.13 Modified Bligh and Dyer lipid extraction

Lipids were extracted from freeze-dried biomass following the procedure reported by Cavonius *et al.* (2014), based on the commonly used Bligh and Dyer method (Bligh & Dyer, 1959). To avoid oxidation of lipid species, centrifuge tubes and flasks were flushed with argon or nitrogen to displace any air whenever possible. Flasks and tubes were also shielded from light with aluminium foil whenever possible to avoid degradation of pigments or solvents. All chemicals used were of analytical reagent or HPLC grade. The chloroform used in all cases contained between 1% and 3% ethanol as a stabiliser.

A typical extraction was carried out as follows: 200 mg of freeze-dried biomass was reconstituted with 800 µL of water in a 15 mL centrifuge tube and allowed to stand for one hour at room temperature. Following this, 3 mL of 1:2 (v/v) chloroform/methanol solution was added to the tube to reach a composition of 0.8:1:2 (v/v) water/chloroform/methanol and the mix was vortexed for two minutes on medium-high speed. To this, 1 mL of chloroform was added, the tube vortexed for approximately 30 seconds, 1 mL of water added to reach a final composition of 1.8:2:2 (v/v) water/chloroform/methanol, and the tube vortexed again for 30 seconds. The tube was then centrifuged in a fixed-angle rotor centrifuge at 2500 × rcf for six minutes. Using a glass Pasteur pipette, the upper aqueous phase was discarded. Using another glass Pasteur pipette, the lower chloroform phase was recovered by carefully punching thorough the biomass layer to collect the lower solvent layer. The chloroform phase was collected in a capped glass test tube. 1 mL of chloroform was added to the remaining biomass in the centrifuge tube, the tube vortexed for 30 seconds and then centrifuged under the same conditions as before. The chloroform phase was recovered as before, and the combined recovered phases were transferred to a pre-weighed 25 mL round-bottom flask. The chloroform phase was passed through a 0.2 µm syringe filter to remove any residual biomass. Glassware was rinsed three times with chloroform (approximately 0.5 mL per rinse) to ensure quantitative recovery of lipids.

A rotary evaporator was used to remove the solvent under vacuum at 332 mbar with the water bath at 40 °C. Lipid extracts were re-dissolved in a small, known volume (typically 250 µL) of chloroform and stored under argon or nitrogen at ≤−18 °C when not processed further immediately following extraction. Lipid yields were determined by weighing a pre-dried aluminium pan and adding a small aliquot of lipid extract (e.g. 50 µL) to the pan. The chloroform was allowed to evaporate and then the pan was

placed in a desiccator. The pan with dried lipid extract was reweighed until a constant weight was reached. This was repeated three times to obtain an average lipid yield.

3.14 Isopropanol lipid extraction

Extraction of lipids by the isopropanol method to prevent degradation of lipids by enzymes was conducted based on the method reported by Kates (1986, p. 107). Approximately 1.5 g of wet biomass was harvested from an actively growing culture by centrifugation (6,500 × rcf, 10 minutes) and the culture media discarded. To the collected wet biomass in a 50 mL centrifuge tube 4 mL of deionised water was added, followed by approximately 20 mL of hot isopropanol at 60 °C. The mix was vortexed on medium-high speed for 5 minutes and then centrifuged (6,500 × rcf, 10 minutes). The supernatant was decanted into a 100 mL round bottom flask and approximately 10 mL of 60 °C isopropanol was added to the biomass pellet in the centrifuge tube. The tube was vortexed again for 5 minutes and centrifuged as before. This process was completed twice with the isopropanol from each step collected in the round bottom flask. Following this, the biomass was extracted once more with approximately 10 mL of isopropanol/chloroform (1:1, v/v), vortexed and centrifuged as before, and the supernatant collected in the round bottom flask. The combined extracts were evaporated under vacuum on a rotary evaporator until the volume was reduced to around < 1 mL. 20 mL of methanol/chloroform (1:1, v/v) was added to the residue and it was transferred to a centrifuge tube where 9 mL of deionised water was added. The mix was centrifuged (2,500 × rcf, 6 minutes) and the lower organic phase collected into another 100 mL round bottom flask. The aqueous layer was washed with 10 mL of chloroform twice and the organic phases collected in the round bottom flask. The combined organic extract was evaporated to near dryness under vacuum on a rotary evaporator, then under a stream of nitrogen at 30 °C to complete dryness. 5 mL of chloroform/methanol (2:1, v/v) was used to dissolve the dried extract and it was stored in a capped glass test tube under nitrogen at ≤−18 °C if not used immediately for further analyses.

3.15 Fatty acid methyl ester derivatisation

Derivatisation of the fatty acids to form methyl esters was carried out according to the methanolic sulphuric acid method reported by Christie (1989, p. 38). The solvent was removed from the lipid extracts to be derivatised by evaporation under vacuum on a rotary evaporator or under a stream of nitrogen and the lipids (up to 50 mg) were then dissolved in 1 mL of toluene. The dissolved lipids were transferred to a glass test tube with

a screw cap and 2 mL of 1 vol% sulphuric acid in methanol was added. Once added, the test tube was capped and shaken briefly before placing into a water bath at 50 °C overnight (12 – 18 hours). After the incubation, 5 mL of 5 wt% aqueous sodium chloride solution was added to the tube and the methyl esters were then extracted using 5 mL of n-hexane twice. The n-hexane phases were recovered with a glass Pasteur pipette and combined then washed with 4 mL of 2 wt% aqueous sodium bicarbonate solution. The resultant n-hexane phase was dried by addition of approximately 2 g of anhydrous sodium sulphate and the solution was then filtered with a 0.2 µm PTFE syringe filter and the n-hexane removed under vacuum on a rotary evaporator. The resultant fatty acid methyl esters were then dissolved in the desired solvent for GC analysis as below.

3.16 Gas chromatographic (GC) analysis of fatty acid methyl esters

The method used for GC analysis of fatty acid methyl esters was based on the BS EN 14103:2011 standard (British Standards Institution, 2011) with adaptions made as described below. Analysis of fatty acid methyl esters was conducted using a gas chromatograph (GC) equipped with a flame ionisation detector (FID) (GC 2010 Plus, Shimadzu, Japan) and autosampler (AOC-6000, Shimadzu, Japan). The samples were run on a Stabilwax® column (30 m × 0.25 mm × 0.25 µm; Restek, USA). Prepared fatty acid methyl esters were dissolved in toluene and transferred to a 2 mL septum-capped glass vial. The injection volume used was 1 µL and the injection port was held at 240 °C. Ethanol was used as the rinse solvent for the autosampler. Helium was used as the carrier gas at a rate of 1 mL min^{-1} on constant flow mode. The temperature program was as follows: Held at 60 °C for 2 minutes, temperature increased to 200 °C at a rate of 10 °C min^{-1} then increased to 240 °C at a rate of 5 °C min^{-1}. The final temperature was held for 20 minutes. The FID temperature was set at 250 °C.

Chromatograms were analysed using Lab Solutions software (Shimadzu, Japan) and Microsoft Excel. Quantitative results were obtained with comparison of peak areas. Retention times were determined based on comparison with known lipid samples of commercial canola and fish oil and a saturated fatty acid methyl ester standard mix (F.A.M.E Mix C8–C24, Sigma Aldrich, USA).

3.17 Thin layer chromatography (TLC) of lipid extracts

Thin layer chromatography was carried out according to the general methods reported by Kates (1986) and as modified by Xia (2019) and described below. Aluminium

backed pre-coated silica TLC plates were used (0.20 mm silica gel 60, ALUGRAM® SIL G, Macherey-Nagel, Germany). Sheets were cut down to 100 mm x 100 mm squares using a sharp and clean utility knife without chipping the silica coating. A typical plate was eluted by first filling a 1000 mL glass beaker with the desired solvent to a depth of approximately 5 mm. The beaker was then flushed with nitrogen and the beaker covered with aluminium foil. This was allowed to sit at room temperature for at least 10 minutes to allow the atmosphere within the beaker to be saturated with the solvent vapour. The solvents used depended on the separation desired and were as specified in the relevant later sections.

Lipid samples to be separated were added to the TLC plate by spotting 100 µL of lipid extract dissolved in chloroform (with a concentration of approximately 10 mg mL^{-1}) on the bottom of the plate around 15 mm from the edges of the plate. For two-dimensional plates the spot was placed to the bottom-left corner of the plate. The sample solvent was allowed to evaporate under a nitrogen atmosphere for around 10 minutes or until all residual solvent had evaporated. Once the sample spot was dry, the plate was loaded into the beaker so the edge of the plate closest to the sample spot was at the base of the beaker. In all cases the solvent level in the beaker was high enough to be in contact with the bottom edge of the silica coating, but never so high that it was in contact with the sample spot. The beaker was briefly flushed with nitrogen again and the aluminium foil was replaced. The plate was exposed to the solvent until the solvent front on the silica coating was observed to reach approximately 5–10 mm from the top edge of the plate (typically 30–50 minutes depending on the solvent). At this point the plate was removed from the beaker and placed into a nitrogen atmosphere to dry at room temperature until all solvent was removed from the plate. For two-dimensional plates the plate was then introduced into another beaker, prepared similarly to the first, containing the second elution solvent but this time at 90 ° to the direction of the first elution by rotating the plate 90 ° anti-clockwise. The plate was allowed to dry under nitrogen as before.

Once the plate was fully dry the lipids were visualised using iodine by introducing the plate into a watchglass-covered beaker containing approximately 3 g of iodine crystals which had been allowed to vaporise for around 10 minutes prior to introducing the plate. Plates were exposed to the iodine vapour for around 5 minutes or until bands or spots could be seen clearly developing on the plate. Separated lipid classes were seen as yellow-brown bands or spots on the plate. A translucent weighing paper was placed over the stained plate and used to trace the locations of the separated lipid regions on the plate.

As iodine interfered with further analysis of lipid spots by reacting with lipid species, the traced outlines from the stained plate were used to determine the location of the classes on a non-stained plate prepared in an identical fashion.

Once the regions of the plate had been identified which contained the lipid classes of interest, the silica coating was carefully scraped from the non-stained plate using a clean metal spatula. The removed silica containing the lipids of interest was collected on a weighing paper and added to a centrifuge tube with approximately 1 mL of chloroform and vortexed on medium-high speed for 30 seconds to extract the lipids from the silica. The silica-chloroform mix was centrifuged (2500 × rcf, 6 minutes), and the chloroform recovered to a glass test tube. This process was repeated with the silica pellet twice more to ensure quantitative recovery of lipids. The recovered chloroform from each extraction was combined in the same test tube and then evaporated under a stream of nitrogen at 30 °C to allow redissolution of the lipids in another solvent for further analysis or preparation, such as fatty acid analysis, as described in other sections.

3.18 High performance liquid chromatographic (HPLC) analysis of lipid extracts

The HPLC apparatus used for this study was an UltiMate 3000 series HPLC equipped with a charged aerosol detector (CAD) (Thermo Fisher Scientific, USA). In all cases HPLC grade solvents were used and were degassed by sonication prior to use. The general method used for HPLC analysis was as follows. Lipid samples to be analysed were evaporated and dissolved in the injection solvent required for HPLC analysis. The dissolved lipids were filtered with a 0.2 µm PTFE syringe filter and transferred to a 2 mL septum-capped glass vial which was placed in the HPLC autosampler. Mobile phases were prepared by measuring out the required volumes of individual solvents and mixing in 1 L glass Schott bottles. The column was equilibrated with the initial solvent at the required flow rate and temperature. Once the system was equilibrated, the sample was injected, and the mobile phase was altered as desired for the method being run. Separation of lipids was determined by detection by the CAD. Results from the HPLC were analysed using the Chromeleon software (Thermo Fisher Scientific, USA). Individual HPLC methods and solvents used were as described in the relevant sections.

3.19 Mass spectrometric analysis of lipids

Mass spectrometry of lipids was conducted by two parties in this study. In-house mass spectrometric analysis was conducted by Dr. Marie Squire and Dr. Amanda Inglis at the School of Physical and Chemical Sciences at the University of Canterbury using a MaXis II UHR-QToF mass spectrometer (Bruker, USA). Electrospray ionisation (ESI) was used as the ion source in positive mode. The scan range was 50 to 1300 m/z, the capillary voltage was 3000 V, plate offset was −500 V and collision cell RF was 1800 Vpp. The nebuliser was set to 1.0 bar, the dry heater at 120 °C and dry gas flow rate of 6.6 L min^{-1} (Xia, 2019).

External mass spectrometric analysis of lipids was conducted by Dr. Alastair Ross at AgResearch Limited (Lincoln, New Zealand) using a LCMS 9030 LC-qToF mass spectrometer (Shimadzu, Japan). LC-MS was used to analyse lipid classes that had been separated by TLC prior to analysis. Fragmentation of lipid species was also attempted to search for characteristic fragments of possible head groups of lipid classes. The LC-MS solvents used were water/acetonitrile and water/acetonitrile/isopropyl alcohol and the column was a C_{18} column (Waters CSH, Waters, USA). ESI was used in positive ion mode and fragmentation was attempted by ramping up the collision energy between 17–29 eV as well as tests up to 60 eV.

3.20 Fatty acid analysis by an external party

External analysis of the fatty acid composition of microalgae biomass was conducted by Callaghan Innovation (Wellington, New Zealand). Biomass samples were freeze-dried as described previously before being sent for analysis. The method they used for analysis was as follows (K. Lagutin, 18th October 2019, personal communication). Freeze-dried biomass was methylated directly according to Carreau and Dubacq (1978) at 80 °C. Samples were analysed by an Agilent 7890B gas chromatograph equipped with a flame ionization detector (FID) and DB-WAX UI (30 m x 0.25 mm i.d., 0.25 µm) capillary column. Helium was used as the carrier gas with a split ratio of 1:100. The injector and detector temperatures were both 280 °C. The oven temperature was held at 200 °C. 23:0 methyl ester was used as an internal standard. GLC-714 standard (Nu-Check, USA) was used to calculate the empirical correction factors for FID. Fatty acids were identified by comparison with standards and by using equivalent chain lengths.

4 Tubular Photobioreactor Design and Characterisation

4.1 Introduction and design objective

Tubular photobioreactors are the most promising photobioreactor for large-scale culturing of microalgae for high-value products (Acién Fernández *et al.*, 2013; Tredici *et al.*, 2013). Due to this it was desired to investigate how cultures of *Trachydiscus* sp. LCR-Awa-9-2 performed in this style of photobioreactor. To investigate this, a laboratory scale tubular photobioreactor was constructed. For this project the objectives of the laboratory scale reactor were to:

- Allow axenic culturing of *Trachydiscus* sp. LCR-Awa-9-2
- Allow control and measurement of culture parameters such as temperature, liquid and gas flow rates, pH, light intensity, and dissolved oxygen
- Allow batch and continuous culturing
- Investigate and determine the optimal culture conditions in tubular photobioreactors to maximise EPA productivity
- Provide data for refinement of the design of future tubular photobioreactors for *Trachydiscus* sp. LCR-Awa-9-2
- Provide data for potential scale up and modelling

The major design constraint for the reactor was that it was to be laboratory scale and limited to approximately 50 L in total volume. The following sections cover the design process used to design the reactor and a summary of the final reactor that was used for this study.

4.2 Design of the tubular photobioreactor

4.2.1 Bubble column

The bubble column of a tubular photobioreactor performs two main functions: stripping of oxygen from the culture, and supply of carbon dioxide (Chisti, 2007). The main considerations in the design of the bubble column are mass transfer of these two gasses. Additionally, the bubble column is where the heat exchanger is often located to control the temperature of cultures. The bubble column design involved selection of the bubble column material, design of the column geometry, gas sparger and heat exchanger, and determination of the expected mass transfer characteristics for oxygen and carbon dioxide. The following section covers the design process of these aspects.

Material selection

Bubble columns can be constructed from a variety of materials, typically being glass or plastics (Becker, 1994; Tredici *et al.*, 2013). Acrylic was chosen as the material for the bubble column in this study. Acrylic was readily available in suitable diameters, provided good optical properties and allowed easy addition of ports for sensors. It is also relatively chemically inert and was unlikely to leach chemicals into cultures or be damaged by the chemicals used for the culture media or cleaning. 316 stainless-steel was used for the concentric reducer at the base of the column and for the pipework located within the bubble column such as the heat exchanger and sparger due to its chemical stability.

Geometry

The aspect ratio (height to diameter) is one of the key design characteristics for bubble columns. The aspect ratio should be in the region of 2 to 5 (height/diameter) for biochemical applications (Kantarci *et al.*, 2005). However, many tubular photobioreactors employ aspect ratios in the region of 10 (Bosma *et al.*, 2014; Fernández *et al.*, 2014; Luangpipat, 2013). Increasing the diameter decreases the liquid velocity in the column and increasing the length results in a longer residence time. However, the volume had to be kept within the laboratory scale constraints which limited the dimensions of the column. Typical volume ratios for the bubble column are approximately 15% to 30% of the total reactor volume (Becker, 1994; Bosma *et al.*, 2014) which gave a volume constraint of approximately 20 L for the column.

For laboratory scale tubular photobioreactors of similar volumes, a bubble column diameter of approximately 150 mm is common (Becker, 1994; Luangpipat, 2013). This diameter provides a balance between liquid velocity, residence time and total volume. Allowing for a maximum aspect ratio of 10, the total liquid height should be approximately 1.5 m. Thus, the maximum volume of the bubble column of this geometry was 23 L which complied with the standard volume ratio of up to approximately one-third of the total reactor volume. Of the available standard diameters, a tube of 150 mm outside diameter (OD) and 140 mm inside diameter (ID) was the best compromise for cost and suitable dimensions. Head space must also be supplied above the operating liquid level to allow for bubble disengagement and formation of foam (Chisti, 1998). Due to this, the total height of the bubble column was 1.8 m in order to allow for head space above the operating liquid level.

The inlet to the bubble column from the solar receiver is generally located at the top of the bubble column in tubular photobioreactors (Acién Fernández *et al.*, 2013). However, due to the diameter of the bubble column on this scale the inlet was chosen to enter in the side of the bubble column in the head space. Placing the inlet above the liquid level provides additional mixing and can help to control potential foam formation, although it can also cause it (Vardar-Sukan, 1998). The inlet was located so that if foam was produced by the inlet being above the liquid level the level could be increased so that the inlet was below the liquid surface but still maintain sufficient head space for bubble disengagement.

The transition between the diameter of the bubble column base and the tubing connecting to the pump was made with a concentric reducer to minimise entrance effects from dramatic diameter changes which may damage cells. The angled reducer was also chosen to prevent potential settling of cells that could happen on a horizontal surface.

Bubble size, rise velocity, entrainment, and gas holdup

For ideal operation, bubble columns should operate in the homogeneous bubbly regime as shown in Figure 4.1. As the ID of the bubble column was 140 mm, the theoretical upper limit for the superficial gas velocity was approximately 0.05 m s^{-1} as per Figure 4.2.

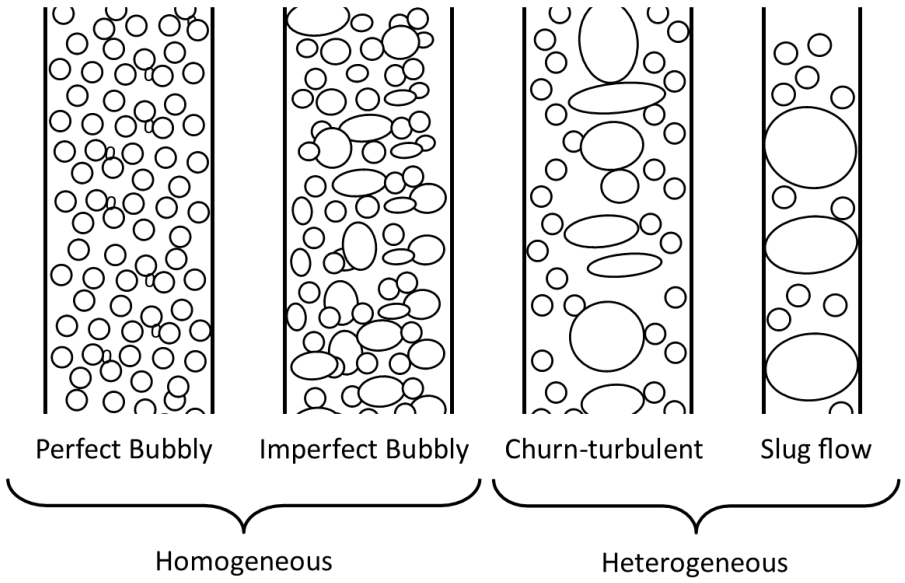

Figure 4.1 – Flow regime patterns in bubble columns. Based on Kantarci et al. (2005).

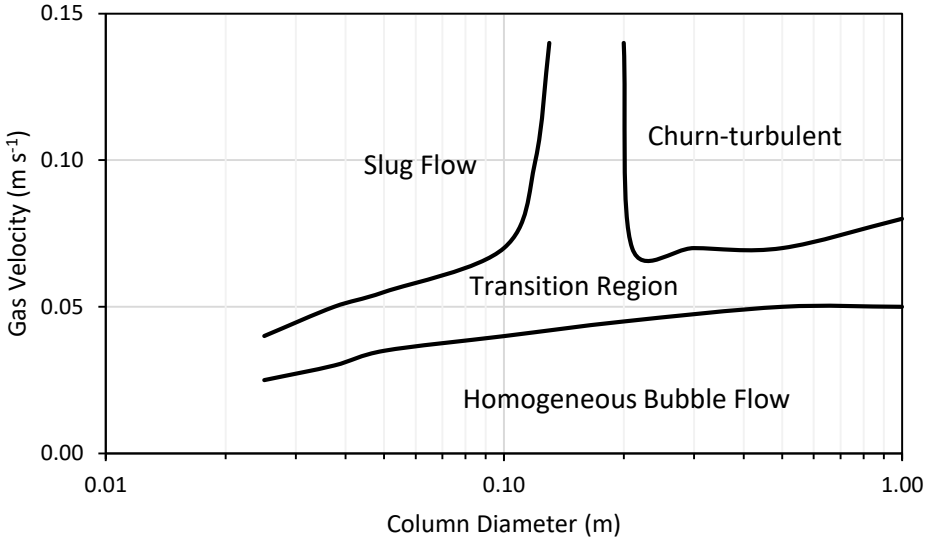

Figure 4.2 – Flow regimes in bubble columns for a given column diameter and superficial gas velocity. Based on Kantarci et al. (2005).

The bubble rise velocity can be estimated by a variety of different relationships (Holland & Bragg, 2002). It is important that bubbles are not entrained in the liquid flowing out of base of the bubble column as entrainment of bubbles in the liquid flow into the solar receiver leads to formation of small bubbles as the mixture passes through the pump. The dispersed small bubbles attenuate light, are difficult to remove when the fluid returns to the bubble column, and can kill cells due to shear stresses when the bubbles burst (van't Riet & Tramper, 1991). This constraint placed a limit on the maximum downward liquid velocity in the bubble column to less than that of the bubble rise velocity.

Gas-liquid flow in bubble columns has been reviewed by Holland and Bragg (2002) as follows. The void fraction, α, in the bubble column is defined as the cross-sectional area of gas, $A_{CS,G}$, over the total cross-sectional area, A_{CS} (Equation (4.1)).

$$\alpha = \frac{A_{CS,G}}{A_{CS}} \tag{4.1}$$

The void superficial gas velocity, $u_{G,V}$, is given by the volumetric flowrate of gas through the gas cross-sectional area (Equation (4.2)).

$$u_{G,V} = \frac{Q_G}{\alpha\, A_{CS}} \tag{4.2}$$

Similarly, the void liquid superficial velocity, $u_{L,V}$, is found with Equation (4.3) from the volumetric liquid flowrate through the liquid cross-sectional area.

$$u_{L,V} = \frac{Q_L}{(1-\alpha)A_{CS}} \tag{4.3}$$

The bubble Reynolds number, Re_{bubble}, is given by Equation (4.5) depending on the bubble diameter, d_b, and terminal rise velocity, u_t.

$$Re_{bubble} = \frac{\rho_L \, u_t \, d_b}{\eta_l} \tag{4.4}$$

The slip velocity is the difference between the gas velocity and liquid velocity, which is related to the terminal bubble velocity by Equation (4.5).

$$\text{slip velocity} = u_t(1-\alpha)^{n-1} \tag{4.5}$$

Here, $n = 4.6$ for $Re_{bubble} < 1$ and $n = 2.4$ for $Re_{bubble} > 500$. The variables above are related by Equation (4.6).

$$\frac{Q_G}{A_{CS}}(1-\alpha) - \frac{Q_L}{A_{CS}}\alpha = u_t \, \alpha(1-\alpha)^{n-1} = (\text{slip velocity})\alpha(1-\alpha) = u_{G,L} \tag{4.6}$$

The terminal velocity of the bubbles determines their rise velocity. The Peebles and Garber correlations for bubble rise velocities are shown in Table 4.1 (Equations (4.7) to (4.10)). Additionally, the bubble rise velocity for large bubbles can be given by Equation (4.11) (Holland & Bragg, 2002).

Table 4.1 – Correlations for terminal bubble rise velocities. Adapted from Holland and Bragg (2002, p. 235).

Terminal velocity	Conditions	
$u_t = \frac{2\, r_{be}^2(\rho_L - \rho_G)g}{9\,\eta_L}$	$Re_{bubble} < 2$	(4.7)
$u_t = 0.33 g^{0.76} \nu_L^{-0.52} r_{be}^{1.28}$	$2 < Re_{bubble} < 4.02\, G_1^{-0.214}$	(4.8)
$u_t = 1.35\left(\frac{\sigma}{\rho_L r_{be}}\right)^{0.5}$	$4.02 G_1^{-.0214} < Re_{bubble} < 3.10 G_1^{-.025}$ Or $16.32 G_1^{0.144} < G_2 < 5.75$	(4.9)
$u_t = 1.18\left(\frac{g\sigma}{\rho_L}\right)^{0.25}$	$3.10 G_1^{-0.25} < Re$ Or $5.75 < G_2$	(4.10)
$u_t = 1.00\sqrt{g r_{be}}$	$r_{be} > 2\sqrt{\frac{\sigma}{g\rho_L}}$	(4.11)

In these correlations r_{be} is the bubble radius, G_1 is the Morton number as given by Equation (4.12), and G_2 is given by Equation (4.13). For a bubble diameter of 6 mm the bubble rise velocity was estimated to be 0.21 m s^{-1}.

$$G_1 = \frac{g\,\eta_L^4}{\rho_L\,\sigma^3} \tag{4.12}$$

$$G_2 = \frac{g\,r_{be}^4\,u_t^4\,\rho_L^3}{\sigma^3} \tag{4.13}$$

In order to determine the void fraction, the system above could be solved through use of a Wallis plot, an example for counter-current flow is shown in Figure 4.3. The void fraction is found from the intersection of the plots of $u_t\,\alpha(1-\alpha)^{n-1}$ and $\frac{Q_G}{A_{CS}}(1-\alpha) - \frac{Q_L}{A_{CS}}\alpha$.

At low liquid flow rates there are two solutions for the void fraction and normally the lower fraction of the two is achieved. As the liquid flow increases there is one solution possible until liquid flow increases to the point that no solution is found. At this point the bubbles coalesce resulting in a change in the terminal rise velocity.

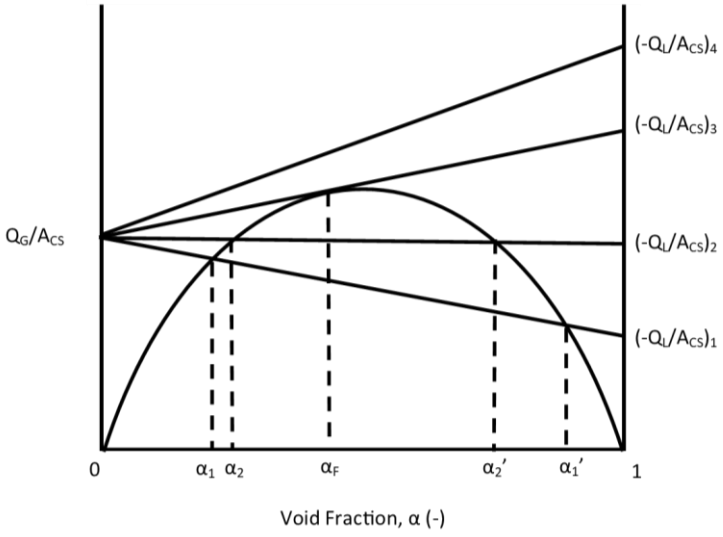

Figure 4.3 – Wallis plot for counter-current flow in a bubble column. Conditions 1 and 2, increasing liquid flow; condition 3, maximum liquid flow where flooding (F) occurs; condition 4, a further increase in liquid flow results in no solution at these conditions. Based on Holland and Bragg (2002, p. 232).

For a 140 mm ID bubble column the predicted void fractions were as shown in Figure 4.4. The void fraction varied with bubble size and liquid and gas superficial velocities.

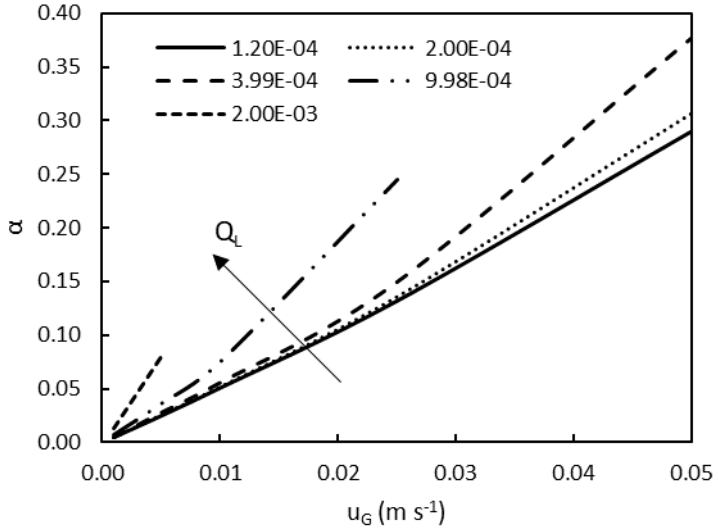

Figure 4.4 – Estimated void fractions (α) as a function of gas superficial velocities (u_G) and downward liquid flowrate ($Q_L, m^3\ s^{-1}$ given in the legend). Missing data points indicate no solution at these conditions. $d_{BC} = 140\ mm$, $d_b = 6\ mm$.

Increasing downward liquid velocity resulted in higher void fractions, as did increasing superficial gas velocity. For liquid flowrates greater than 3.23×10^{-3} m³ s⁻¹ the liquid velocity in the bubble column began to exceed that of the bubble rise velocity and so the bubbles would be entrained in the liquid flow. At this condition, no solution was found for the system under the assumed conditions. When the superficial gas velocity was increased to the point that no solution resulted, the assumed bubble diameter was no longer valid and other coalescence effects would occur resulting in non-homogenous flow regimes (Holland & Bragg, 2002; van't Riet & Tramper, 1991)

Sparger design

There are many different sparger designs reported in the literature, from ring shaped to sintered blocks and perforated plates (Chisti, 1998; Kulkarni & Joshi, 2011). For ease of construction and due to the bubble column diameter, a ring-type sparger was used for the reactor. The size of bubbles at an orifice can be controlled by the diameter of the orifices in the sparger and the gas flow rates (Kulkarni, 2010). Kantarci *et al.* (2005) have summarised correlations for bubble diameter, d_b, formed at an orifice with a diameter d_o (Table 4.2).

Table 4.2 –Correlations for bubble size for bubbles produced at an orifice. Adapted from Kantarci et al. (2005). Correlations are from Moo-Young and Blanch (1981).

Correlation	
$d_b = \left[\frac{6\,\sigma\,d_o}{g(\rho_l-\rho_g)}\right]^{1/3}$ (low gas flow rates)	*(4.14)*
$d_b = 0.19 d_o^{0.48}\, Re_o^{0.32}$	*(4.15)*
$d_b = 0.18 d_o^{1/2}\, Re_o^{1/3} \quad (Re_o < 2000)$	*(4.16)*
$V_b = \left(\frac{4\,\pi}{3}\right)^{1/3} \left(\frac{15\,\eta_L\,Q_G}{2\,\rho_L\,g}\right)^{3/4}$	*(4.17)*
$\frac{d_b}{d_o} = 3.23 \left(\frac{4\,\rho_L\,Q_G}{\pi\,\eta_L\,d_o}\right)^{-0.1} \left(\frac{Q_G^2}{d_O^5\,g}\right)^{0.21}$	*(4.18)*

Re_o is the orifice Reynolds number as given by Equation (4.19) where Q_G is the volumetric gas flow rate, ρ_G is the gas density, and η_G is the gas viscosity.

$$Re_o = \frac{4\,Q_G\,\rho_G}{\pi\,d_o\,\eta_G} \tag{4.19}$$

Bubble diameters can also be calculated using Equation (4.20), where Fr is the Froude number (Equation (4.22)), Bd_o is the orifice Bond number (Equation (4.21)), and Ga is the Galileo number (Equation (4.23)) (Jamialahmadi *et al.*, 2001).

$$\frac{d_b}{d_o} = \left[\frac{5}{Bd_O^{1.08}} + \frac{9.261 Fr^{0.36}}{Ga^{0.39}} + 2.14 Fr^{0.51}\right]^{\frac{1}{3}} \tag{4.20}$$

$$Bd_o = \rho_L\,g\,d_o^2\,\sigma^{-1} \tag{4.21}$$

$$Fr = \frac{u_{so}^2}{d_o\,g} \tag{4.22}$$

$$Ga = \frac{\rho_L^2\,d_o^3\,g}{\eta_L^2} \tag{4.23}$$

Bubble diameters at the sparger vary due to sparger design and orifice size. However, for most bioreactor operations at equilibrium the bubbles can be assumed to coalesce and form bubbles approximately 6 mm in diameter as used in previous calculations (van't Riet & Tramper, 1991).

When determining the number and size of holes in the sparger the orifice superficial velocity, u_{so}, should exceed the critical weep velocity, u_{cw}, by at least 15% (Kulkarni & Joshi, 2011). The critical weep velocity for ring type spargers is given by

Equation (4.24) (Kulkarni & Joshi, 2011). u_{cw} depends on the spacing of sparger holes, Δx_o, the total length of the sparger, L_S, and the static liquid height, H_L.

$$u_{cw}^2 = \left(\frac{0.44(\rho_L - \rho_G)d_o\, g}{\rho_G}\right)\left(\frac{L_s}{d_o}\right)^{-0.12}\left(\frac{\Delta x_o}{d_o}\right)^{-0.145}\left(\frac{H_L}{d_o}\right)^{0.67} \qquad (4.24)$$

For a minimum expected volumetric gas flow rate for the tubular photobioreactor of 7.7×10^{-5} m^3 s^{-1}, six 1 mm holes in a 100 mm diameter ring sparger maintained the orifice superficial velocity to >15% above the critical weep velocity. This was the design used for the sparger.

Mass Transfer

The major mass transfer operation in the bubble column is the stripping of oxygen from the culture (Molina Grima *et al.*, 2001). For an oxygen-and-water system it was found that the major resistance to mass transfer was in the liquid phase (van't Riet & Tramper, 1991). The overall oxygen mass transfer rate, $\frac{dC_{O_2}}{dt}$, can be given by Equation (4.25), where k_l is the liquid-side mass transfer coefficient for oxygen, a is the mass transfer area between the liquid and gas, C_{O_2} is the bulk liquid concentration of oxygen and $C_{O_2}^*$ is the concentration of oxygen in the liquid in equilibrium with the gas (van't Riet & Tramper, 1991). $(k_l a)_{O_2}$ is the overall mass transfer coefficient for oxygen in water.

$$\frac{dC_{O_2}}{dt} = (k_l a)_{O_2}\left(C_{O_2}^* - C_{O_2}\right) \qquad (4.25)$$

k_l and a depend on a range of factors, notably the bubble size. The mass transfer coefficient can be theoretically estimated by a variety of correlations for different conditions. Equation (4.26) is one estimation of the mass transfer coefficient suitable for the typical conditions expected in the bubble column of the tubular photobioreactor (van't Riet & Tramper, 1991).

$$k_l = \sqrt{\frac{4\,\mathcal{D}_{il}\,u_b}{\pi\,d_b}} \qquad (4.26)$$

Here, $\mathcal{D}_{il}$ is the diffusion coefficient of the gas in the liquid phase, u_b is the bubble rise velocity, and d_b is the bubble diameter. The specific surface area of the bubbles in the liquid phase, a, with an average diameter of d_b can be determined by Equation (4.27) where ε_g is the gas hold-up ($\varepsilon_G = V_G/(V_L + V_G)$).

$$a = \frac{6}{d_b}\frac{\varepsilon_G}{1 - \varepsilon_G} \qquad (4.27)$$

The inaccuracy of models used to determine mass transfer coefficients and interfacial area in bubble columns means they are rarely able to be relied upon. As such, experimental determination of mass transfer coefficients for a particular system is preferred; however, this cannot be done in the design stage. Generally, the lumped parameter $(k_l a)_{O_2}$ is determined for a particular reactor geometry and set of flow conditions (Chisti, 1998).

One correlation reported for bubble column bioreactors is given by Equation (4.28). This is suitable for oxygen and water systems at 20 °C with an uncertainty of approximately 30% (van't Riet & Tramper, 1991). u_G here is the superficial gas velocity adjusted for the local pressure.

$$(k_l a)_{O_2} = 0.32\ (u_G)^{0.7} \qquad (4.28)$$

A variety of other correlations have been reported for estimating $k_l a$ in different bubble column systems (Kantarci *et al.*, 2005). A summary of a selection of these is shown in Table 4.3.

Table 4.3 - Mass transfer coefficient correlations for bubble column reactors. Adapted from Kantarci et al. (2005).

Correlation	Reference	
$\frac{k_l a\, d_b^2}{\mathcal{D}_{AB}} = 0.62 \left(\frac{\eta_L}{\rho_L\, \mathcal{D}_{AB}}\right)^{0.5} \left(\frac{g\, \rho_L^2\, d_b^2}{\eta_L^2}\right)^{0.33} \left(\frac{u_G}{\sqrt{g\, d_b}}\right)^{0.68} \left(\frac{\rho_g}{\rho_l}\right)^{0.04}$	a	*(4.29)*
$\frac{k_l a\, D_T^2}{\mathcal{D}_{AB}} = 0.6 \left(\frac{\nu_L}{\mathcal{D}_{AB}}\right)^{0.5} \left(\frac{g\, D_T^2\, \rho_L}{\sigma}\right)^{0.62} \left(\frac{g\, D_T^3}{\nu_L^2}\right)^{0.31} \varepsilon_G^{1.1}$	b	*(4.30)*
$k_l a = 0.467\, u_G^{0.82}$	b	*(4.31)*
$\frac{k_l a\, D_T^2}{\mathcal{D}_{AB}} = 0.452 \left(\frac{\nu_l}{\mathcal{D}_{AB}}\right)^{1/2} \left(\frac{D_T\, u_G}{\nu_l}\right)^{3/4} \left(\frac{g\, D_T^3\, \rho_L}{\sigma}\right)^{3/5} \left(\frac{u_G^2}{D_T\, g}\right)^{7/60}$	b	*(4.32)*
$\frac{k_l a\, u_g}{g} = 14.9 \left(\frac{u_G\, \eta_L}{\sigma}\right)^{1.76} \left(\frac{\eta_L^4\, g}{\rho_L\, \sigma^3}\right)^{-0.248} \left(\frac{\eta_G}{\eta_L}\right)^{0.243} \left(\frac{\eta_L}{\rho_l \mathcal{D}_{AB}}\right)^{-0.604}$	c	*(4.33)*
$k_l a = K_1 \times 10^{-3.08} \left(\frac{D_T\, u_G\, \rho_g}{\eta_L}\right)^{0.254}$	c	*(4.34)*
$k_l a = K_2\, u_g^{0.82}\, \eta_{\text{eff}}^{-0.39}$	c	*(4.35)*

K_1 is the correlation dimension, $K_2 = 0.063$ (water/salt solution), $K_2 = 0.042$ (water, 0.8 M Na_2SO_4)

a: Öztürk *et al.* (1987); b: Shimizu *et al.* (2000); c: Behkish *et al.* (2002)

Using these correlations, the $k_l a$ for the oxygen-water system can be estimated. The results of the suitable correlations for superficial gas velocities up to 0.05 m s^{-1} are shown in Figure 4.5.

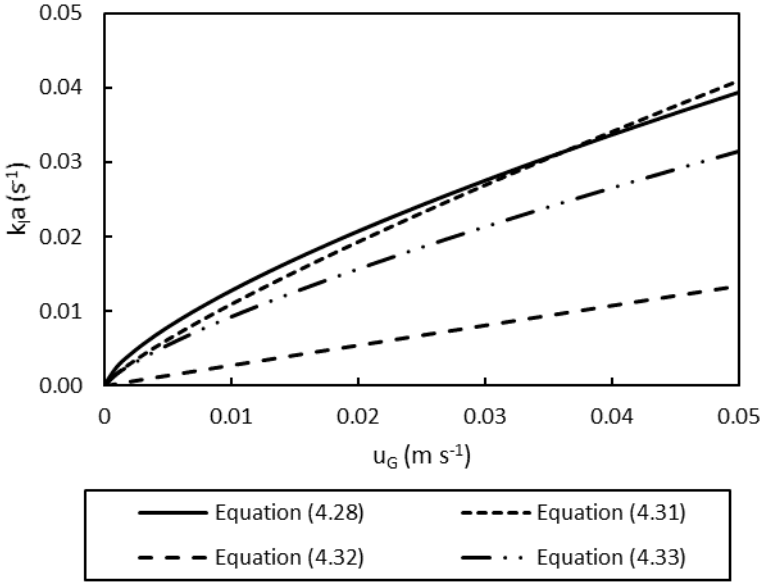

Figure 4.5 – Variation of predicted $k_l a$ values for oxygen in water at 20 °C in a bubble column of 140 mm ID.

Oxygen stripping

The oxygen produced during the microalgae's residence in the solar receiver must be removed in the bubble column. The dissolved oxygen concentration at the exit of the solar receiver will be highest when the liquid velocity is the minimum and hence the residence time is longest. As liquid velocity increases, the time for mass transfer to occur in the bubble column is reduced and so less oxygen can be stripped. The bubble column needed to be sized to perform under both low and high liquid velocities.

The concentration of oxygen in the media entering the bubble column is given by Equation (4.36) and the dissolved oxygen concentration leaving the bubble column can be found by Equation (4.37) where $\frac{dC_{O_2}}{dt} = (k_l a)_{O_2}\left(C^*_{O_2} - C_{O_2}\right)$ as per Equation (4.25), R_{O_2} is the oxygen evolution rate of the microalgae, and t_R is the residence time of the liquid in the bubble column.

$$C_{O_2,BC,i} = C_{O_2,BC,o} + \left(R_{O_2}\,\frac{L_{SR}}{u_{L,SR}}\right) \qquad (4.36)$$

$$C_{O_2,BC,o} = C_{O_2,BC,i} - \left(\int_{t=0}^{t=t_R} \frac{dC_{O_2}}{dt}\, dt \right) \qquad (4.37)$$

It was assumed that the maximum oxygen evolution rate was in the region of 3–4 × 10^{-3} mol m^{-3} s^{-1} based on results from other microalgae in tubular photobioreactors (Acién Fernández *et al.*, 2001; Bosma *et al.*, 2014; Rebolloso Fuentes *et al.*, 1999). For this condition the maximum dissolved oxygen concentrations calculated leaving the bubble column were as shown in Figure 4.6. The maximum dissolved oxygen concentration reached leaving the bubble column was found to be 150% of air saturation, which is within the typical threshold range reported for dissolved oxygen of 120% to 200% of air saturation for other microalgae (Posten, 2009). This condition was reached at the maximum expected liquid velocity and cell concentrations. In the event that *Trachydiscus* sp. LCR-Awa-9-2 was highly sensitive to dissolved oxygen, oxygen-free nitrogen could be used as the sparging gas which would lower the dissolved oxygen concentrations further.

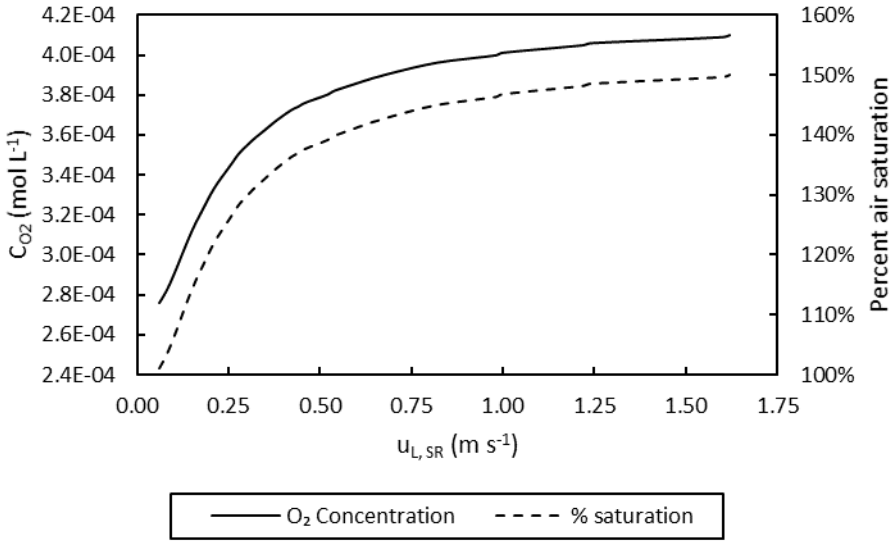

Figure 4.6 – Maximum predicted dissolved oxygen concentrations at exit of the bubble column in laboratory scale tubular photobioreactor. Air-water system, $k_l a = 0.03\ s^{-1}$, $T = 20$ °C, $d_{BC} = 0.14\ m$, $R_{O_2,max} = 0.003\ mol\ m^{-3} s^{-1}$, $h_{BC} = 1.5\ m$.

Carbon dioxide supply

CO_2 can be supplied in two locations, either in the bubble column or at the entrance to the solar receiver. When supplied in the bubble column it can either be mixed with the air supply or injected separately. For this reactor, the CO_2 was supplied mixed with the air inlet, but it could be altered to a separate injection system if it was found that the culture was carbon limited due to mass transfer. As CO_2 is much more soluble than oxygen in

water its overall mass transfer rate is greater (Sander, 2015; Sobczuk *et al.*, 2000). The $k_l a$ for CO_2 can be related to that for oxygen by Equation (4.38) (Talbot *et al.*, 2004).

$$(k_l a)_{CO_2} = (k_l a)_{O_2} \left(\frac{\mathcal{D}_{CO_2}}{\mathcal{D}_{O_2}} \right)^{0.5} \tag{4.38}$$

It was assumed that the carbon dioxide demand was approximately 3–4 × 10^{-3} mol m^{-3} s^{-1} (due to the photosynthesis reaction, 1 mole of O_2 produced per 1 mole of CO_2, and the oxygen evolution rate from above). If CO_2 was supplied at 3% concentration in the air supply the CO_2 concentration in the bubble column could be determined similarly to as above for oxygen. The predicted CO_2 concentration at the exit of the solar receiver for various liquid flow rates is shown in Figure 4.7 which was used to determine the predicted CO_2 depletion. As the predicted CO_2 concentration did not reach zero at the exit of the solar receiver it was likely that enough CO_2 could be supplied to prevent carbon limitation. The percentage of CO_2 in the sparging gas could also potentially be increased to avoid CO_2 limitation at low liquid flow rates.

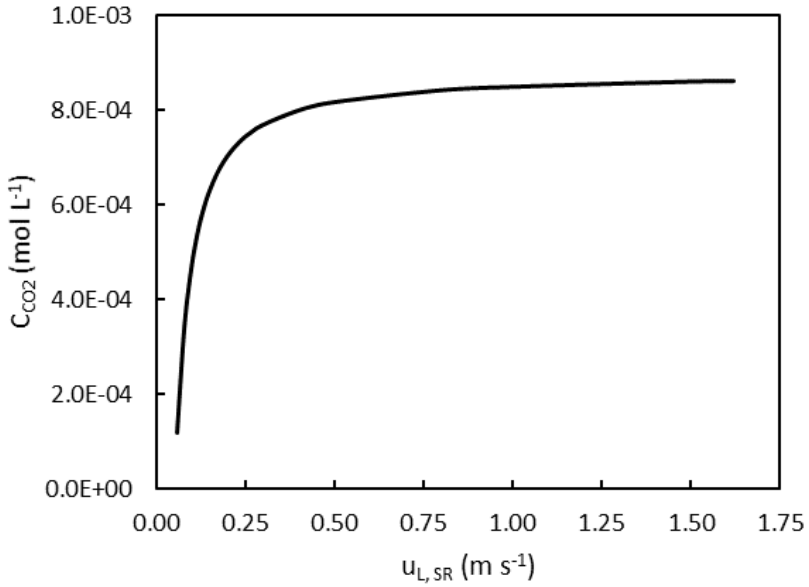

Figure 4.7 – Predicted CO_2 concentrations at the exit of the solar receiver. $k_l a = 0.033\ s^{-1}$, $T = 20$ °C, $y_{CO_2} = 0.03$, $R_{CO_2} = 0.003\ mol\ m^{-3} s^{-1}$, $h_{BC} = 1.5\ m$, $d_{BC} = 0.14\ m$.

Heat transfer

Heat is supplied to the reactor from the lighting system, power input from pumping, and the outside environment. If the temperature of the reactor was lower than that of the surrounding air there would be convective heat transfer to the reactor, and vice versa. The surrounding air temperature was assumed to be 20 °C (controlled by air conditioning). The minimum expected temperature that would be required for operation was assumed to be 12 °C which required removal of approximately 2.5 kW of heat. In order to maintain the desired temperature, an internal heat exchanger was the best option due to poor heat transfer through the acrylic column and construction constraints which made jacketing impractical. For large tubular photobioreactors internal heat exchangers are also commonly used (Fernández *et al.*, 2014) and so using a similar design would also help to mimic those conditions.

The heat transfer from the culture to an internal heat exchanger can be given by Equation (4.39). Typical overall heat transfer coefficients, U, for liquid-liquid heat exchangers are 850–1700 W m^{-2} K^{-1} (McDonald & Magande, 2012).

$$q = U\,A\,\Delta T \tag{4.39}$$

As mentioned above, the heat exchanger needed to remove up to 2.5 kW of heat, q, from the reactor. The lowest expected temperature required for the culture was 12 °C and cooling water could be supplied at approximately 7 °C.

The cooling water was expected to increase in temperature by approximately 1 °C during its passage through the heat exchanger and could be supplied at a flow rate of approximately 2 m^3 h^{-1}. Under these conditions a surface area of approximately 0.45 m^2 was required for heat exchange. Six metres of 25.4 mm OD stainless steel pipe supplied 0.48 m^2 of surface area which met the required area. In order to fit this within the bubble column, four passes were made to allow inlet and outlet connections at the top of the column.

4.2.2 Solar receiver

Solar receivers have been designed in a variety of geometries, the most common of these being vertically stacked or fence-style (Molina Grima *et al.*, 2009), flat horizontal (Acién Fernández *et al.*, 2001), and spiral or helical (Hall *et al.*, 2003) as shown in Figure

4.8. The vertically stacked style gives the best use of land space of the options available and is the most commonly employed style in industrial scale plants (Molina Grima *et al.*, 2009; Pulz, 2001). Due to this, it was the style chosen for this reactor. Tubes in this arrangement are normally spaced one tube-diameter apart to allow light to reach all sides of the tubes while maximising the vertical density of the tubes.

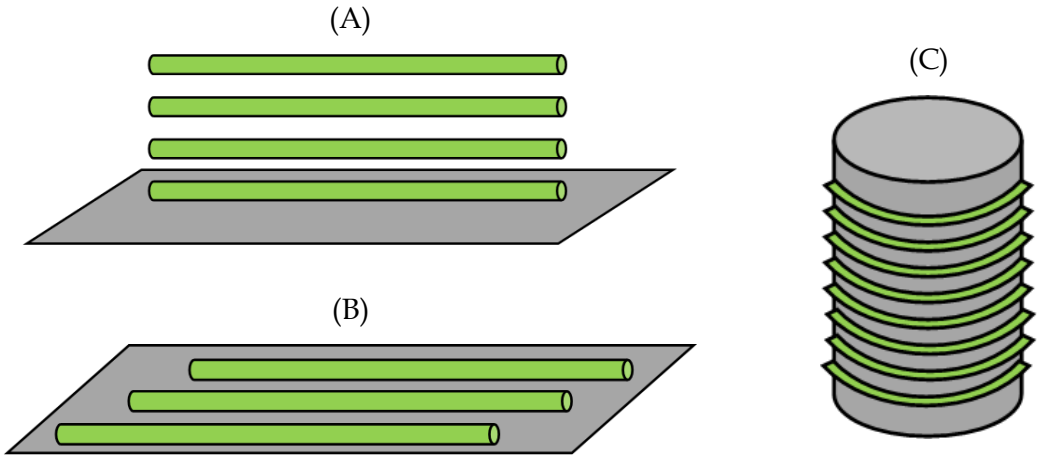

Figure 4.8 – Examples of different tubular photobioreactor solar receivers. A) vertically stacked, B) horizontal, and C) spiral.

The material that solar receivers are made of must fulfil some critical criteria; namely it must:

- Be transparent to photosynthetically active radiation
- Be chemically compatible with culture media and common disinfection compounds, such as sodium hypochlorite
- Have sufficient mechanical strength to support itself and the culture without needing excessive support structures
- Not leach compounds which are toxic to microalgae
- Be resistant to biofouling

There are four materials typically used in tubular photobioreactor construction that meet most of these criteria: clear acrylic, polycarbonate, glass, and clear PVC. These materials are transparent to photosynthetically active radiation as shown in Figure 4.9. Glass provided the best transmittance with >90% of radiation between 300 nm and 1000 nm being transmitted (SCHOTT AG, 2017a).

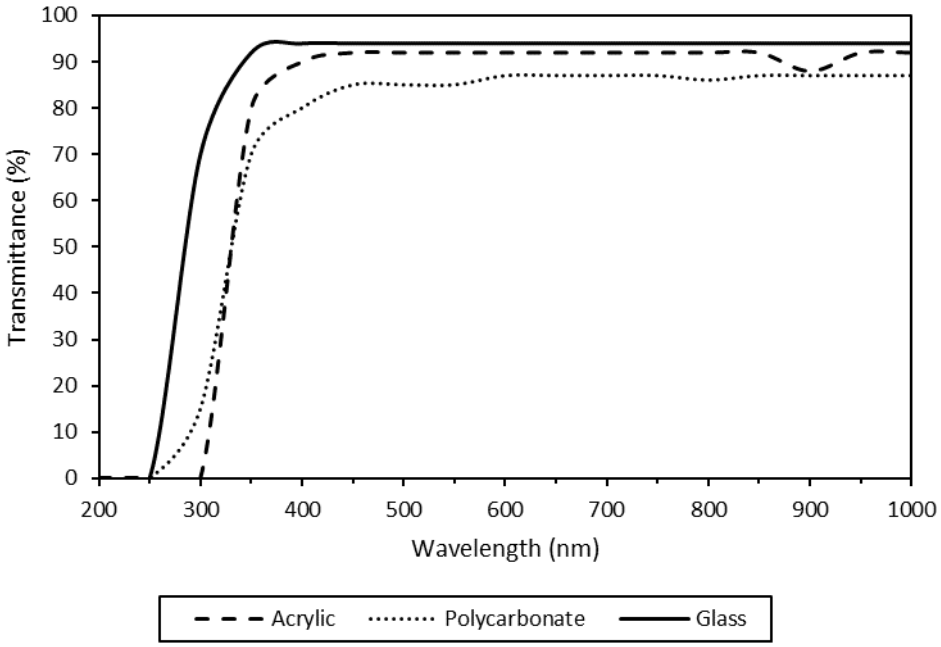

Figure 4.9 – Typical transmittance profiles of potential solar receiver materials of approximately 3 mm thickness. Data sourced from Shannon and Wyant (1979) and SCHOTT AG (2017a).

There were two main parameters to consider when designing the solar receiver: the tube diameter and total length. Total length was constrained by oxygen build-up in the culture as it travels along the solar receiver. This can be determined by Equation (4.40) where the maximum permittable length, $L_{SR,max}$, is given by the liquid velocity in the tubes, $u_{L,SR}$, the inlet dissolved oxygen concentration, $C_{O_2 in}$, the maximum volumetric rate of oxygen production, $R_{O_2,max}$, and the maximum permittable dissolved oxygen concentration in the reactor, $C_{O_2 max}$ (Molina Grima *et al.*, 2001). For an ideally designed reactor, the inlet concentration of dissolved oxygen at the entrance of the solar receiver will be 100% of air saturation (provided air is being used as the sparging gas in the bubble column).

$$L_{SR,max} = \frac{(C_{O_2 max} - C_{O_2 in}) \cdot u_{L,SR}}{R_{O_2,max}} \qquad (4.40)$$

The diameter is constrained by allowing sufficient light to the culture while maintaining a viable volume and minimising the pressure drop. Typical diameters for solar receivers range from approximately 30 mm up to 300 mm, with most reactors using a diameter in the range of 50–100 mm (Becker, 1994; Tredici *et al.*, 2013). As the desired material for the solar receiver was glass the diameter was limited to standard glass tubing

diameters for practicality. Schott AG (Germany) supplied glass solar receiver systems in two outer diameter options, 54 mm and 65 mm (SCHOTT AG, 2016). Due to the scale of the reactor in this study the 54 mm option was chosen as a compromise between volume and allowing light/dark cycling to occur in the tubes which was important for simulating large-scale conditions (Chisti, 2007; Molina Grima *et al.*, 2000).

Liquid flow rates are bounded at the minimum by the turbulence requirement for cycling cells between light and dark regions in the solar receiver (Acién Fernández *et al.*, 2013). Turbulent flow in pipes can be quantified using the pipe Reynolds number, Re_{pipe}, as calculated in Equation (2.32) (de Nevers, 2005). A minimum Reynolds number of 3000 should be achieved (Acién Fernández *et al.*, 2001) which limited the minimum liquid velocity to 0.06 m s^{-1} (assuming at a temperature of 25 °C the culture broth had a density and viscosity similar to that of water and the inside diameter of the solar receiver was 50.4 mm).

While sufficient turbulence is required to provide mixing, care must be taken to ensure that the turbulence is not so intense that it will damage the cells. The upper limit of the liquid velocity is bounded by shear stress, microeddy length, and entrainment of bubbles in the liquid flow in the bubble column (Acién Fernández *et al.*, 2013; Molina Grima *et al.*, 2000; Molina Grima *et al.*, 2001).

To avoid bubble entrainment into the solar receiver the liquid velocity in the bubble column should be less than the bubble rise velocity. Bubble rise velocities depend on many factors as described in § 4.2.1. The liquid velocity in the bubble column depends on the relative diameters of the bubble column and solar receiver. Bubble rise velocity was estimated to be 0.21 m s^{-1} (as discussed in § 4.2.1) which limited the liquid velocity to 1.62 m s^{-1} to avoid bubble entrainment.

Shear stress due to contact of the cells with the walls of the reactor tubes, τ_0, is given by Equation (4.41) (Molina Grima *et al.*, 2000). C_f is the Fanning friction factor which can be determined graphically or from empirical relationships (Holland & Bragg, 2002). For a turbulent flow regime and smooth pipe, as is present in the solar receiver, the Fanning friction factor can be found using the Blasius equation as seen in Equation (4.42) (Michels *et al.*, 2016). As there is a broad range of shear stress tolerances for microalgae (see § 2.5.7), the liquid velocity was limited to between 0.6 m s^{-1} and 7.4 m s^{-1}. The shear

stress tolerance of *Trachydiscus* sp. LCR-Awa-9-2 was unknown, but due to its morphology it was expected to be able to tolerate shear stresses at the higher end of the range.

$$\tau_0 = \frac{1}{2} C_f \rho_L u_L^2 \quad (4.41)$$

$$C_f = \frac{0.0791}{Re_{pipe}^{\frac{1}{4}}} \quad (4.42)$$

Damage to cells can be caused by microeddies which form as turbulence increases, creating an upper limit on the liquid velocity that can be used (Sánchez Mirón *et al.*, 1999). When the length of the microeddies, l_{eddy}, approaches that of the size of the cells, damage can occur and thus the liquid velocity should be restricted as to avoid this (Molina Grima *et al.*, 2000; Posten, 2009; Tredici *et al.*, 2013). The length of the microeddies can be quantified by Equation (4.43) where the energy dissipation per unit mass, ξ, can be calculated using Equation (4.44) (Batchelor, 1947; Molina Grima *et al.*, 1999).

$$l_{eddy} = \left(\frac{\eta_L}{\rho_l}\right)^{\frac{3}{4}} \xi^{-\frac{1}{4}} \quad (4.43)$$

$$\xi = \frac{2 C_f {u_L}^3}{d_t} \quad (4.44)$$

For the liquid velocity to be maintained such that microeddies did not approach the cell size of approximately 5–10 µm, the liquid velocity was limited to 9 m s^{-1}. This velocity was far higher than any reasonable operating velocity for tubular photobioreactors (Sánchez Mirón *et al.*, 1999). It was expected that this phenomenon would not cause an issue with cultures of *Trachydiscus* sp. LCR-Awa-9-2 due to the microalga's morphology and the operating liquid velocities in the reactor.

4.2.3 Pump

The pump for the photobioreactor was required to be capable of supplying a flow rate of at least 430 L h^{-1} to reach a liquid velocity of 0.06 m s^{-1}, as determined from the calculations in the previous sections. As tubular photobioreactors are typically operated with a solar receiver liquid velocity in the region of 1 m s^{-1} the pump was desired to be able to supply 7200 L h^{-1} or more. Achieving a flow rate above this would allow testing of the shear tolerance of the microalgae. A flow rate of greater than 11000 L h^{-1} was predicted to result in bubble entrainment.

As the culture medium was a salt solution and the reactor was to be sterilised with bleach solutions, the pump had to also be constructed of materials compatible with these chemicals. Inlet and outlet diameters also needed to be similar to the solar receiver tube diameter to avoid venturi effects at the entrance and exit of the pump. The most suitable pump for these constraints was a centrifugal-style swimming pool pump. These pumps have 40 or 50 mm diameter connections and can supply maximum flow rates from 11000 L h^{-1} up to 32000 L h^{-1}. They are constructed from plastic which does not degrade with salt-water or chlorine used for pool treatment. This style of pump has also been used successfully on large-scale tubular photobioreactors (Fernández *et al.*, 2014).

Shear stress should be kept within a suitable range for the microalgae; thus, the impeller diameter and speed are limited by the tolerance of the microalgae. Shear stresses are imposed on the cells by impellers present in the pump and any venturi effects that may occur due to diameter variations (Michels *et al.*, 2016).

Shear stress in centrifugal pumps can be determined using Equation (4.45) (Michels *et al.*, 2016). Shear stress imposed by the pump, τ_{pump}, depends on the liquid viscosity, η_L, the impeller rotational speed, N_{pump}, and local Reynolds number, Re_L. The local Reynolds number (Equation (4.46)), and thus shear stress, is greatest at the tip of the impeller, with diameter d_L.

$$\tau_{pump} = 6.30\, \eta_L\, N_{pump}\, Re_L^{0.5} \tag{4.45}$$

$$Re_L = \frac{N_{pump}\, d_L^2\, \rho_L}{\eta_L} \tag{4.46}$$

The maximum impeller diameter for pool pumps is approximately 20 cm. This limited the pump speed to between 250 rpm and 1600 rpm depending on the shear stress tolerance of the microalgae. The maximum speed of pool pumps is approximately 3500 rpm. The variation of shear stress with impeller diameter and rotational speed is shown in Figure 4.10 for typical ranges for swimming pool pumps.

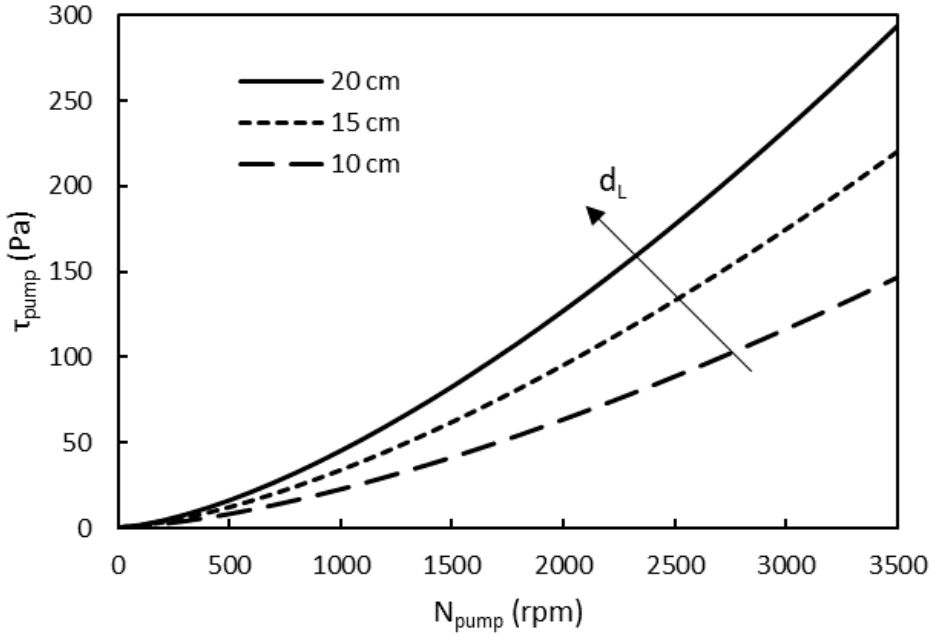

Figure 4.10 – Variation of pump shear stress with impeller diameter and rotational speed for typical pool pump ranges.

The pump chosen for the tubular photobioreactor was a single-phase pool pump with a maximum flow rate of 19,000 L h^{-1} with a 106 mm diameter impeller and 2900 rpm no load motor speed (SWPP-800, Ozito, Australia). The pump was constructed from plastic and could withstand the chemicals used for cleaning and in the culture media. The maximum shear stress expected to be produced by the pump was approximately 100 Pa which was at the upper end of shear stress tolerances reported for other microalgae (§ 2.5.7).

4.2.4 Support structure

The support structure was constructed from square steel tube and was designed to allow the reactor to be relocated by use of castors on the base. The overall dimensions of the reactor were approximately 2 m tall by 2.5 m long by 0.8 m wide. The solar receiver tubes were located approximately one tube diameter apart in a similar fashion to outdoor tubular photobioreactors attached to vertical supports. Rubber-lined pipe supports were used to hold the solar receiver tubes at the desired positions. Two similar pipe supports were used to support the bubble column with a vertical support bar. The pump was mounted near the base of the bubble column.

4.2.5 Electrical, lighting and control system

The lighting used for the tubular photobioreactor was LED strip lights. Four colour 24 V SMD5050 LED strips with 60 LED/m spacing were used to provide red, green, blue, and warm white (RGBWW) light for the reactor. To illuminate the solar receiver tubes, 1350 mm lengths of 100 mm diameter PVC pipe were lined with the LED strips with a total of 15 strips running the entire length of each tube. Each LED strip was 1300 mm long. The tubes were split in half lengthwise and hinged so they could be attached in a clamshell-style around each of the solar receiver tubes. The intensity of the lights was controlled by PWM from an Arduino Uno microcontroller via IRF520N MOSFET modules, with each colour channel being able to be controlled individually. Two 3 kW 24 V power supplies (RSP-3000-24, Meanwell, Taiwan) were used to power the lighting system.

pH was measured by a probe located in the bubble column connected to a pH meter/controller (HI8711, Hanna Instruments, USA) and dissolved oxygen was measured with a galvanic-style dissolved oxygen probe located in the bubble column connected to a dissolved oxygen meter/controller (HI8410, Hanna Instruments, USA). Both of these meters outputted an analogue signal which was measured by the Arduino Uno. Temperature was measured with a DS18B20 temperature probe located in the bubble column which was also connected to the Arduino Uno. Measurements recorded by the Arduino Uno were sent to a Raspberry Pi 3 B+ for datalogging.

The speed of the pump was controlled with an Optidrive E3 single-phase variable frequency dive (VFD) (Invertek Drives Ltd, UK). Air and CO_2 flow rates were controlled with mass flow controllers, MCR-50SLPM and MCS-10SLPM models, respectively (Alicat Scientific, USA). Both the VFD and mass flow controllers were controllable from the Raspberry Pi or via their built-in keypads. Data from the controllers was datalogged by the Raspberry Pi. A diagrammatic overview of the control system is shown in Figure 4.11.

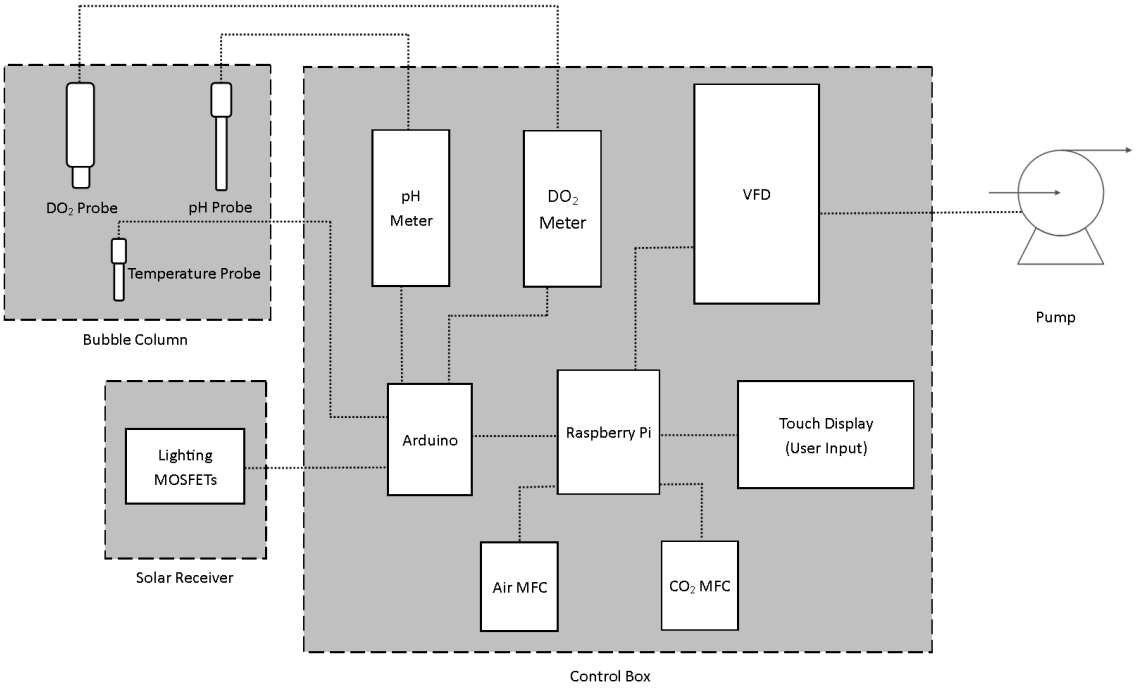

Figure 4.11 – Overview of tubular photobioreactor control system. MFC: mass flow controller; VFD: variable frequency drive; DO_2: dissolved oxygen.

4.3 Final design summary

The final design of the tubular photobioreactor can be seen in the photos and drawings below in Figure 4.12 and Figure 4.13. The final working volume of the reactor was approximately 76 L with 23 L in the bubble column and 53 L in the solar receiver. The solar receiver was constructed from borosilicate glass tubing (Schott, Germany) in a 'fence' style as seen in Figure 4.12. 12 straight tubes were used of 1500 mm length and 50.4 mm ID (54 mm OD), connected by glass U-bends and plastic couplers (Schott, Germany). The horizontal tubes were spaced one tube diameter apart on each side. The bubble column was constructed from acrylic tube, 140 mm ID and 150 mm OD, 1800 mm in height from base to top. Inside the bubble column was a stainless-steel heat exchanger through which temperature-controlled water was circulated from a water bath with a pump. Also located in the bubble column was the pH, dissolved oxygen, and temperature probes.

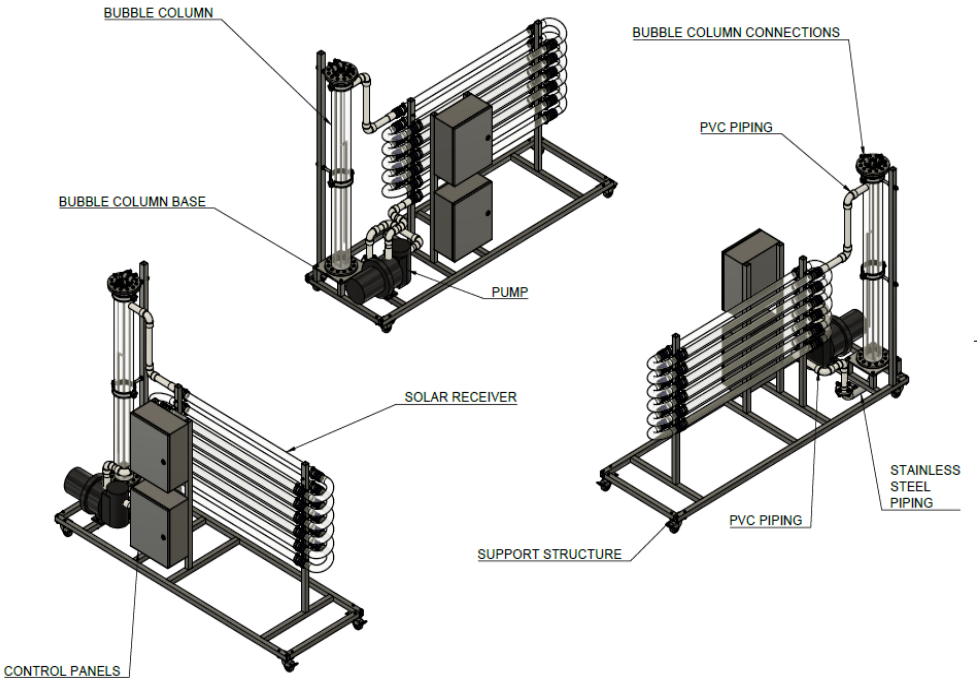

Figure 4.12 – Design drawings of the overview of the tubular photobioreactor.

(A)

(B)

(C)

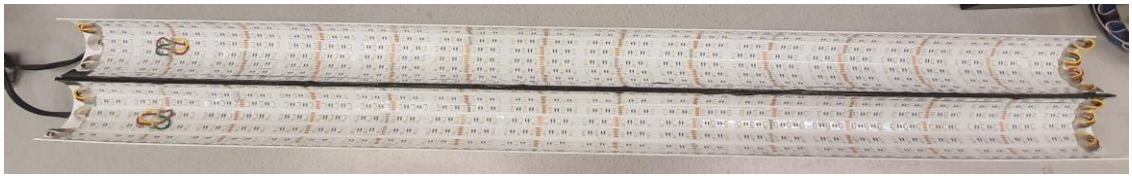

Figure 4.13 – Photos of the tubular photobioreactor. A) bubble column and pump; B) solar receiver; C) lighting clam shell.

The sparger was a ring-type sparger with six 1 mm holes. It was located at the centre of the base of the bubble column, suspended from a length of stainless-steel tubing running from the top of the bubble column down the centre which was supported by the cap of the bubble column. The base of the bubble column was constructed from a stainless-steel concentric reducer connected to 50.4 mm ID stainless steel elbows and a tee where the main drain valve was located.

40 mm PVC pressure piping was used to connect the stainless-steel pipe from the base of the bubble column to the pump inlet by a flanged joint. The same PVC pipe was also used to connect the pump outlet to the solar receiver input and the solar receiver output to the top of the bubble column. Transitions between the PVC pipe and inlets/outlets were tapered to provide a smooth transition between different IDs.

Lighting was provided by RGBWW LED strips attached to the inside of 100 mm PVC pipe which was split lengthwise to be able to clam shell around each of the solar receiver tubes. Each lighting tube contained a total length of 19.5 m of LED strips. Light intensity was controlled by PWM.

Air and CO_2 flow rates were controlled with MCR-50SLPM and MCS-10SLPM mass flow controllers, respectively (Alicat Scientific, USA). Air was supplied from an air compressor and food grade CO_2 was supplied from cylinders (BOC, New Zealand). The air and CO_2 mix was filtered with an inline 0.2 µm PTFE filter (Whatman™ Polycap 75 TF, GE Healthcare, USA) prior to entering the bubble column. A swimming pool pump was used to recirculate the culture and the pump speed was controlled with a single phase VFD. Datalogging and control signals were managed by a Raspberry Pi with custom Python software. pH, dissolved oxygen, and temperature were datalogged.

4.4 Characterisation

4.4.1 Liquid velocity

Liquid velocity in the solar receiver of the reactor was determined by residence time of a pulse of saline solution. The solution was introduced through a septum located at the beginning of the solar receiver and the conductivity was measured at the exit of the solar receiver inside the bubble column. The total length of solar receiver from injection point to the conductivity probe was 24.0 ± 0.2 m. A stopwatch was used to time from the injection of the saline solution until the peak conductivity was registered on the conductivity meter. 10 mL of saturated NaCl solution was used for each test and injected

using a 25 mL syringe with a 1.6 mm diameter bore needle, it took approximately 0.5 seconds to inject the entire 10 mL. Residence time was determined from the average of three trials.

The minimum frequency that the pump could run at was 7 Hz, below this point the pump stalled and there was no flow. The maximum frequency used was 30 Hz as above this point the flow exiting the solar receiver into the bubble column would splash excessively and potentially damage the sensors. The calculated average liquid velocity in the solar receiver over the 7–30 Hz range of the pump is shown in Figure 4.14. Error bars represent the measurement error in the calculated values.

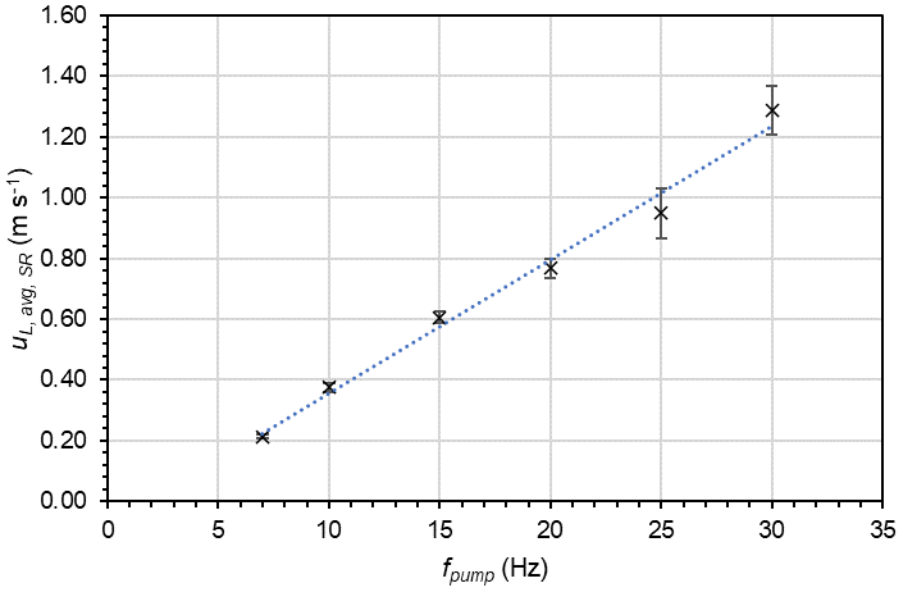

Figure 4.14 – Average liquid velocity in the solar receiver as a function of the frequency supplied to the pump from the VFD. Error bars represent measurement uncertainty.

For frequencies in the range of 7–30 Hz, the average liquid velocity in m s^{-1} in the solar receiver, $u_{L,SR,avg}$, can be related to the pump frequency by the empirical formula in Equation (4.47) where f_{pump} is the frequency of the electricity supplied to the pump.

$$u_{L,SR,avg} = 0.0439\, f_{pump} - 0.0828 \qquad (4.47)$$

4.4.2 Light intensity and spectra

The spectrum of the LEDs was measured as described in § 3.6 and can be seen in Figure 4.15. Measurements were taken in a darkened room to avoid external light sources. The light intensity of the tubes was calibrated by measuring the intensity as in § 3.6. The

light intensity was measured over the range of 400–700 nm. The spherical sensor was located in the centre of the light tube at the mid-point in the length of the tube as shown in Figure 4.16 with the light tubes removed from the tubular photobioreactor. Readings were taken at other locations in the tube to estimate the homogeneity of the light and ambient light readings also taken. Results of the light intensity calibrations for each LED colour are shown in Figure 4.17.

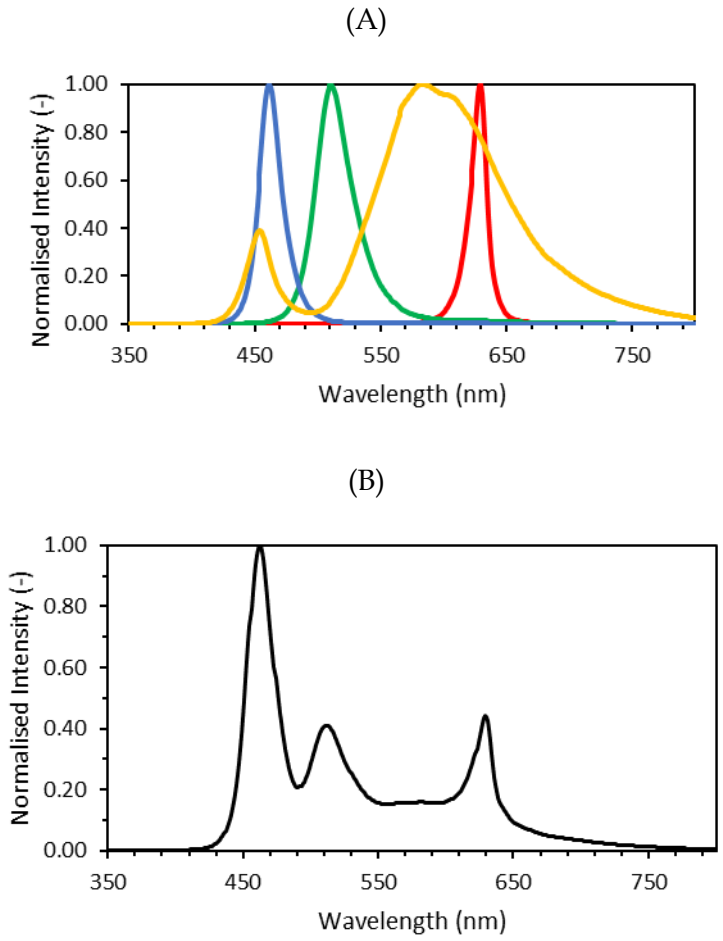

Figure 4.15 – Spectra of LEDs used for the tubular photobioreactor. A) Red (—), Green (—), Blue (—) and Warm White (—) LEDs, B) All LEDs on.

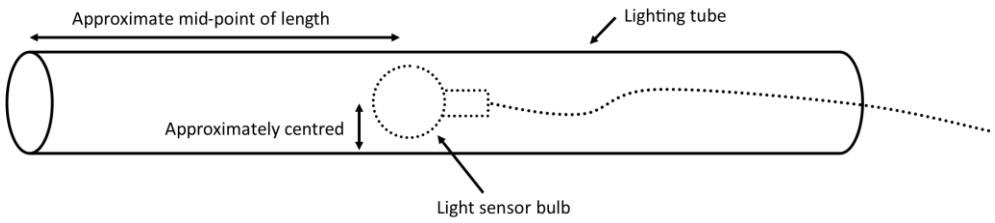

Figure 4.16 – Location of light measurements for tubular photobioreactor lighting. Clam shell was closed during measurements.

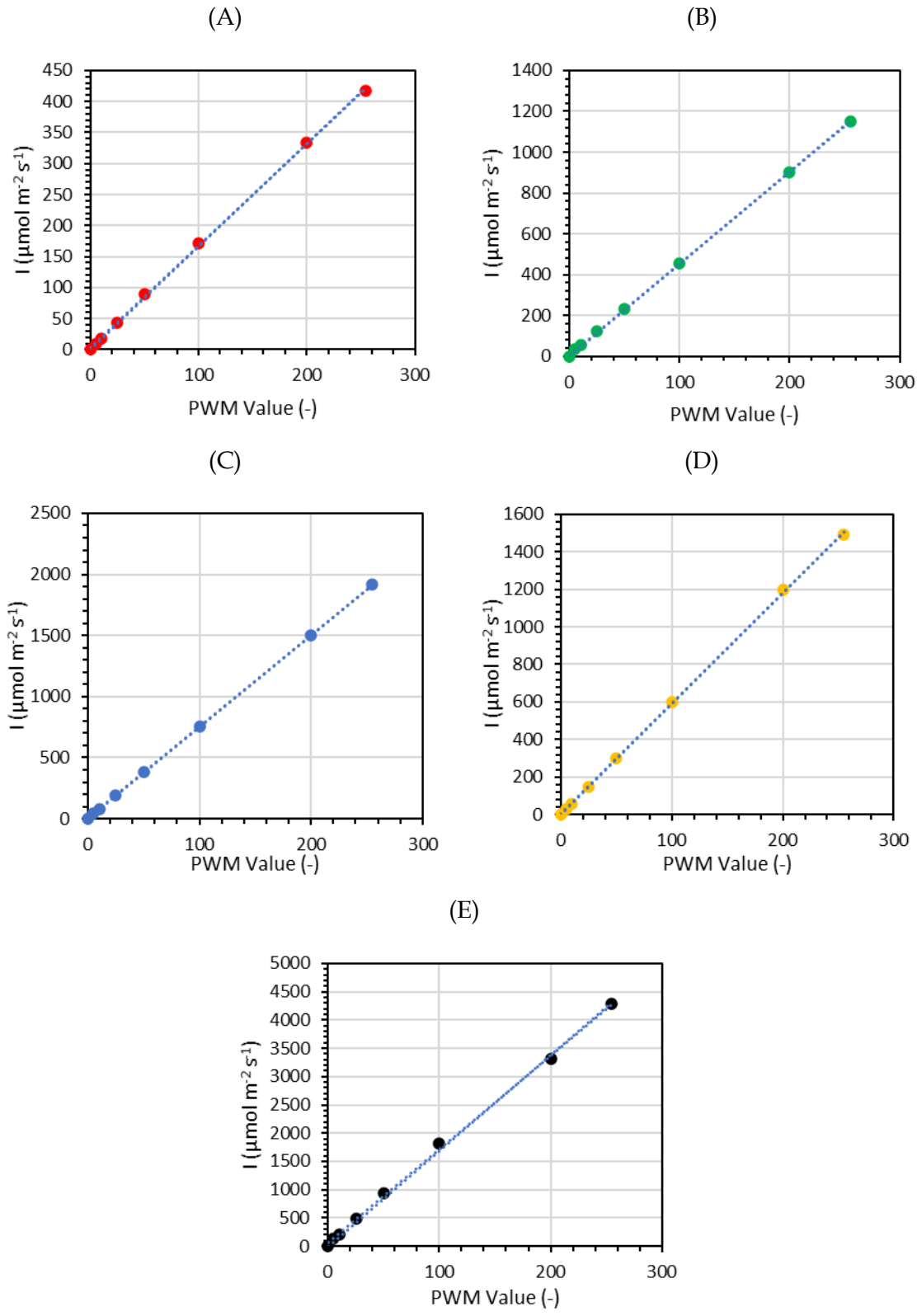

Figure 4.17 – Calibration curves for LED light intensities, I, of the tubular photobioreactor. A) Red, B) Green, C) Blue, D) Warm white, E) All colours combined.

The calibration curves for the intensity in µmol m^{-2} s^{-1} of each colour for a given PWM level, V_{PWM}, are given by Equations (4.48) to (4.52) for $0 < V_{PWM} < 255$.v

$$I_{Red} = 1.66\, V_{PWM} \tag{4.48}$$

$$I_{Green} = 4.53\, V_{PWM} \tag{4.49}$$

$$I_{Blue} = 7.52\, V_{PWM} \tag{4.50}$$

$$I_{White} = 5.91\, V_{PWM} \tag{4.51}$$

$$I_{All} = 16.9\, V_{PWM} \tag{4.52}$$

4.4.3 Gas holdup

Gas holdup was determined by measuring the liquid height against a scale on the outside of the bubble column under a range of conditions. The initial liquid height was recorded with no gas bubbling and then again with a controlled flow of gas. As the liquid height was variable due to bubbles bursting at the surface, an average value was taken, and the range estimated by observing the level over approximately 10 seconds. Both gas flow and liquid flow rates were varied for the trials and the system was allowed to equilibrate for 60 seconds prior to any level measurements being taken. The gas used for all tests was air and the liquid used was tap water. The temperature was constant at 24.3 ± 0.1 °C during the tests.

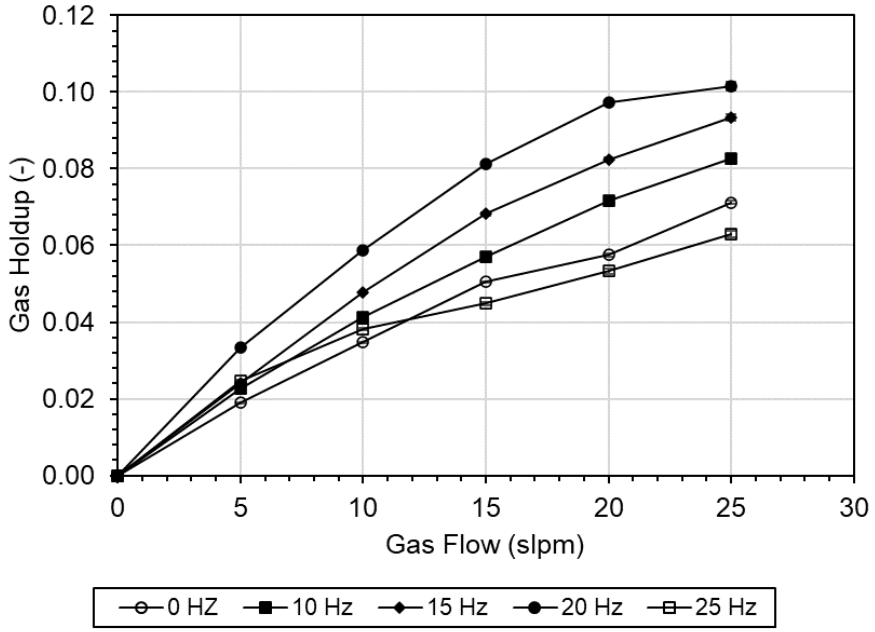

Figure 4.18 – Gas holdup in the bubble column for different gas flow rates and pump speeds. Error bars represent measurement uncertainty.

5 Investigation of the Lipidome of *Trachydiscus* sp. LCR-Awa-9-2

5.1 Introduction

In order to maximise the EPA content and productivity of *Trachydiscus* sp. LCR-Awa-9-2 it was important to understand its lipidome to determine the potential limitations and effects of different treatments. As discussed in § 2.4, most literature associates EPA with the galactolipids in microalgae. In particular, other eustigmatophytes such as *Nannochloropsis* sp. are reported to contain the vast majority of EPA in this lipid fraction, namely concentrated in the MGDG lipids associated with the chloroplast. Additionally, EPA is typically associated with a select few fatty acids in the MGDG species such as another EPA (20:5/20:5), palmitic (20:5/16:0), or palmitoleic acid (20:5/16:1) (Cohen, 1999). It was hypothesised that *Trachydiscus* sp. LCR-Awa-9-2 would show similar characteristics to these related strains of microalgae. Confirmation of the lipids associated with EPA would allow further understanding of the potential for increasing EPA content of the cells and the behaviour exhibited under different culture conditions.

Investigation into the lipidome of *Trachydiscus* sp. LCR-Awa-9-2 was conducted using a series of stages and techniques, with a particular focus on EPA. The general fatty acid composition of the microalgae was determined by extraction, derivatisation, and then GC-FID analysis of the fatty acid methyl esters. To refine the fatty acid composition of different lipid classes of the microalga, thin layer chromatography (TLC) was used to fractionate the lipid classes prior to derivatisation and GC analysis. To determine the individual lipid species mass spectrometry was used to analyse non-derivatised samples. Both liquid chromatography mass spectrometry (LC-MS) and TLC followed by direct infusion or LC-MS were used to analyse individual lipid classes. Investigation of the biosynthetic and metabolic pathways or associated enzymes was beyond the scope of this study.

5.2 Development of lipidomic chromatographic and analytical methods

Development of methods was conducted with commercially available freeze-dried *Chlorella vulgaris* biomass powder (Lifestream International Ltd, New Zealand) as well as *Trachydiscus* sp. LCR-Awa-9-2 biomass. As *Chlorella vulgaris* is a widely studied microalga

this allowed comparison with expected results from published lipidomic analyses to validate results. A stated dietary composition of the *Chlorella vulgaris* powder used can be found in Appendix E. The following sections focus on the development of lipid extraction, HPLC, TLC, and MS methods used in the lipidomic analyses attempted.

5.2.1 HPLC method development

Development of the HPLC method for separation of lipid extracts was conducted collaboratively with two undergraduate students during the course of this study, and was as reported by Dever (2018) and Xia (2019). There were many methods described in the literature for HPLC separation of microalgal lipids, of which a selection that were considered in this study are summarised in Appendix B. For this study, the method reported by Li *et al.* (2014) was used as the basis for development of the HPLC method. The HPLC apparatus used in this work was that described in § 3.18. Lipid samples for analysis were prepared by the modified Bligh and Dyer extraction method covered in § 3.13 from freeze-dried biomass. Briefly, the preliminary HPLC method used, and that was developed further, was as follows. The column used was a C_8 column with a 3 µm particle size, 150 mm × 2.1 mm (Restek, USA). Mobile phase A was water/acetonitrile 1:2 (v/v) and mobile phase B was acetonitrile/tetrahydrofuran/ isopropyl alcohol 1:1:1 (v/v). Lipid samples were dissolved in water/acetonitrile 1:2 (v/v). The flow rate was 0.25 mL min^{-1}, the column temperature was held at 40 °C, and the injection volume was 10 µL. The mobile phase composition gradient was as follows: B was ramped from 0% to 50% over 15 minutes then ramped to 80% over 30 minutes, held for 2 minutes at 80% and then returned to 0% and equilibrated for 11 minutes. The balance was made up by mobile phase A. Analytes were detected by a charged aerosol detector (CAD).

Improvement of the preliminary method in collaboration with Dever (2018) involved altering the sample solvent, mobile phase gradient, injection volume, and column temperature. The improved method was as follows (with the same column, HPLC apparatus, and mobile phases as used previously). The lipid sample was dissolved in water/tetrahydrofuran 1:1 (v/v) to a concentration of approximately 1 mg mL^{-1} and the injection volume was 25 µL. The column was held at 20 °C and the mobile phase gradient was 0% B to 50% B over 25 minutes, then increased to 80% B over 40 minutes where it was held at 80% for 2 minutes. The composition was returned to 0% B over 3 minutes and the column allowed to re-equilibrate for 10 minutes. The mobile phase flow rate was 0.25 mL min^{-1}.

The improved HPLC method was used to perform HPLC-MS in order to determine the nature of the of the separated lipids. HPLC-MS analyses were conducted in collaboration with Xia (2019) using the apparatus and methods outlined in § 3.19 by the School of Physical and Chemical Sciences (University of Canterbury).

5.2.2 Thin layer chromatography method development

Work in collaboration with Xia (2019) focussed on separation of lipids from *Chlorella vulgaris* and *Trachydiscus* sp. LCR-Awa-9-2 on silica gel TLC plates using a variety of methods and solvent systems that were reported in literature. The general method that was used for TLC separations is outlined in § 3.17; however, the solvent system used for each separation was varied. Fatty acids from the separated lipid classes were analysed by GC-FID according to the methods in § 3.15 and 3.16. Lipid extracts were obtained by two different methods: a modified Bligh and Dyer method from freeze-dried biomass (§ 3.13) and an isopropanol extraction method from fresh biomass (§ 3.14).

The original two-dimensional TLC solvent system trialled by Xia (2019) (Method A) was as reported by Christie (2019) of chloroform/methanol/water (75:25:2.5, v/v) for the first direction and chloroform/methanol/acetic acid/water (80:9:12:2, v/v) for the second direction. Lipids were visualised by iodine staining. Individual spots were scraped from the plate, lipids extracted with chloroform and derivatised for GC analysis as described earlier.

One-dimensional separations were trialled to obtain the major bulk classes of lipids, as well as loading the plate with a greater total lipid mass (Method B). The one-dimensional separations used the same chloroform/methanol/water (75:25:2.5, v/v) solvent as used previously, but the second direction was omitted. Lipids were loaded in a line across the bottom edge of the plate to increase the total mass of lipids. Lipid spots were visualised with iodine staining. Lipids were then analysed from non-stained plates prepared identically to the stained plates by using the stained plates to locate lipid bands on the non-stained plates.

An alternative two-dimensional TLC method was used based on the solvent systems used by Gašparović *et al.* (2015) in an attempt to separate the EPA-containing fraction from the other neutral lipids and pigments eluting in the same band in previous TLC separations (Method C). In this case, the solvent for the first direction was

acetone/toluene/water (91:30:7.5, v/v) and the solvent for the second direction was chloroform/acetone/formic acid (95:5:0.6, v/v).

As EPA is normally associated with galactolipids in other microalgae the presence of carbohydrates in the TLC spots was tested for using Molisch's test. The test involved spraying the TLC plate with a 2.4 g L^{-1} α-naphthol-10 vol% sulfuric acid-80 vol% ethanol solution and then baking the sprayed plate in an oven at 120 °C for 5–10 minutes until a red-purple colour change was observed on the lipid spots (Wang & Benning, 2011). Plates were sprayed using an airbrush to apply the Molisch's test solution until the entire plate was covered by a light, even covering. A purple or red colour change of the lipid spot after baking the sprayed plate indicated presence of carbohydrates.

Separation of potential monoglucosyl diacylglycerides (GlcDG) was conducted using one-dimensional TLC with the solvent system reported by Sato (2015) (Method D). The solvent mix used was chloroform/n-hexane/isopropanol/tetrahydrofuran/water (25:50:40:0.5:1, v/v). Lipid spots were identified by iodine staining.

In all cases the lipid classes were identified based on their relative elution positions on the TLC plates based on the reported literature results, Molisch's test results, or mass spectrometry. Canola oil was used a triacylglyceride standard and *Chlorella vulgaris* as a known microalgae standard. Mass spectrometric analysis of the spots was conducted by extracting the spots with acetonitrile/isopropanol (1:1, v/v) and then analysing the separated classes by the mass spectrometric methods outlined in § 3.19.

5.3 Results and discussion

5.3.1 HPLC-CAD and HPLC-MS analyses

The original HPLC method from Li *et al.* (2014) trialled with the *Chlorella vulgaris* lipid extract showed some separation of the lipid classes upon inspection of the CAD chromatograms; however, improvement was required to separate the lipid classes in a fashion that was suitable for further analysis and mass spectrometry. As can be observed in Figure 5.1, analyte peaks showed significant overlap and the majority of lipid species eluted all within a short time range around the 20 minute mark. Improvement was desired of the peak resolution to reduce overlap of peaks. Chromatograms of lipid separations from the improved HPLC method are shown in Figure 5.2 for both *Chlorella vulgaris* and *Trachydiscus* sp. LCR-Awa-9-2 lipid extracts. The *Chlorella vulgaris* result showed better peak resolution and elution of the analytes over a longer time period compared to the

preliminary method above. The result from the *Trachydiscus* sp. LCR-Awa-9-2 lipids showed that there were distinct differences between the lipid composition of this microalga and *Chlorella vulgaris* based on the chromatograms.

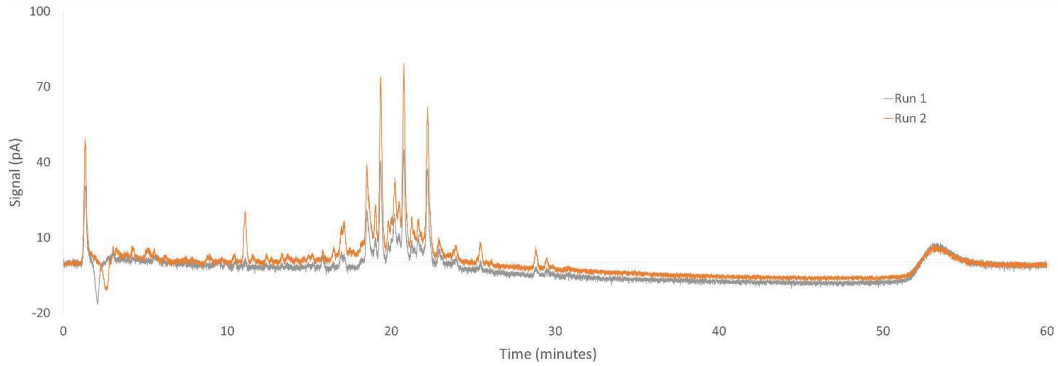

Figure 5.1 - Example of HPLC-CAD chromatograms of Chlorella vulgaris lipid separation with the preliminary HPLC method. Reprinted with permission from Dever (2018).

(A)

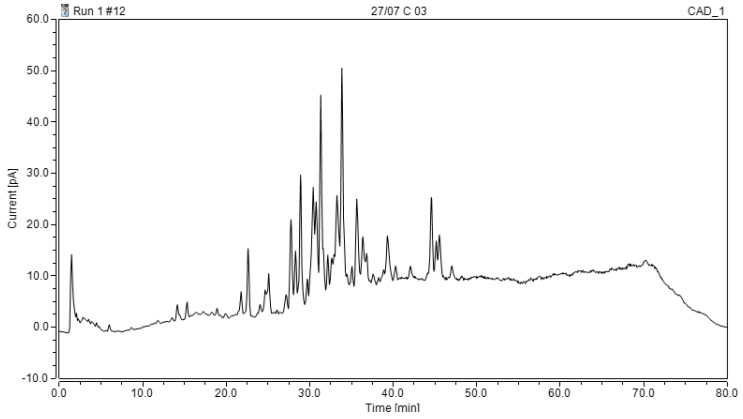

(B)

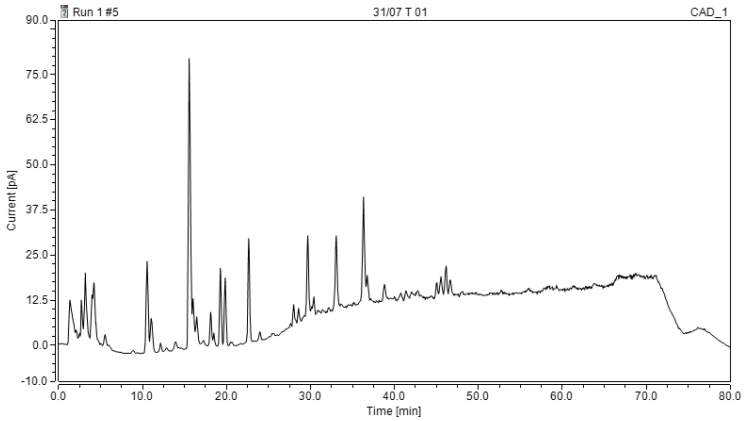

Figure 5.2 - Examples of HPLC-CAD chromatograms of A) Chlorella vulgaris and B) Trachydiscus sp. LCR-Awa-9-2 lipid separations with the improved HPLC method. Reprinted with permission from Xia (2019).

HPLC-MS was attempted with the improved HPLC lipid separation achieved above for *Trachydiscus* sp. LCR-Awa-9-2; however, the result from this did not show presence of the expected lipid species such as MGDG. Additionally, the chromatogram achieved from HPLC-CAD was not able to be replicated by HPLC-MS with the total ion count chromatogram. An example of the chromatogram obtained from HPLC-MS is shown in Figure 5.3.

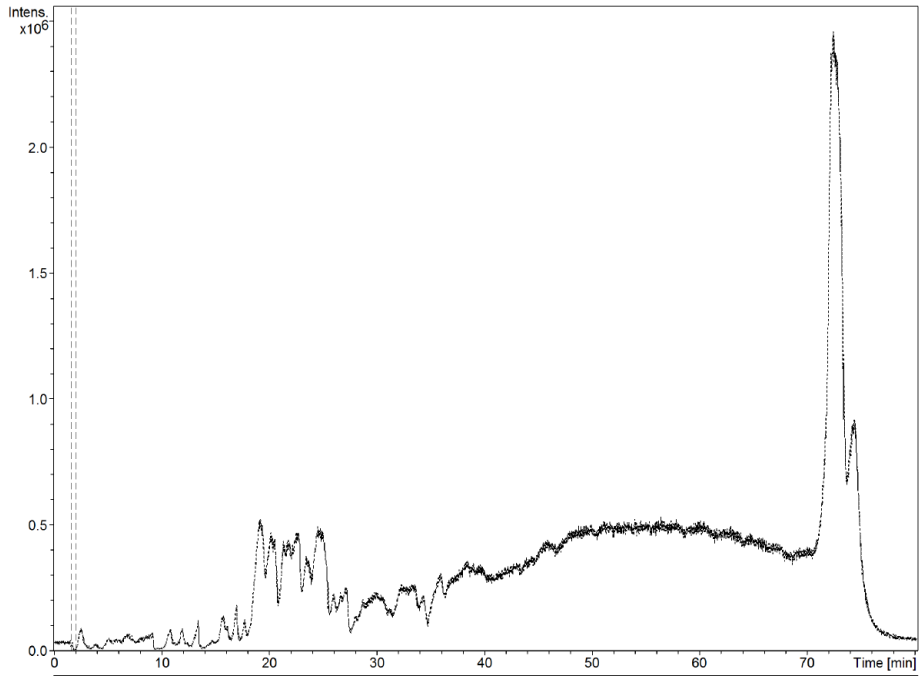

Figure 5.3 – Example of a total ion chromatogram obtained from HPLC-MS for Trachydiscus sp. LCR-Awa-9-2. Reprinted with permission from Xia (2019).

The mass spectra obtained from the HPLC-MS analysis did not show m/z ratios consistent with probable lipid species and almost all mass spectra were dominated by a major peak at 413 m/z which would not have been expected if separation of the sample was occurring. It was deduced that the use of tetrahydrofuran in the mobile phases and sample solvent was possibly causing reactions to occur with lipids and other species which obscured any meaningful results (Katritzky & Rees, 1984) (despite tetrahydrofuran being used in the work by Li *et al.* (2014) as well as in other studies (Appendix B)). This indicated the tetrahydrofuran used in this study had likely degraded and formed peroxides (Katritzky & Rees, 1984; Zagorevskii *et al.*, 2006). Due to the issues encountered with the HPLC-MS method that was developed further work focussed on TLC separations as discussed below in order to simplify the analysis and determine where issues encountered in the HPLC-MS analysis may be occurring.

5.3.2 TLC-GC-FID, TLC-MS, and TLC-LC-MS analyses

Development of TLC methods

Preliminary TLC separations that were trialled using Method A showed that separations for *Chlorella vulgaris* lipid extracts behaved as expected from the reported method; however, the results from *Trachydiscus* sp. LCR-Awa-9-2 showed differences in the location of the expected MGDG lipid class. TLC plates prepared using the initial two-dimensional TLC method are shown in Figure 5.4 with some of the relevant lipid spots identified by Xia (2019) based on typical literature results.

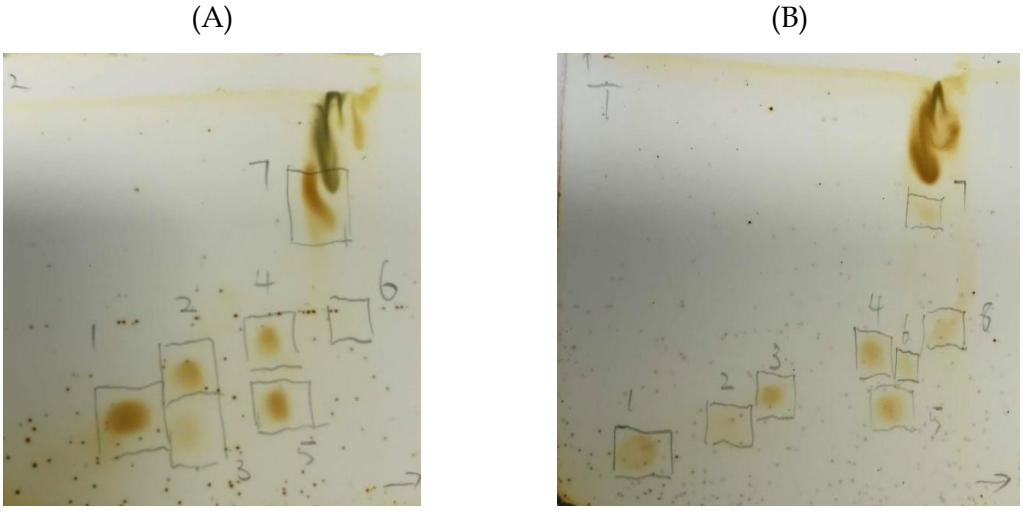

(A)	(B)
1: PC	1: PI
2: DGDG	2: PC
3: unknown	3: PG
4: PE	4: DPG
5: PG	5: unknown
6: unknown	6: unknown
7: MGDG	7: MGDG
	8: unknown

Figure 5.4 – Iodine-stained TLC plates from Method A for and A) Chlorella vulgaris and B) Trachydiscus sp. LCR-Awa-9-2 with likely lipid classes numbered. Direction 1: left to right; direction 2: bottom to top. Reprinted with permission from Xia (2019).

Initial GC-FID results of the fatty acid composition of the spots isolated from the above TLC separations by Xia (2019) suggested that the quantity of lipids obtained from the spots may have been too low to reliably assess the fatty acid composition due to negligible EPA being detected and noisy chromatograms. One-dimensional TLC separations were trialled using Method B to increase the quantity of lipids for GC analysis. However, GC analysis of the separated lipid bands from the one-dimensional TLC plate

from Method B again showed negligible total EPA compared to the total extract and it was discovered at this point that this result was due to use of spots from the iodine stained plate. This was due to the iodine reacting with the lipids on the stained plates and these spots being used for GC analyses (Kates, 1986). GC analysis of the fatty acids from non-stained plates was more promising, with the total fatty acid composition of the combined spots matching closely with that of the original total lipid extract, confirming that iodine was reacting with the lipids on the plate and affecting the GC results.

In other microalgae EPA is mainly associated with the galactolipids as discussed earlier, but GC analysis of the TLC spots from *Trachydiscus* sp. LCR-Awa-9-2 showed that EPA was mainly located in what was expected to be the neutral lipid band. This band had an EPA fraction of approximately 33 g/100 g total fatty acids and around 90 wt% of the total EPA present in the cells. Meanwhile, the expected galactolipid band did not show a notable peak for EPA in the GC chromatograms (Xia, 2019). As the EPA-containing lipid class was not sufficiently separated from the pigments and other neutral lipids an alternative two-dimensional separation was trialled with Method C where the second solvent system was changed to separate the neutral lipid classes. This separation again showed distinct differences between the *Chlorella vulgaris* and *Trachydiscus* sp. LCR-Awa-9-2 lipid separations as seen in Figure 5.5.

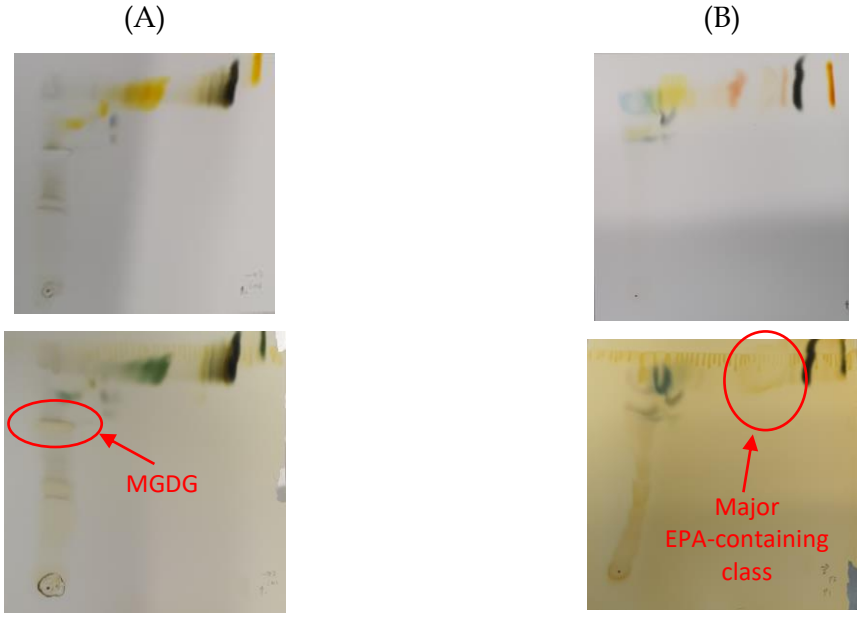

Figure 5.5 – Two-dimensional TLC plates of lipid separations with (bottom) and without (top) iodine staining for A) Chlorella vulgaris, and B) Trachydiscus sp. LCR-Awa-9-2 using Method C. Direction 1: bottom to top; direction 2: left to right.

A lipid spot was detected that was separated from the pigments and other neutral lipids in *Trachydiscus* sp. LCR-Awa-9-2 (circled spot in Figure 5.5 B) but was not present in the separation for *Chlorella vulgaris*. GC analysis of this spot for *Trachydiscus* sp. LCR-Awa-9-2 showed that it contained a high proportion of total EPA (approximately 80 wt% of all EPA).

Molisch's test was used on the plate to test for carbohydrate-containing lipids and this confirmed the presence of carbohydrates in the unknown lipid class spot of interest. This indicated that the lipid class present was likely some class of glycolipid, but different from those which are typically present in *Chlorella vulgaris* such as MGDG. Additionally, due to the unknown lipid class eluting in a similar fashion to neutral lipids it was assumed to be a less-polar species than the typical galactolipids. The major lipid classes separated on the TLC plate were identified as outlined in Figure 5.6 and Table 5.1 below for *Trachydiscus* sp. LCR-Awa-9-2.

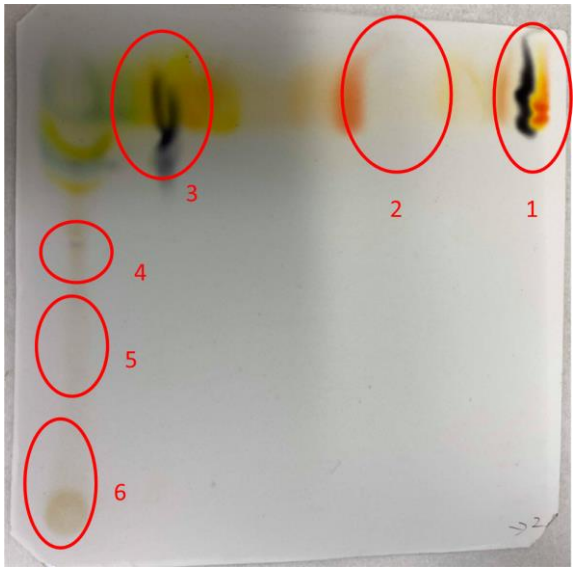

Figure 5.6 – Two-dimensional TLC plate of lipid separation of Trachydiscus sp. LCR-Awa-9-2 with method C. Direction 1: bottom to top; direction 2: left to right. Adapted with permission from Xia (2020).

As spot 2 contained the vast majority of EPA in the cells but its class was unable to be conclusively identified from the TLC elution results mass spectrometric analysis was focussed on this unknown lipid class in an effort to identify the class as discussed below.

Table 5.1 – Fraction of total EPA present in TLC spots in Figure 5.6 from GC-FID analysis. Data from Xia (2020).

Spot Number	Likely Lipid Class	Proportion of Total EPA (g / 100 g EPA)
1	Triacylglycerides	4
2	Unknown (carbohydrate-containing)	84
3	Other neutral lipids	8
4	MGDG	4
5	DGDG/SQDG	Negligible
6	Phospholipids	Negligible

The mass spectrum from the TLC spot analysed for *Trachydiscus* sp. LCR-Awa-9-2 was as shown in Figure 5.7. There were notable peaks for the $[M+H]^+$ and $[M+Na]^+$ adducts of free EPA (m/z 303.2319 and 325.2142 respectively) which was expected due to the high EPA content determined by GC analysis. These could have been due to either the presence of free EPA or fragmentation of EPA-containing lipid species.

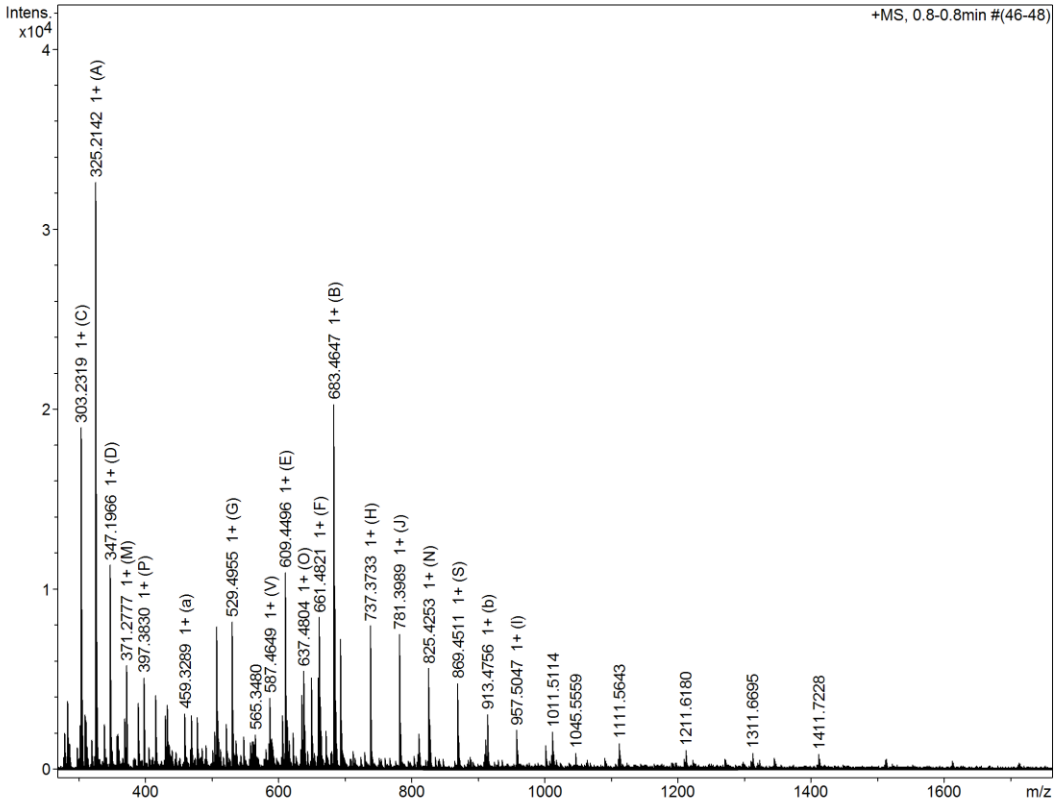

Figure 5.7 – Mass spectrum of Trachydiscus sp. LCR-Awa-9-2 major EPA-containing TLC spot (Spot 2, Figure 5.6, TLC Method C). ESI positive mode.

Further notable peaks were also present for the $[M+H]^+$ and $[M+Na]^+$ adducts corresponding to the EPA-containing diacylglyceride (DG) of DG 20:5/20:5 at m/z of 661.4821 and 683.4647 respectively. The likely structure of this species is shown in Figure 5.8. Peaks were also seen at m/z 637.4802 which could be the $[M+Na]^+$ adduct of a variety of diacylglyceride species: either DG 20:5/16:0, DG 18:2/18:3, DG 16:1/20:4 or DG 16:2/20:3. Another peak at m/z 587.4649 aligned with the expected $[M+Na]^+$ m/z of DG 16:1/16:1 or DG 18:2/14:0. All of these species are expected from the typical biosynthetic pathways of EPA and other lipids in microalgae that were discussed in § 2.4.

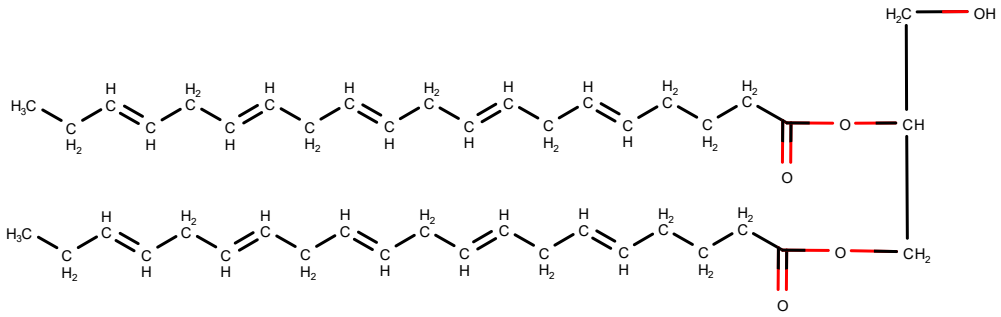

Figure 5.8 – Expected structure of DG 20:5/20:5 species present in the Trachydiscus sp. LCR-Awa-9-2 mass spectrum.

Of greatest interest was that there was no peak seen for the presence of MGDG 20:5/20:5 at m/z 823.535 for $[M+H]^+$ or 845.417 for $[M+Na]^+$ which would have been expected, at least at trace levels, if this species had been present and fragmented to form DG 20:5/20:5 during mass spectrometry. Additionally, no peaks at the expected m/z of typical MGDG head group fragments were seen (da Costa *et al.*, 2016). Lack of detection of both of these further confirmed that the TLC spot was unlikely to be a typical MGDG species.

Contamination of the samples was detected with peaks that occurred at m/z from 737.373 to 1045.556 with a m/z difference of 44.026 attributed to polyethylene glycol contamination and peaks at m/z greater than 1011.511 with m/z differences of 100.053 mainly attributed to PMMA contaminants (L. Schneider, 20th March 2020, personal communication).

While only diacylglycerides and associated fragments were found in the mass spectrum of *Trachydiscus* sp. LCR-Awa-9-2, the Molisch's test that was carried out on the lipid spot on the TLC plate indicated presence of carbohydrates and so it was expected that this lipid class may be some form of glycolipid. The presence of diacylglycerides in

the mass spectrum was proposed to be due to fragmentation of the glycolipid species resulting in the loss of the sugar head group from the lipids. One potential reason for the possible glycolipid species not being detected could be that the species was neutral, and thus unable to be detected by mass spectrometry (da Costa *et al.*, 2016). If both the sugar fragment from the head group and the overall glycolipid were neutral species then these would not have appeared in the mass spectrum. However, MGDG and other glycolipid species have been detected by mass spectrometry in other studies and in this study for *Chlorella vulgaris* as below, so this was unlikely to be the case.

As the glycolipids appeared to have undergone cleavage of the sugar group prior to mass spectrometric analysis it was possible that the sugar group was bonded to the glycerol back bone via a weaker bonding group (C. Costello, 21st March 2020, personal communication). One option that could have been present were glycophospholipids, where a phosphate group bonds the sugar to the glycerol (Gurr & Harwood, 1991). However, as phosphate groups are charged it was not expected that this class of lipid would elute near the neutral lipid classes and it was unlikely to be the class of the unknown lipids. Additionally, peaks with m/z values consistent with glycophospholipid fragments were not seen in the mass spectra.

To confirm that the suspected MGDG spot from the *Chlorella vulgaris* TLC Method C separation (circled spot in Figure 5.5 A) was indeed MGDG it was also analysed by mass spectrometry. The mass spectrum from the *Chlorella vulgaris* TLC spot is shown in Figure 5.9. Notable peaks detected in the mass spectrum confirmed the presence of MGDG species such as the $[M+Na]^+$ adduct of MGDG 16:0/16:1 at 749.516. The major peak at 773.516 could indicate $[M+Na]^+$ adducts of MGDG 18:3/16:1 or MGDG 18:2/16:2 species. The peak at m/z 589.481 could indicate the $[M+Na]^+$ adduct of DG 16:0/16:1 which could be a fragment of MGDG 16:0/16:1, further confirming the likelihood of presence of this MGDG species.

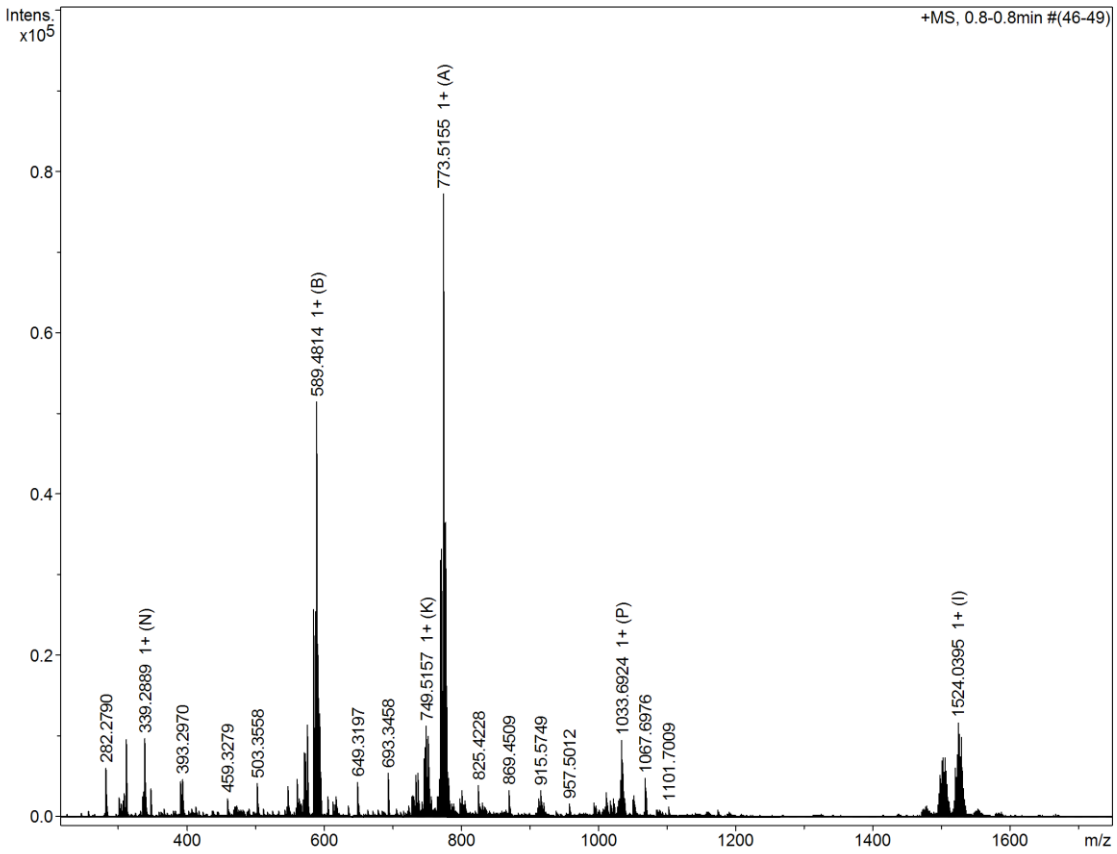

Figure 5.9 – Mass spectrum of Chlorella vulgaris MGDG TLC spot (TLC method C, circled spot from Figure 5.5 A). ESI positive ion mode.

The mass spectrometric results from *Chlorella vulgaris* showed that the spot in question was indeed likely to be MGDG and that MGDG species were able to be detected by the methods used in this study. This further indicated that the lipids analysed for *Trachydiscus* sp. LCR-Awa-9-2 above were unlikely to MGDG lipids.

LC-MS results from AgResearch also showed that the lipid composition of the spots from *Chlorella vulgaris* and *Trachydiscus* sp. LCR-Awa-9-2 TLC plates were substantially different, from both their total ion chromatograms and mass spectra. The LC-MS total ion chromatograms for the two spots are shown in Figure 5.10. Peaks corresponding to the lipids of interest eluted with retention times between approximately 4 and 10 minutes and the peaks before and after this range were attributed to contaminants (as seen in the control chromatograms in Appendix C).

(A)

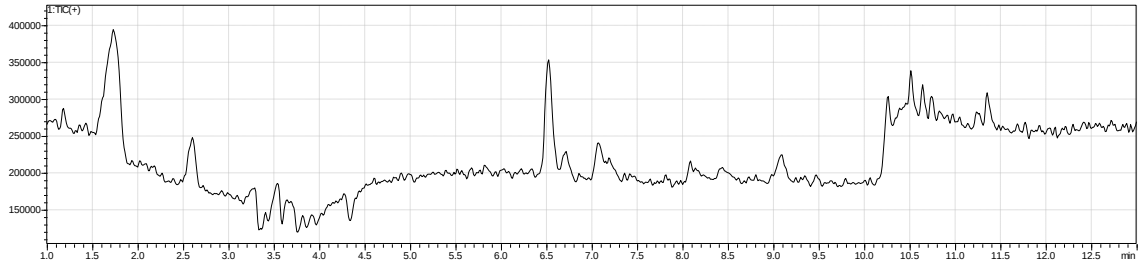

(B)

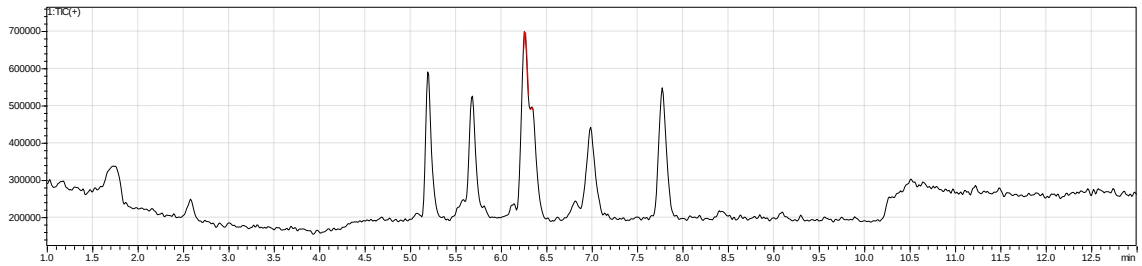

Figure 5.10 – Total ion chromatograms of LC-MS analysis of A) Trachydiscus sp. LCR-Awa-9-2 unknown lipid class and B) Chlorella vulgaris MGDG lipids.

The mass spectrum of the major *Trachydiscus* sp. LCR-Awa-9-2 peak at 6.5 minutes is shown in Figure 5.11. Similar large peaks were seen at m/z of 661.4835 and 683.4653 as were seen in the direct infusion mass spectrum in Figure 5.7 for the $[M+H]^+$ and $[M+Na]^+$ adducts of DG 20:5/20:5, respectively. An additional peak was noted at m/z 699.3492 which corresponded to the $[M+K]^+$ adduct of DG 20:5/20:5. The intensity of the peaks observed for EPA as a free fatty acid relative to the diacylglyceride species were lower than what was seen in the direct infusion result in Figure 5.7. This indicated that either fragmentation was occurring to a lesser degree than seen previously or that free fatty acids present in the TLC spot extract were separated from the DG species during the LC-MS process.

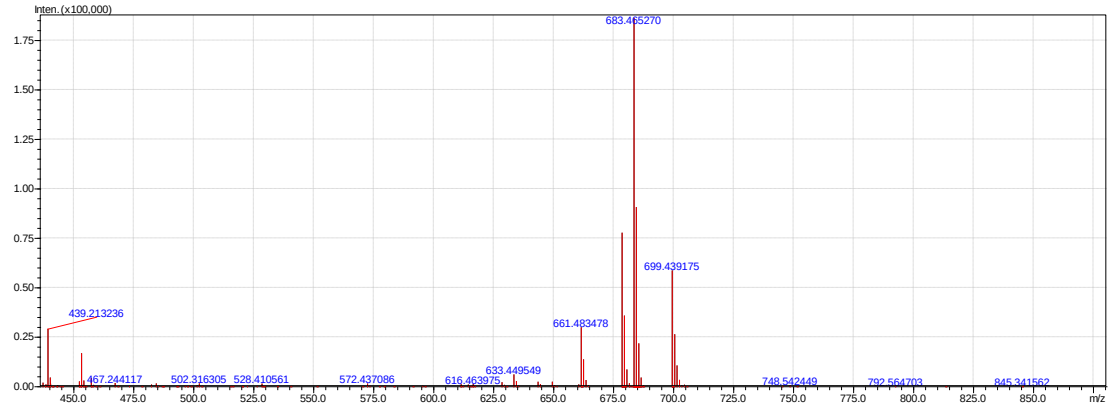

Figure 5.11 – Mass spectrum of the major chromatogram peak from the unknown lipid class of Trachydiscus sp. LCR-Awa-9-2.

Fragmentation of the notable 661, 683 and 699 m/z peaks was attempted, and the results were as summarised in Figure 5.12. Limited fragmentation was observed of these species. The $[M+H]^+$ adduct of EPA was observed at m/z of 359.258 for the 661 and 683 fragmentation patterns confirming the presence of EPA in the species. Fragments corresponding to the loss of sugar groups such as galactose or glucose were not observed; however, if a sugar group was present this fragment is unlikely to be seen from the species that were fragmented as they appeared to be diacylglyceride species that have already lost any sugar moiety that may have been present prior to mass spectrometric analysis.

Mass spectrometry of the peaks from *Chlorella vulgaris* again showed a different composition to the results from *Trachydiscus* sp. LCR-Awa-9-2 as seen in Figure 5.13. Notable peaks that were seen in the mass spectra were again consistent with MGDG species. For example, the peak at m/z of 769.487 was consistent with the $[M+Na]^+$ adduct of MGDG 16:3/18:3, 771.502 with the $[M+Na]^+$ adduct of MGDG 16:2/18:3 or MGDG 16:3/18:2, and 775.534 with the $[M+H]^+$ adduct of MGDG 18:3/18:3. Structures of these lipid species are shown in Figure 5.14. All of these species were expected to be present based on the typical biosynthesis pathways of MGDG lipids discussed in § 2.4.2. Attempts at fragmentation of the major m/z peaks from *Chlorella vulgaris* did not show strong fragmentation patterns (see Appendix D).

(A)

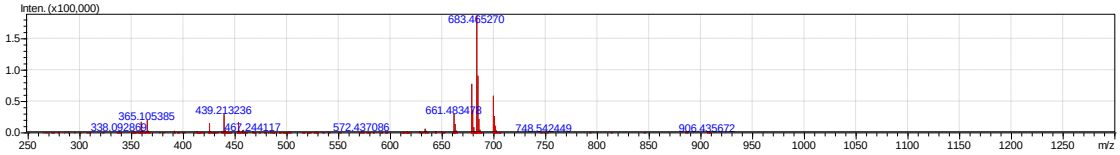

(B)

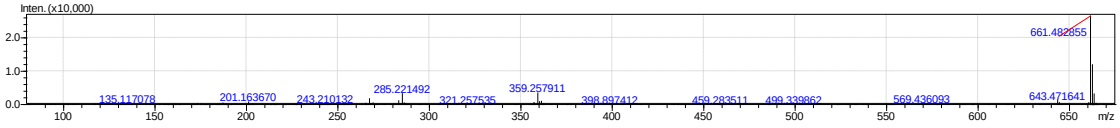

(C)

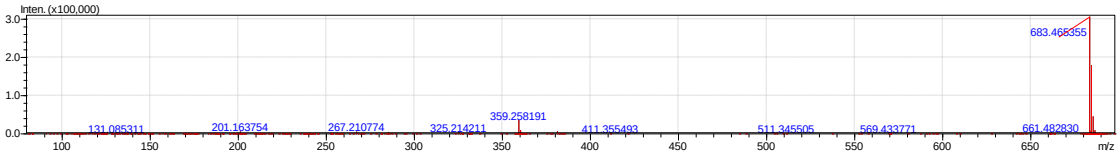

(D)

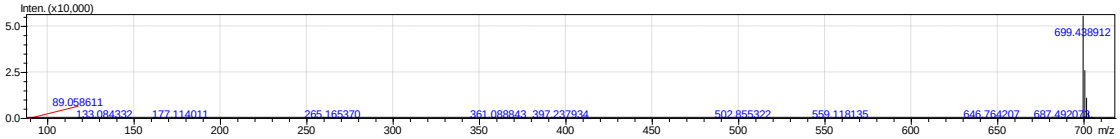

Figure 5.12 – Fragmentation patterns of major m/z peaks from the A) overall mass spectrum for Trachydiscus sp. LCR-Awa-9-2 for peaks at m/z of B) 661, C) 683, and D) 699.

(A)

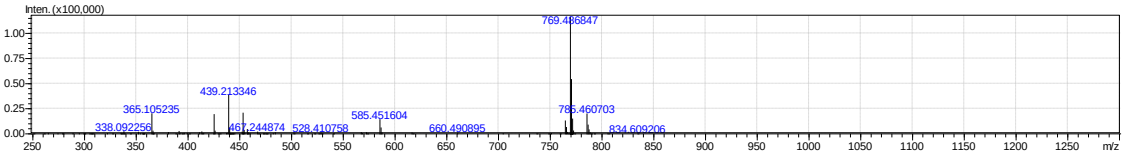

(B)

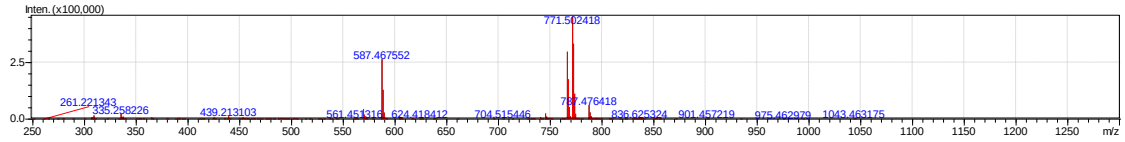

(C)

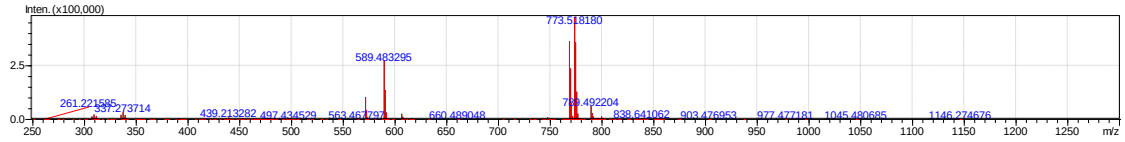

(D)

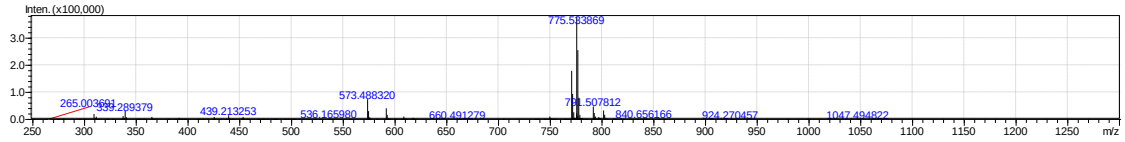

(E)

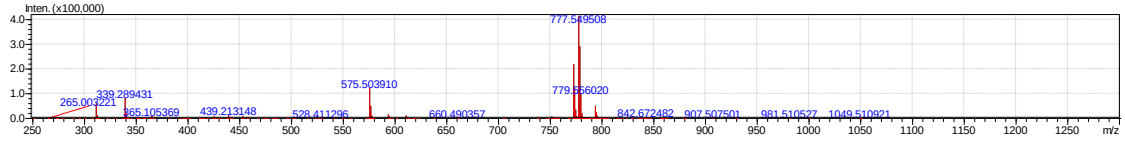

Figure 5.13 – Mass spectra of the five major chromatogram peaks from Chlorella vulgaris at retention times of A) 5.25 min, B) 5.75 min, C) 6.25 min, D) 7 min, and E) 7.75 min.

(A)

$[M+Na]^+ = 769$

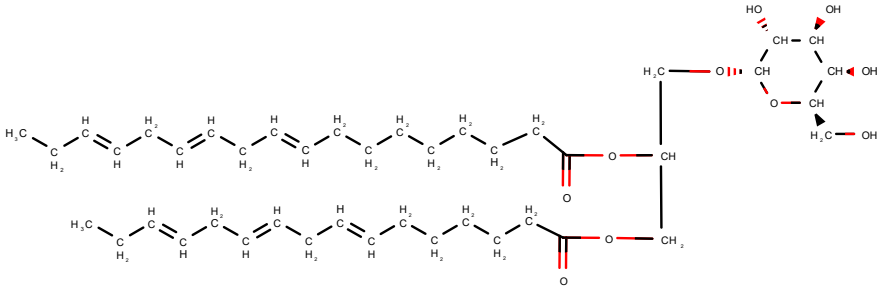

(B)

[M+Na]+ = 771

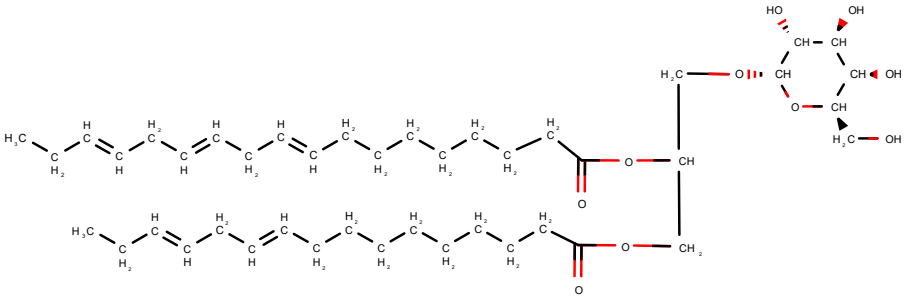

(C)

$[M+H]^+ = 775$

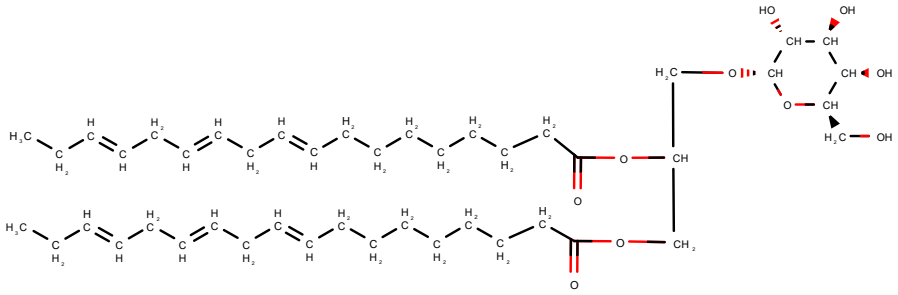

Figure 5.14 – Structures of likely MGDG species present in the Chlorella vulgaris sample. A) MGDG 16:3/18:3 B) MGDG 16:2/18:3 C) MGDG 18:3/18:3.

The results from the mass spectrometric analyses did not show conclusively the class of the EPA containing lipids in *Trachydiscus* sp. LCR-Awa-9-2. However, it was clear that the majority of the EPA containing lipids had EPA as the associated fatty acid on both positions of the glycerol backbone. This indicated that the lipid class was more likely associated with the typical 'eukaryotic' pathway as this results in a greater proportion of 20:5/20:5 species (Cohen, 1999). A higher proportion of 20:5/14:0, 20:5/16:0 or 20:5/16:1 species would indicate preference of the prokaryotic pathway. Additionally, a peak was

seen corresponding to DG 16:1/16:1 which is one important precursor to production of 20:5 fatty acids.

Separation of monoglucosyl diacylglycerides

Despite the mass spectrometry results indicating the unknown lipid class present in *Trachydiscus* sp. LCR-Awa-9-2 was diacylglycerides, the Molisch's test indicated the presence of carbohydrates in the lipid spot of interest. There was a remote possibility that the lipid class could be monoglucosyl diacylglycerides (GlcDG) based on results from cyanobacteria showing that these lipids can be accumulated if genes for the enzyme associated with epimerisation to galactose are knocked-out (Awai *et al.*, 2014; Sato, 2015). If a gene transfer event had occurred with *Trachydiscus* sp. LCR-Awa-9-2 it is possible that the microalga may have been able to synthesise these lipids. GlcDG is slightly less polar than MGDG based on their elution on the TLC plates and so this could explain the difference in separation of the lipid classes and the presence of carbohydrates in the spot.

TLC separations from Method D produced results which were consistent with the potential presence of GlcDG in *Trachydiscus* sp. LCR-Awa-9-2 with a lipid spot eluting slightly above the MGDG spot (Figure 5.15) as seen in the results of Sato (2015).

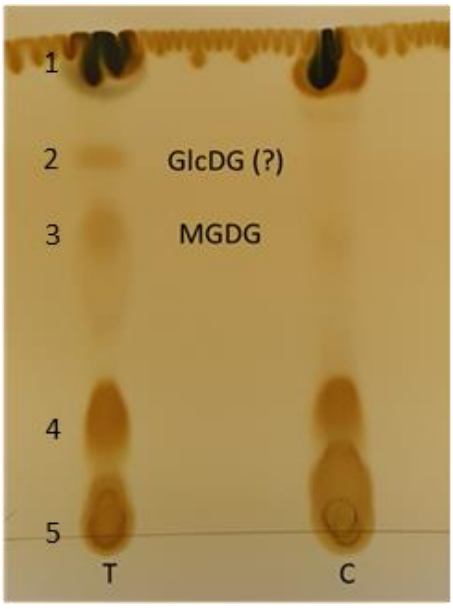

Figure 5.15 – TLC plate from method D separation for Trachydiscus sp. LCR-Awa-9-2 (T) and Chlorella vulgaris (C) with iodine staining. MGDG and possible GlcDG spots labelled.

The use of Molisch's test confirmed the presence of carbohydrates in the potential GlcDG spot. MGDG spots were seen for both *Trachydiscus* sp. LCR-Awa-9-2 and *Chlorella vulgaris*; however, a spot was only observed at the expected GlcDG position for *Trachydiscus* sp. LCR-Awa-9-2. While the position of the spot and Molisch's test result was consistent with GlcDG and the spot was not common to both species of microalga, further work is required to determine if the spot was indeed GlcDG and if it was the same as spot 2 from the Method C separation.

GC analysis of the fatty acids from the spots obtained from Method D for *Trachydiscus* sp. LCR-Awa-9-2 showed that there was negligible EPA (or any other fatty acids) in the GlcDG spot compared to the other lipid classes. The majority of EPA was present in the neutral lipid fraction as seen in Table 5.2. This confirmed that the spot previously analysed from Method C was not the same as the GlcDG spot obtained in this separation.

Table 5.2 – Proportion of EPA present in the separated lipid classes from the Method D TLC plate for Trachydiscus sp. LCR-Awa-9-2.

Spot number	Likely lipid class	Proportion of total EPA (g / 100 g total EPA)
1	Neutral lipids	84
2	GlcDG	Negligible
3	MGDG	0.6
4	SQDG/DGDG	0.3
5	Phospholipids	15

This result further indicated that the EPA-containing lipids were likely to be diacylglycerides as determined during the mass spectrometric results, rather than GlcDG. Further analysis of the results from the Molisch's test from Method C showed that it was likely that the suspected GlcDG class was eluting in the same region as the diacylglycerides and the spots were overlapping, as seen by presence of a smaller purple spot within the broader charred lipid spot in Figure 5.16. This was likely the reason for the positive Molisch's test despite the lack of detection of glycolipids during mass spectrometry of the lipid spot. As the GlcDG were present at a negligible concentration compared to the other lipids the concentration would likely have resulted in any peaks from GlcDG species present in the mass spectra being lost in the background noise.

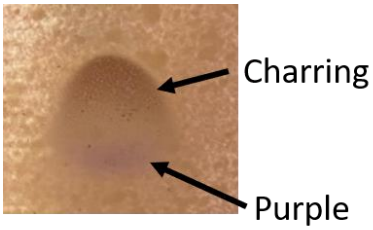

Figure 5.16 – Molisch's test of likely GlcDG and DG spot from Method C TLC plate showing overlap of lipid species. Adapted with permission from Xia (2020).

Degradation of lipids

Diacylglycerides are precursors to the production of other lipid species as well as degradation products of lipid species (Kates, 1986). As the presence of large quantities of diacylglycerides is uncommon in microorganisms it was highly likely that these were degradation products of the lipid classes containing the EPA (Christie, 1993). As diacylglycerides were not observed in the analyses for *Chlorella vulgaris*, the degradation of the lipid classes was not likely to be occurring due to chemical reasons such as due to the TLC solvents. However, it was likely to be due to enzymatic degradation during the extraction or freeze-drying process of the *Trachydiscus* sp. LCR-Awa-9-2 biomass. In order to test this, lipids were extracted using the hot isopropanol technique in § 3.14 from fresh biomass and separated by TLC using Method C as previously described. The result from this separation still showed a spot eluting at the same position as for diacylglycerides in the previous analyses; however, it was smaller in size than in the previous separations. Molisch's test also indicated the presence of carbohydrates in this spot as was seen previously.

GC-FID analysis of the fatty acids from the lipid spots showed that 50 ± 2 g/100 g total EPA was located in the MGDG lipids while only 3 ± 2 g/100 g total EPA was present in the GlcDG/DG lipids (Table 5.3). This result was consistent with what has been reported for other microalgae as discussed earlier and confirmed that significant degradation had occurred of the lipids extracted from freeze-dried biomass using the Bligh and Dyer method.

Table 5.3 – Proportion of EPA present in the separated lipid classes from the isopropanol extraction using Method C TLC for Trachydiscus sp. LCR-Awa-9-2.

Likely lipid class	Proportion of total EPA (g / 100 g total EPA)
Neutral lipids	20 ± 2
GlcDG/DG	3 ± 2
MGDG	50 ± 2
SQDG/DGDG/Phospholipids	14 ± 2
Phospholipids	13 ± 2

It was evident from this result that the presence of the large quantity of diacylglycerides in earlier results was due to degradation of MGDG and other lipid species. In the earlier work conducted in this study, freeze-dried biomass from both *Trachydiscus* sp. LCR-Awa-9-2 and *Chlorella vulgaris* was extracted with a modified Bligh and Dyer extraction method. While negligible degradation of lipids was observed with *Chlorella vulgaris* using this method, significant degradation of lipids was observed for *Trachydiscus* sp. LCR-Awa-9-2. Many lipidomic studies have used the Bligh and Dyer method to extract lipids from wet biomass for analysis (da Costa *et al.*, 2016); however, the work by Li *et al.* (2014) that was originally used as a basis for this work used a Bligh and Dyer method with freeze-dried biomass from a variety of strains, apparently without degradation. The isopropanol extraction method used, as recommended by Kates (1986), successfully inhibited degradation of lipid species based on the results obtained here. This indicated that lipids from *Trachydiscus* sp. LCR-Awa-9-2 were degraded either during the process of freeze-drying the biomass or the Bligh and Dyer method used in this study.

As the harvested biomass was frozen using a domestic −18 °C freezer during this work, the slow freezing rate likely lead to formation of ice crystals which ruptured membranes in the cells and allowed contact of lipids with degradative enzymes (Christie, 1993). Snap-freezing by use of liquid nitrogen or a −80 °C freezer could serve to avoid this effect. Additionally, the freeze-dryer used in this study did not provide temperature control of the samples and so the temperature of samples was only maintained during the freeze-drying process by the sublimation of ice from the frozen biomass. This could also have allowed degradation of lipids to occur during the freeze-drying process itself. In order to determine the cause of lipid degradation in the *Trachydiscus* sp. LCR-Awa-9-2 samples it is recommended that a variety of freezing and freeze-drying methods are

trialled such as using liquid nitrogen to freeze the biomass as mentioned above. Exposure of the biomass to different freezing conditions over different time periods may also indicate the rate at which the lipids are degraded. Additionally, extraction of wet biomass directly using the original Bligh and Dyer method should be attempted to determine if degradative enzymes are able to remain active in the organic solvents used in this process. As some proteins are also extracted in the Bligh and Dyer process it may also be required to thoroughly clean the lipid extract of any non-lipid contaminants to avoid degradation of extracted lipids which may not be required for other microalga strains (Christie, 1993). While enzymes appeared to have degraded the lipids by cleavage of head groups from lipids such as MGDG and fatty acids from the glycerol, the fatty acids themselves did not appear to be appreciably degraded. This was based on the GC-FID results obtained being consistent with the fatty acid profiles from other studies (Alfiarty, 2018; Tangestani, 2019) and so the overall fatty acid profile of the biomass was unlikely to be affected by the lipid degradation seen here.

The large amount of diacylglycerides produced and relatively small proportion of MGDG that remained in early results indicated that it was possible that the microalga possessed particularly aggressive degradative enzymes or preferable conditions for degradation compared to other strains. Due to these effects it is important to further investigate the mechanisms resulting in lipid degradation which may impact the future extraction methods that can be utilised depending on the final application of the EPA extracted from the cells. Many industrial oil extraction processes require rupturing of the cells (Cooney *et al.*, 2009); however, these processes would cause lipids to come into contact with degradative enzymes as the cells are ruptured. Due to this it is likely that these processes would not be able to be used to extract EPA from *Trachydiscus* sp. LCR-Awa-9-2 without lipid degradation occurring and so techniques such as supercritical fluid extraction may be preferred. It is possible that diacylglycerides could be a preferential form of EPA delivery for humans as diacylglycerides themselves may have a beneficial impact on obesity as well as being absorbed differently in the digestive tract compared to triacylglycerides (Lairon, 2009; Lo *et al.*, 2008). Due to the potential benefits of diacylglycerides it is possible that the degradation effect seen in this study could be beneficial in producing a desirable health product and so further investigation should be conducted of this aspect.

While it was promising that the diacylglycerides containing EPA were largely detected as DG 20:5/20:5 species by mass spectrometry which can lead to high EPA fractions, it also indicated that there was potentially little in the way of room for improvement to increase the EPA fraction beyond the current maximums achieved. As the lipid molecules that contained EPA were already largely 'saturated' with EPA it does not allow for the potential of further increase in the EPA fraction of the lipids as there would be if the majority of species had contained EPA associated with other fatty acids (e.g. 20:5/16:1 or 20:5/16:0 etc.). However, as the lipids analysed had been degraded from their original lipid class, investigation of the non-degraded lipids is required to draw further conclusions on this aspect. As EPA is mainly associated with the MGDG lipids which typically make up the thylakoid membranes there is a limit to the absolute amount of this lipid class that can be accumulated in the cells depending on the size limit of the chloroplasts and packing of the thylakoid membranes.

Further investigation is required to elucidate the full lipidome of *Trachydiscus* sp. LCR-Awa-9-2 with non-degraded lipids. Investigation of the changes in the lipidome under different growth conditions is also required to determine the biosynthesis pathways of EPA which may be present and which lipid classes are associated with EPA accumulation under different conditions. The presence of lipids consistent with GlcDG in *Trachydiscus* sp. LCR-Awa-9-2 indicated similar biosynthetic pathways to those in cyanobacteria may be present and thus may indicate that associated genes were transferred from cyanobacteria for this to occur. Further mass spectrometric and NMR studies are recommended to conclusively confirm the presence of GlcDG. Full metabolomic and genomic analyses would be also required to investigate the possibility of a gene transfer event.

5.4 Conclusions

The aim of investigating the lipidome of *Trachydiscus* sp. LCR-Awa-9-2 was to determine which lipids EPA was associated with and whether this microalga was consistent with the lipidomes of other microalgae. The results from this study showed that EPA was likely primarily associated with MGDG lipids like it is in other microalgae. Lipids extracted from freeze-dried biomass of *Trachydiscus* sp. LCR-Awa-9-2 with the modified Bligh and Dyer method used resulted in significant degradation of the lipid species which was not observed to occur with *Chlorella vulgaris*. Mass spectrometric analyses indicated that the degraded lipid class was a diacylglyceride species with m/z

peaks indicating the presence of DG 20:5/20:5 species. However, results from TLC plates suggested that the diacylglyceride lipid class was eluting alongside a carbohydrate-containing class and there was a possibility that the glycolipid class could be monoglucosyl diacylglycerides which are known to be present in cyanobacteria. TLC results showed that the suspected GlcDG class present in *Trachydiscus* sp. LCR-Awa-9-2 was not present in *Chlorella vulgaris* and that the lipid compositions of the two microalgae species were distinctly different. Further investigation into the lipidome of *Trachydiscus* sp. LCR-Awa-9-2 is required to fully elucidate its lipidome and the mechanisms responsible for the degradation of lipids that was observed to avoid degradation during further studies.

6 Effect of Light on the Growth, Oxygen Evolution Rate, and EPA Content of *Trachydiscus* sp. LCR-Awa-9-2

6.1 Introduction

Light is the energy source for photoautotrophic growth and so it is one of the most important factors to optimise for growing microalgae cultures. The intensity and wavelength of light has been shown to affect the growth and composition of microalgae as discussed in § 2.5.1. Previous work with *Trachydiscus* sp. LCR-Awa-9-2 has investigated growth and EPA content and productivity under different light intensities and colours; however, the light requirements for cultures in tubular photobioreactor cultures was not known. There were also still questions around the light requirements for cells and the maximum light intensity that had been used was 500 µmol m^{-2} s^{-1}. In outdoor cultures light intensities can exceed 3–4000 µmol m^{-2} s^{-1} (Acién Fernández *et al.*, 2001) and so the behaviour of cells at higher light intensities than had been previously studied was also of interest. Light cycling had not been investigated with this microalga although it had been shown to grow under 24-hour illumination.

6.2 Light saturation and limitation

6.2.1 Introduction

Light is the major limiting factor for photoautotrophic cultures of microalgae. As discussed earlier, the photosynthesis and growth rate of microalgae increases as light intensity increases, until the culture becomes light saturated and a further increase in light intensity does not increase the rate of growth. In order to grow cultures efficiently under artificial lights the saturation point for growth is important to determine in order to avoid wasting energy by oversaturating the culture. It is also important to ensure the culture is not light limited in order to maximise the growth rate. Additionally, the light intensity determines the maximum cell density that is able to be achieved in a culture which is key to determining its potential productivity.

Most studies report the incident light intensity on a culture as this is simple to measure; however, under a constant incident intensity, as the culture progresses the light available per cell decreases. Due to this, a culture may transition from being light saturated to light limited over the course of the culture. It was hypothesised that the light available per cell was the determining factor for maintaining maximum growth in cultures if all

other environmental factors were non-limiting. This study focussed on determining the light saturation or limitation point for growth of *Trachydiscus* sp. LCR-Awa-9-2 in a tubular photobioreactor and shake flasks. The light saturation point for photosynthesis was also investigated by measuring the oxygen evolution rate of cells in a homogenously illuminated environment.

6.2.2 Experimental methods

Light saturation and limitation of cultures were determined using three different methods: measurement of oxygen evolution, growth of shake flask cultures, and growth of tubular photobioreactor cultures. The oxygen evolution rate under different light intensities was measured using the methods outlined in § 3.12. Oxygen evolution rate measurements were taken at a range of light intensities between 0 and 1337 µmol m^{-2} s^{-1} with warm white LEDs. Light saturation was determined by the point where the rate of oxygen evolution did not increase despite an increase in light intensity. Inoculum for these experiments was harvested fresh from a tubular photobioreactor culture (as described below) grown under combined RGBWW light. Experiments were conducted at an initial dissolved oxygen concentration of 100 ± 5% air saturation, 25.0 ± 0.4 °C, and an initial pH of 4.60 ± 0.05.

Light saturation in shake flasks was investigated by growing cultures as described in § 3.8. Cultures were grown under light intensities of 250 µmol m^{-2} s^{-1} and 500 µmol m^{-2} s^{-1} and the growth curves from the cultures were used to determine the point of light limitation, as described in the results section below. Tubular photobioreactor cultures were conducted using the general methods and apparatus in § 3.11 and 4. Different light intensities were used to grow cultures in the tubular photobioreactor with cultures conducted at 217 and 500 µmol m^{-2} s^{-1} as well as a culture where the light intensity was increased each day to maintain light limitation or saturation as the cell density increased. The point of light limitation in the cultures was determined from the growth curves as covered in the results section below. Additionally, once the cell density had reached its maximum for 500 µmol m^{-2} s^{-1} cultures, the light intensity was increased to 1000 or 2000 µmol m^{-2} s^{-1} to determine the maximum cell density achievable for each intensity.

Oxygen evolution rates in the tubular photobioreactor were measured by turning off the gas supply and measuring the increase in dissolved oxygen concentration for around one hour. Following this, the gas supply was turned back on to strip the

accumulated oxygen and supply CO_2 again. Oxygen evolution rates were measured on alternate days to allow the culture to recover from any oxygen poisoning or carbon limitation effects. The light intensity was increased during the culture from 500 to 1000 µmol m^{-2} s^{-1} on day 17 and the oxygen evolution rate measured before and after the increase in light intensity.

6.2.3 Results and discussion

The oxygen evolution rate at different light intensities are shown in Figure 6.1 for warm white LED light. In all tests the cell density was 1.0 ± 0.2 × 10^6 cells mL^{-1} and the surface area of the flask exposed to light was 1.3 × 10^{-2} m^2. The saturation point for the cells was determined by the light intensity above which an increase in light intensity did not result in an increase of oxygen evolution rate.

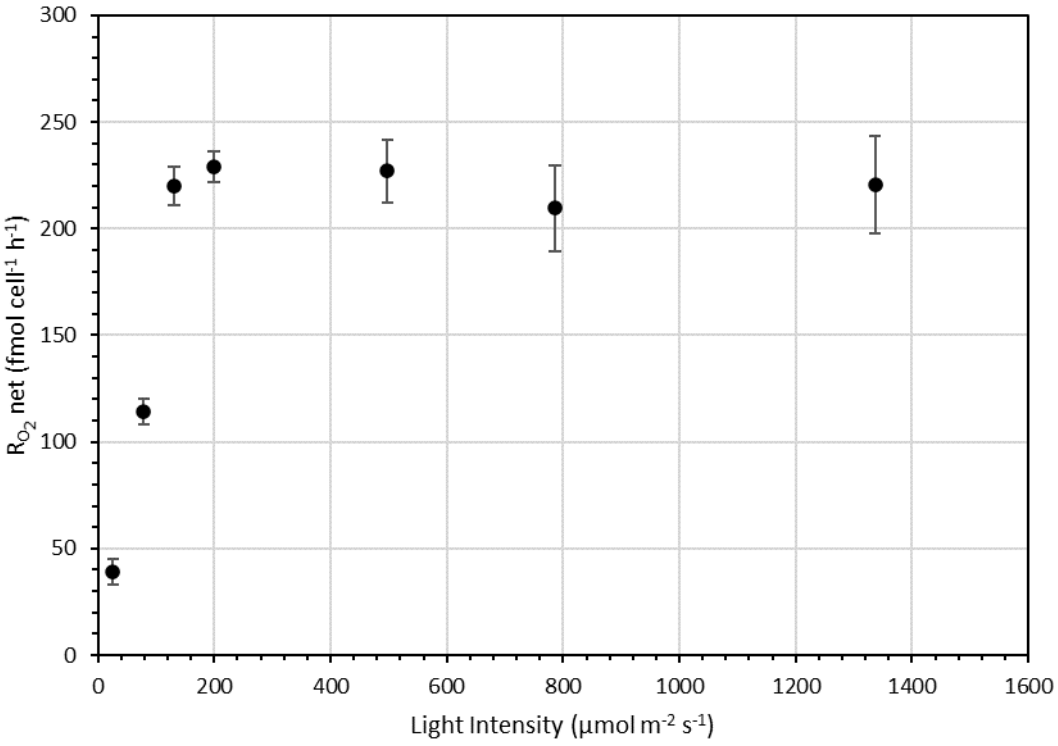

Figure 6.1 – Net oxygen evolution rate, R_{O_2}, under different light intensities of warm white LED light. Data points are the mean of three tests. Error bars are the standard deviation from triplicate experiments.

The results of the oxygen evolution rate measurements showed that at incident intensities of 199 µmol m^{-2} s^{-1} and above the cells were light saturated and no increase of oxygen evolution rate was observed. The cell specific light intensity was determined to be 1.5 × 10^{10} photons $cell^{-1}$ s^{-1} at the point of light saturation. The photosynthesis-irradiance

curve obtained followed the general form that was expected for microalgae with the rate of oxygen evolution increasing with light intensity at low intensities but then remaining relatively constant once the cells became light saturated. No noticeable photoinhibition was observed at a light intensity of 1337 µmol m^{-2} s^{-1} under the test conditions.

The light saturation point for cultures in shake flasks was determined by examining the growth curves such as those in Figure 6.2. It was assumed that while cultures were light saturated they grew at their maximum growth rate, but once the cell specific photon flux decreased below the saturation point the growth rate started to decrease and the culture was light limited. The point at which the growth curve transitioned from exponential to the beginning of stationary phase, as marked on the curves in Figure 6.2, was used to determine the saturation point for shake flask cultures. This was taken as the point where the gradient of the log-linear growth curve noticeably started to steeply decrease compared to the previous day's growth.

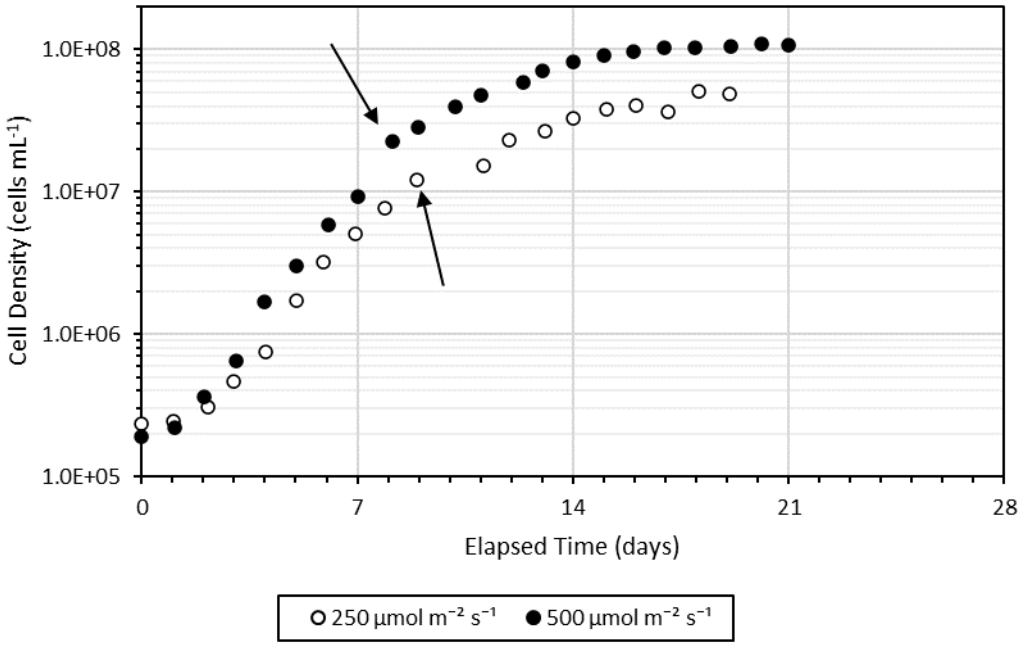

Figure 6.2 – Growth curves for shake flask cultures showing the cell density at which light levels were assumed to transition from saturation to limitation.

The incident light intensity for the cultures in the curves was 250 or 500 µmol m^{-2} s^{-1} and it was assumed that the surface area through which the light acted was approximately 9.3×10^{-3} m^2. The area here was assumed to be the surface area of the culture in the flask through which light passed through (i.e. the surface area of a truncated cone, including the top face but not the bottom) and all the light was assumed to be

absorbed by the 100 mL of culture. From this, the light saturation value for *Trachydiscus* sp. LCR-Awa-9-2 was found to be approximately 1.2×10^9 photons $cell^{-1}$ s^{-1} for the 250 µmol m^{-2} s^{-1} condition and 1.3×10^9 photons $cell^{-1}$ s^{-1} for the 500 µmol m^{-2} s^{-1} condition. The cultures were still able to grow after the saturation point was reached and the culture became light limited, but at a continually decreasing growth rate until the maximum cell density was reached. At this point it was assumed to have reached a compensation point where the rate of photosynthesis was only sufficient to maintain the culture.

The light saturation point in the tubular photobioreactor was determined similarly to the approach used for the shake flask cultures. The area for light transmission was assumed to be the surface area of the solar receiver tubes over which the lights were acting (approximately 2.65 m^2). The volume used was the entire culture volume of 76 L.

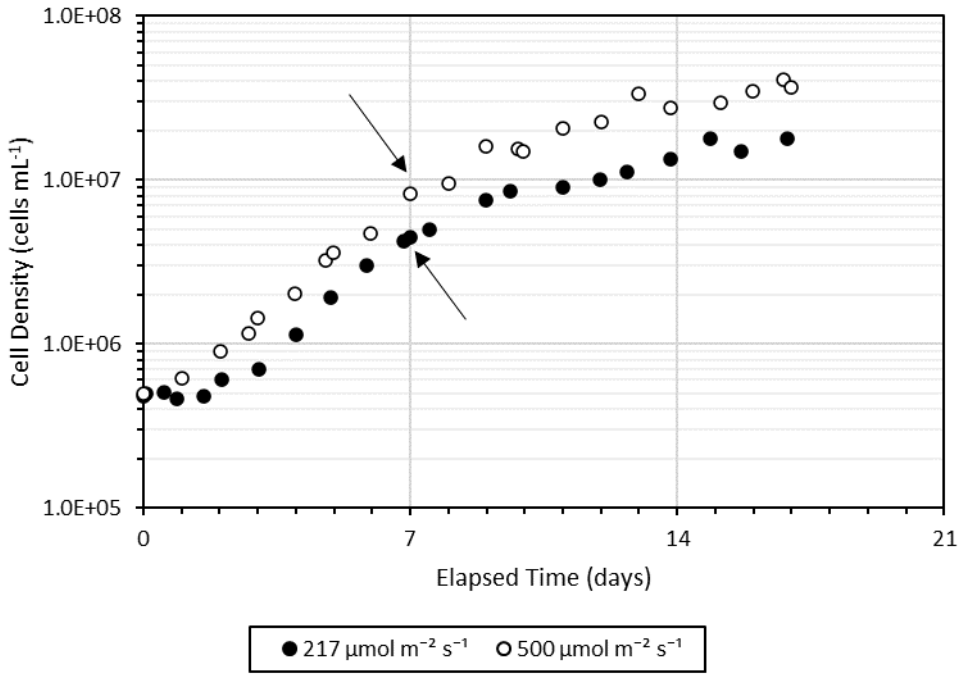

Figure 6.3 – Growth curves from tubular photobioreactor cultures showing the point at which light levels were assumed to transition from saturation to limitation.

The light saturation point was found to be 1.0×10^9 photons $cell^{-1}$ s^{-1} for the 217 µmol m^{-2} s^{-1} condition and 1.3×10^9 photons $cell^{-1}$ s^{-1} for the 500 µmol m^{-2} s^{-1} condition. These values were consistent with the light saturation values calculated for cultures in shake flasks under similar incident light intensities.

The light saturation values obtained for the shake flask and tubular photobioreactor cultures were similar; however, the result obtained from the oxygen evolution rate measurement was greater by an order of magnitude. One possible explanation is due to the different methods being used in each case to determine the saturation point. It is possible that the rate of photosynthesis does not directly correspond to the growth of the cells and so a greater light intensity is required to maximise the oxygen evolution rate than is required for growth. This could be due to energy from photosynthesis not being directly used for growth. Additionally, at the points used in the growth curve, the rate of growth was still in the exponential phase, but the growth rate had already started to decrease from what it was earlier in the exponential curve. Due to this, the cells may not be truly light saturated at the point taken in the growth curves, but it is still the point where the growth rate began to drop off far more rapidly and thus the observed change in gradient of the growth curve.

The light colour used in the different methods was different, with warm white LEDs used for the oxygen evolution rate, a mix of warm and cold white and violet for the shake flasks, and RGBWW for the tubular photobioreactor. However, all cultures used warm white LEDs either exclusively or as part of the light mix, so the spectral composition of the light sources was still comparable. Also, the results between the shake flasks and tubular photobioreactor were similar despite the different light spectrum so it was not expected to have made a significant difference to the result that would be on an order of magnitude different (light wavelength effects are covered further below in § 6.4).

The cell densities used for the calculation of the saturation points were around one order of magnitude different between the oxygen evolution rate measurement and the growth curves, but the light intensities were similar between both cases and so the cell density was the most likely cause of the discrepancy between the results from the two experimental techniques. At similar cell densities in the growth curves as were used in the oxygen evolution rate measurements (1.0×10^6 cells mL^{-1}) the specific growth rate of cultures was higher than at the saturation point that was used for the growth-based calculations. At cell specific light intensities where growth was assumed to become strongly light limited, the corresponding net oxygen evolution rate was still positive, but it was far lower (approximately one-tenth of what it was at saturation).

The growth curve for the tubular photobioreactor culture grown under maintained light saturation is shown in Figure 6.4. For this culture, the cell specific light saturation

level was assumed to be approximately 1.5×10^9 photons $cell^{-1}$ s^{-1} based on the results that were obtained from the growth saturation points above. To simulate light limitation the culture was illuminated at a level of below approximately 1.0×10^9 photons $cell^{-1}$ s^{-1} for the first five days of the culture, and then increased to a level of approximately 2.0×10^9 photons $cell^{-1}$ s^{-1} from day five onwards to light saturate the culture. During the first 5 days of the culture where the light intensity was held below the saturation point a decreased growth rate was seen than in the light saturated condition. Once the light intensity was increased above the saturation point the growth rate of the culture increased.

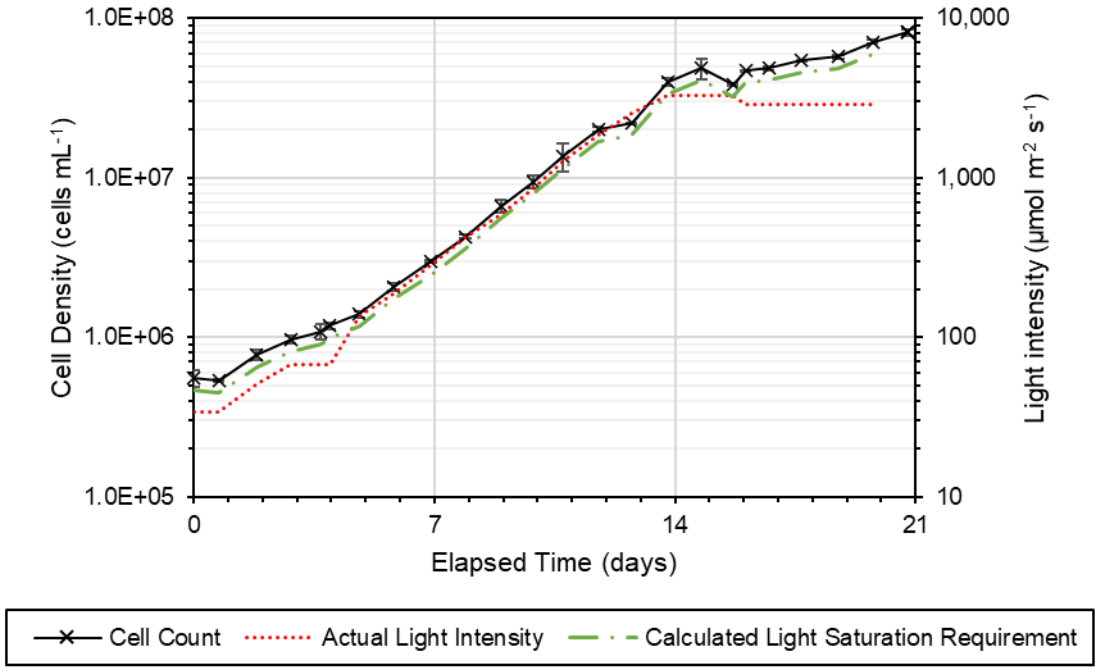

Figure 6.4 – Growth curve for the tubular photobioreactor culture grown under maintained light saturation. Error bars represent the standard deviation of duplicate cell counts of one culture.

The growth curve showed that strong exponential growth was able to be maintained whilst light saturation was maintained, up to around 4×10^7 cells mL^{-1}. Due to the limitations of the apparatus used to maintain the culture temperature, the light intensity was limited to 3260 µmol m^{-2} s^{-1} briefly and then reduced to 2872 µmol m^{-2} s^{-1} where it was able to be maintained for the remainder of the culture while maintaining the culture temperature at 25 °C. Due to this limitation, light saturation was not able to be maintained indefinitely. It was seen that as soon as the light intensity was no longer able to be increased and the culture became light limited (day 15) the growth rate began to decrease in a similar fashion to what had been seen in other cultures.

Maximum specific growth rates for the abovementioned cultures are summarised in Table 6.1. μ_{max} was similar under different light intensities in each culture apparatus, but growth rates were slower in the tubular photobioreactor than in shake flasks. The reduction in growth rate was seen in the tubular photobioreactor was assumed to be due to the difference in light and dark volumes in the apparatus which was tested in § 6.3. Additionally, the growth rate under the light saturation condition in the tubular photobioreactor was lower than under constant illumination. This could be due to the cells not being sufficiently light saturated as the light intensity was held only just higher than the calculated saturation point throughout the culture. This result indicated that cultures were light limited at a cell density lower than that used to calculate the point of light limitation in Figure 6.2 and Figure 6.3. As cells still appeared to be growing strongly at this point this could indicate that the cells were using up energy stores to maintain the growth rate and were already under light limitation. Therefore, the true light saturation requirement would be higher than that which was calculated.

Table 6.1 – Maximum specific growth rates for shake flask and tubular photobioreactor (TPBR) light saturation cultures.

Apparatus	**Light Intensity (µmol m^{-2} s^{-1})**	**μ_{max} (d^{-1})**
Shake flask	250	0.61 ± 0.02
Shake flask	500	0.62 ± 0.02
TPBR	217	0.48 ± 0.02
TPBR	500	0.47 ± 0.02
TPBR	Saturation	0.40 ± 0.02

As the light intensity was increased the maximum cell density achieved in the tubular photobioreactor also increased as seen by Figure 6.5. The rate that the cell density increased with increasing light intensity was not linear and there was diminishing return in maximum cell density as the light intensity was increased.

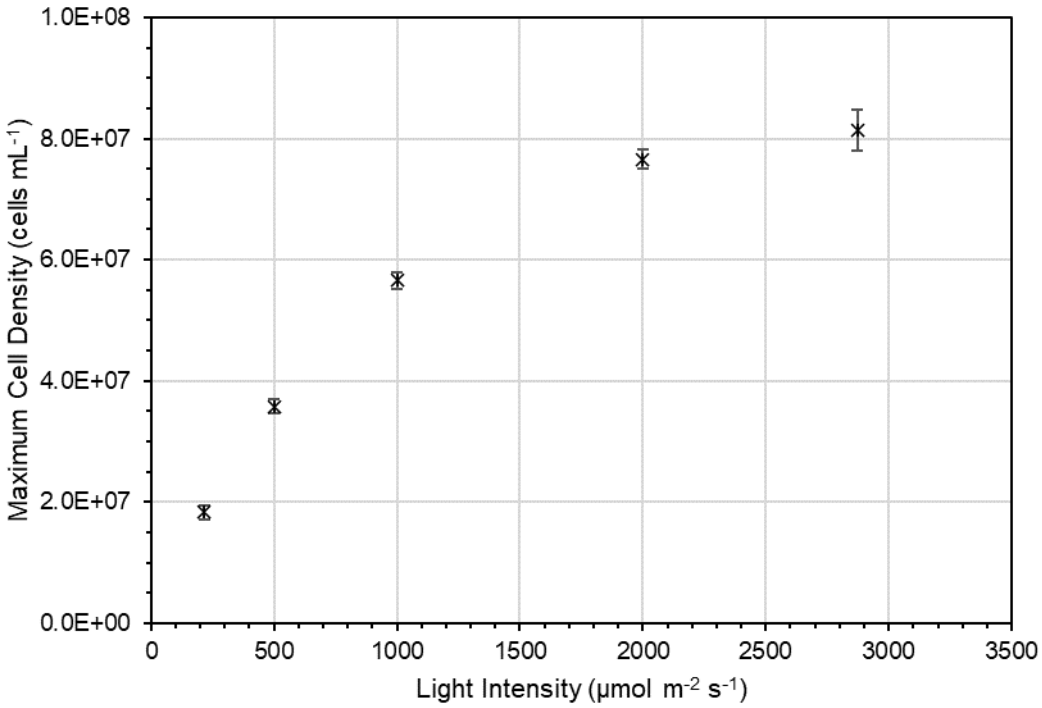

Figure 6.5 – Maximum cell density achieved under different light intensities in the tubular photobioreactor. Data points are the mean of two counts taken from the same culture. Error bars represent the standard deviation of replicate cell counts on a single culture.

The maximum light intensity that could be used was limited by the experimental apparatus due the ability to remove heat from the reactor at high light intensities in order to maintain the culture temperature at 25 °C. Additionally, the lighting rig itself was limited to a maximum intensity of 4300 µmol m^{-2} s^{-1}. While the light intensity was limited by these factors, it is unlikely that artificial lighting of this intensity would be economically feasible for cultures due to the energy consumption of supplying this quantity of light (see § 9.6.2). The increase in cell density achieved above 2000 µmol m^{-2} s^{-1} was unlikely to be great enough to warrant the increase in energy consumption, with an increase in cell density of approximately 6% for a light intensity increase of 44% when increased to 2872 µmol m^{-2} s^{-1}. In comparison, increasing the light intensity at lower light intensities a greater payoff was observed with a 95% increase in cell density for a 130% increase in light intensity from 217 to 500 µmol m^{-2} s^{-1}.

The EPA and biomass productivities of the cultures in the tubular photobioreactor are summarised in Table 6.2 for the light saturation conditions investigated. EPA productivity was highest under the light saturation condition, largely due to the increase in biomass concentration compared to the other conditions. EPA content was highest for the culture grown at 500 µmol m^{-2} s^{-1} compared to the other conditions.

Table 6.2 – EPA and biomass productivities of tubular photobioreactor batch cultures under different light saturation conditions.

Light Intensity (µmol m^{-2} s^{-1})	EPA content (g / 100 g dry biomass)	Biomass concentration (g L^{-1})	EPA productivity (mg L^{-1} d^{-1})	Biomass productivity (g L^{-1} d^{-1})
217	4.5 ± 0.1	1.3 ± 0.1	3.4 ± 0.3	0.076 ± 0.006
500	5.3 ± 0.1	2.5 ± 0.1	8.0 ± 0.7	0.15 ± 0.01
Saturation (max. 2872)	5.0 ± 0.1	5.0 ± 0.1	12 ± 1	0.23 ± 0.01

One of the driving motivations behind maintaining the culture at a light level just above saturation of the cells was to minimise the energy consumption of artificial lighting of cultures by only using the amount of light that was required. The energy required for lighting is directly related to the total quantity of photons the culture was supplied with over the course of the culture. As summarised in Table 6.3, the total photon input to the cultures was lowest for the 217 µmol m^{-2} s^{-1} culture, followed by the 500 µmol m^{-2} s^{-1} culture then the saturation culture.

Table 6.3 – Total photon requirements of tubular photobioreactor cultures for different light intensities.

Light Intensity (µmol m^{-2} s^{-1})	Culture time to maturity (days)	Total photon requirement (mol photons)
217	17	$8.5 \pm 0.9 \times 10^5$
500	17	$1.9 \pm 0.2 \times 10^6$
Saturation (max. 2872)	21	$7.4 \pm 0.7 \times 10^6$

While the light saturated culture required the greatest quantity of photons of the conditions tested, by increasing the light intensity incrementally over the course of the culture to maintain light saturation it only required 50% of the photons (and thus energy) that would have been required had the culture been run at a constant light intensity of 2872 µmol m^{-2} s^{-1}.

If the light saturation culture had been harvested at the point that the same quantity of photons had been supplied as was used for the constant light intensity cultures the culture would have been harvested at day 12 and 14 for the equivalent photon supply in the 217 and 500 µmol m^{-2} s^{-1} cultures, respectively. At elapsed times of 12 and 14 days

the cell density in the light saturated culture was 2.0 and 1.4 times higher than at the same elapsed time in the respective constant illumination cultures. The cell densities in the light saturated culture at these elapsed times were also similar to the maximum cell densities that were reached in the respective constant-illumination cultures. This was due to the cultures growing faster for a longer period in the saturation-maintained culture and so the culture could reach a higher cell density in a shorter elapsed culture time. This approach of maintaining light saturation with artificial lighting of cultures could allow harvesting of the culture sooner than under constant intensity illumination and could increase the productivity of batch cultures due to decreased batch times.

Oxygen evolution rates were measured in the tubular photobioreactor during the culture shown in Figure 6.6. The light intensity was held at 500 µmol m^{-2} s^{-1} until day 17 of the culture when the light intensity was increased to 1000 µmol m^{-2} s^{-1}. The oxygen evolution rates measured on a selection of days during the culture are shown in Figure 6.7.

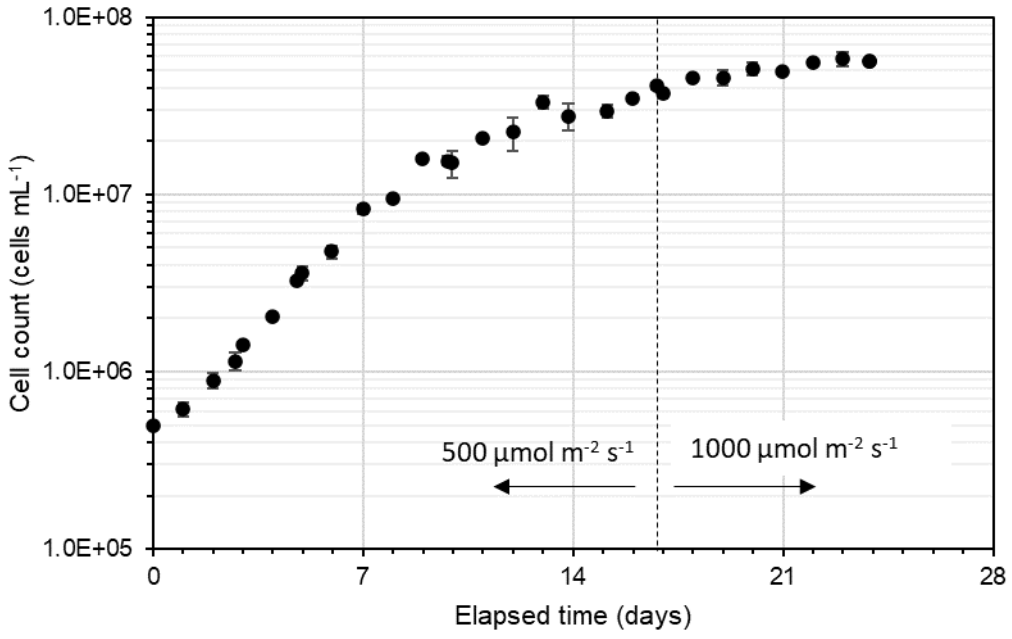

Figure 6.6 – Growth curve of tubular photobioreactor culture used during measurement of the oxygen evolution rate. Light intensity was changed from 500 to 1000 µmol m^{-2} s^{-1} on day 17 of the culture. Error bars denote standard deviation of duplicate cell counts from the same culture.

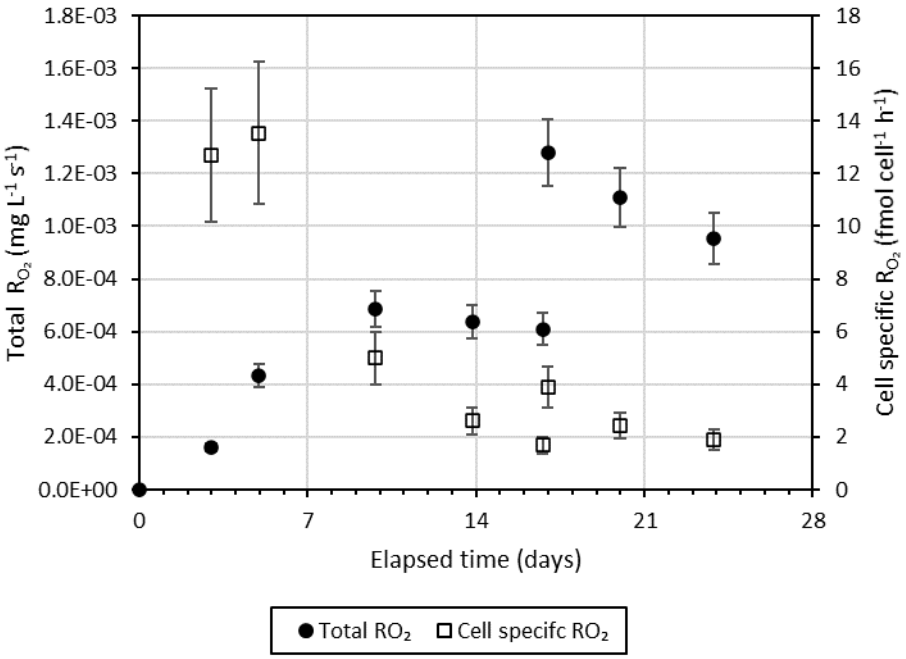

Figure 6.7 – Oxygen evolution rates, R_{O_2}, of Trachydiscus sp. LCR-Awa-9-2 over the course of a tubular photobioreactor culture. Light intensity was changed from 500 to 1000 µmol m^{-2} s^{-1} on day 17 of the culture. Error bars denote measurement error.

During the first 10 days of the culture the total rate of oxygen evolution increased as the cell density increased; however, after day 10 the rate of oxygen evolution plateaued and slightly decreased. On day 17 when the light intensity was doubled the total rate of oxygen evolution also approximately doubled. These results indicated that the culture was light limited from day 10 and this was also confirmed by the gradient of the growth curve also sharply decreasing around day 10. The increase in cell density and oxygen evolution rate when the light intensity was increased indicated that light limitation was occurring, rather than a nutrient limitation or other effects. After the light intensity was increased the rate of total oxygen evolution rate started to decrease as the cell density increased and the light available per cell decreased. The cell specific oxygen evolution rate was highest during the early days of the culture but drastically decreased between day 5 and 10 of the culture. On day 17 when the light intensity was doubled the cell specific oxygen evolution rate also roughly doubled and then continued to decrease as the cell density increased on the following days. The maximum cell specific oxygen evolution rates measured in the tubular photobioreactor were around 5% of that which had been measured in the oxygen evolution rate apparatus that were reported earlier. This was likely due to the culture in the tubular photobioreactor receiving a lower cell specific photon flux due to the geometry of the lighting arrangement and higher cell densities (approximately

7×10^9 photons $cell^{-1}$ s^{-1} at the highest for the tubular photobioreactor compared to around 4×10^{10} photons $cell^{-1}$ s^{-1} in the oxygen evolution apparatus for the equivalent incident light intensity). Unlike the oxygen evolution apparatus, the tubular photobioreactor was non-homogeneously illuminated and so the cells were not being continuously supplied with light which would also result in a decreased oxygen evolution rate. Other causes of the lower rate could be due to mixing of the culture in the bubble column due to circulation of the culture which could cause dissolved oxygen to be released to the atmosphere which did not occur appreciably in the oxygen evolution apparatus.

6.2.4 Conclusions

The key findings from these studies showed that for an artificially illuminated culture the lighting energy consumption could be minimised by increasing the light intensity over the course of a culture to maintain light saturation and thus avoid excess light being wasted while still maintaining sufficient culture growth. For *Trachydiscus* sp. LCR-Awa-9-2 there was no marked benefit to increasing the light intensity beyond around 2000 µmol m^{-2} s^{-1} when attempting to increase the cell density of the culture in the tubular photobioreactor. EPA productivity was greatest under the light saturated culture conditions, due mostly to the increase in final biomass concentration when compared to constant illumination cultures at 217 or 500 µmol m^{-2} s^{-1}. Results from the growth and oxygen evolution rate measurements indicated that light intensity limited growth during cultures. Cultures were shown to be able to grow at high light intensities comparable to sunlight which is promising for potential outdoor culturing of this microalga. Despite the increase in light intensity for the tubular photobioreactor cultures, the maximum specific growth rate and cell density achieved in shake flasks was not able to be replicated. Further investigation was required to determine the cause of decreased growth in the tubular photobioreactor; however, it was hypothesised that this could likely be due to light and dark volumes present in the tubular photobioreactor which were not present in shake flasks.

6.3 Light cycling

6.3.1 Introduction

In nature, microalgae are exposed to varying light intensities across the day and night known as diurnal cycles. These cycles can vary in length depending on the season, with longer days and shorter nights during summer and vice versa for winter. In addition, some strains of microalgae require diurnal cycling as part of their growth cycles, often affecting mechanisms such as cell division (Andersen, 2005). *Trachydiscus* sp. LCR-Awa-9-2 had already been shown to be able to grow under 24-hour light regimes; however, any beneficial or detrimental effects of diurnal cycling had not yet been explored. Additionally, many commercial microalgal strains are grown using natural light and so the behaviour of *Trachydiscus* sp. LCR-Awa-9-2 under similar diurnal cycles was important to understand to predict potential culture productivity in these conditions.

Microalgae also undergo shorter light cycles in photobioreactor cultures of a variety of times scales. In tubular photobioreactors, the cultures traverse the illuminated solar receiver section and 'dark' bubble column section which exposes the cells to dark and light cycles on the order of minutes or tens of seconds. As cell densities increase, and thus light attenuation, cells are also cycled between light and dark regions in the solar receiver tubes themselves due to turbulent flow through the pipes. This turbulent flow can result in light cycling on the order of seconds or shorter (Chisti, 2007).

Short light cycling has been reported to increase the photosynthetic efficiency of some strains of microalgae, and so may be beneficial to growth of cultures. Light cycling can also improve cultures' tolerance to high light intensities by allowing time for cells to repair damage caused by intense light during the time spent in dark regions (Chisti, 2007). Conversely, the time spent by cells in dark regions can decrease their growth and cause excessive respiration to occur, resulting in reduced biomass concentrations and culture productivities. The effects of these shorter-scale light cycles on *Trachydiscus* LCR-Awa-9-2 had not been investigated before and so this study looked to investigate these effects on this strain.

6.3.2 Experimental methods

Growth and EPA content of *Trachydiscus* sp. LCR-Awa-9-2 grown under diurnal cycles was conducted in shake flasks using the general methods described in § 3.8. Diurnal cycles were achieved by switching the LED lights on and off using a plug timer in-line

with the LED power supply. A light shield was installed on the glass incubator door to block any external light reaching the flasks during dark periods. In all tests the light intensity used was 500 µmol m^{-2} s^{-1} and the lights were timed to produce light cycles of 24:0, 16:8, and 12:12 (hours light : hours dark). In all cases the lights were turned on at 08:00 each day and then switched off at the required time depending on the light cycle. Cell counts or harvests were taken at around 10:00.

Tubular photobioreactor cultures were conducted using the general methods and apparatus in § 3.11 and 4. To investigate the effect of light cycling due to light and dark regions in the tubular photobioreactor, a control culture was run under an incident light intensity of 500 µmol m^{-2} s^{-1} with all light tubes in use. This was then compared with another culture run using half the light tubes, but with the light intensity increased to 1000 µmol m^{-2} s^{-1}. The total photon flux supplied (photons L^{-1} s^{-1}) was the same in both cultures; however, the ratio of residence time between light and dark sections was different between the cultures. The 'light volume' was defined as the volume of the tubular photobioreactor that was illuminated by the lighting apparatus (i.e. the volume within the straight lengths of the solar receiver that were covered by the lighting clamshells). The light volume ratio was defined at the ratio of the light volume to the total culture volume.

6.3.3 Results and discussion

Diurnal light cycling

The growth curves for shake flasks under diurnal cycles are shown in Figure 6.8. The highest maximum cell density was achieved under a 24:0 regime, with the cell density for 16:8 and 12:12 regimes both reaching lower maximum densities. The maximum specific growth rate achieved was lower for 12:12 than 16:8 and they were both lower than the 24:0 treatment. Maximum cell densities and specific growth rates for each condition are summarised in Table 6.4. The maximum cell density achieved with the 12:12 cycle was not significantly lower than that achieved with the 16:8 cycle ($p = 0.455$); however, this result could be due to the unusually high uncertainty of the final cell count for the 12:12 culture.

As light energy is key for photoautotrophic growth the decrease in the total quantity of photons received during diurnal cycling directly impacted the maximum cell density achieved under each regime. Under a 16:8 regime cultures were supplied with 33% fewer photons than 24:0 over the course of each day; however, the maximum cell density only decreased by 27%. Similarly, under 12:12 regime the cultures were supplied

with 50% fewer photons per day than 24:0 but only a 41% decrease in cell density was observed. In both cases, the relative decrease in cell density was only approximately 80% of the magnitude of the decrease in photons supplied.

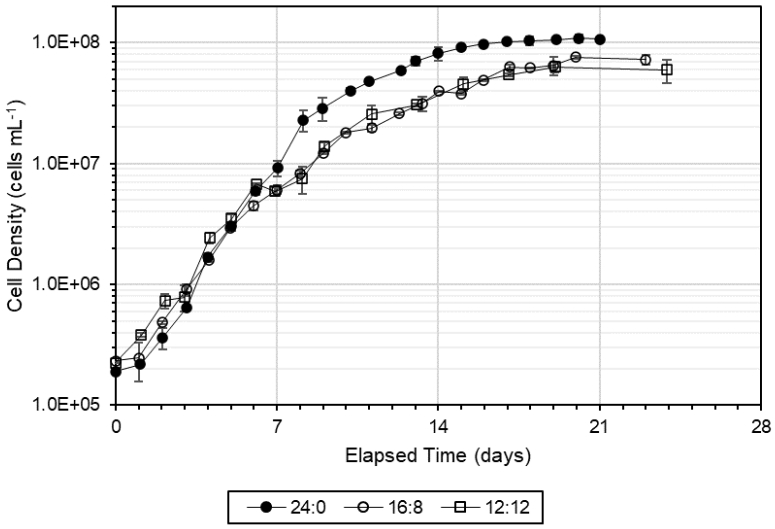

Figure 6.8 – Growth curves for diurnal cycle lighting experiment in shake flasks. Error bars denote standard deviation of cell counts from two flasks in replicate.

Table 6.4 – Maximum specific growth rates and cell densities for different diurnal light cycles in shake flasks.

Light cycle (hours light : hours dark)	μ_{max} **(d^{-1})**	$C_{cell,max}$ **(cells mL^{-1})**
24:0	0.62 ± 0.02	$1.0 \pm 0.1 \times 10^8$
16:8	0.58 ± 0.02	$7.3 \pm 0.5 \times 10^7$
12:12	0.54 ± 0.02	$6 \pm 1 \times 10^7$

One explanation as to why the cell density did not decrease by the equivalent decrease in photons supplied could be that the cells were able to store energy while light was available and then use this to maintain the culture through the dark period (Schulze *et al.*, 2017). This would indicate that cells were sufficiently light saturated during the light period and able to store any surplus energy supplied during this time. *Trachydiscus* sp. LCR-Awa-9-2 has been shown to produce both lipid and polysaccharide bodies (Tangestani, 2019), either of which could be potential energy storage materials to maintain the cells over dark periods. As the cell density increased there was less light available per

cell and thus less in excess to devote to energy storage, leading to a lower cell density as the cultures had a smaller energy reservoir to draw from.

The maximum specific growth rates under diurnal cycles only decreased by 6% and 13% for the 16:8 and 12:12 treatments respectively when compared to 24:0. This showed that with increasing dark time that the maximum growth rate decreased, but the cultures were not severely light limited during the exponential growth phase when the growth rate decrease was compared to the decrease in photons. Although the maximum specific growth rates did not decrease to the same relative extent as maximum cell densities, the point that cultures became light limited, and thus growth significantly slowed, occurred sooner and at a lower cell density as dark times increased. This can be observed in the growth curves in Figure 6.8 where the growth curves shifted from strong exponential growth to a significantly slower growth rate at around Day 8 for 24:0 (2.3×10^7 cells mL^{-1}), Day 5 for 16:8 (3.0×10^6 cells mL^{-1}), and Day 4 for 12:12 (2.4×10^6 cells mL^{-1}).

The fatty acid composition of the cells was affected by the diurnal cycle length, as is shown in Figure 6.9. EPA fraction increased under a 12:12 regime compared to 24:0, but the fraction of EPA under 16:8 decreased compared to both 24:0 and 12:12 regimes. The EPA content was highest under the 12:12 regime and decreased for both 16:8 and 24:0.

The maximum EPA productivity was achieved with the 24:0 regime due to the higher biomass productivity achieved. Although the EPA content was higher under 16:8 and 12:12, the relative increase in EPA content did not overcome the decrease in cell density and increased culture time to reach the maximum cell density, resulting in lower productivities. While the maximum cell densities achieved with 16:8 and 12:12 cycles were not significantly different, the resulting biomass concentration was significantly lower for the 12:12 cycle culture than the 16:8 culture ($p = 0.071$, 90% confidence). EPA and biomass productivities for each treatment are summarised in Table 6.5.

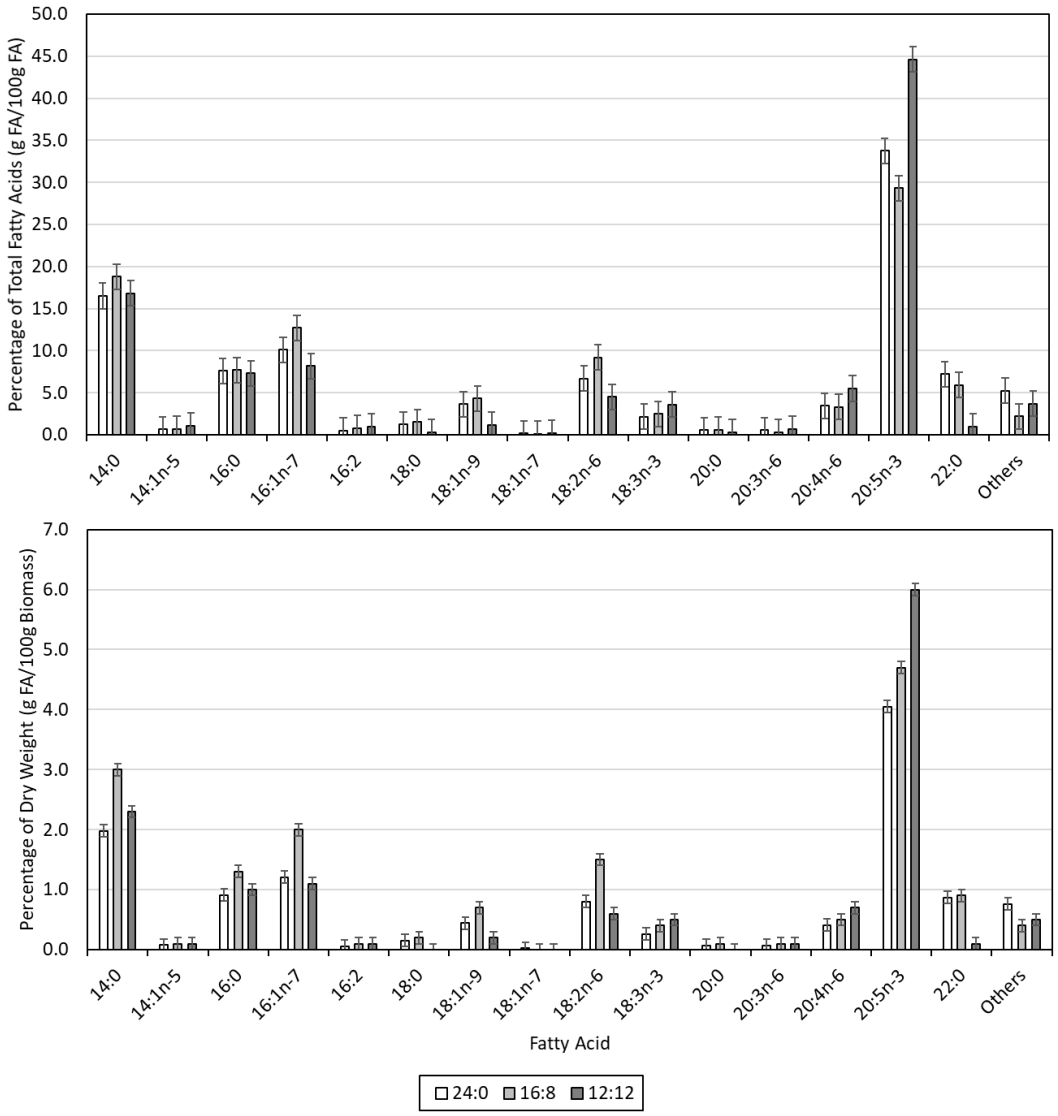

Figure 6.9 – Fatty acid composition of biomass grown under different diurnal cycles. Error bars denote the typical uncertainty from duplicate analyses.

Table 6.5 – Summary of EPA and biomass productivities for batch cultures under different diurnal light cycles.

Light cycle (hours light : hours dark)	EPA content (g / 100 g dry biomass)	Biomass concentration (g L^{-1})	EPA productivity (mg L^{-1} d^{-1})	Biomass productivity (g L^{-1} d^{-1})
24:0	4.1 ± 0.1	5.7 ± 0.1	14 ± 1	0.34 ± 0.01
16:8	4.7 ± 0.1	5.1 ± 0.2	12 ± 1	0.26 ± 0.01
12:12	6.0 ± 0.1	3.1 ± 0.1	9.8 ± 0.8	0.16 ± 0.01

The total fatty acid content of the cells increased with increasing dark time which reinforced the possibility that cells were storing greater quantities of lipids in order to tide them over the dark period. Dark incubation experiments conducted by Tangestani (2019) showed an increase in EPA content for *Trachydiscus* sp. LCR-Awa-9-2 and it is proposed that a similar mechanism was at play here. As was discussed earlier in § 2.4.3, dark conditions can cause a decrease in chloroplastic ω-3 desaturation of lipids and instead result in the majority of EPA being formed via the eukaryotic pathway. This can produce a greater proportion of 20:5/20:5 species (as opposed to 20:5/16:0, for example) increasing the EPA fraction of the lipids. However, this does not explain the decrease of EPA fraction in the 16:8 case. It is possible that the shorter dark cycle does not strongly promote either pathway to be preferred and results in less EPA being produced overall compared to the other conditions. A result that supports this is that for the 12:12 condition the total fatty acid content of the cells decreased to 13.4 ± 0.1 g/100 g dry biomass from 16.2 ± 0.1 g/100 g dry biomass for 16:8 and the fraction of saturated fatty acids 14:0 and 16:0 decreased. This indicated that the cells under the 12:12 regime likely consumed more of their energy stores due to the longer dark period and so the cells may require a longer dark period to trigger greater consumption of energy stores. This could be due to cells preferentially using other energy stores such as polysaccharides before using up lipid stores.

While these results show that diurnal light cycles do not have a beneficial effect on growth and EPA productivity, they do provide information to predict the potential productivity for outdoor culturing. When using natural light there is no control over the timing of sunlight hours (unless supplemental lighting is also supplied) and so predicting the behaviour of cultures of *Trachydiscus* sp. LCR-Awa-9-2 under diurnal cycles was important to understand. The increase in EPA content was promising and so there may be scope for applying light cycles as a secondary treatment to increase the EPA content of cultures while maintaining higher biomass concentrations than complete darkness treatments.

Photobioreactor light cycling

The growth curves for cultures grown in the tubular photobioreactor with different light and dark volumes are shown in Figure 6.10. It was clear that despite the same quantity of photons being available per litre of culture in the reactor in both experiments, the relative residence time of the cells in the dark and light sections of the reactor affected the growth rate and maximum cell density.

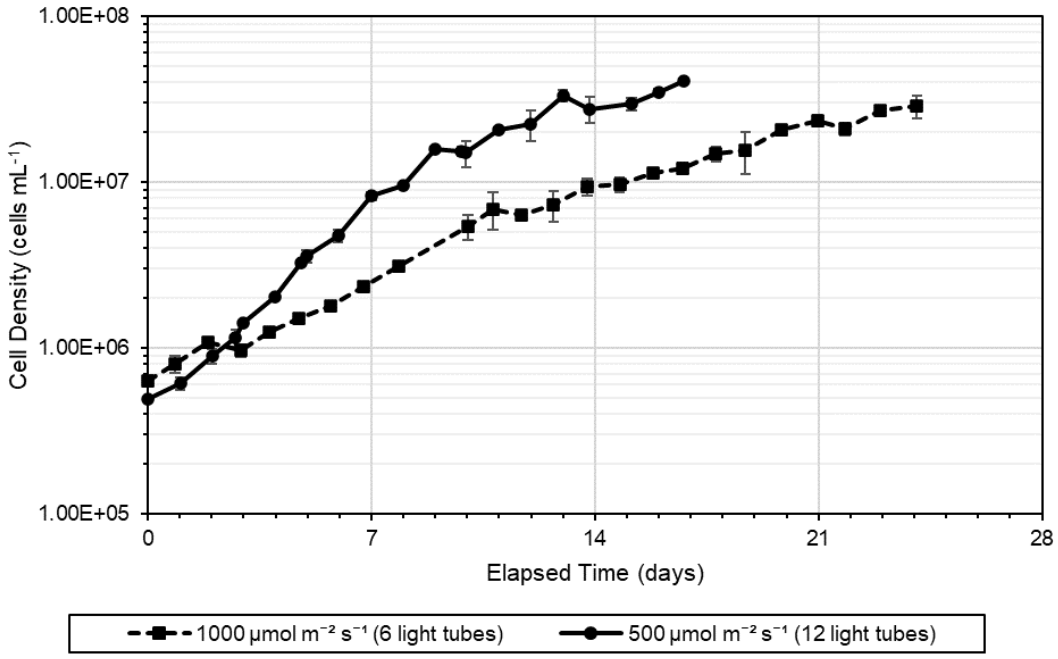

Figure 6.10 – Growth curves for cultures grown under different light volume ratios in a tubular photobioreactor. Error bars represent the standard deviation of duplicate cell counts from the same culture.

The maximum specific growth rate and cell density for each condition is summarised in Table 6.6. Specific growth rates and maximum cell densities decreased with decreasing light volume ratio as expected, despite the same total quantity of photons being supplied per unit volume of the total reactor.

Table 6.6 – Comparison of specific growth rate and maximum cell densities for cultures in a tubular photobioreactor with different light volume ratios.

Light Intensity (µmol m^{-2} s^{-1})	**$\frac{\text{Light volume}}{\text{Total volume}}$**	**μ_{max} (d^{-1})**	**$C_{cell,max}$ (cells mL^{-1})**
1000	0.21	0.24 ± 0.01	$3.0 \pm 0.5 \times 10^7$
500	0.43	0.47 ± 0.02	$4.1 \pm 0.2 \times 10^7$

The decrease in growth rate and maximum cell density with decreasing light volume ratio confirmed the hypothesis that the reason that higher growth rates and cell densities were achieved in shake flasks compared to the tubular photobioreactor was due to the lack of dark and light sections in the flask. It is therefore suggested than in order to improve the productivity of future tubular photobioreactor designs that the dark volume is minimised. The light volume ratio would likely increase with larger scale tubular photobioreactors as the contribution to the dark volume from components such as the pump and connecting pipework between the bubble column, pump, and solar receiver would contribute a smaller percentage of the total reactor volume. As a similar sized pump to the one used in the laboratory scale reactor in this study could recirculate a culture of a far greater volume (more than one cubic metre based on similar pumps used for the tubular photobioreactors in the work by Fernández *et al.* (2014)) the contribution of dark volume of the pump alone would decrease by up to 13-fold. Due to this, it is expected that a larger reactor could have improved growth characteristics.

Alteration of the light supply setup could also improve the light volume ratio of the reactor. The lighting setup used in this study was limited by the length of the solar receiver tubes that could be illuminated due to fixings and couplings on the tubes. The bubble column was not illuminated in this study, apart from by ambient light which was negligible. By illuminating the bubble column and changing the geometry of the lighting setup on the solar receiver the light volume ratio could be increased which would likely result in a greater specific growth rate and maximum cell density. However, this approach increases the complexity and cost of the system as well as requiring a greater energy input for artificial lighting. Additionally, the light path lengths in the bubble column are far longer than for the solar receiver and so in order to illuminate the culture completely in the bubble column would require light sources located inside the column which would add even further complexity to the system.

The fatty acid composition of the cells grown under the different light volume ratios are shown in Figure 6.11. The EPA fraction and content decreased with decreased light volume ratio. This is possibly due to the cells growing less strongly which can be detrimental to EPA production (Acién Fernández *et al.*, 2000). The EPA productivities for each condition are summarised in Table 6.7. EPA productivity was 3.2 times lower for the lower light volume ratio. This decrease was contributed to by both the decrease in EPA content as well as the decrease in biomass concentration.

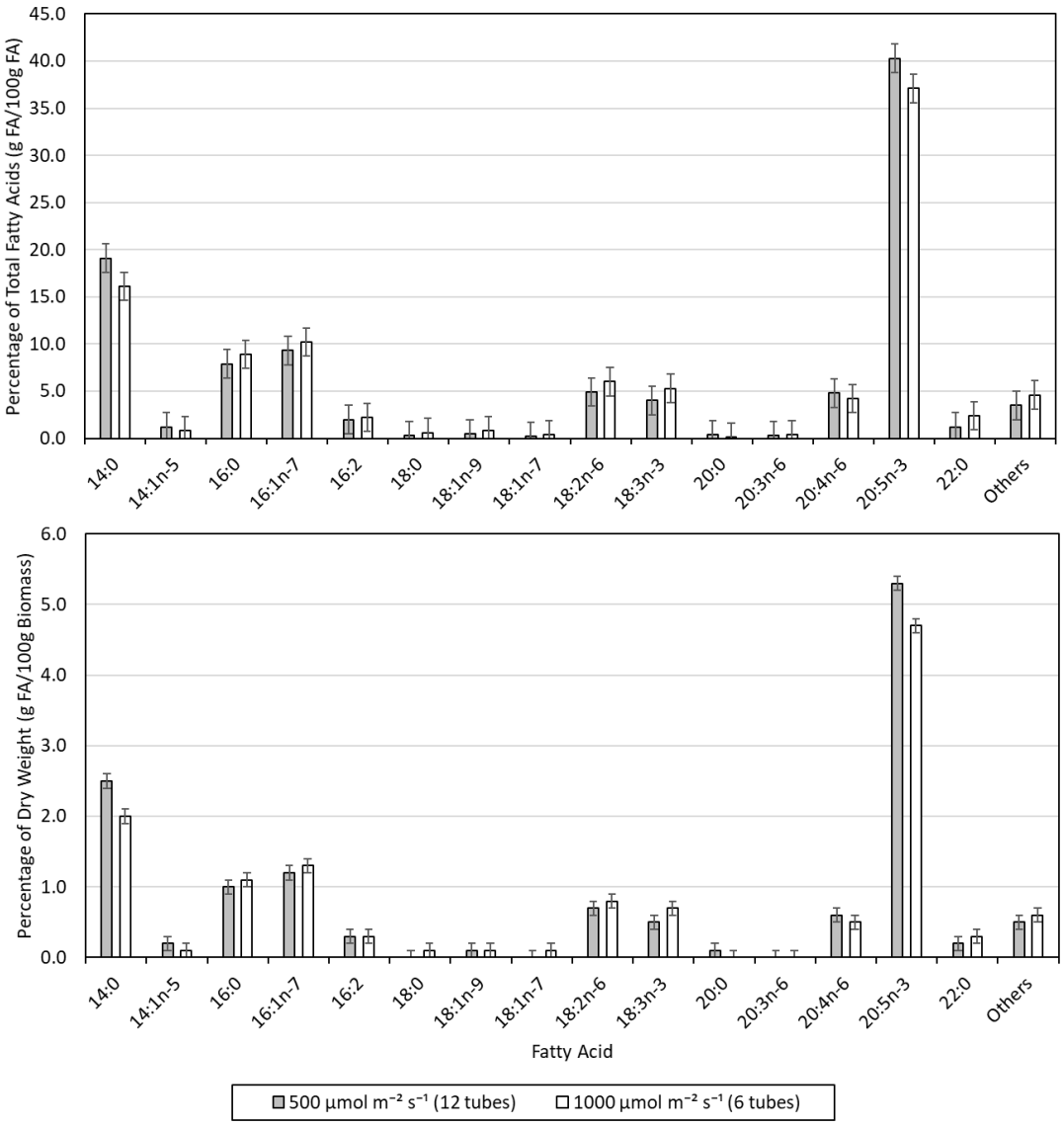

Figure 6.11 – Fatty acid fraction and content of biomass grown under different light volume ratios in a tubular photobioreactor.

Table 6.7 – Summary of EPA and biomass productivities for tubular photobioreactor batch cultures with different light volume ratios.

Light volume / Total volume	EPA content (g / 100 g dry biomass)	Biomass concentration (g L^{-1})	EPA productivity (mg L^{-1} d^{-1})	Biomass productivity (g L^{-1} d^{-1})
0.21	4.7 ± 0.1	1.4 ± 0.1	2.7 ± 0.2	0.058 ± 0.004
0.43	5.3 ± 0.1	2.5 ± 0.1	8.0 ± 0.7	0.15 ± 0.01

The maximum cell density achieved at the higher light volume ratio was approximately 1.4 times higher than that achieved for the lower light volume ratio despite a 2-fold increase in illuminated volume. This indicated that the cells may be able to store energy absorbed in the illuminated section to use while in the dark volume to continue growing.

6.3.4 Conclusions

The results from studies investigating the effect of light cycling on *Trachydiscus* sp. LCR-Awa-9-2 showed that diurnal cycling resulted in an increase in EPA content of the cells with increasing dark time, but EPA productivity was reduced due to reduced biomass concentrations. Diurnal cycles are not required for the growth of this microalga. The dark and light volumes present in the tubular photobioreactor were shown to reduce the growth of cultures compared to shake flasks and a decrease in the light volume ratio decreased the growth rate and maximum cell density. Improved productivity of cultures would likely be obtained if the dark volumes in the tubular photobioreactor could be reduced, either by different reactor geometries or lighting arrangements. While diurnal cycles negatively impacted growth, results from this work are useful to predict the behaviour of cultures if they were to be grown with natural light.

6.4 Light wavelength

6.4.1 Comparison of light wavelengths with whole-cell absorbance spectrum

Introduction

As discussed in § 2.3 light must be able to be absorbed by cells in order for it to be used for photosynthesis. When using artificial lights such as LEDs which produce narrow wavelength ranges of light it is important to match the supplied light wavelengths with those which are absorbed by the cells. Previous work has investigated the influence of light wavelengths on the growth of *Trachydiscus* sp. LCR-Awa-9-2 and the cells were able to grow under a wide range of light colours (Tangestani, 2019). The LED lights used in this study for the tubular photobioreactor and oxygen evolution rate apparatus were different than those used in other studies so comparison of these LED spectra with the absorbance of the cells was required to understand how these spectra compared.

Experimental methods

Measurement of LED emission spectra was conducted as outlined in § 3.6 and the spectra of the LEDs were as reported in § 3.12.1 for the oxygen evolution rate apparatus and § 4.4.2 for the tubular photobioreactor. Whole-cell absorbance spectra were measured from cultures of *Trachydiscus* sp. LCR-Awa-9-2 grown in BBMA medium in shake flasks in the incubator outlined in § 3.8. The absorbance spectrum was measured using a UV-Vis spectrophotometer (UV-1600PC, VWR, USA) using matched quartz cuvettes with 10 mm path lengths. Cells harvested from the shake flask culture were diluted using fresh BBMA medium to achieve a maximum absorbance of approximately 1. The spectrophotometer was blanked with fresh BBMA medium. Absorbances were measured in 1 nm increments over the range of 350 to 850 nm.

Results and discussion

The LED light spectra and whole-cell absorbance comparison is shown in Figure 6.12. Red led light aligned closely with a peak in absorbance of the cells around 625 nm; however, no light colours in this study aligned with the strong absorbance peak at 682 nm apart from some overlap from warm white light in this region.

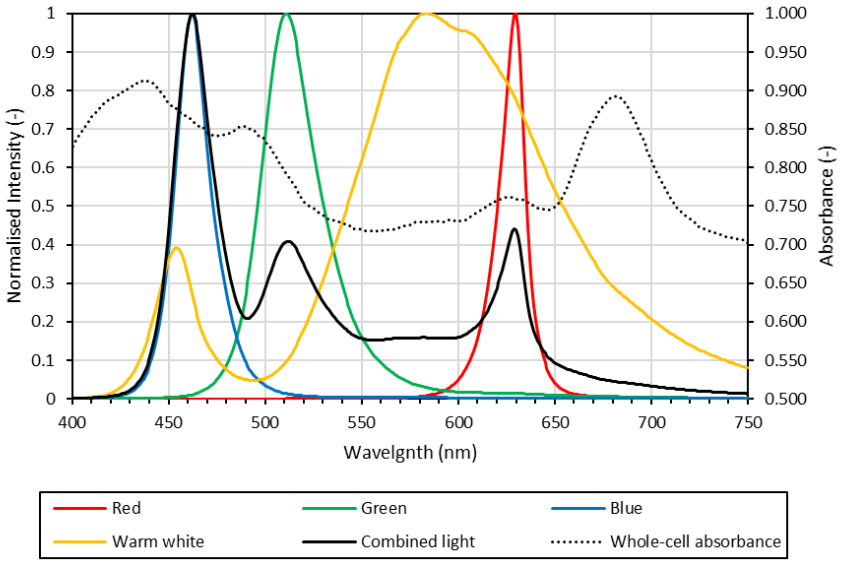

Figure 6.12 – Comparison of whole-cell absorbance spectrum and emission spectra of different LED colours.

The relative absorption of each light colour is summarised in Table 6.8 where the relative absorption is the ratio of photons absorbed compared to the photons supplied for each colour based on the whole-cell absorbance. Blue light showed the highest relative absorption which was expected as the wavelength of this light fell in the region where the

cells absorb most strongly at around 400–500 nm. Combined light also showed a high relative absorption due mainly to a high proportion of the light produced in the blue wavelength range.

Table 6.8 – Relative absorbance of different light colours used in this study based on whole-cell absorbance.

Light Colour	Relative Absorption (-)
Red	0.76
Green	0.78
Blue	0.86
Warm white	0.76
Combined light	0.80

Red and warm white light both showed the lowest relative absorption due to producing wavelengths of light mainly in the region where the cells do not strongly absorb. The green light used in this study had a relative absorption in the mid-range of the colours tested. This was due to the LED producing a relatively wide range of wavelengths compared to the other single colour LEDs and the wavelengths aligning with the end of the upper range where the cells strongly absorb in the blue region around 500 nm. Based on the absorbance of the cells, green light with a longer peak wavelength would be expected to have a lower relative absorption.

The results from this study showed that the LEDs used were able to be absorbed by the cells based on the absorbance spectra. Growth of cultures in the tubular photobioreactor in § 6.4.5 and oxygen evolution rates in § 6.4.2 also showed that all these wavelengths were able to be utilised by the cells for photosynthesis. It is possible that LEDs with wavelengths tuned to match the peak absorbances of the cells would be more efficient and have a higher relative absorption which could improve growth. However, this may not necessarily produce better growth as growth can be preferred under wavelengths that do not necessarily correspond to the highest absorbance (Schulze *et al.*, 2014).

6.4.2 Oxygen evolution rate under different light colours

Introduction

The wavelength of light determines the amount of energy a given photon of light has, with shorter wavelengths having greater energy than longer wavelengths. Due to this, fewer photons of shorter wavelengths are required to supply the equivalent amount of energy required for photosynthesis. However, light also needs to be able to be absorbed to utilise its energy, therefore light wavelengths which align with the absorbance of pigments in microalgae are typically the most useful for photosynthesis compared with those with poor absorbance (Schulze *et al.*, 2014). From the results in § 6.4.1 it was expected that the response of photosynthesis rate would mirror that of the relative absorption of the different light colours. However, the quantum yield of different light wavelengths can vary as discussed in § 2.3.1 and so absorbance of light colours is not the only factor influencing which light colour is optimal for photosynthesis. In order to maximise energy efficiency of artificially illuminated cultures the optimal light colour should be used to avoid supplying light that is not used by the culture.

Experimental methods

Oxygen evolution rates were measured using the general apparatus and methods described in § 3.12. To investigate the effect of different light colours, the apparatus was illuminated using just one colour of light (red, green, blue, or warm white) for each experiment. Each colour of light was tested over a range of PWM values to determine the saturation point for each light colour.

Results and discussion

The oxygen evolution rates under red, green, blue, and warm white LED light for different intensities are shown in Figure 6.13. The point of light saturation varied for each light colour as summarised in Table 6.9. As the light intensity for red was limited to 325 µmol m^{-2} s^{-1} the true point of saturation could not be determined.

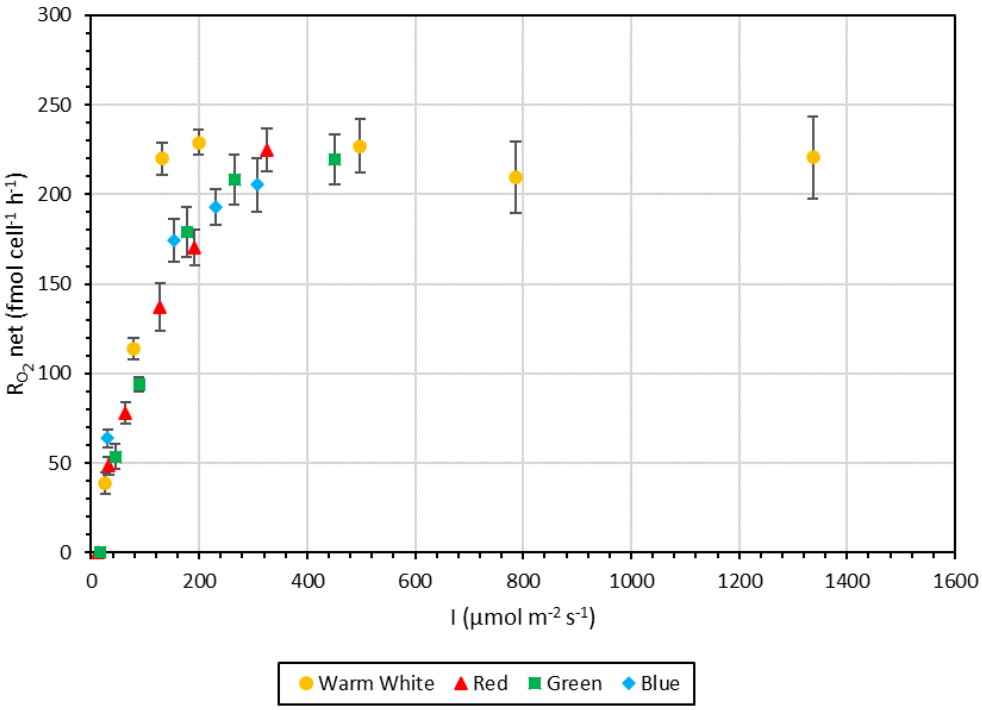

Figure 6.13 – Net oxygen evolution rate under different light intensities for different LED colours.

Table 6.9 – Light saturation point for oxygen evolution rate for different light colours. Uncertainties estimated from graph and typical measurement error.

Light Colour	**Light Saturation Point**	
	(µmol m^{-2} s^{-1})	**(× 10^{10} photons cell^{-1} s^{-1})**
Red	>325 ± 25	>2.5 ± 0.2
Green	451 ± 50	3.4 ± 0.4
Blue	307 ± 25	2.3 ± 0.2
Warm White	199 ± 25	1.5 ± 0.2

Warm white required the lowest cell specific light intensity to reach saturation, followed by blue, then red and green. Based on the results from § 6.4.1 it was expected that the light saturation requirement would be related to the relative absorption of each light colour; however, despite warm white having one of the lowest relative absorbances it required the lowest light intensity to achieve light saturation. Conversely, green light had a higher relative absorption than warm white light but required the highest light intensity to reach light saturation. As the warm white light used produced a broad

distribution of wavelengths it is possible that this broad light spectrum could be used more efficiently than narrow wavelength ranges produced by single colour LEDs. This could be due to light being harvested by a variety of different pigments and of different photon energies which may be able to be used more effectively (Larkum *et al.*, 2003; Schulze *et al.*, 2014). Additionally, the spectrum of warm white light is the most similar to natural sunlight of the light colours tested due to its broad range of wavelengths and as cells have evolved to use sunlight for photosynthesis this may explain why it was used more efficiently than single light colours with narrow wavelength ranges.

6.4.3 Acclimation to light wavelengths

Introduction

Work by Tangestani (2019) suggested that *Trachydiscus* sp. LCR-Awa-9-2 showed acclimation when grown under blue light but acclimation was not required when grown under red light. This was seen by a lag phase occurring in the growth curve of cultures grown under blue light which was not observed in cultures grown in red light under otherwise identical conditions. In both cases the inoculum culture had been grown under white LEDs. Differences were also observed in the visual colour of cultures grown under different light wavelengths. It was hypothesised that the cells may be adapting their pigment composition to shift their absorption spectrum to favour the light they are receiving and thus requiring time to acclimatise and grow effectively. To investigate this, the cells were grown under red light initially and their absorbance spectra recorded and then exposed to blue light and the absorbance spectra recorded again over time to see if there was an observable shift in the absorbance profile of the cells to match the light colour that was supplied.

Experimental methods

Cultures were grown in an airlift photobioreactor as described in § 3.10. The cultures were inoculated from shake flasks grown under a warm white, cool white and violet LED light mix as described previously in § 3.8 The cultures in the airlift photobioreactor were grown under red LED lights for the first three days and then the light switched to blue for a further eight days. The light intensity used for both red and blue light was approximately 40 µmol m^{-2} s^{-1} (the maximum achievable intensity of the red LEDs used in the apparatus). The absorbance spectrum was recorded daily (except for day 6 and 7 of the blue light) using a UV-Vis spectrophotometer (UV-1600PC, VWR, USA) and a quartz cuvette with a 10 mm path length. The spectrophotometer was blanked with

microalgae-free BBMA culture medium. Absorbances were measured in 1 nm increments for the range of 350 nm to 750 nm. As the culture density increased it was diluted prior to measurement with fresh culture medium to result in a maximum peak absorbance of approximately 1 over the entire spectrum.

Results and discussion

The absorbance spectra over the course of the culture are shown in Figure 6.14. No noticeable trend in the change of the whole-cell absorbance spectra was seen when the culture was grown under red and blue light. Some change was observed in the peak seen at 625 nm as shown in Figure 6.15; however, there was no consistent trend observed, with the absorbance initially decreasing then increasing again after switching from red to blue light. The red LED used for the culture growth had a peak at 629 nm which aligned with this peak.

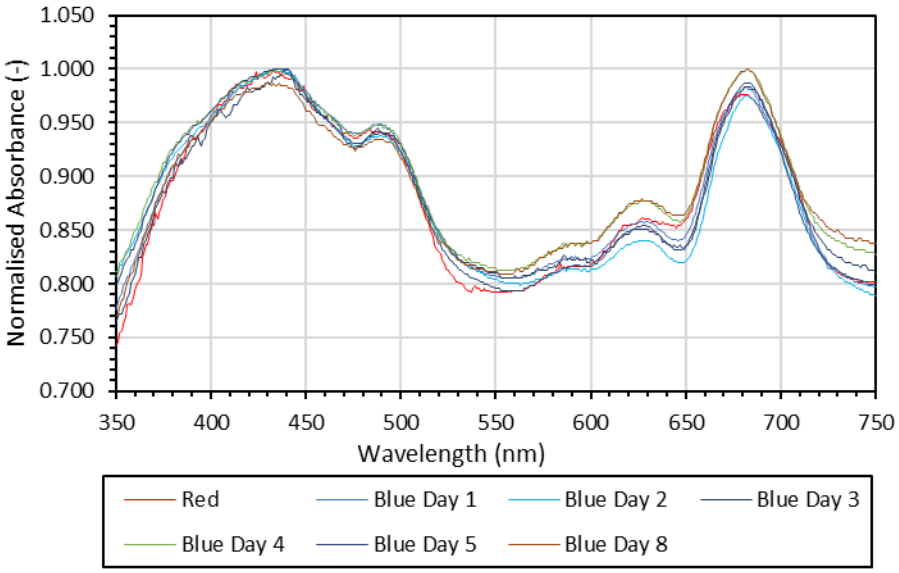

Figure 6.14 – Whole-cell absorbance spectra over the course of a culture initially exposed to red light then switched to blue light.

Measurement of the absorbance spectra indicated that the acclimation happening in cells under blue light was unlikely to be due to pigment composition changes. However, it is possible that the cells were undergoing an acclimation at another level in order to utilise blue light. This could be with apparatus associated with light harvesting and utilisation or could be triggering production of enzymes associated with growth that are not normally triggered under red light (Schulze *et al.*, 2016). It is also possible that the cells were also inhibited by blue light in the initial stages of the culture due to the increased energy per photon and the light is inhibiting their growth. However, from the experiments

in § 6.2 and § 6.4.5 cells were able to grow under far higher light intensities (around 10 times higher) than were used here and in the work by Tangestani (2019) and so it is unlikely that photoinhibition was a factor.

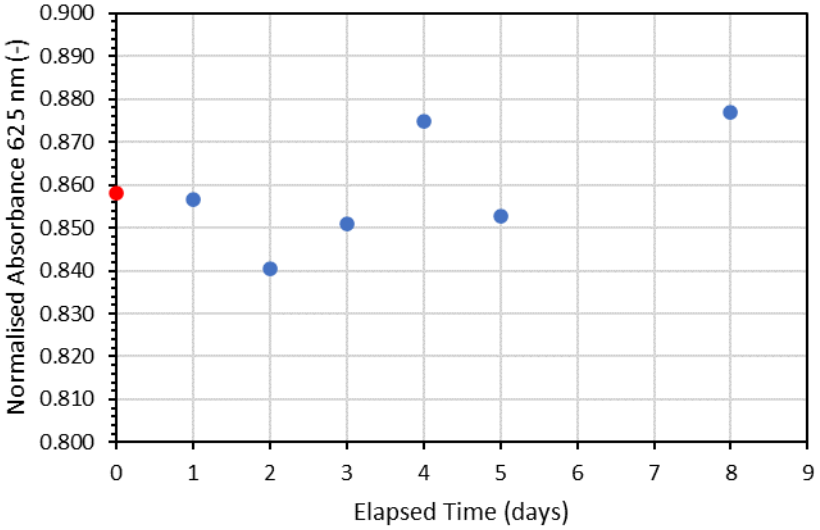

Figure 6.15 – Change in absorbance at 625 nm with change from red (day 0) to blue light.

6.4.4 Pigment composition of lipid extracts of *Trachydiscus* sp. LCR-Awa-9-2

Introduction

Microalgae are a source of many different pigment compounds which are used by the cells for absorption of light for use in photosynthesis as well as protection of cells from light (Richmond, 2008). Pigments can be high value products and have a wide range of uses in food and cosmetic industries (Grubišić *et al.*, 2019; Spolaore *et al.*, 2006). During the lipidomic study undertaken in § 5 it was noted that the pigment composition of *Trachydiscus* sp. LCR-Awa-9-2 was different that that seen in *Chlorella vulgaris* and there appeared to be a greater number of different pigment bands present. Additionally, these pigments were extracted as a by-product during the process of extracting the other lipids of interest containing EPA. As the pigment composition of *Trachydiscus* sp. LCR-Awa-9-2 had not yet been investigated, identification of the pigments present was important as both a tool to investigate the absorption of light for photosynthesis as well as identify any commercially interesting pigments that may be produced by the microalga. Quantification of different pigment contents was beyond the scope of this study.

Experimental methods

Pigment extracts were obtained from freeze-dried biomass by the Bligh and Dyer method outlined in § 3.13 or from fresh biomass using the isopropanol extraction method in § 3.14. Extracted pigments were analysed by separation by one-dimensional TLC as outlined in § 3.17 with hexane/acetone (7:3, v/v) used as the solvent system (Mikami & Hosokawa, 2013; Quach *et al.*, 2004). The separated pigments were dissolved off the scraped silica spots with 750 µL of ethanol to be analysed. Throughout the process pigments were shielded from light wherever practicable and kept cool with ice to prevent degradation. A UV-Vis spectrometer (UV-1600PC, VWR, USA) was used to record the absorbance spectra of the pigments using a quartz cuvette (10 mm path length) over the range of 350 to 750 nm (0.5 nm step size). Ethanol was used as the blanking solution. Pigments were identified based on their absorbance profiles and comparisons with literature values from Clementson and Wojtasiewicz (2019) and Jeffrey *et al.* (1997) as well as relative retentions on the TLC plate.

Results and discussion

The TLC plate obtained for the separation of the Bligh and Dyer lipid extract of *Trachydiscus* sp. LCR-Awa-9-2 and *Chlorella vulgaris* freeze-dried biomass is shown in Figure 6.16 with the pigments spots that were analysed labelled. Pigment spectra can be found in Appendix F. It could be seen that there were distinct differences in the pigment composition of the two microalgae, as was expected, with some pigments common to both species.

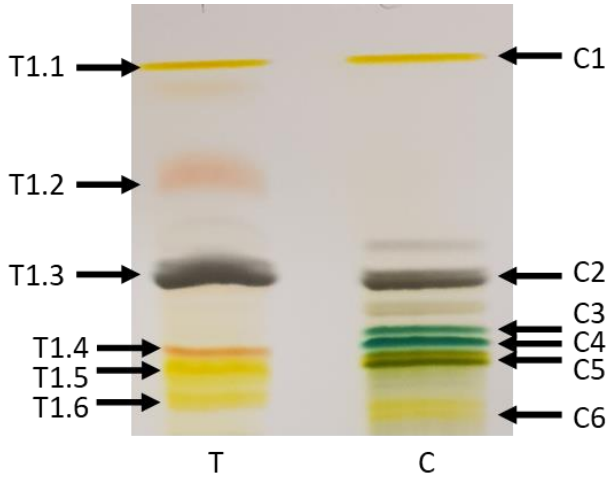

Figure 6.16 – TLC plate of pigment separation Bligh and Dyer lipid extracts of Trachydiscus sp. LCR-Awa-9-2 (T) and Chlorella vulgaris (C).

Pigment bands were identified as summarised in Table 6.10. Degradation of pigments had occurred in the *Trachydiscus* sp. LCR-Awa-9-2 and *Chlorella vulgaris* samples due to the presence of chlorophyllide *a* which is a degradation product of chlorophyll *a* (Hörtensteiner, 1999). Additionally, the large bands of phaeophytin also indicated that chlorophyll was likely degraded during the extraction process by loss of the Mg^{2+} centre, despite phaeophytin also being present as a component of photosystem II in the cells (Klimov, 2003). β-carotene was present in both species; however, astaxanthin was only detected in *Trachydiscus* sp. LCR-Awa-9-2.

Table 6.10 – Pigment species identified from the TLC separation shown in Figure 6.16.

***Trachydiscus* sp. LCR-Awa-9-2**		***Chlorella vulgaris***	
Spot number	**Pigment**	**Spot Number**	**Pigment**
T1.1	β-carotene	C1	β-carotene
T1.2	Astaxanthin	C2	Phaeophytin *a*
T1.3	Phaeophytin *a*	C3	Chlorophyllide *a*
T1.4, 1.5, 1.6	Unconfirmed *	C4	Chlorophyll *a*
		C5	Unconfirmed *
		C6	Antheraxanthin

* Pigment spectrum was not able to be matched conclusively to any in the references used. Possibly due to being degradation products or multiple pigment species present.

It was clear from the above result that many of the pigments present were degraded by either the freeze-drying or Bligh and Dyer extraction process as had been seen in the lipid studies in § 5. As the isopropanol method had been applied in the lipidomic study to prevent degradation of lipids by extraction from fresh biomass, the pigment composition of this extract was also of interest. The TLC separation of the pigments from the isopropanol extraction for *Trachydiscus* sp. LCR-Awa-9-2 is shown in Figure 6.17 and the pigments bands identified as in Table 6.11. A drastic reduction in the size of the phaeophytin band and the presence of chlorophyll *a* confirmed that significant degradation had occurred of the pigments present in the Bligh and Dyer extract.

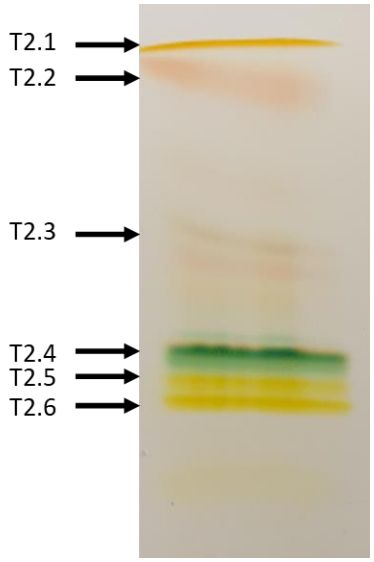

Figure 6.17 – TLC separation of pigments from the isopropanol extraction of Trachydiscus sp. LCR-Awa-9-2.

Table 6.11 – Pigments identified from the isopropanol extraction of Trachydiscus sp. LCR-Awa-9-2 from the TLC plate in Figure 6.17.

Spot number	Pigment
T2.1	β-carotene
T2.2	Astaxanthin
T2.3	Phaeophytin *a*
T2.4	Chlorophyll *a*
T2.5	Antheraxanthin
T2.6	Lutein

The results from pigment analyses showed that *Trachydiscus* sp. LCR-Awa-9-2 was consistent with the typical pigments present in other microalgae and eustigmatophytes such as *Trachydiscus guangdongensis* (Gao *et al.*, 2019; Lubián *et al.*, 2000); however, it also showed the presence of pigments that were not identified in *Trachydiscus guangdongensis* such as astaxanthin. Vaucheriaxanthin ester that was present in *Trachydiscus guangdongensis* was not detected for *Trachydiscus* sp. LCR-Awa-9-2 in this study. The presence of chlorophyll *a* but not *b* or *c* was consistent with the traits of eustigmatophytes; however, violaxanthin which is typically the major carotenoid in this class of microalgae was not identified (Heimann & Huerlimann, 2015). It is possible that this pigment was not sufficiently separated from other pigments on the TLC plate and was obscured by the

spectra of the other pigments present, or that it had been converted to antheraxanthin by the cells due to growth conditions or by degradation during the extraction process (Latowski *et al.*, 2011). The results showed that the lipid extract from *Trachydiscus* sp. LCR-Awa-9-2 contained a variety of pigments that could be commercially interesting, such as astaxanthin and β-carotene (Spolaore *et al.*, 2006). Further investigation into the content of these different pigments in the biomass is required to determine their potential value; however, as these pigments would be by-products in the production of EPA the potential of their use as a supplementary revenue stream from this microalga should be considered.

Pigments are essential for microalgae to absorb light to conduct photosynthesis as discussed earlier. Differences in the amount of different pigments can change the absorbance profile of the cells and thus their utilisation of different light wavelengths. Further investigation of the changes of the contents of the pigments identified here under different conditions may provide information on the effects of light on growth and EPA content that were observed by Tangestani (2019). In particular, the presence of antheraxanthin but not violaxanthin may indicate that cells were stressed due to excessive light (Larkum *et al.*, 2003) and so could serve to indicate which light conditions are preferable for the cells.

Pigments are typically extracted from biomass using different methods than those used in this study, such as with acetone (Gao *et al.*, 2019). However, as the Bligh and Dyer and isopropanol extraction methods were already used to extract the lipids from the biomass the composition of pigments in this extract was of interest as they were by-products of the desired lipid extraction. Full investigation is suggested of the pigment composition using other pigment-specific extraction methods to determine the presence of pigments which may not have been extracted from the cells with the methods used here. In addition, HPLC studies and comparison with standard pigment samples or other spectrometric techniques such as mass spectrometry are recommended to obtain more reliable pigment species confirmation due to the variability of UV-Vis absorbance peaks for pigments in different solvents and conditions (Clementson & Wojtasiewicz, 2019; Jeffrey *et al.*, 1997). Despite its limited scope, this study showed that during the extraction processes already used to obtain the EPA that pigments of commercial interest are also extracted. Further work is suggested to fully characterise the pigment composition of the

cells as well as to develop methods to economically collect the pigments from the lipid extract by-product once the EPA has been obtained.

6.4.5 Growth and EPA productivity under RGBWW, blue, and warm white LED light in a tubular photobioreactor

Introduction

As discussed earlier in § 2.5.1, light colour can impact both the growth and composition of microalgae. Previous work by Tangestani (2019) with *Trachydiscus* sp. LCR-Awa-9-2 showed that EPA productivity and content was improved under blue light compared to white or red light. To investigate whether this effect could improve the EPA productivity of cultures in the tubular photobioreactor cultures were grown under blue and warm white LEDs and compared to the mixed RGBWW light that was used in other experiments.

Experimental methods

Cultures in the tubular photobioreactor were grown under three different light colour conditions: a combination of RGBWW, blue only, and warm white only. The cultures were conducted as described in § 3.11 with only the light colour being altered. The light intensity used was the maximum possible for all light colours in order to investigate the maximum growth possible in the apparatus. The maximum intensity for the blue and white lights were 1900 µmol m^{-2} s^{-1} and 1500 µmol m^{-2} s^{-1}, respectively. For RGBWW light the maximum maintainable intensity was 2300 µmol m^{-2} s^{-1}.

Results and discussion

The fatty acid compositions of the biomass grown under different light colours are shown in Figure 6.18. Blue light did not show an increase in EPA content or fraction compared to warm white or RGBWW light and produced the lowest EPA fraction and content of the conditions tested. Warm white light showed a slight increase in EPA fraction compared to RGBWW; however, EPA content was highest under RGBWW light. It was predicted based on other studies that the use of blue light would increase the EPA content of the cells (Tangestani, 2019); however, this was not observed in this study.

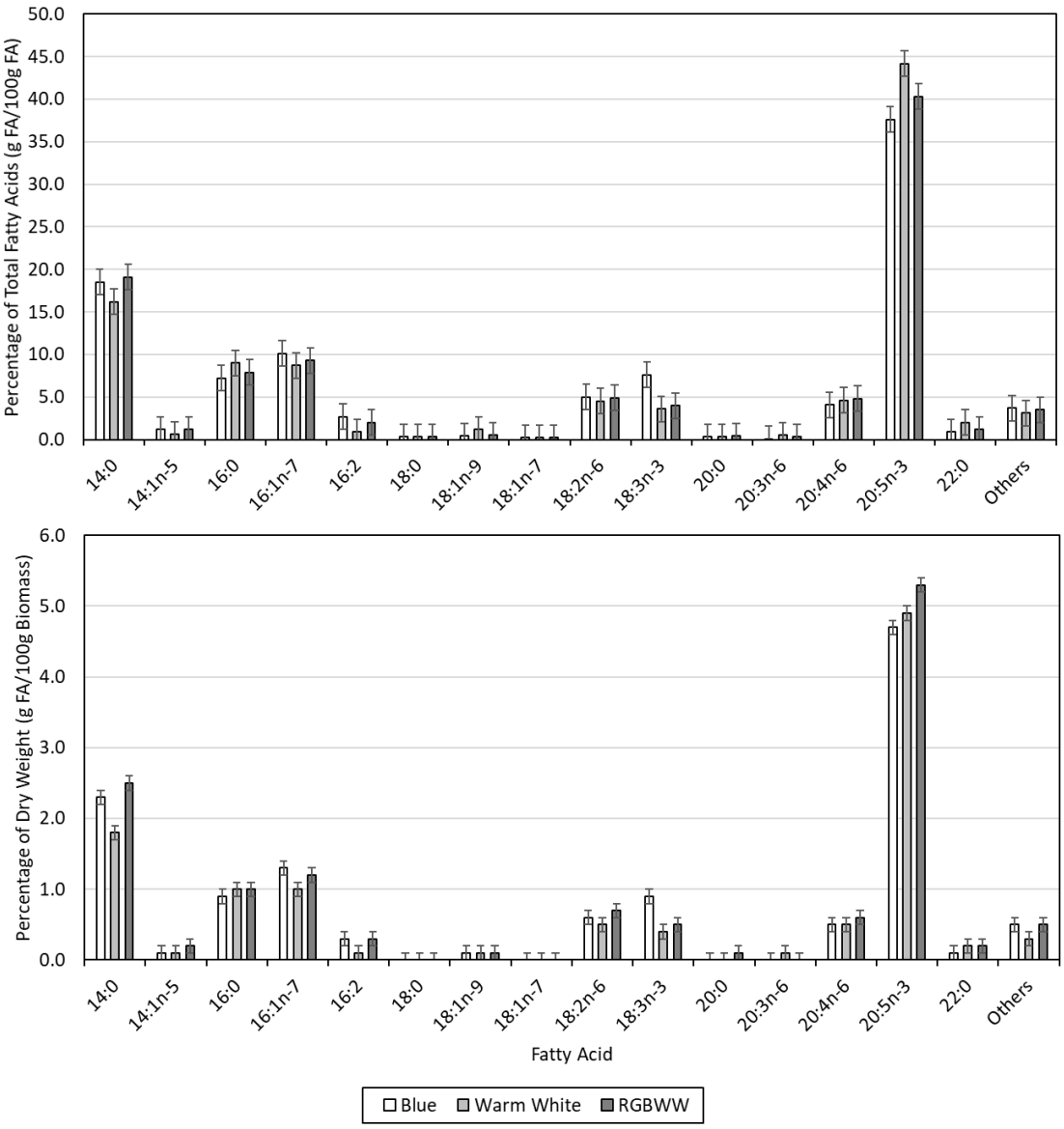

Figure 6.18 – Fatty acid composition of biomass grown in tubular photobioreactor cultures under blue, warm white and RGBWW light.

The maximum specific growth rates and cell densities achieved for each light colour are summarised in Table 6.12. In all cases the culture was saturated with light during the exponential phase and so comparison between these values can be made. As the light intensity was different between cultures, direct comparison of the maximum cell density could not be made. However, the ratio of cell density to light intensity required was used to determine the efficiency of each colour to reach the given cell density.

Table 6.12 – Maximum specific growth rates and cell densities achieved under different light colours in the tubular photobioreactor.

Light Colour	Light Intensity (µmol m^{-2} s^{-1})	μ_{max} (d^{-1})	$C_{cell,max}$ (cells mL^{-1})
Blue	1900	0.50 ± 0.02	$4.5 \pm 0.4 \times 10^7$
Warm white	1500	0.49 ± 0.02	$5.2 \pm 0.6 \times 10^7$
RGBWW	2300	0.54 ± 0.02	$6.0 \pm 0.3 \times 10^7$

There was no marked difference in specific growth rate under different light colours, but the maximum specific growth rate was highest under RGBWW, followed by blue and warm white. This could be in part due to the different light intensity between each colour as the trend follows the light intensity of each colour. Warm white was the most efficient colour for maximum cell density achieved with a cell density to light ratio of approximately 8.3×10^2 cells μmol^{-1}. RGBWW light resulted in a ratio of 6.6×10^2 cells μmol^{-1}, while blue light resulted in the lowest ratio of 4.7×10^2 cells μmol^{-1}. It was expected that blue light would be the most efficient as the wavelengths of light supplied are strongly absorbed by the cells; however, it is possible that the broader distribution of light wavelengths provided by the other light colours used were able to be used more efficiently by the cells. As different wavelengths of light are harvested by different pigments this may have allowed the cells to use all the light available as it was spread over more harvesting pathways and so no singular one would be overwhelmed, whereas the blue light would have only been able to be utilised via fewer pathways which may have been oversaturated. The EPA productivities achieved for the different light colours trialled are summarised in Table 6.13

Table 6.13 – Summary of EPA and biomass productivities for tubular photobioreactor batch cultures under different light colours.

Light Colour	EPA content (g / 100 g dry biomass)	Biomass concentration (g L^{-1})	EPA productivity (mg L^{-1} d^{-1})	Biomass productivity (g L^{-1} d^{-1})
Blue	4.7 ± 0.1	3.0 ± 0.1	8.5 ± 0.7	0.18 ± 0.01
Warm White	4.9 ± 0.1	3.1 ± 0.1	11 ± 1	0.22 ± 0.01
RGBWW	5.3 ± 0.1	3.6 ± 0.1	15 ± 1	0.28 ± 0.01

The best EPA productivity was achieved with the RGBWW light due to both the higher EPA content and biomass concentration. EPA productivity was poorest with blue light, with warm white performing slightly better. While the increase in EPA content under blue light was not observed in this study, other factors may have influenced this result. The medium used in this study was not the same and the light intensity was more than 14 times higher than in previous work. Additionally, the photobioreactor style used was different between the studies. Further investigation is required to determine any combined effects of nutrients or photobioreactor geometry and light colour in order to increase EPA content and productivity.

6.4.6 Conclusions

Light wavelength was shown to influence the growth and fatty acid composition of *Trachydiscus* sp. LCR-Awa-9-2. The results from light wavelength experiments showed that cells did not adapt their pigment composition appreciably in response to blue light. Warm white light was the most efficient light colour for growth and photosynthesis. EPA productivity and content were greatest when cultures were grown under RGBWW light in the tubular photobioreactor compared to blue or warm white light. Comparison of the whole-cell absorbance with the light wavelengths of the LEDs used in this study showed that all wavelengths used were able to be absorbed by the cells and results from the oxygen evolution experiments showed that all light colours used in this study could be utilised for photosynthesis. The pigment composition of *Trachydiscus* sp. LCR-Awa-9-2 was distinctly different from that of *Chlorella vulgaris* based on TLC separations of pigment compounds from the cells but consistent with the pigments present in other eustigmatophytes. The presence of pigments such as β-carotene and astaxanthin in the lipid extracts showed there may be potential for these pigments to be harnessed as alternative revenue streams alongside EPA. Further work is required to understand the potential interaction of light wavelength and other culture conditions to improve EPA content to levels obtained in other studies.

7 Effect of Nutrients on the Growth, Oxygen Evolution Rate, and EPA Content of *Trachydiscus* sp. LCR-Awa-9-2

7.1 Introduction

Carbon dioxide is one of the key nutrients required for microalgal growth (Chisti, 2007). Atmospheric air contained approximately 400 ppm CO_2 at the time of this study (National Institute of Water and Atmospheric Research (NIWA), 2020a); however, it is widely reported that supplementing air with additional CO_2 improves the growth of microalgal cultures (Andersen, 2005). Previous work with *Trachydiscus* sp. LCR-Awa-9-2 has used air supplemented with 3 vol% CO_2 (Tangestani, 2019) but work had not been conducted investigating the CO_2 tolerance of the microalga or optimal CO_2 concentration. Additionally, the effect of CO_2 on the EPA content and productivity had not been investigated.

Other nutrients that are important for microalgae supplied via the culture medium had been investigated by Alfiarty (2018) and Tangestani (2019). The improved BBMA medium produced by Alfiarty (2018) did not show nitrate limitation but the rate of nitrate consumption had not been measured. Additionally, the EPA content that had been achieved in studies by Tangestani (2019) with Z medium had been higher than the results from BBMA medium in this study so a direct comparison between these media and the nutrients that were different was of interest. As the microalga had been cultured concurrently in different conditions prior to this study, the behaviour of the microalga from these two culture sources also needed to be compared. This was to ensure there were not differences due to acclimation to different conditions or carryover of compounds such as trace nutrients which could affect the behaviour of cultures.

Sodium chloride has been shown to increase lipid contents in other microalgae (Pal *et al.*, 2011) and this was of interest to investigate. *Trachydiscus* sp. LCR-Awa-9-2 is a freshwater microalga; however, the peatland the microalga was isolated from was located near the Pacific Ocean and so it was hypothesised that the microalga may be tolerant of saltwater. As there was interest in using the microalga as an aquaculture feed in saltwater environments the tolerance of the microalga to seawater would be of benefit.

7.2 Culture acclimation to nutrient conditions and hangover effects

7.2.1 Introduction

The culture stock inherited for this study had been exposed to a variety of culture medium studies over the course of around one year during the work by Alfiarty (2018). Meanwhile, concurrent studies were conducted at Landcare Research as reported by Tangestani (2019) with the same strain under different conditions. Both culture stocks had originated from the same original stock prior to these two studies. As the microalga had been grown for many generations under different conditions there was cause to investigate whether adaption or acclimation had occurred and that the microalga culture stocks still performed similarly despite this.

In order to confirm that the culture inherited for this study did not show any long-term change from exposure to different conditions, culture stocks from the University of Canterbury and Landcare Research were both grown under identical conditions to confirm that the growth characteristics were the same.

7.2.2 Experimental methods

Cultures were grown in shake flasks according to the general method outlined in § 3.8. Both cultures were grown in BBMA medium at a light intensity of approximately 250 µmol m^{-2} s^{-1}. Cell counts were taken each day according to the method in § 3.1.1. The inoculum for the Landcare Research culture was obtained from the cultures used in the work by Tangestani (2019) and had been previously grown in Z medium (see § 7.5 for details of this medium). The inoculum for the University of Canterbury culture was obtained from the cultures used in the work by Alfiarty (2018) and had been previously grown in BBMA medium.

7.2.3 Results and discussion

Growth curves for the cultures are shown in Figure 7.1. Both cultures exhibited near identical growth behaviour reaching similar maximum cell densities ($p = 0.728$) and maximum specific growth rates ($p = 0.553$) as summarised in Table 7.1. This indicated that the cultures were not substantially different despite being exposed to different conditions in the preceding studies. Additionally, this experiment served to show the reproducibility of culture experiments. Despite both cultures originating from different sources the cultures still behaved similarly when exposed to the same conditions. This showed that the results from cultures could be relied on to be reproducible despite the low number of

replicate flasks (typically conducted in duplicate). Due to the time taken for cultures to grow and apparatus limitations the number of replicates that could be conducted in the course of this study was limited.

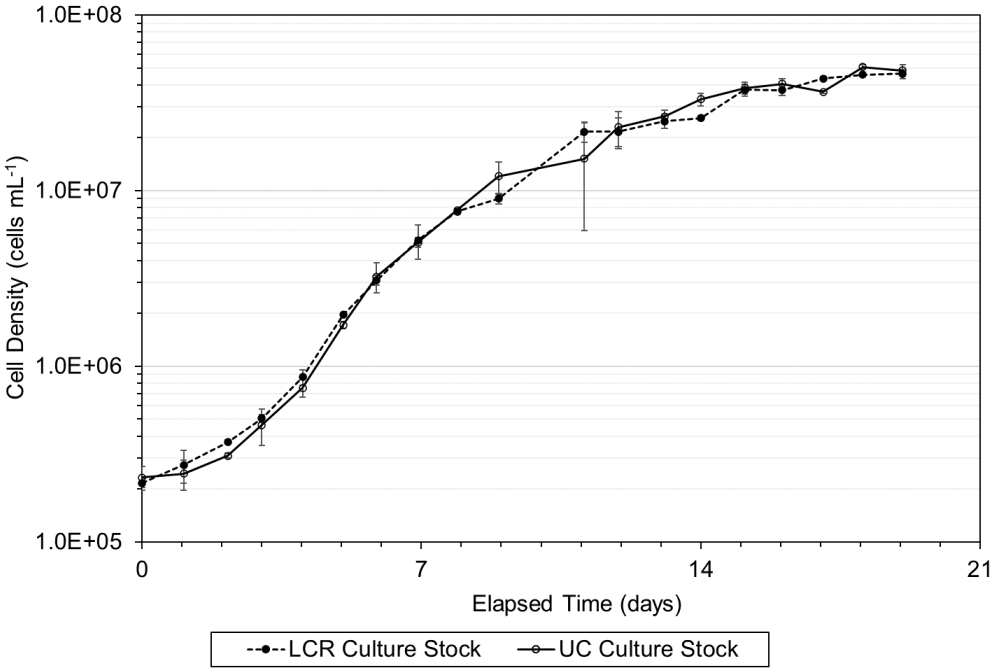

Figure 7.1 – Growth curves for cultures inoculated from different culture stocks. Error bars denote standard deviation of counts from two flasks. LCR: Landcare Research; UC: University of Canterbury.

It was expected that a significant lag phase would have been observed in the Landcare Research culture stock curve while the cells acclimatised to the new medium conditions if cells had adapted to the conditions that they were previously cultured under. It was also expected that there may be some carry over of trace elements from previous studies in the biomass of the cells. This would have been seen as a difference in the growth characteristics between the cultures, but this was not seen in the results.

Table 7.1 – Maximum specific growth rates and cell densities of cultures from different culture stock origins.

Culture Stock Origin	μ_{max} **(d^{-1})**	$C_{cell,max}$ **(cells mL^{-1})**
Landcare Research	0.55 ± 0.02	$4.6 \pm 0.3 \times 10^7$
University of Canterbury	0.57 ± 0.02	$4.8 \pm 0.4 \times 10^7$

7.3 Effect of carbon dioxide concentration

7.3.1 Introduction

While microalgae are able to grow in the wild from the carbon dioxide present in the atmosphere, beneficial results are obtained for most microalgae species with supplementation of CO_2 (Andersen, 2005; Becker, 1994). *Trachydiscus* sp. LCR-Awa-9-2 had been grown with air and air supplemented with 3 vol% CO_2; however, it was not known whether this level of CO_2 supplementation was optimal and what the tolerance of this alga was to different concentrations of CO_2. Some microalgae, such as *Nannochloris eucaryotum* (Concas *et al.*, 2013), were shown to be able to grow under 100% CO_2, while other microalgae such as *Nannochloropsis oculata* were unable to grow at 10% CO_2 (Hsueh *et al.*, 2009). As CO_2 tolerance was strain specific, the behaviour of *Trachydiscus* sp. LCR-Awa-9-2 with different CO_2 concentrations needed to be investigated.

7.3.2 Experimental methods

Growth of cultures under different CO_2 concentrations was conducted in shake flasks grown as described in § 3.8. Different CO_2 concentrations were investigated by altering the flow rates of CO_2 and air to reach the desired concentration of CO_2. Six CO_2 concentration conditions were tested: 0.04 % (air, approximately 400 ppm CO_2 at the time of experiments (National Institute of Water and Atmospheric Research (NIWA), 2020a)), 0.4%, 3%, 10%, 30% and 100%. The pH of the cultures was measured each day and cell counts were also taken as described in § 3.1.1. Cultures were harvested once they had reached their maximum cell density and fatty acid composition analysis was conducted as described in § 3.20.

7.3.3 Results and discussion

Growth curves for the cultures grown with different CO_2 concentrations are shown in Figure 7.2. The growth of cultures was seen to be influenced by the CO_2 concentration. Results show that the 3% CO_2 concentration used in previous work was sufficient to prevent carbon limitation and produced the highest cell density of the conditions investigated. While air (0.04%) did not supply enough carbon for the cell density to reach that of 3% CO_2, increasing the CO_2 concentration 10-fold to 0.4% was enough to produce cell densities comparable to 3% CO_2 with only slight evidence of carbon limitation due to reaching a slightly lower maximum cell density. Increasing the CO_2 concentration to 10% and beyond had a detrimental effect on culture growth and no growth was seen at 100%

CO_2. The maximum growth rates and cell densities for each treatment are summarised in Table 7.2.

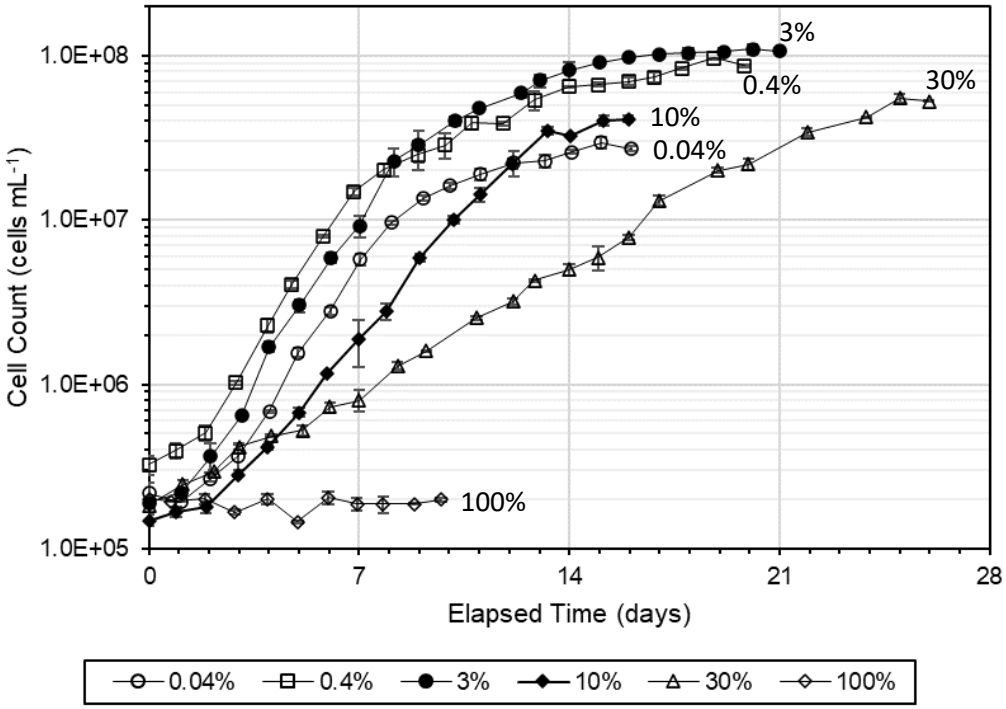

Figure 7.2 – Growth curves for cultures in shake flasks with different CO_2 concentrations. Data points are the mean of counts from duplicate flasks. Error bars denote standard deviation of two flasks in replicate.

Table 7.2 – Specific growth rate and maximum cell densities for cultures grown with different CO_2 concentrations in shake flasks.

CO_2 Concentration (vol%)	**μ_{max} (d^{-1})**	**$C_{cell,max}$ (cells mL^{-1})**
0.04	0.64 ± 0.02	$2.7 \pm 0.1 \times 10^7$
0.4	0.63 ± 0.02	$8.7 \pm 0.1 \times 10^7$
3	0.62 ± 0.02	$1.0 \pm 0.1 \times 10^8$
10	0.50 ± 0.02	$4.1 \pm 0.2 \times 10^7$
30	0.24 ± 0.01	$5.3 \pm 0.1 \times 10^7$
100	0	$2.0 \pm 0.1 \times 10^5$

While other studies investigating the influence of CO_2 concentration on microalgal cultures cite low pH as potentially being the reason for poor growth at high CO_2 concentrations (Hsueh *et al.*, 2009), this was ruled out as a cause in this study. Cultures were shown to be able to grow at a pH as low as 4 (Tangestani, 2019) and continued to

photosynthesise at a pH as low as 2, as discussed later in § 8.2. The pH of the cultures with different CO_2 concentrations is shown in Figure 7.3. The lowest pH reached for 100% CO_2 was 4.0 ± 0.1 and well within the pH range in which cultures could continue to grow. For the culture grown with air (0.04% CO_2) the pH on the final days of the culture reached above pH 9. From results in § 8.2, the photosynthesis rate was seen to decrease above pH 7 and at pH 9 the rate was reduced to around 20% of the maximum rate. This was attributed to the dissolved CO_2 in the medium transitioning to HCO_3^- and CO_3^{2-} and the cells not being able to use these forms of inorganic carbon. However, as discussed in § 2.5.3 and 2.5.4, if CO_2 is continually supplied to the system then the amount of dissolved CO_2 remains relatively constant as pH increases which was the case in the cultures in this experiment. Due to this, the result of poor growth is likely to be a combination of both high pH and carbon limitation in the 0.04% CO_2 culture.

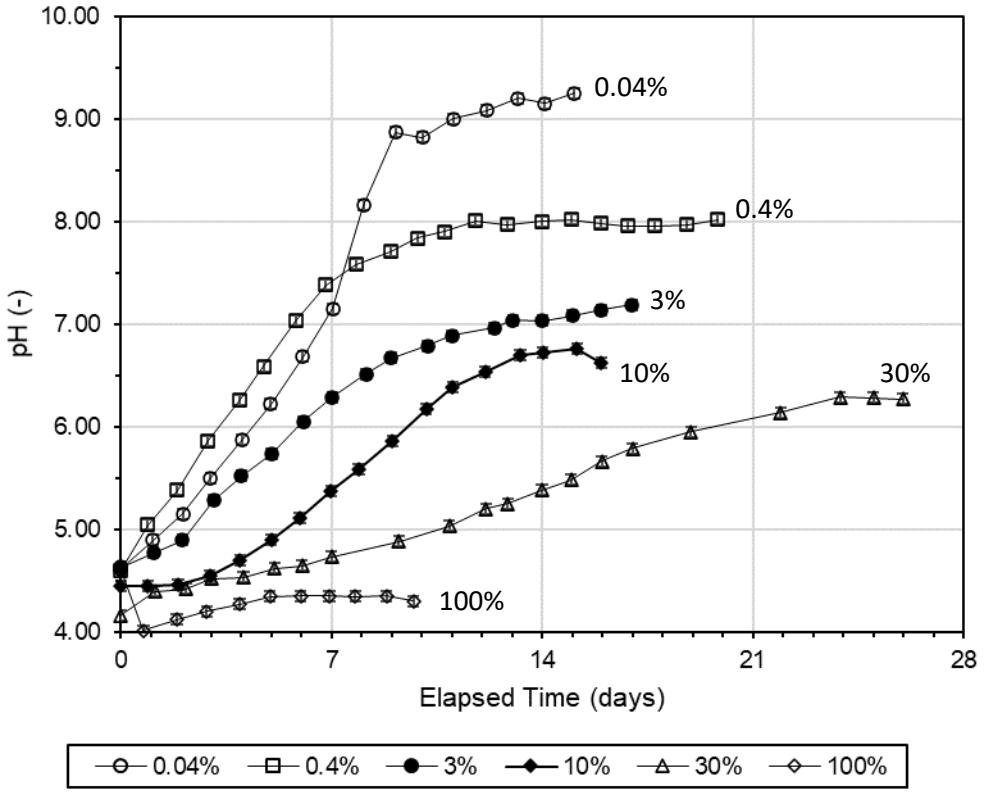

Figure 7.3 – pH of cultures in shake flasks with different CO_2 concentrations. Error bars denote typical measurement error.

While growth was slower at low pH it was not the limiting factor for growth of cultures under high CO_2 concentrations and this indicated that there was some form of poisoning or inhibition effect resulting from high CO_2 concentrations. While growth was observed with a concentration of 30% CO_2, an initial culture inoculated from cells grown

with 3% CO_2 showed a lag of around one week before adapting to the higher CO_2 concentration and growing strongly. Subsequent cultures grown at 30% CO_2 inoculated from a 30% CO_2 adapted culture did not show any lag period, as seen in Figure 7.4. It has been reported that microalgae can alter the structure and location of organelles in their cells to cope with high CO_2 concentrations (Salih, 2011) and it is possible that the lag phase seen in this study was due to this cellular 'rearrangement' taking time to occur and growth being hindered until the cells had acclimatised. The maximum cell density in the non-acclimatised culture was higher than the acclimatised culture, but this was deemed to be due to evaporation of water from the medium over the extended culture time.

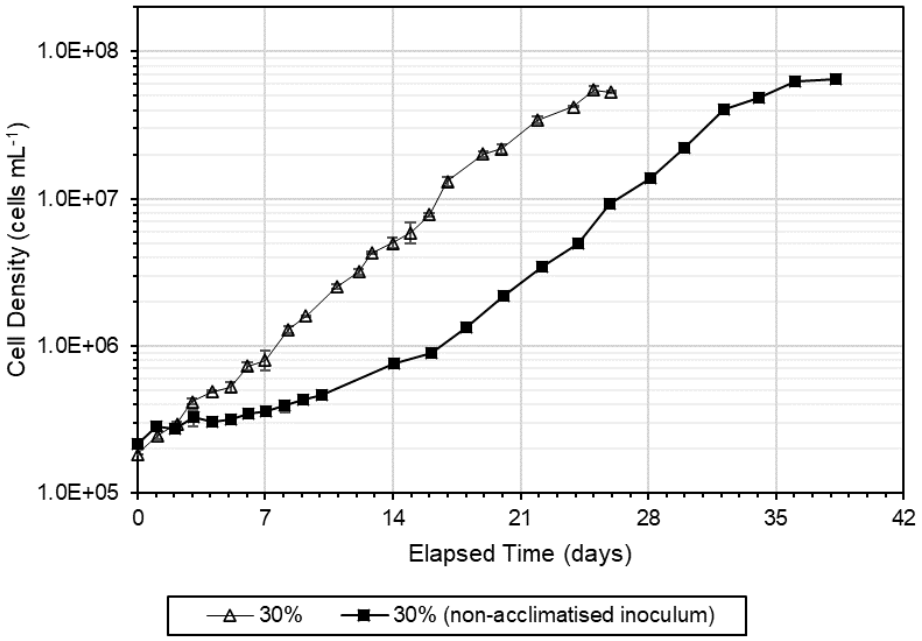

Figure 7.4 – Growth curves showing acclimation of cultures to 30% CO_2. Data points are the mean of counts from duplicate flasks. Error bars denote standard deviation of cell counts from duplicate flasks.

After ten days no acclimation was observed of the cultures grown at 100% CO_2 and so it is assumed that the cells were unable to adapt to this high of a concentration. It is possible that high CO_2 concentrations lead to feedback inhibition of enzymes associated with the metabolism of the cells and that *Trachydiscus* sp. LCR-Awa-9-2 does not have the required apparatus to manage the CO_2 concentration within the cell to prevent these effects. Other strains of microalgae have been shown to grow at 100% CO_2 concentrations as described earlier and it is assumed that these cells are able to regulate CO_2 concentrations within the cell and adapt their cellular structure to mitigate inhibition from high CO_2 concentrations (Salih, 2011).

The fatty acid composition of *Trachydiscus* sp. LCR-Awa-9-2 was affected by the CO_2 concentration as shown in Figure 7.5. The greatest EPA content was achieved with 30% CO_2; however, this condition also produced the lowest EPA fraction. It can be seen from the growth curve that the culture was stressed under this condition, resulting in a lower growth rate, and this in turn could trigger the increase in total fatty acid content of the cells resulting in higher EPA content despite the lower fraction. Conversely, air (0.04% CO_2) showed the highest EPA fraction and second highest EPA content. The cells were assumed to be under carbon limitation stress due to the maximum cell density being lower than at 0.4% or 3% CO_2.

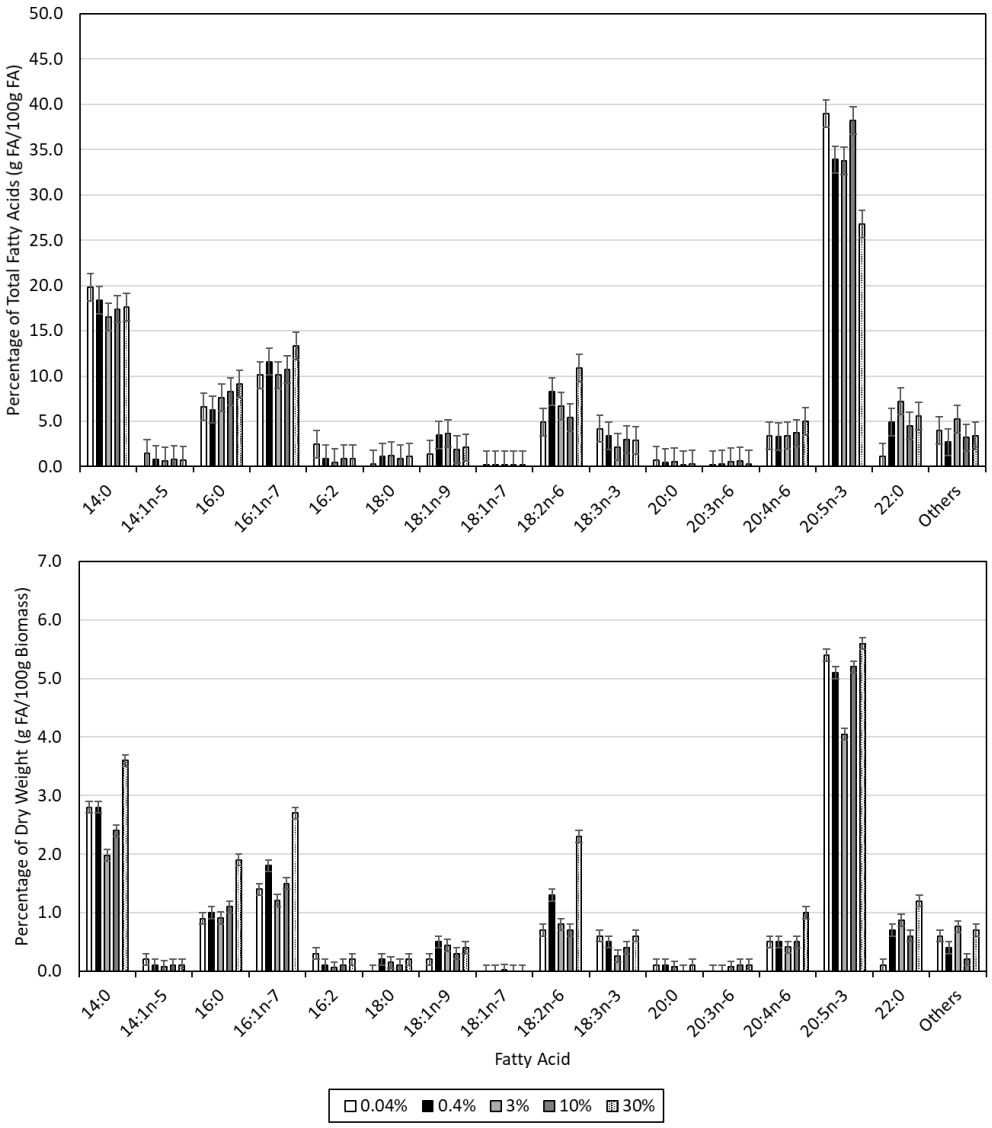

Figure 7.5 – Fatty acid (FA) composition of biomass grown under different carbon dioxide concentrations. Note: as cultures did not grow at 100% CO_2 sufficient biomass could not be collected for fatty acid analysis for this condition.

Growth was inhibited at both high and low CO_2 concentrations and this had a notable effect on the productivity of cultures. The EPA productivities under each CO_2 concentration are summarised in Table 7.3. EPA productivity was best at 10% CO_2 due to both a high EPA content and biomass concentration. While EPA content was higher at 30% CO_2 the biomass concentration achieved was much lower and the culture took longer to grow resulting in a lower productivity. At 3% CO_2 the biomass concentration was higher but a lower EPA content was achieved; however, the productivity achieved was not significantly lower than that at 10% CO_2.

Table 7.3 – EPA productivities of shake flask batch cultures at different CO_2 concentrations.

CO_2 Concentration (vol %)	**EPA content (g / 100 g dry biomass)**	**Biomass concentration (g L^{-1})**	**EPA productivity (mg L^{-1} d^{-1})**	**Biomass productivity (g L^{-1} d^{-1})**
0.04	5.4 ± 0.1	1.9 ± 0.1	6.4 ± 0.7	0.12 ± 0.01
0.4	5.1 ± 0.1	4.1 ± 0.2	11 ± 1	0.21 ± 0.01
3	4.1 ± 0.1	5.7 ± 0.1	14 ± 1	0.34 ± 0.01
10	5.2 ± 0.1	4.8 ± 0.4	16 ± 2	0.30 ± 0.03
30	5.6 ± 0.1	3.6 ± 0.1	8.0 ± 0.7	0.14 ± 0.01

Tolerance of high CO_2 concentrations such as 10% and 30% is beneficial if the use of CO_2 sources such as flue gases is to be considered. Flue gases can provide a free source of CO_2 for microalgae cultures and the cultures themselves can be used for CO_2 sequestration (Saifuddin *et al.*, 2015; Salih, 2011).

7.4 Mixotrophic growth at low pH

7.4.1 Introduction

Light was identified as the key limiting factor for achieving high cell densities in photoautotrophic cultures. However, as *Trachydiscus* sp. LCR-Awa-9-2 had been shown to grow on organic carbon sources such as lactose and galactose, mixotrophic or heterotrophic growth was proposed as an option to overcome the limitations of light on culture density (Tangestani, 2019). A disadvantage of adding inorganic carbon to cultures is the susceptibility to contamination by growth of bacteria and fungi which, coupled with the comparatively slow growth rate of microalgae, can hinder the viability of mixotrophic cultures. As it had been shown that *Trachydiscus* sp. LCR-Awa-9-2 can grow at a low pH, down to around pH 4 (Tangestani, 2019), and photosynthesise down to pH 2 (§ 8.2)

cultivation at low pH was one potential option to mitigate the growth of other undesirable microorganisms in mixotrophic cultures (Posten & Walter, 2012).

7.4.2 Experimental methods

Cultures were grown in shake flasks using the general methods outlined in § 3.8. BBMA medium was supplemented with either 10 g L^{-1} lactose or galactose for mixotrophic cultures and they were compared with a non-supplemented BBMA culture subjected to otherwise identical conditions. The pH of the medium was lowered by addition of 1 mol L^{-1} HCl until the pH was approximately pH 3. pH readings of the cultures were taken each day by taking a small aliquot (typically approximately 100 µL) and measuring the pH with a small volume pH probe. The pH of the cultures was adjusted with additional HCl solution until the pH was reduced to around pH 3 as required. Cell counts were taken at the same time as pH measurements according to the method in § 3.1.1. Checks for contamination were made by visual inspection of the cultures in the flasks and by presence of bacteria or fungi during cell counting.

7.4.3 Results and discussion

The growth curves for the cultures with and without lactose and galactose supplementation are shown in Figure 7.6. During the cultures significant bacterial and fungal contamination was observed in the mixotrophic cultures; however, no noticeable contamination was seen in the photoautotrophic culture. Cultures could grow at the pH used but grew slower than in cultures without pH adjustment from previous experiments. Maximum specific growth rates for each condition are summarised in Table 7.4.

Maximum specific growth rates were higher with lactose and galactose supplementation than without, with galactose producing the highest specific growth rate. However, due to contamination of the cultures, growth was best overall with the non-supplemented medium. Overall, reducing the pH of the culture to pH 3 reduced the maximum specific growth rate compared to cultures where the pH was not controlled in other experiments where the maximum specific growth rate was 0.62 ± 0.02 d^{-1} (see result for 3% CO_2 above in § 7.3.3).

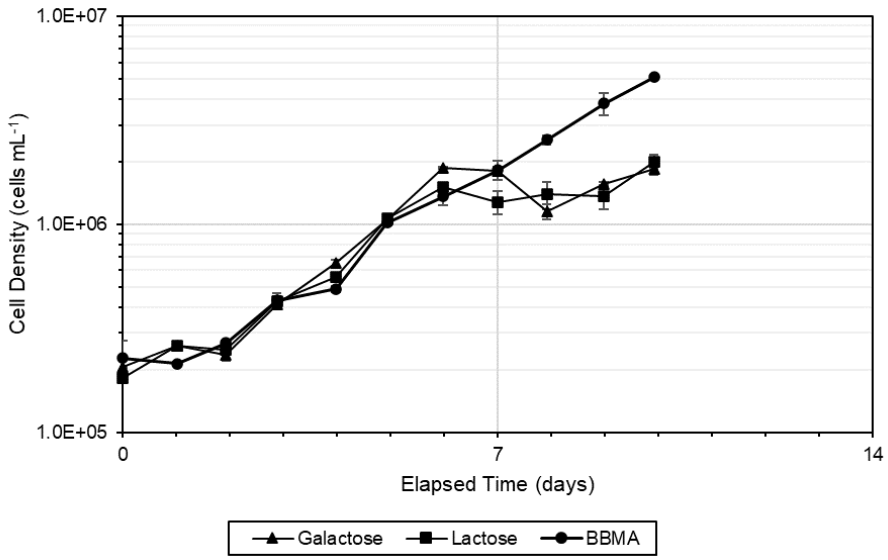

Figure 7.6 – Growth curves of mixotrophic cultures with lactose and galactose compared with a photoautotrophic culture at low pH. Cultures were abandoned after day 10 due to contamination in the mixotrophic cultures.

Table 7.4 – Maximum specific growth rates for mixotrophic cultures grown at pH 3.

Medium	$\boldsymbol{\mu_{max}}$ **(d^{-1})**
BBMA	0.37 ± 0.02
BBMA + lactose	0.41 ± 0.02
BBMA + galactose	0.49 ± 0.02

Tangestani (2019) indicated that lactose was better than galactose for mixotrophic cultures; however, results here indicate that galactose may increase growth rate more than lactose. One reason for this may be due to lactose being a disaccharide of glucose and galactose and so cells have to hydrolyse the sugar with enzyme such as β-galactosidase prior to use which takes additional energy (Girard *et al.*, 2014). Also, as the two supplemented media contained the sugars at the same mass concentration, the effective galactose concentration in the lactose culture was approximately half that of the pure galactose culture. In previous studies, mixotrophic growth with glucose did not perform as well as galactose or lactose (Tangestani, 2019) and so this may have also contributed to the growth rate in this study being lower for lactose than galactose as the glucose produced from hydrolysis of the lactose would not be as useful for growth.

The results from this experiment showed that low pH was not a viable option to control contamination in mixotrophic cultures of *Trachydiscus* sp. LCR-Awa-9-2. While the microalga was able to grow at low pH, the bacteria and fungi present were also able to. As the culture stock used was not free of bacteria and fungi, they were already present in small amounts in the inoculum. Non-supplemented BBMA medium does not contain a source of organic carbon to promote growth of bacteria or fungi and hence showed no visible contamination. However, upon addition of an organic carbon source the contaminant microorganisms had a source of energy and carbon to grow strongly. As the rate of growth of organisms such as bacteria and fungi are typically far higher than that of most microalgae (e.g. around 24 d^{-1} for *Escherichia coli* (Berney *et al.*, 2006) versus around 0.6 d^{-1} for *Trachydiscus* sp. LCR-Awa-9-2) they rapidly use up nutrients in favour of the microalgae. Additionally, the presence of bacteria and fungi attenuates light in the culture further hindering the growth of the microalgae. It was observed that in the contaminated cultures that cells agglomerated, likely due to production of extracellular products from the fungi and bacteria. This was observed by the decrease in cell density from day 6 to 8 of the mixotrophic cultures where clumps of cells hindered cell counting and cells began to attach to the walls of the flasks. This was remedied by vigorously mixing the flasks prior to cell counts to detach the cells from the flasks and resuspend them in the media for counting. As the bacteria and fungi in the culture were most probably also present in the environment that *Trachydiscus* sp. LCR-Awa-9-2 was isolated from which was mildly acidic, the contaminant microorganisms were likely to also be adapted to survive in acidic conditions.

7.5 Comparison of BBMA and Z media

7.5.1 Introduction

Results from Tangestani (2019) showed that EPA content was able to be increased to around 8.7 g/100 g dry biomass but this was not able to be achieved using BBMA media in this study under otherwise similar conditions such as the light colour and temperature. A proposed reason for this was the difference between the Z and BBMA media compositions. A direct comparison had not been made growing *Trachydiscus* sp. LCR-Awa-9-2 in identical conditions with these two culture media and so this was desired to compare results from this study and those by Tangestani (2019) and Alfiarty (2018).

7.5.2 Experimental methods

Z media was prepared according to the recipe in Table 7.5. The general method of preparation was similar to that used for BBMA medium as in § 3.4. Cultures were conducted in shake flasks using the general methods in § 3.8.

Table 7.5 - Composition of prepared Z medium (Alexandrov et al., 2014).

Component	Mass concentration (mg L^{-1})	Molar concentration (mol L^{-1})
$NaNO_3$	467	5.49×10^{-3}
$CaCl_2$	40.0	3.60×10^{-4}
K_2HPO_4	31.0	1.78×10^{-4}
$MgSO_4 . 7\ H_2O$	25.0	1.01×10^{-4}
Na_2CO_3	21.0	1.98×10^{-4}
Fe-EDTA complex	10.0	2.90×10^{-5}
H_3BO_3	6.18	1.00×10^{-4}
$MnSO_4 . 4\ H_2O$	2.23	1.00×10^{-5}
$(NH_4)_6Mo_7O_{24} . 4\ H_2O$	1.96	1.59×10^{-6}
$ZnSO_4 . 7\ H_2O$	2.87	9.98×10^{-6}
$CuSO_4 . 5\ H_2O$	2.49	9.97×10^{-6}
$CoCl_2$	3.00	2.31×10^{-5}

7.5.3 Results and discussion

Growth curves for the cultures grown in Z and BBMA media are shown in Figure 7.7. The maximum cell density achieved with Z medium was lower than for BBMA; however, μ_{max} was similar for both media at 0.65 ± 0.02 d^{-1} for Z medium and 0.66 ± 0.02 d^{-1} for BBMA. As the nitrate concentration in the Z medium was approximately half that of BBMA it was likely that this was the main limiting factor for the cell density that could be achieved with Z medium. This correlated with the maximum cell density achieved with Z medium being approximately half that of BBMA medium.

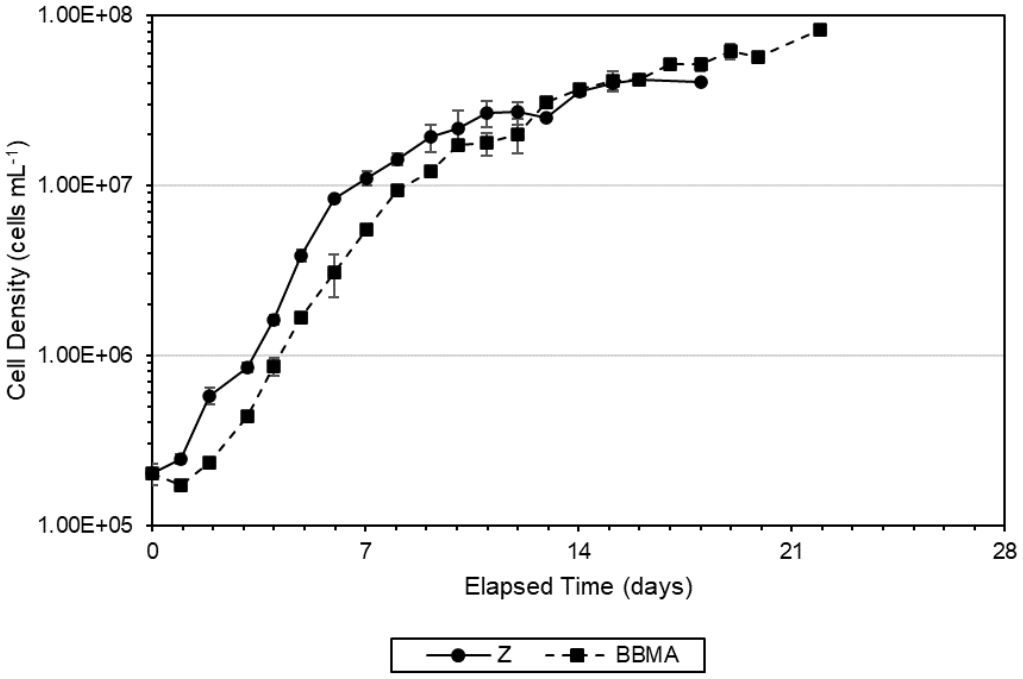

Figure 7.7 – Growth curves for cultures in shake flasks with Z and BBMA media. Error bars denote standard deviation of cell counts from duplicate flasks.

Table 7.6 – Specific growth rate and maximum cell densities for cultures grown in Z or BBMA media in shake flasks.

Medium	μ_{max} **(d^{-1})**	$C_{cell,max}$ **(cells mL^{-1})**
BBMA	0.66 ± 0.02	$8.3 \pm 0.1 \times 10^7$
Z	0.65 ± 0.02	$4.1 \pm 0.1 \times 10^7$

The fatty acid composition of the cells varied with Z and BBMA media as seen in Figure 7.8. EPA content was highest with Z medium, but the EPA fraction was highest with BBMA medium. The total fatty acid (TFA) content was higher with Z medium at 26.4 g TFA/100 g dry biomass compared to BBMA with 12.6 g TFA/100 g dry biomass. These effects could also be due to the nitrate concentration of the two media as nitrate stress has been shown to increase the fatty acid content of microalgae (Mühlroth *et al.*, 2013). While EPA content was higher with Z medium, the cell density was lower and so the EPA productivity was lower than that for BBMA as seen in Table 7.7.

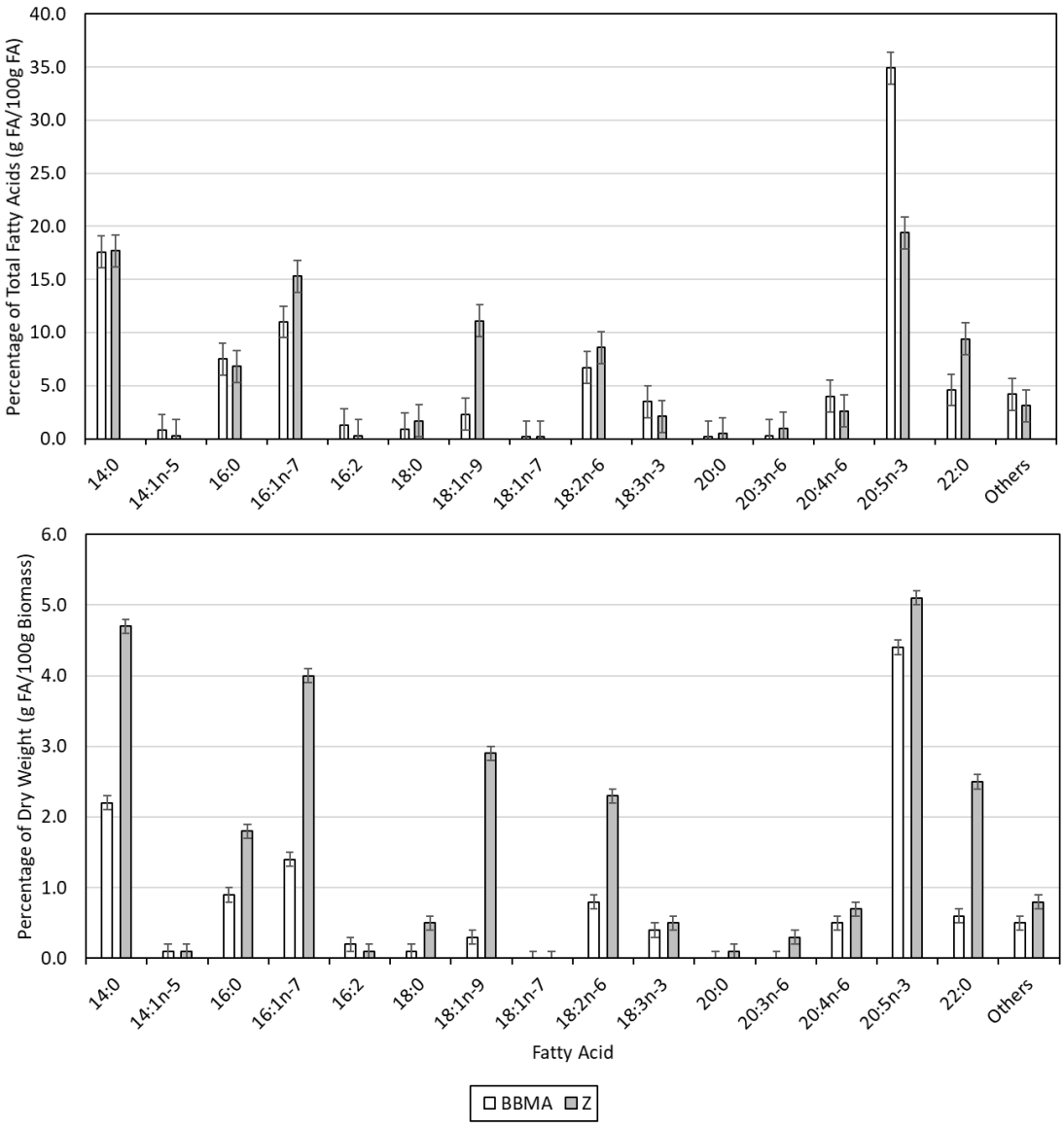

Figure 7.8 – Fatty acid composition of biomass grown in Z and BBMA media.

Table 7.7 – EPA productivities of shake flask cultures grown in Z and BBMA media.

Medium	EPA content (g / 100 g dry biomass)	Biomass concentration (g L^{-1})	EPA productivity (mg L^{-1} d^{-1})	Biomass productivity (g L^{-1} d^{-1})
BBMA	4.4 ± 0.1	4.0 ± 0.2	8.4 ± 0.6	0.19 ± 0.01
Z	5.1 ± 0.1	3.7 ± 0.1	11 ± 1	0.21 ± 0.01

These results showed that the increased EPA content seen in work by Tangestani (2019) compared to this study was likely to be due in part to the use of different media between these two studies. Two components present in Z media but not present in BBMA

were cobalt and boron. Alfiarty (2018) showed that these elements were not required for growth of *Trachydiscus* sp. LCR-Awa-9-2; however, it was possible that these elements may play a role in lipid synthesis by the microalga. The biomass concentration of cultures was better with BBMA medium and so if the EPA content achieved with Z medium could be combined with the growth from BBMA medium this would be promising for further improvement of EPA productivity than what was achieved individually.

7.6 Effect of Co and B trace elements

7.6.1 Introduction

Research conducted by Alfiarty (2018) showed that cobalt and boron were not essential for the growth of *Trachydiscus* sp. LCR-Awa-9-2; however, the effect of these trace elements on EPA content were not investigated. As discussed in § 7.5, Tangestani (2019) was able to achieve a higher maximum EPA using Z media than what was able to be achieved using BBMA media. BBMA and Z media have similar recipes; however, BBMA media does not contain cobalt or boron while Z media does. It was hypothesised that one or both of these trace nutrients may be important in the biosynthesis pathway for EPA, thus resulting in a lower EPA content despite the same environmental conditions when using BBMA medium.

7.6.2 Experimental methods

Cultures were grown in shake flasks according to the general methods outlined in § 3.8. The media used for the cultures was BBMA medium and BBMA medium supplemented with B or Co to reach the equivalent concentration as was present in Z medium (see § 7.5.2 above). Boron was added in the form of H_3BO_3 to a final concentration of 6.18 mg L^{-1} for the B supplemented medium, and cobalt was added in the form of $CoCl_2$ to reach a final concentration of 3.00 mg L^{-1} for the Co supplemented medium. Cell counts were taken each day according to the method in § 3.1.1.

7.6.3 Results and discussion

As seen in Figure 7.9, the growth of cultures with Co supplementation was better than BBMA and B supplemented cultures. The maximum specific growth rate was similar for all cultures, but the culture supplemented with Co showed stronger growth past day 7 than the other two cultures. All cultures reached a similar maximum cell density.

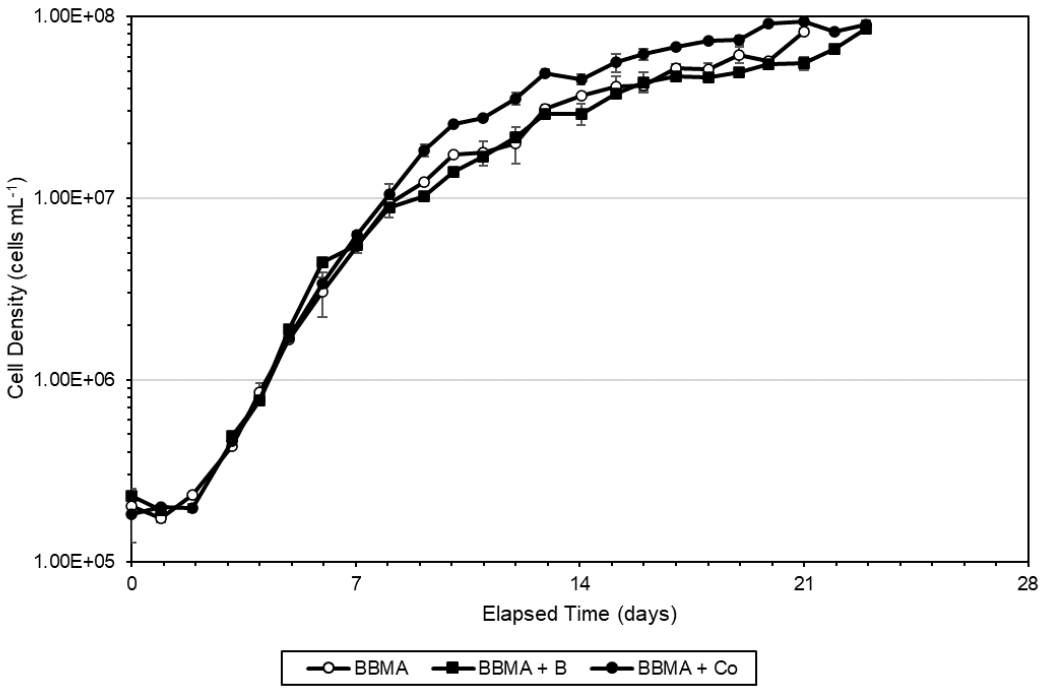

Figure 7.9 – Growth curves for cultures grown with BBMA media supplemented with Co or B.

Table 7.8 – Specific growth rate and maximum cell densities for cultures grown in Z or BBMA medium in shake flasks.

Medium	$\boldsymbol{\mu_{max}}$ **(d^{-1})**	$\boldsymbol{C_{cell,max}}$ **(cells mL^{-1})**
BBMA	0.66 ± 0.02	$8.3 \pm 0.1 \times 10^7$
BBMA + B	0.65 ± 0.02	$8.6 \pm 0.3 \times 10^7$
BBMA + Co	0.66 ± 0.02	$9.0 \pm 0.5 \times 10^7$

Addition of Co and B had an impact on the fatty acid composition of the cells compared to BBMA medium without supplementation as seen in Figure 7.10. The highest EPA fraction was observed in BBMA medium, with the B and Co supplemented media cultures showing decreased EPA fractions. However, the EPA content of the cells showed an opposite trend, with Co supplemented media producing the highest EPA content followed by B and non-supplemented media.

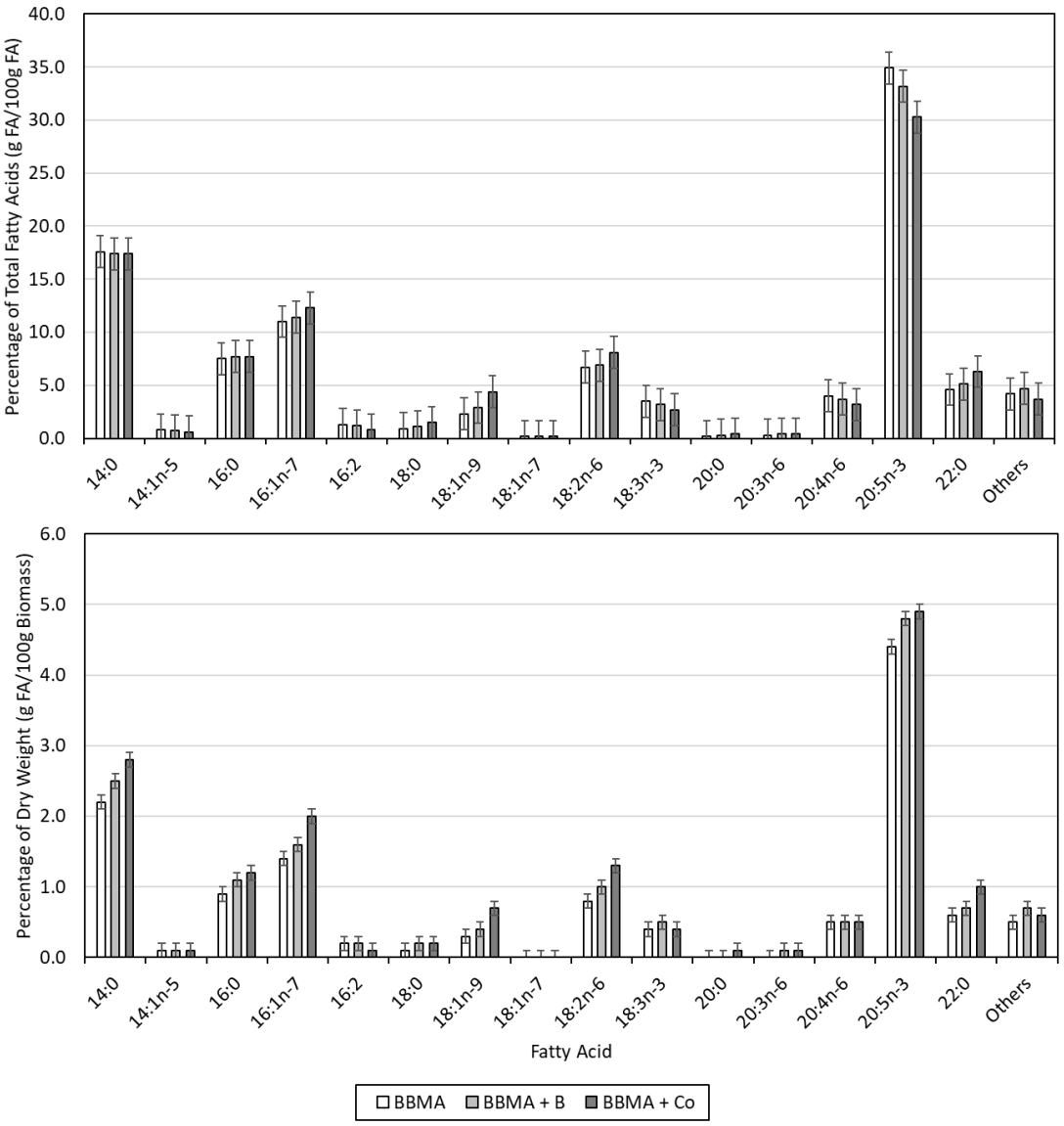

Figure 7.10 – Fatty acid profiles of biomass grown with BBMA media supplemented with Co or B.

Co and B increased the total fatty acid content of the cells compared to non-supplemented media and shows that these two elements may play a role in the increased EPA content seen from the Z media results in § 7.5. Alfiarty (2018) showed that Co and B were not essential for growth and could be potentially toxic to the cells. However, supplementing BBMA medium with only B or Co was not investigated previously. This study showed that the addition of Co may produce slightly favourable growth, but growth was inhibited slightly by addition of B. Neither cobalt or boron appear to be essential in the biosynthesis of EPA and are more likely to inhibit its production due to the slightly lower EPA fractions achieved with these elements present. However, these elements may play a role in overall fatty acid production of the cells, either as an element

involved in the fatty acid synthesis pathway or by causing stress which induces greater overall fatty acid production.

The EPA productivities for the cultures are summarised in Table 7.9. EPA productivity was highest for the cobalt supplemented medium, followed by the boron supplemented and non-supplemented medium. However, the biomass concentration achieved for the non-supplemented medium was lower than what had been achieved in other experiments with the same conditions except for the number of flasks in the incubator. Due to this, it was likely that the light interference from the other flasks might be responsible for the lower productivity in this experiment. Flasks were rotated through different positions in the incubator during the course of the cultures to expose them to a similar 'average' light intensity. However, for the final days of the cultures the BBMA flasks may have been in an unfavourable position compared to the others, resulting in a lower biomass content. The EPA content was similar for BBMA medium between this and other experiments.

Table 7.9 – EPA productivities with BBMA medium and BBMA medium supplemented with B or Co.

Medium	EPA content (g / 100 g dry biomass)	Biomass concentration ($g\ L^{-1}$)	EPA productivity ($mg\ L^{-1}\ d^{-1}$)	Biomass productivity ($g\ L^{-1}\ d^{-1}$)
BBMA	4.4 ± 0.1	4.0 ± 0.2	8.4 ± 0.6	0.19 ± 0.01
BBMA + B	4.8 ± 0.1	4.4 ± 0.1	9.6 ± 0.7	0.20 ± 0.01
BBMA + Co	4.9 ± 0.1	5.3 ± 0.1	11 ± 1	0.23 ± 0.01

7.7 Nitrate consumption rate

7.7.1 Introduction

Nitrate is one of the major macronutrients that is required for microalgae cultures and is closely associated with EPA content, growth rates and photosynthesis in other microalgae (Andersen, 2005; Converti *et al.*, 2009). Alfiarty (2018) concluded that nitrate was not limiting for *Trachydiscus* sp. LCR-Awa-9-2 cultures with BBMA medium over 14 days in shake flasks (a cell density of approximately 8.1×10^7 cells mL^{-1}); however, the true rate of nitrate consumption of *Trachydiscus* sp. LCR-Awa-9-2 had not been measured.

7.7.2 Experimental methods

Cultures were grown in the tubular photobioreactor as described in § 3.11 and 4. Nitrate concentration was measured during tubular photobioreactor cultures under warm white light at 1500 µmol m^{-2} s^{-1} and RGBWW light at maintained light saturation during the experiments in § 6.2 and 6.4.5. Nitrate concentrations were monitored daily at the same time as cell counts were taken using the method outlined in § 3.7 and 3.1.1. The nitrate consumption rate was calculated by minimising the sum of squared errors between the measured nitrate concentration and the modelled nitrate concentration determined by Equation (7.1). The nitrate concentration, $C_{NO_3^-}$, was estimated based on the rate of nitrate consumption, Y_N, the increase in the biomass concentration, $\Delta C_{biomass}$, and the initial concentration of nitrate in the medium, $C_{NO_3^-,0}$.

$$C_{NO_3^-} = C_{NO_3^-,0} - (\Delta C_{biomass}\, Y_N) \qquad (7.1)$$

7.7.3 Results and discussion

The change in nitrate concentrations during the cultures studied are shown in Figure 7.11. The nitrate consumption rate determined by modelling by Alfiarty (2018) predicted a rate of 0.1113 g NO_3^-/g dry biomass. The average nitrate consumption rate calculated from the data in this study was 0.22 ± 0.02 g NO_3^-/g dry biomass and 0.25 ± 0.02 g NO_3^-/g dry biomass for the warm white and RGBWW cultures, respectively.

The results from the nitrate measurement and modelling showed that cultures with BBMA medium were likely nitrate limited at cell concentrations above approximately 4×10^7 cells mL^{-1}. The nitrate consumption rates determined in this study were approximately 2-fold greater than that which had been previously determined. This showed that nitrate is used faster than previously thought and cultures were nitrate limited sooner. However, light was still the major limiting factor for growth of cultures as upon feeding additional nitrate during continuous culturing (§ 8.5) the cell density was not seen to increase proportionally.

(A)

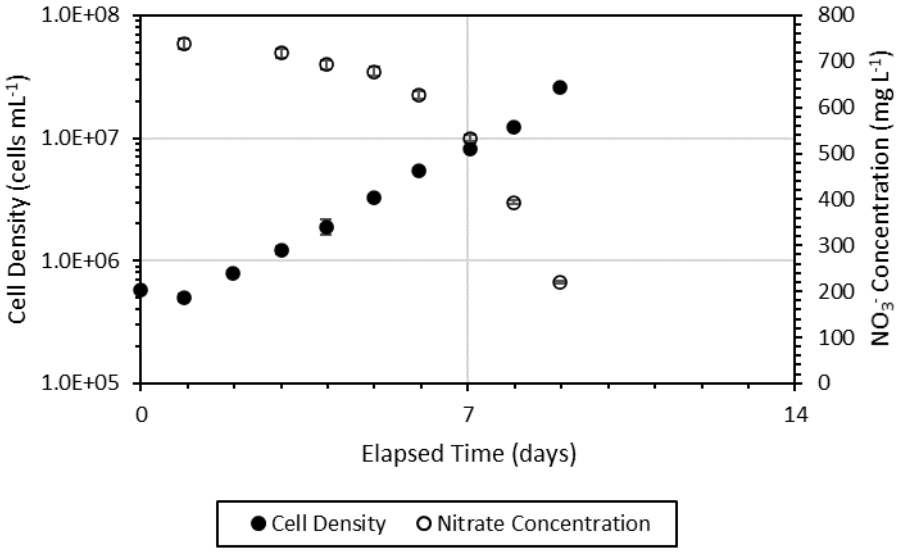

(B)

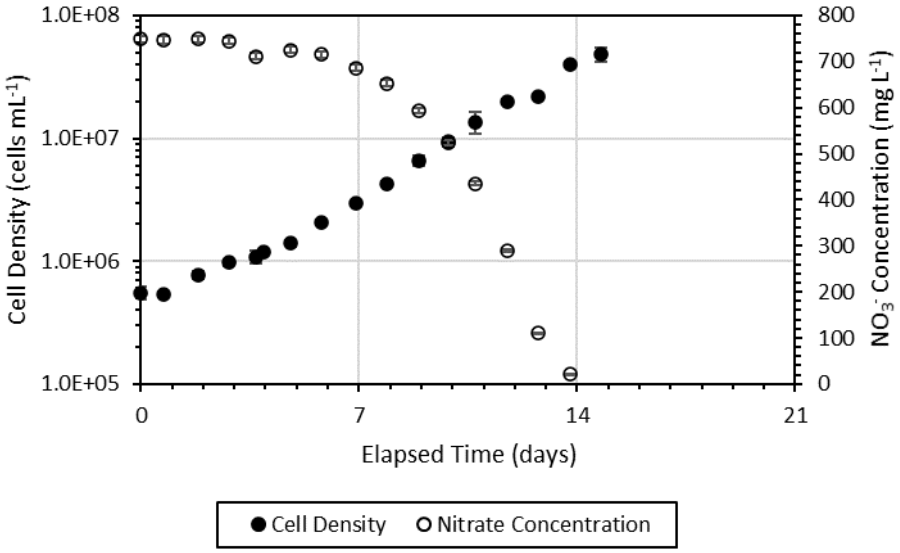

Figure 7.11 – Growth curves showing the change in nitrate concentration in the culture for tubular photobioreactor cultures. A) warm white light, 1500 µmol m^{-2} s^{-1}, B) RGBWW light, light saturation (see § 6.2 and 6.4.5).

7.8 Effect of sodium chloride concentration

7.8.1 Introduction

Salinity has been reported to influence the fatty acid composition of other microalga strains (Mühlroth *et al.*, 2013). For marine microalgae a high salinity is required for growth, whereas for freshwater microalgae there is a range of tolerance for sodium chloride (Andersen, 2005). *Trachydiscus* sp. LCR-Awa-9-2 was isolated from a wetland near

the Pacific Ocean and so it was hypothesised that the microalga could potentially harbour genes that allow it to cope with high salinities, despite being a freshwater microalga. Salinity influences the osmotic pressure which can stress cells. Alfiarty (2018) showed that cultures were not significantly affected by osmotic pressures between 0.312 and 1.926 bar; however, these osmotic pressures were far lower than that of seawater (approximately 30 bar). Seawater is abundant and cheap and so strains which can grow in seawater are beneficial as they do not need to use freshwater supplies which are otherwise needed for drinking water or irrigation (Silva *et al.*, 2014; Waltz, 2009).

7.8.2 Experimental methods

Cultures were grown in shake flasks using the general methods outlined in § 3.8. BBMA medium was supplemented with additional NaCl to increase the salinity of the final media to concentrations of 1, 5, 10 and 35 g L^{-1}, where 35 g L^{-1} was the approximate salinity of seawater (Andersen, 2005). Standard BBMA media with a NaCl concentration of 0.05 g L^{-1} was used as the control. Cell counts were taken daily as outlined in § 3.1.1 and fatty acid contents of harvested biomass were analysed as per § 3.20.

7.8.3 Results and discussion

The growth curves for shake flasks cultures grown with different NaCl concentrations are shown in Figure 7.12.

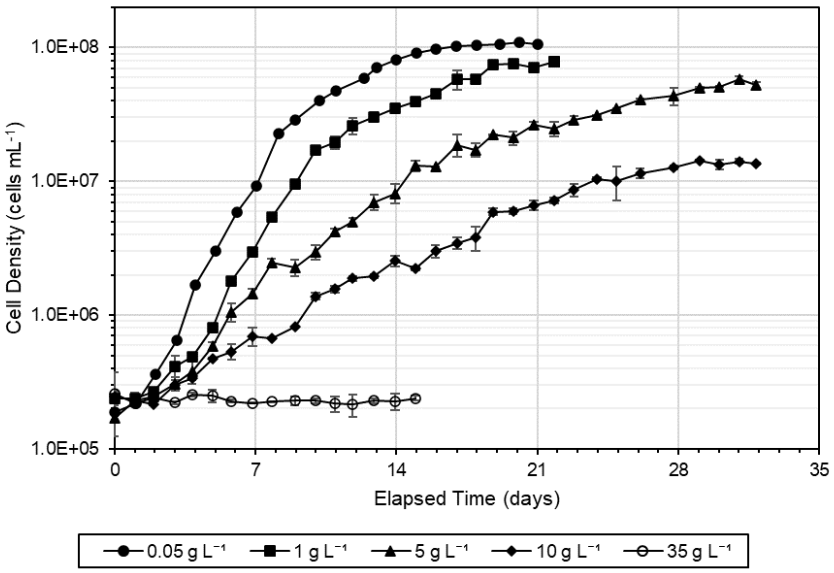

Figure 7.12 – Growth curves for shake flask cultures with different NaCl concentrations. Each data point is the mean of two flasks. Error bars denote standard deviation of two flasks in replicate.

The maximum growth rate and cell density achieved for each NaCl concentration are summarised below in Table 7.10. The maximum cell density and specific growth rate decreased as NaCl concentration was increased. Cultures were unable to grow at a salinity of 35 g L^{-1}.

Table 7.10 – Maximum specific growth rates and cell densities for different NaCl concentrations.

NaCl Concentration ($g\ L^{-1}$)	μ_{max} **(d^{-1})**	$C_{cell,max}$ **(cells mL^{-1})**
0.05	0.62 ± 0.02	$1.0 \pm 0.1 \times 10^8$
1	0.54 ± 0.02	$7.6 \pm 0.1 \times 10^7$
5	0.35 ± 0.02	$5.3 \pm 0.3 \times 10^7$
10	0.22 ± 0.01	$1.4 \pm 0.1 \times 10^7$
35	0 †	$2.5 \pm 0.1 \times 10^5$ †

† Negligible growth was observed in this culture, but cell density was not observed to decrease

As the salinity of the medium was increased the osmotic pressure also increased. The specific growth rate of the cultures decreased with increasing osmotic pressure as seen in Figure 7.13. Growth rates rapidly decreased as osmotic pressure was increased initially but the rate of decrease in growth rate decreased as the osmotic pressure increased.

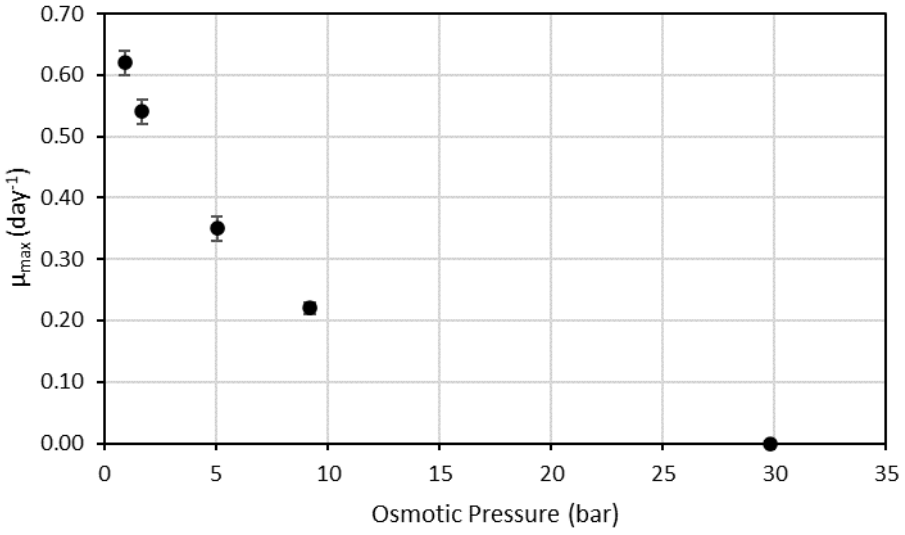

Figure 7.13 – Specific growth rates of cultures at different osmotic pressures due to increased sodium chloride concentration.

The fatty acid composition of the cells was influenced by the sodium chloride concentration as seen in Figure 7.14. The EPA fraction decreased as the concentration of sodium chloride increased; however, the greatest EPA content was achieved at a sodium chloride concentration of 1 g L^{-1}. An increase in salinity increased the total fatty acid content of the cells, as has been seen in other strains of microalgae (Mühlroth *et al.*, 2013).

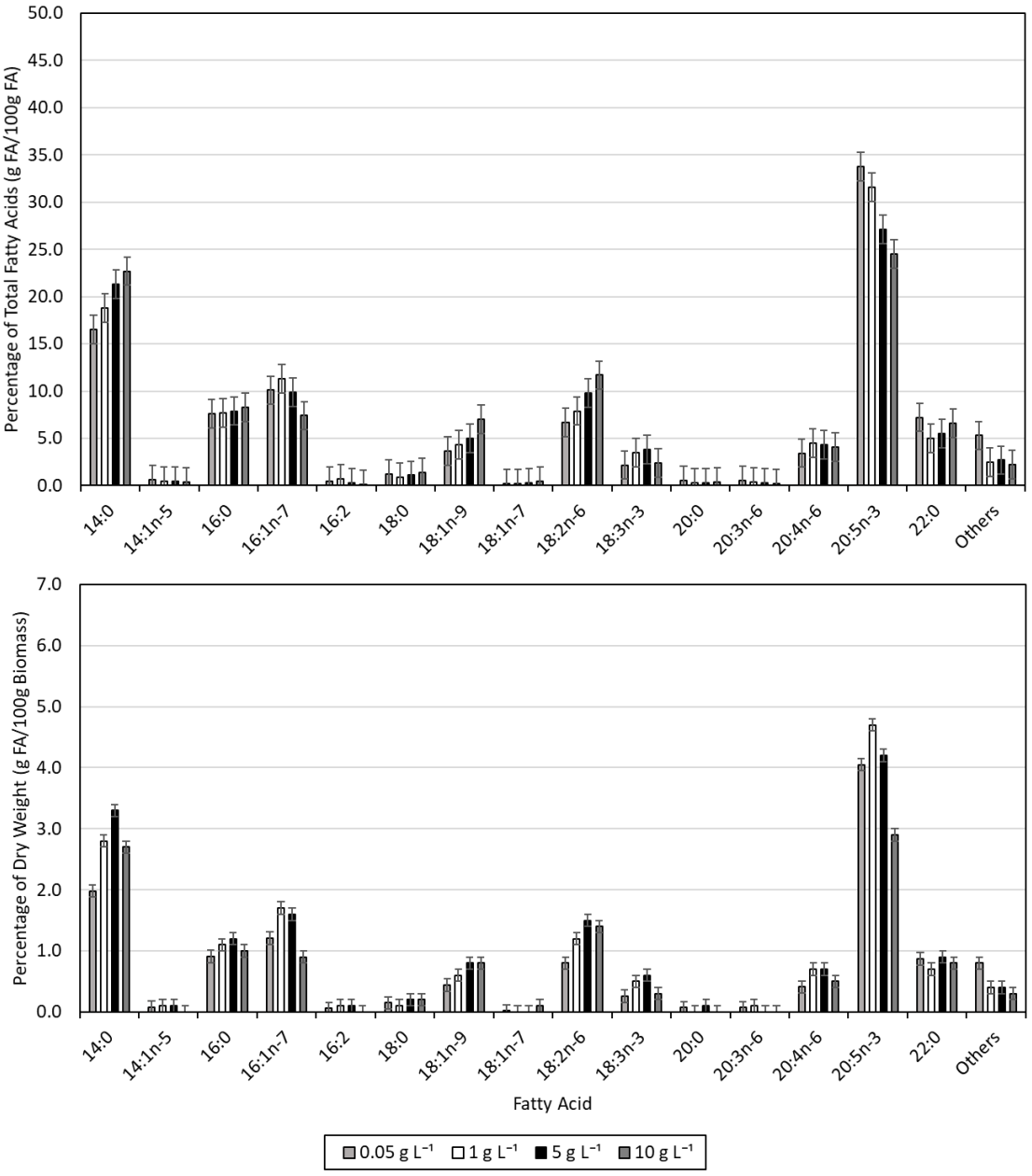

Figure 7.14 – Fatty acid composition of biomass grown with different NaCl concentrations. Note: due to negligible growth there was not enough biomass produced to analyse fatty acids for 35 g L^{-1} NaCl.

As *Trachydiscus* sp. LCR-Awa-9-2 was a freshwater microalga it was not expected to grow optimally at high salinities. However, as could be seen in the growth curves the cells were not able to adapt to the higher sodium chloride concentrations and showed inhibited growth. EPA productivities for the different NaCl concentrations are summarised in Table 7.11. EPA productivity decreased with increasing salinity, with the greatest EPA productivity achieved at 0.05 g L^{-1} NaCl. Despite a higher EPA content at 1 g L^{-1} NaCl, the decrease in biomass concentration and increased culture time due to slower growth negatively impacted productivity.

Table 7.11 – EPA productivities of cultures grown with different NaCl concentrations in BBMA medium.

NaCl Concentration (g L^{-1})	EPA content (g / 100 g dry biomass)	Biomass concentration (g L^{-1})	EPA productivity (mg L^{-1} d^{-1})	Biomass productivity (g L^{-1} d^{-1})
0.05	4.1 ± 0.1	5.7 ± 0.1	14 ± 1	0.34 ± 0.01
1	4.7 ± 0.1	4.4 ± 0.6	9 ± 2	0.20 ± 0.03
5	4.2 ± 0.1	3.4 ± 0.3	4.6 ± 0.5	0.11 ± 0.01
10	2.9 ± 0.1	0.9 ± 0.1	0.9 ± 0.3	0.03 ± 0.01

These results show that freshwater media produced the best EPA productivity and that salinity stress did not improve EPA productivity despite a slight increase in EPA content at 1 g L^{-1} NaCl. While cells could tolerate higher NaCl concentrations than those in freshwater media, salinity stress did not improve EPA production from this microalga.

7.9 Conclusions

Investigations into the effects of nutrients on the growth and EPA content and productivity of *Trachydiscus* sp. LCR-Awa-9-2 showed that the cells were tolerant of CO_2 concentrations up to 30% CO_2 but were unable to grow at 100% CO_2. Air (0.04% CO_2) caused carbon limitation of the culture and growth was best with 3% CO_2. EPA productivity was highest with 10% CO_2. These results show that CO_2 supplementation of cultures is required for optimal EPA productivity and tolerance of high CO_2 concentrations could allow the use of CO_2 sources such as flue gases. Z media produced a higher EPA content than BBMA medium and studies conducted with boron and cobalt supplementation showed that these nutrients may play a role in this difference. Cultures were tolerant of NaCl concentrations up to 10 g L^{-1}; however, cells were unable to grow at a salinity comparable to seawater. Increased NaCl concentration had a detrimental effect on growth, EPA productivity and EPA fraction, but 1 g L^{-1} NaCl showed improved EPA

content. Measurement of the nitrate consumption rate showed that cultures consumed nitrate at a rate around 2-fold higher than previously predicted; however, light was still likely to be the main limiting factor for growth in cultures. Low pH was not able to mitigate growth of bacteria and fungi in cultures during mixotrophic growth and so other approaches are required in order to prevent contamination of cultures when organic carbon sources are added to the growth medium.

8 Effect of Environmental Conditions on the Growth, Oxygen Evolution Rate, and EPA Content of *Trachydiscus* sp. LCR-Awa-9-2

8.1 Introduction

The main environmental factors that influence the growth of microalgae other than light are temperature and pH (Acién Fernández *et al.*, 2013; Molina Grima *et al.*, 2009). In addition to these, the liquid velocity of the culture in tubular photobioreactors can affect the growth of cultures due to shear stress and mixing effects. The effects of all these environmental factors on *Trachydiscus* sp. LCR-Awa-9-2 were important to understand the tolerance of the cells and requirements for cultures. Tangestani (2019) had investigated the effect of pH and temperature on growth; however, the range of test conditions was limited and the oxygen evolution rate of the cells under these conditions had not yet been investigated.

8.2 Effect of pH

8.2.1 Introduction

pH influences many factors in microalgal cultures from cellular processes to the availability of inorganic carbon. The pH ranges that microalgae are tolerant to are highly strain specific and so the pH tolerance of *Trachydiscus* sp. LCR-Awa-9-2 needed to be investigated. In large-scale cultures pH is often difficult to control accurately and economically and can vary depending on the cell's position in the cultivation system (Acién Fernández *et al.*, 2013).

8.2.2 Experimental method

The effect of pH on the oxygen evolution rate of *Trachydiscus* sp. LCR-Awa-9-2 was investigated using the apparatus and general methods outlined in § 3.12. To observe the effect of pH, the pH of the media was adjusted using hydrochloric acid or sodium hydroxide solutions until the required pH was reached. To avoid precipitation of divalent components under high or low pH a simplified BBMA medium was used with the composition as outlined in Table 8.1. As the cultures were exposed to this condition for less than one hour the lack of other nutrients was not likely to be significant.

Table 8.1 – Composition of simplified BBMA medium.

Component	Mass Concentration (mg L^{-1})	Molar Concentration (mol L^{-1})
$NaNO_3$	1000	1.18×10^{-2}
KH_2PO_4	440	3.23×10^{-3}
NaCl	50.0	8.56×10^{-4}

8.2.3 Results and discussion

The net oxygen evolution rate at different pH values were as seen in Figure 8.1. Net oxygen evolution rates were similar over the pH range of 3 to 7 but decreased outside this range.

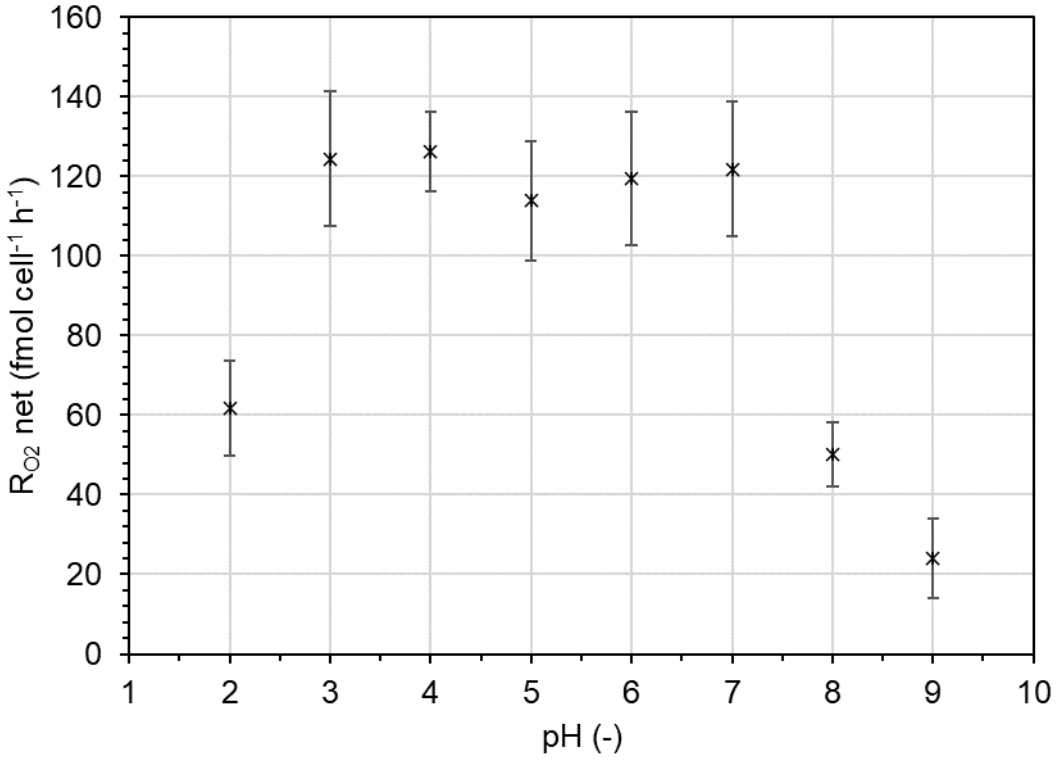

Figure 8.1 – Net oxygen evolution rate for different media pH at 500 µmol m^{-2} s^{-1}, 25.0 °C, 100% air saturation. Data points are the average of triplicate tests. Error bars represent standard deviation of triplicate tests.

As discussed earlier in § 2.5.3, pH has an influence of many factors of microalgal growth. In particular, the ratio of inorganic carbon species in the media changes at different pH values which can have a direct influence on carbon availability for photosynthesis. All microalgae are able to utilise CO_2 by passive diffusion across their

membranes; however, HCO_3^- and CO_3^{2-} require active membrane transport in order to be utilised. Not all strains of microalgae possess the capability to actively transport inorganic carbon species (as discussed in § 2.5.4). As the pH increases the proportion of HCO_3^- and CO_3^{2-} increases and so less CO_2 is available for the cells to use if CO_2 is not continually supplied to the medium. As the rate of oxygen evolution decreased rapidly above pH 7 it was likely that *Trachydiscus* sp. LCR-Awa-9-2 was unable to utilise HCO_3^- and CO_3^{2-}.

The environment that *Trachydiscus* LCR-Awa-9-2 was isolated from was moderately acidic (approximately pH 4–6) and so it was expected that the cells would tolerate acidic environments. Oxygen evolution was observed at a similar rate from pH 7 down to pH 3. At pH 2 the rate of oxygen evolution decreased to around half of that at pH 3. It was assumed that at below pH 3 the cells were unable to sufficiently maintain the pH within the cell against the H^+ concentration gradient present. As many enzymes and other cellular processes must operate in narrow pH ranges (Reece *et al.*, 2010), if the pH inside the cell is unable to be maintained then cellular processes can be affected and this is what was assumed to be happening at low pH with *Trachydiscus* sp. LCR-Awa-9-2. Despite this, the cells were shown to be tolerant of a wide pH range at moderately acidic conditions which is beneficial for large-scale culturing where pH may not be able to be finely controlled. *Trachydiscus* sp. LCR-Awa-9-2 performed more favourably when compared to other microalgae, such as *Isochrysis galbana* (Ippoliti *et al.*, 2016), which showed a small pH range tolerance and so would require more tightly controlled conditions for optimal photosynthesis rate. While *Trachydiscus* sp. LCR-Awa-9-2 was tolerant of a wide range of acidic pH values, results from CO_2 concentration experiments in § 7.3 showed that the pH in cultures without supplemental CO_2 (0.04%) increased to around pH 9. From the results obtained here the photosynthesis rate was greatly reduced at this pH and so this indicated that supplemental CO_2 is a requirement to maintain the pH of cultures in the tolerable range.

8.3 Effect of temperature

8.3.1 Introduction

Temperature can strongly influence both the rate of growth and composition of cells as was discussed in § 2.5.2. Growth and fatty acid composition of the cells had been previously investigated between 15 and 35 °C (Tangestani, 2019); however, questions had been raised about the cells' tolerance to high temperatures where growth was not observed but cultures did not collapse. To further investigate the role photosynthesis rate

could be playing in this effect the oxygen evolution rate of *Trachydiscus* sp. LCR-Awa-9-2 over a range of temperatures was investigated. In this study a broader range of temperatures were trialled to determine the tolerance range of the cells.

8.3.2 Experimental method

The effect of temperature on the oxygen evolution rate was conducted using the previously described apparatus and general methods in § 3.12. To investigate the effect of temperature the experiments were conducted at a range of different temperatures from 5 °C to 40 °C in 5 °C increments. The apparatus was allowed to equilibrate fully prior to measurements. Inoculum for the experiment was added to the medium once the system had equilibrated.

8.3.3 Results and discussion

The effect of temperature on the oxygen evolution rate is shown in Figure 8.2. The maximum oxygen evolution rate was achieved at 20 °C with a similar rate also recorded at 25 °C. Above 25 °C and below 20 °C the rate of oxygen evolution was observed to decrease.

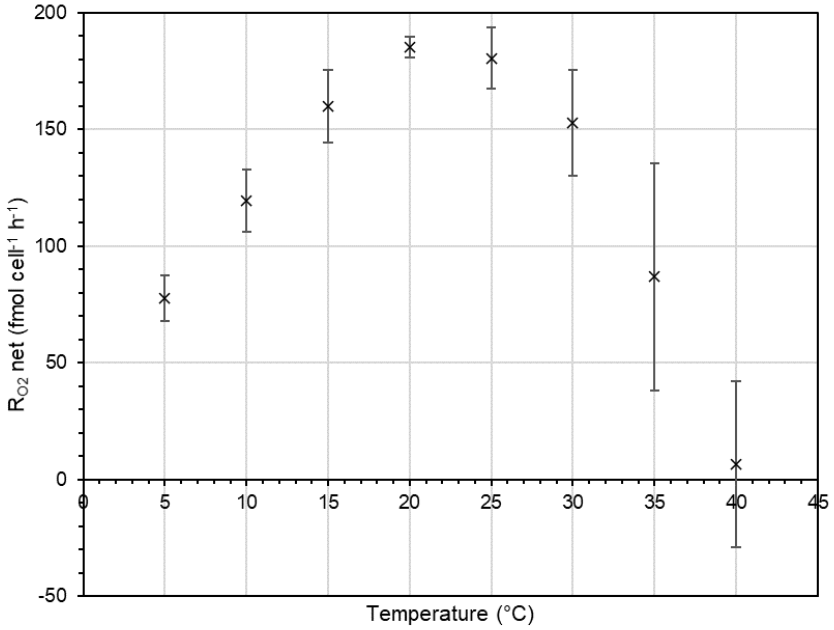

Figure 8.2 – Net oxygen evolution rate at different temperatures. pH 4.6, 500 µmol m^{-2} s^{-1}, 100% air saturation. Error bars represent the standard deviation of triplicate tests.

In previous studies, cultures were shown to grow strongest at 20 and 25 °C, but growth was slower at 15 °C and severely limited above 27 °C (Tangestani, 2019). The results from this study showed that the maximum oxygen evolution rate occurred in the

region of 20 to 25 °C and oxygen evolution rate was lower at 15 °C which agreed with previous results. However, at temperatures higher than 27 °C the oxygen evolution rate was still net positive and rapidly decreased as temperature increased to near net zero at 40 °C. This showed that the cells were able to continue photosynthesising up to 40 °C despite not being able to actively grow at these higher temperatures. It is proposed that other mechanisms associated with processes such as cell division were inhibited at higher temperatures, resulting in the lack of culture growth; however, cells were still able to photosynthesise and maintain themselves at these higher temperatures, thus explaining the cultures not collapsing at these temperatures. The rate of decrease of the rate of oxygen evolution was observed to be greater as temperature increased above 25 °C compared to the rate it decreased when temperatures were decreased below 20 °C. This indicated again that the cells were more tolerant of lower temperatures than higher temperatures.

A broad temperature tolerance range of microalgal strains is one beneficial factor for outdoor culturing to minimise the energy required to maintain culture temperatures in an acceptable range (Borowitzka & Vonshak, 2017). As monthly-average daily temperatures in New Zealand rarely exceed 25 °C or dip below 2 °C in many regions (National Institute of Water and Atmospheric Research (NIWA), 2020b) this showed that *Trachydiscus* sp. LCR-Awa-9-2 could be a suitable species for outdoor cultivation in a New Zealand climate. However, consideration of the heating due to the energy supplied from sunlight would be needed to ensure culture temperatures did not exceed 27 °C which would result in poor growth based on other studies (Tangestani, 2019).

8.4 Effect of liquid velocity

8.4.1 Introduction

Of the parameters that can be controlled in tubular photobioreactors, liquid velocity is unique compared to most other photobioreactors as it can be set independently of other culture parameters such as aeration rate. Increasing the liquid velocity can increase turbulence which leads to improved mixing; however, it also causes higher shear stresses on cells in the culture (Chisti, 2007; Molina Grima *et al.*, 2009). Increased liquid velocities also increase the required pumping power and the energy lost to friction in the pipes. Low liquid velocities are gentler on cells and require less pumping power but can lead to settling of cells and poor mixing.

To determine the effect of liquid velocity on cultures of *Trachydiscus* sp. LCR-Awa-9-2 in the tubular photobioreactor, cultures were grown under three different liquid velocities to observe the effects on growth.

8.4.2 Experimental methods

Cultures were grown in the tubular photobioreactor previously described in § 3.11 and 4. Different liquid velocities were tested by altering the pump speed via the VFD according to the calibration curve previously determined for the liquid velocity in the solar receiver at different frequencies (see § 4.4.1). A control culture was run at a liquid velocity in the solar receiver of 0.6 m s^{-1} and then another culture was grown initially at a liquid velocity of 0.3 m s^{-1} which was then increased to 1.2 m s^{-1} on day 5 of the culture. In all cases BBMA medium was used, the light intensity was 500 µmol m^{-2} s^{-1} and the temperature was 25 °C.

8.4.3 Results and discussion

The growth curves from the liquid velocity experiments are shown in Figure 8.3. The growth curves for 0.6 and 1.2 m s^{-1} were similar but there was a significant lag phase seen for 0.3 m s^{-1} and the culture exhibited slower growth than that for the other conditions. The maximum specific growth rates for each condition are summarised in Table 8.2.

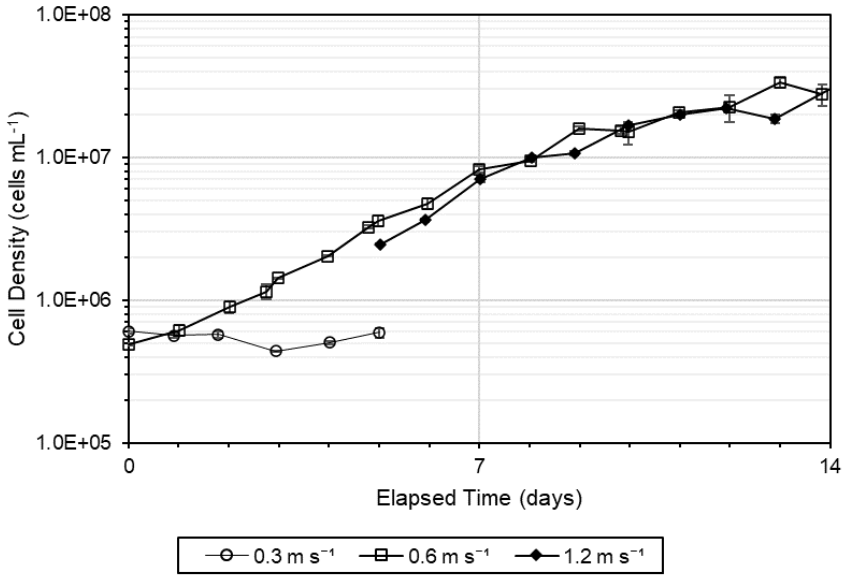

Figure 8.3 – Growth curves for cultures grown in a tubular photobioreactor with different solar receiver liquid velocities. Each data point is the mean of two cell counts taken of the same culture. Error bars denote standard deviation of replicate cell counts of the same culture.

Table 8.2 – Maximum specific growth rates at different liquid velocities.

Liquid Velocity ($m\ s^{-1}$)	**μ_{max} (d^{-1})**
0.3	0.14 ± 0.01
0.6	0.51 ± 0.02
1.2	0.53 ± 0.02

As was seen from the growth curves, the growth rate at 0.6 and 1.2 m s^{-1} were similar, but the growth rate for 0.3 m s^{-1} was far lower. It was also observed that during the first three days at 0.3 m s^{-1} the cell density decreased before starting to increase again on day 4. This was attributed to cells settling out in the reactor and was observed by accumulation of cells along the bottom half of the solar receiver tubes as can be been in Figure 8.4. Upon increasing the liquid velocity to 1.2 m s^{-1} the cells were rapidly resuspended (within 10 minutes) which showed that the cells had most likely settled out of the culture, rather than forming a biofilm. This was also seen by the sudden increase in cell density on day 5 after the liquid velocity was increased. If the cells had attached to the walls of the solar receiver tubes by formation of biofilms it was expected that the cells would not have resuspended appreciably upon increasing the liquid velocity.

(A) (B)

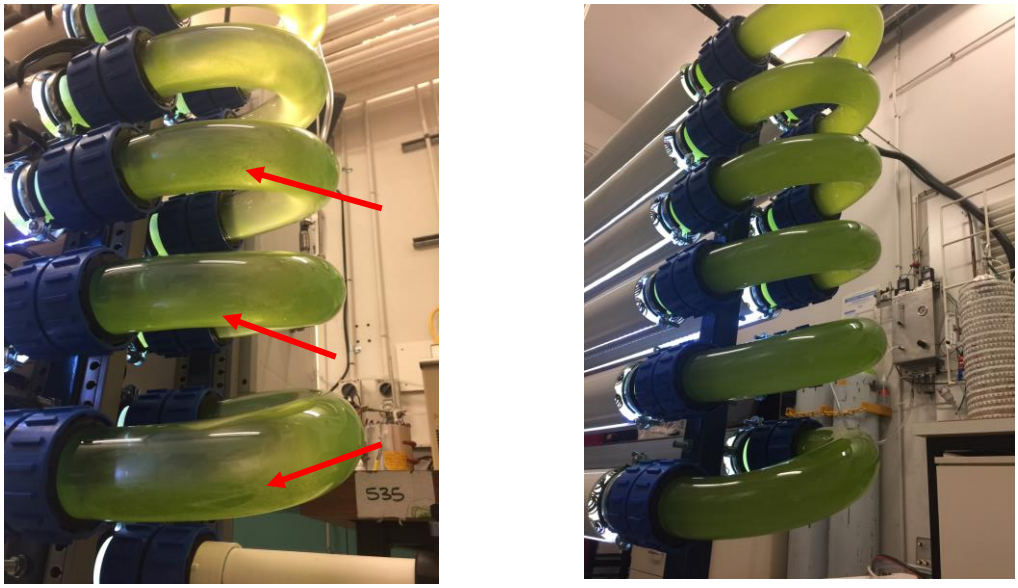

Figure 8.4 – A) Settling of cells in the solar receiver at liquid velocity of 0.3 m s^{-1}, B) resuspension of cells upon increase of liquid velocity to 1.2 m s^{-1}.

The low specific growth rate for 0.3 m s^{-1} was likely artificially low as the cells that had settled out were unable to be counted and so the cell density appeared lower than it truly was in the reactor. Although the cells were not suspended in the medium, they appear to have still been able to grow as otherwise there would not have been a significant jump in cell density when the liquid velocity was increased and the cells were resuspended. Due to this, the true cell density including the settled cells would have been closer to 2.4×10^6 cells mL^{-1} on day 5 and so the maximum specific growth rate would be closer to 0.29 d^{-1}.

The results show that *Trachydiscus* sp. LCR-Awa-9-2 was tolerant of the shear stress levels present in tubular photobioreactors and growth was unlikely to be hindered by shear stress at reasonable liquid velocities that may be used in operation. However, even though at a liquid velocity of 0.3 m s^{-1} the flow was in the turbulent regime the cells still settled out. It was proposed that this could be due to the increase in the laminar boundary layer thickness, δ, which increases with decreasing liquid velocity. Thicker boundary layers result in smaller wall shear stresses on the cells which could cause them to stick to the walls of the solar receiver and not remain suspended in the medium. δ can be found by Equation (8.1) (Wilkes & Bike, 1999), where d_t is the tube diameter and the Reynolds number is given by Equation (2.32).

$$\frac{\delta}{d_t} = 62\ Re_{pipe}{}^{-\frac{7}{8}} \qquad (8.1)$$

For the solar receiver, the boundary layer thickness varied with liquid velocity as shown in Figure 8.5. At 0.3 m s^{-1} the boundary layer was approximately 86 times thicker than the diameter of a typical cell while at 0.6 and 1.2 m s^{-1} it was approximately 50 and 25 times thicker, respectively.

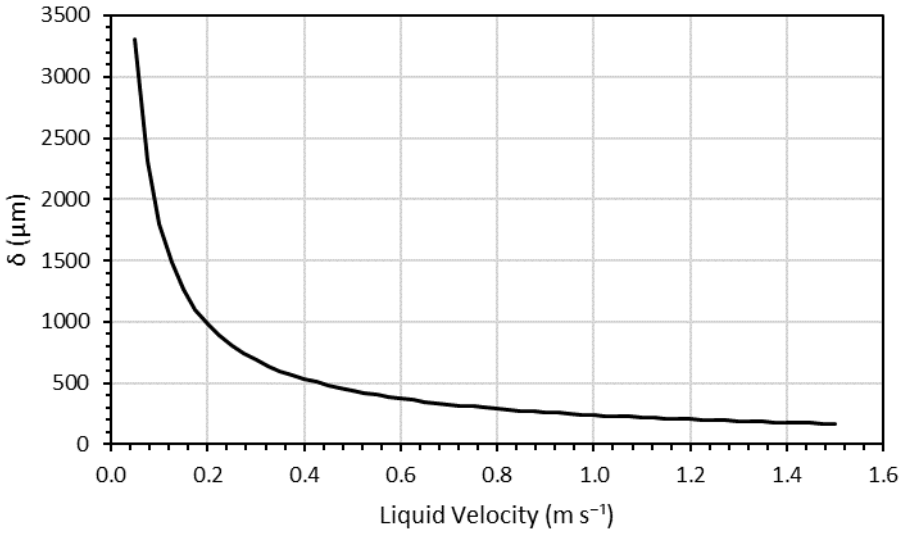

Figure 8.5 – Calculated laminar boundary layer thickness, δ, for different liquid velocities in the solar receiver.

The wall shear stress, τ_0, on the cells given by Equation (4.41) varied with liquid velocity as shown in Figure 8.6. As cells are able to attach to surfaces with substances such as exopolysaccharides, sufficient shear forces must be applied to detach the cells again (Zeriouh *et al.*, 2017). Based on the calculated shear stress at the wall of the tubes, a shear stress between 0.32 and 1.08 Pa was required to prevent attachment of cells to the walls of the tubes. Above this range the cells were not seen to form biofilms or settle in the tubes.

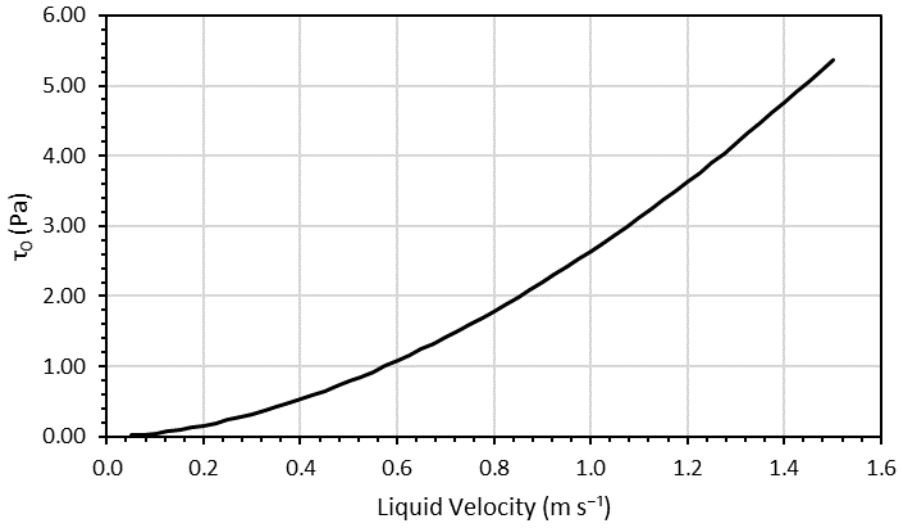

Figure 8.6 – Calculated wall shear stress, τ_0, for different liquid velocities in the solar receiver.

Another key concern was the shear stress due to the centrifugal pump in the tubular photobioreactor. According to Equation (4.45), the shear stress at the tip of the

impeller in the pump was approximately 54 Pa at a liquid velocity of 1.2 m s^{-1}. This showed that *Trachydiscus* sp. LCR-Awa-9-2 had a shear tolerance of at least 54 Pa which was at the higher range of reported shear stress tolerances of microalgae (see § 2.5.7). Due to the morphology of the cells it was expected that *Trachydiscus* sp. LCR-Awa-9-2 would be tolerant of shear stress and the results of this study confirmed this. As shear tolerance is a key requirement for successful culturing of microalgae in large-scale tubular photobioreactors this indicated that *Trachydiscus* sp. LCR-Awa-9-2 was a promising candidate for large-scale culturing in this type of system.

8.5 Effect of semi-continuous and batch culturing

8.5.1 Introduction

Prior to this study *Trachydiscus* sp. LCR-Awa-9-2 had only be grown as batch cultures; however, many large-scale microalgal cultures are run as continuous cultures (Borowitzka & Vonshak, 2017; Posten & Walter, 2012). Additionally, continuous culturing has shown improved EPA productivity for a range of microalga strains compared to batch cultures as discussed in § 2.5.6. Continuous culturing can improve efficiency of processes by minimising the downtime required for cleaning and sterilisation between batches by allowing continuous harvesting of a portion of a culture for, in theory, an indefinite length of time.

One major limitation to continuous culturing of microalgae is the formation of biofilms in photobioreactors (Zeriouh *et al.*, 2017). Biofilms reduce the availability of nutrients to cells that are within the biofilm due to mass transfer limitations resulting in poor growth. The accumulation of biofilms on the surfaces of photobioreactors also greatly hinders the light penetration into cultures and limits growth of the bulk culture. To remedy this, the reactor must be cleaned of the biofilms which often requires complete harvesting of the biofouled reactor, cleaning of the surfaces, and inoculating a new culture. Other approaches to prevent formation of biofilms can include adding abrasive particles to the culture, recirculation of a close-fitting ball through the solar receiver which scours the tubes, or introduction of slugs of air (Chisti, 2006). Biofilms are typically formed from extracellular products such as polysaccharides from the cells which allow them to attach to the walls of photobioreactors and to each other. Contamination of cultures can often lead to increased formation of biofilms in microalgae cultures. Due to these reasons,

microalgae strains which do not cause excessive biofouling over extended culture times and are not prone to contamination are of greatest benefit to continuous culturing.

8.5.2 Experimental methods

Cultures were grown in the tubular photobioreactor as described in § 4 and the general methods in § 3.11. Batch cultures were run by inoculating the culture then allowing it to run until maturity where the entire reactor volume was harvested. For semi-continuous cultures the reactor was inoculated as usual but once the culture had grown to the desired cell density a set volume of the culture was harvested and topped up with an equivalent volume of fresh culture medium.

The culture medium used to top up the culture during semi-continuous culturing was prepared as per the usual recipe (i.e. full strength) apart from the sodium nitrate which was added to bring the total nitrate concentration in the reactor up to the original concentration at the beginning of the culture. This was achieved by measuring the nitrate concentration in the culture using the method outlined in § 3.7 and then adding the required amount of sodium nitrate to the replacement media to bring the sodium nitrate concentration to 1.0 g L^{-1} in the entire culture volume.

Semi-continuous cultures were conducted at a variety of cell densities under both warm white and RGBWW light at intensities of 1500 and 2300 µmol m^{-2} s^{-1}, respectively. To assess the performance of semi-continuous cultures at different cell densities, harvests were conducted over a minimum of five days at each condition. To increase the cell density the culture was allowed to grow for two or three days until the cell density reached the desired level and then harvesting was resumed.

The volume harvested each day was determined based on the specific growth rate of the previous day so that the cell density would replenish within a 24-hour period between harvests. Cell counts were taken according to the methods in § 3.1.1 before and after daily harvests which occurred 24 hours apart. Nitrate concentrations were also analysed before and after harvests each day. Biomass samples were collected at the start, middle and end of each semi-continuous culture condition for fatty acid analysis and to determine the dry biomass concentration as per § 3.20 and 3.1.2.

8.5.3 Results and discussion

The growth curve for the semi-continuous culture under warm white light is shown in Figure 8.7. Semi-continuous culturing was conducted in three parts at cell

densities of approximately 3×10^7, 4×10^7 and 5×10^7 cells mL^{-1}. During part 1 and 2, 20 L of culture was harvested per day (dilution rate of 0.26 d^{-1}) and this was reduced to 15 L per day (dilution rate of 0.19 d^{-1}) during part 3 as the growth rate was not high enough to maintain the culture at a rate of 20 L per day. This was observed by the culture starting to wash out during the initial days during part 3 of the culture. The EPA productivities achieved during each part of the semi-continuous culture were as reported in Table 8.3.

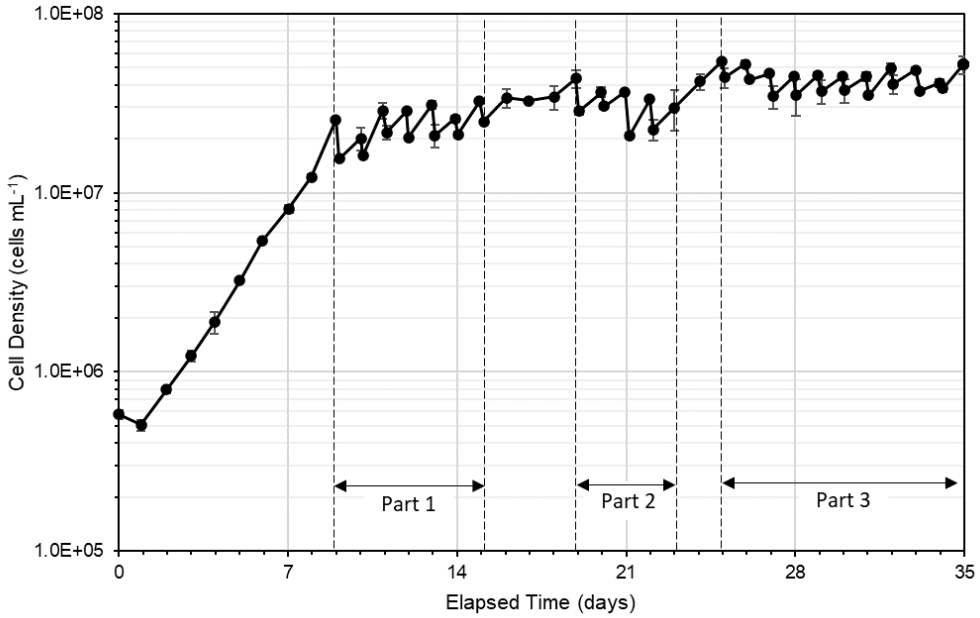

Figure 8.7 – Growth curve of semi-continuous tubular photobioreactor culture under warm white light at 1500 µmol m^{-2} s^{-1}.

Table 8.3 – EPA productivities of semi-continuous cultures in the tubular photobioreactor.

Elapsed Time	Dilution rate (d^{-1})	EPA content (g / 100 g dry biomass)	Biomass concentration (g L^{-1})	EPA productivity (mg L^{-1} d^{-1})	Biomass productivity (g L^{-1} d^{-1})
Day 9	0.26	6.1 ± 0.1	1.7 ± 0.1	27 ± 2	0.45 ± 0.03
Day 15	0.26	4.9 ± 0.1	1.7 ± 0.1	22 ± 2	0.45 ± 0.03
Day 19	0.26	4.6 ± 0.1	2.4 ± 0.1	29 ± 2	0.63 ± 0.03
Day 25	0.26	4.8 ± 0.1	3.4 ± 0.1	43 ± 2 ▲	0.89 ± 0.03
Day 30	0.19	4.4 ± 0.1	3.4 ± 0.1	30 ± 2	0.67 ± 0.02
Day 35	0.19	4.4 ± 0.1	3.1 ± 0.2	27 ± 2	0.61 ± 0.04

▲ Culture was not able to be maintained at a dilution rate of 0.26 d^{-1} but could be at 0.19 d^{-1}. This gives a true maintainable EPA productivity of approximately 32 ± 2 mg L^{-1} d^{-1}.

EPA productivity was greatest during part 3 of the culture. Although an initial EPA productivity of 43 ± 2 mg L^{-1} d^{-1} was achieved at the beginning of part 3, the culture started to wash out this productivity was unable to be maintained. The maximum maintainable productivity was 30 ± 2 mg L^{-1} d^{-1} on day 30 of the culture. This was due to the higher biomass concentration of the culture harvested at this condition. EPA content decreased during the course of the culture but stabilised at 4.4 ± 0.1 g/100 g dry biomass during part 3. Productivities during part 1 and 2 were only marginally lower than that achieved in part 3 due to a combination of a higher EPA content of the biomass and a greater volume harvested per day, despite a lower biomass concentration. Based on previous experiments (§ 6) it was possible that an increase in the light intensity could improve the growth rate at high cell densities and so this was tested during the second semi-continuous culture trialled.

As the first semi-continuous culture trialled started to wash out at a dilution rate of 0.26 d^{-1} at 5 × 10^7 cells mL^{-1} another semi-continuous culture was trialled using RGBWW light but at a higher light intensity of 2300 µmol m^{-2} s^{-1} in an attempt to maintain a higher growth rate at this cell density. The growth curve for this culture is shown in Figure 8.8. During the course of this culture a pump failure occurred on day 17 which may have affected the performance of the culture as it was not circulated for one day while the pump replacement took place.

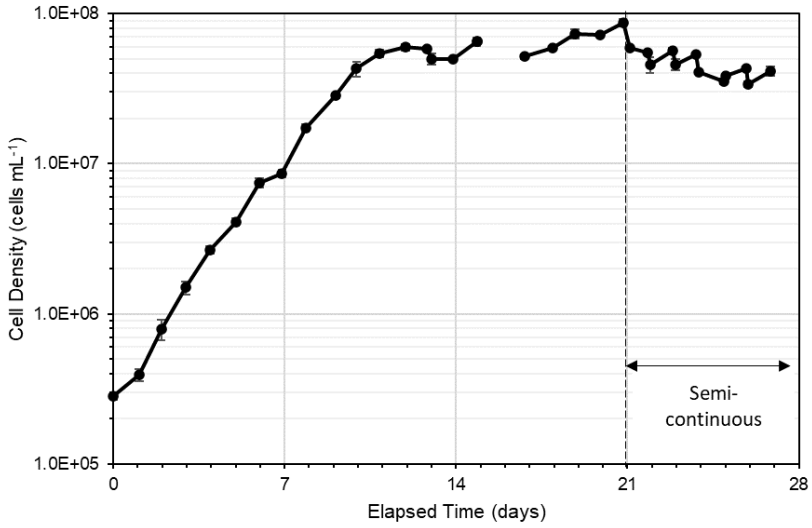

Figure 8.8 – Semi-continuous culture growth curve under 2300 µmol m^{-2} s^{-1} light intensity with RGBWW lighting. Error bars denote standard deviation of duplicate counts from the same culture.

As can be seen in the growth curve, the culture again suffered from wash out and the growth rate was not high enough to maintain a dilution rate of 0.26 d^{-1} (20 L d^{-1} harvest). It was not known whether this was in part due to the pump failure during the culture, but from other experimental results it was expected that the culture should recover from a change of condition such as this within approximately one week. From results obtained from the light limitation experiments, one approach that could be used instead to improve the growth rate at higher cell densities was to increase the volume of the reactor that is illuminated. At the end of this semi-continuous culture the EPA fraction was 40 ± 1 g/100 g fatty acids and the EPA content was 4.7 ± 0.1 g/100 g dry biomass which were comparable with the results that were achieved previously with semi-continuous cultures at this cell density with warm white light.

Compared to batch cultures from previous experiments, even the lowest EPA productivity achieved from semi-continuous culturing (22 ± 2 mg L^{-1} d^{-1}) was greater than the greatest achievable with batch cultures (16 ± 2 mg L^{-1} d^{-1}). Due to this it is recommended that semi-continuous culturing is used for maximising the EPA productivity of *Trachydiscus* sp. LCR-Awa-9-2. One barrier that can hinder continuous culturing of microalgae is the formation of biofilms (Zeriouh *et al.*, 2017). However, from the experiments conducted with *Trachydiscus* sp. LCR-Awa-9-2, no appreciable biofilm formation was observed over the course of 35 days which indicated that this microalga was well-suited to continuous culturing.

8.6 Conclusions

Investigations into the effect of environmental conditions on *Trachydiscus* sp. LCR-Awa-9-2 showed that the cells were tolerant of a wide range of conditions. Cells were able to photosynthesise over a broad range of moderately acidic pH values. The optimal temperature for photosynthesis rate was between 20 and 25 °C but cells continued to photosynthesise down to 5 °C and up to 40 °C. Cultures were able to be grown in the tubular photobioreactor at liquid velocities up to 1.2 m s^{-1} which showed that the cells were tolerant of the typical shear stresses present in this style of photobioreactor. Cells settled out of the culture at lower liquid velocities and so the minimum liquid velocity that can be used for operation is between 0.3 and 0.6 m s^{-1}. Semi-continuous culturing improved the EPA productivity of cultures compared to batch culturing and cultures were able to be grown for 35 days without signs of significant biofilm formation in the tubular photobioreactor. The ability to be effectively semi-continuously cultured in conjunction

with tolerance of a wide range of environmental conditions showed that *Trachydiscus* sp. LCR-Awa-9-2 was a good candidate for large-scale cultivation.

9 General Discussion and Conclusions

9.1 Summary of experimental results

The following section is a summary of the key results that were obtained in the preceding sections. The lipidomic studies conducted on *Trachydiscus* sp. LCR-Awa-9-2 showed that the majority of EPA (50 ± 2 g/100 g total EPA) was located in the MGDG lipids which was consistent with results published for other eustigmatophytes. Results from early lipidomic work showed that lipids were degraded in the lipid extracts obtained from freeze-dried biomass from *Trachydiscus* sp. LCR-Awa-9-2 during extraction with a modified Bligh and Dyer method. The main lipid specie detected by mass spectrometry in the degraded lipids was a DG 20:5/20:5 species which showed that the majority of EPA was likely produced through the eukaryotic pathways of ω-3 fatty acid synthesis and confirmed that degradation of lipids had occurred due to the high content of diacylglycerides.

While a carbohydrate-containing lipid species was not detected in the mass spectra of the TLC spot, staining with Molisch's test on the TLC plate indicated the presence of carbohydrates in what was determined by mass spectrometry as diacylglycerides. Further TLC separations indicated that monoglucosyl diacylglycerides (GlcDG) may be present in the microalga and were likely eluting alongside the diacylglycerides in the TLC method used. However, results from fatty acid analyses showed that the potential GlcDG lipids were a minor component of the total lipid profile of the cells (approximately < 3 wt% of total lipids). Further work is required to elucidate the full lipidome of *Trachydiscus* sp. LCR-Awa-9-2 now that hurdles with degradation of lipids have been overcome with direct extraction of lipids from wet biomass with the isopropanol method to prevent the action of degradative enzymes. Further work is also required to determine the cause of degradation of lipids as this was not observed with extractions from *Chlorella vulgaris* in this study and other species used in other studies (Li *et al.*, 2014). It was likely that the freezing process used during freeze-drying of the biomass in this study was the key cause of lipid degradation due to rupturing of cell organelles and subsequent contact of lipids with degradative enzymes. This may be able to be overcome with snap freezing of the biomass using liquid nitrogen, for example. However, further work is required to determine the mechanisms of lipid degradation in the microalga and their potential implications for large-scale extraction of EPA.

Oxygen evolution rate measurements were conducted to investigate the effect of light intensity, light wavelength, pH, and temperature. Warm white LED light saturated the cells with light at the lowest intensity, followed by blue, green and red LED light. Oxygen evolution was shown to occur over a temperature range of 5 to 40 °C with the optimum rate achieved at 20 to 25 °C. Photosynthesis was also shown to occur over a broad pH range, with similar results obtained for pH values of 3 to 7. Above pH 7 the rate of oxygen evolution decreased, as it also did below pH 3. The light saturation point for cells under warm white light was approximately 1.5×10^{10} photons $cell^{-1}$ s^{-1}.

The following tables summarise the results of culture studies that were conducted. Table 9.1 summarises the results from batch cultures in the tubular photobioreactor and Table 9.2 summarises the results from semi-continuous culturing. The conditions tested in the tubular photobioreactor included light intensity, light colour, liquid velocity, and light volume ratios. Table 9.3 summarises the results from shake flask cultures that were conducted. Conditions that were investigated were the effects of diurnal light cycles, carbon dioxide concentration, sodium chloride concentration, mixotrophic growth at low pH, Z and BBMA media and Co and B trace nutrients.

Table 9.1 – Summary of results from tubular photobioreactor batch cultures. BBMA medium, 3 vol% CO_2, 25 °C, 24:0 light regime.

Treatment	I (µmol m^{-2} s^{-1})	Light colour	$u_{L,SR}$ (m s^{-1})	μ_{max} (d^{-1})	$C_{cell,max}$ (cells mL^{-1})	$C_{cell,max}$ (g L^{-1})	EPA fraction (g EPA/ 100 g total fatty acids)	EPA content (g EPA/ 100 g dry biomass)	EPA productivity (mg L^{-1} d^{-1}) ♦
Light intensity	217	RGBWW	0.6	0.48 ± 0.02	$1.8 \pm 0.1 \times 10^7$	1.3 ± 0.1	37 ± 1	4.5 ± 0.1	3.4 ± 0.3
Light Intensity	500	RGBWW	0.6	0.47 ± 0.02	$4.1 \pm 0.2 \times 10^7$	2.5 ± 0.1	40 ± 1	5.3 ± 0.1	8.0 ± 0.7
Liquid velocity	500	RGBWW	0.3	0.14 ± 0.01 ▲	-	-	-	-	-
Liquid velocity	500	RGBWW	1.2	0.53 ± 0.02	$4.7 \pm 0.5 \times 10^7$	-	38 ± 1	5.5 ± 0.1	-
Light intensity	Saturation †	RGBWW	0.6	0.40 ± 0.02	$8.1 \pm 0.3 \times 10^7$	5.0 ± 0.1	37 ± 1	5.0 ± 0.1	12 ± 1
Light colour	1900	B	0.6	0.50 ± 0.02	$4.5 \pm 0.4 \times 10^7$	3.0 ± 0.1	38 ± 1	4.7 ± 0.1	8.5 ± 0.7
Light colour	1500	WW	0.6	0.49 ± 0.02	$5.2 \pm 0.6 \times 10^7$	3.1 ±0.1	37 ± 1	4.9 ± 0.1	11 ± 1
Light colour	2300	RGBWW	0.6	0.54 ± 0.02	$6.0 \pm 0.3 \times 10^7$	3.6 ± 0.1	40 ± 1	5.3 ± 0.1	15 ± 1
Light volume ratio	1000 (half light tubes illuminated)‡	RGBWW	0.6	0.24 ± 0.01	$3.0 \pm 0.5 \times 10^7$	1.4 ± 0.1	37 ± 1	4.7 ± 0.1	2.7 ± 0.2

♦: Based on elapsed culture time to harvest of batch culture.
▲: Low growth rate was likely due to settling out of cells from the culture due to low turbulence.
†: Light intensity was increased over the culture duration to maintain saturation. Min I: 34 µmol $m^{-2}s^{-1}$; Max I: 2872 µmol $m^{-2}s^{-1}$.
‡: Solar receiver tubes 1–6 were not illuminated for this culture.

R: red; G: green; B: blue; WW: warm white; I: incident light intensity; $u_{L,SR}$: solar receiver liquid velocity; μ_{max}: maximum specific growth rate; $C_{cell,max}$: maximum cell density.

Table 9.2 – Summary of semi-continuous experiments in the tubular photobioreactor. BBMA medium, 3 vol% CO_2, 25 °C, 24:0 light regime.

Elapsed culture time	I (µmol m^{-2} s^{-1})	Light colour	Harvest volume (L d^{-1})	Dilution rate (d^{-1})	C_{cell} (cells mL^{-1})	(g L^{-1})	EPA fraction (g EPA/100 g total fatty acids)	EPA content (g EPA/100 g dry biomass)	EPA productivity (mg L^{-1} d^{-1})
Day 9 (Start of part 1)	1500	WW	20	0.26	$2.6 \pm 0.1 \times 10^7$	1.7 ± 0.1	46 ± 1	6.1 ± 0.1	27 ± 2
Day 15 (End of part 1)	1500	WW	20	0.26	$3.2 \pm 0.1 \times 10^7$	1.7 ± 0.1	44 ± 1	4.9 ± 0.1	22 ± 2
Day 19 (Start of part 2)	1500	WW	20	0.26	$4.4 \pm 0.5 \times 10^7$	2.4 ± 0.1	41 ± 1	4.6 ± 0.1	29 ± 2
Day 25 (Start of part 3)	1500	WW	20	0.26	$5.4 \pm 0.4 \times 10^7$	3.4 ± 0.1	39 ± 1	4.8 ± 0.1	43 ± 2 ♠
Day 30 (Mid part 3)	1500	WW	15	0.19	$4.5 \pm 0.2 \times 10^7$	3.4 ± 0.1	38 ± 1	4.4 ± 0.1	30 ± 2
Day 35 (End of culture)	1500	WW	15	0.19	$5.2 \pm 0.6 \times 10^7$	3.1 ± 0.2	37 ± 1	4.4 ± 0.1	27 ± 2

♠: Culture started to washout at 20 L d^{-1}, needed to reduce to 15 L d^{-1} to prevent washout (gives a productivity of 32 ± 2 mg L^{-1} d^{-1} at 15 L d^{-1}).

I: incident light intensity; C_{cell}: cell density.

Table 9.3 – Summary of shake flask culture experiments. 150 rpm, 25.0 °C, high light intensity (500 µmol m^{-2} s^{-1}).

Treatment	CO_2 Concentration (vol% in air)	Media	Light cycle (hours light : hours dark)	μ_{max} (d^{-1})	$C_{cell,max}$ (cells mL^{-1})	$C_{cell,max}$ (g L^{-1})	EPA fraction (g EPA/ 100 g total fatty acids)	EPA content (g EPA/ 100 g dry biomass)	EPA productivity (mg L^{-1} d^{-1}) ♦
Diurnal cycles	3	BBMA	24:0	0.62 ± 0.02	$1.0 \pm 0.1 \times 10^8$	5.7 ± 0.1	34 ± 1	4.1 ± 0.1	14 ± 1
	3	BBMA	12:12	0.54 ± 0.02	$6 \pm 1 \times 10^7$	3.1 ± 0.1	45 ± 1	6.0 ± 0.1	9.8 ± 0.8
	3	BBMA	16:8	0.58 ± 0.02	$7.3 \pm 0.5 \times 10^7$	5.1 ± 0.2	29 ± 1	4.7 ± 0.1	12 ± 1
Media	3	BBMA + Co	24:0	0.66 ± 0.02	$9.0 \pm 0.5 \times 10^7$	5.3 ± 0.1	30 ± 1	4.9 ± 0.1	11 ± 1
	3	BBMA + B	24:0	0.65 ± 0.02	$8.6 \pm 0.3 \times 10^7$	4.4 ± 0.1	33 ± 1	4.8 ± 0.1	9.6 ± 1
	3	Z	24:0	0.65 ± 0.02	$4.1 \pm 0.1 \times 10^7$	3.7 ± 0.1	19 ± 1	5.1 ± 0.1	11 ± 1
NaCl	3	BBMA 1 g L^{-1} NaCl	24:0	0.54 ± 0.02	$7.6 \pm 0.1 \times 10^7$	4.4 ± 0.6	32 ± 1	4.7 ± 0.1	9 ± 2
	3	BBMA 5 g L^{-1} NaCl	24:0	0.35 ± 0.02	$5.3 \pm 0.3 \times 10^7$	3.4 ± 0.3	27 ± 1	4.2 ± 0.1	4.6 ± 0.5
	3	BBMA 10 g L^{-1} NaCl	24:0	0.22 ± 0.01	$1.4 \pm 0.1 \times 10^7$	0.9 ± 0.1	25 ± 1	2.9 ± 0.1	0.9 ± 0.3
	3	BBMA 35 g L^{-1} NaCl	24:0	0 ▪	$2.5 \pm 0.1 \times 10^5$	-	-	-	-
CO_2	0.04	BBMA	24:0	0.64 ± 0.02	$2.7 \pm 0.1 \times 10^7$	1.9 ± 0.1	39 ± 1	5.4 ± 0.1	6.4 ± 0.7
	0.4	BBMA	24:0	0.63 ± 0.02	$8.7 \pm 0.1 \times 10^7$	4.1 ± 0.2	34 ± 1	5.1 ± 0.1	11 ± 1
	10	BBMA	24:0	0.50 ± 0.02	$4.1 \pm 0.1 \times 10^7$	4.8 ± 0.4	38 ± 1	5.2± 0.1	16 ± 2
	30	BBMA	24:0	0.24 ± 0.01	$5.3 \pm 0.1 \times 10^7$	3.6 ± 0.1	27 ± 1	5.6 ± 0.1	8.0 ± 0.7
	100	BBMA	24:0	0 ▪	$2.0 \pm 0.1 \times 10^5$	-	-	-	-
Mixotrophy pH 3	3	BBMA + 10 g L^{-1} lactose	24:0	0.41 ± 0.02	- ●	-	-	-	-
	3	BBMA + 10 g L^{-1} galactose	24:0	0.49 ± 0.02	- ●	-	-	-	-
	3	BBMA	24:0	0.37 ± 0.02	- ●	-	-	-	-

♦: Based on elapsed culture time to harvest of batch culture.
■: Growth was not observed or was negligible in this culture, but cell density did not decrease and was able to be maintained after inoculation.
●: Culture was abandoned due to bacterial growth before reaching maximum cell density.

μ_{max}: maximum specific growth rate; $C_{cell,max}$: maximum cell density

9.2 Repeatability and reliability of results

Due to the length of time required for each experiment and the single tubular photobioreactor apparatus used in this study only a few key replicate experiments were able to be conducted. Ideally all experiments would have been repeated to ensure reproducibility of results; however, from the other work conducted with *Trachydiscus* sp. LCR-Awa-9-2 cultures there was reasonable certainty on the reproducibility of results. Studies conducted in shake flasks in § 7.2 showed that, despite cells being previously subjected to different culture conditions, when given identical conditions they still performed similarly. The typical error in specific growth rates calculated from shake flask cultures was approximately ± 3% and cell counts were typically within ± 10% based on counts from duplicate flasks.

In order to confirm the reproducibility of results from the tubular photobioreactor some key experiments were repeated. The experiment which showed the greatest difference from the control was the experiment with the dark volume of the tubular photobioreactor increased by removing light tubes. Due to this the experiment was repeated to confirm that the results were reproducible. The results of the replicate and control cultures are shown in Figure 9.1.

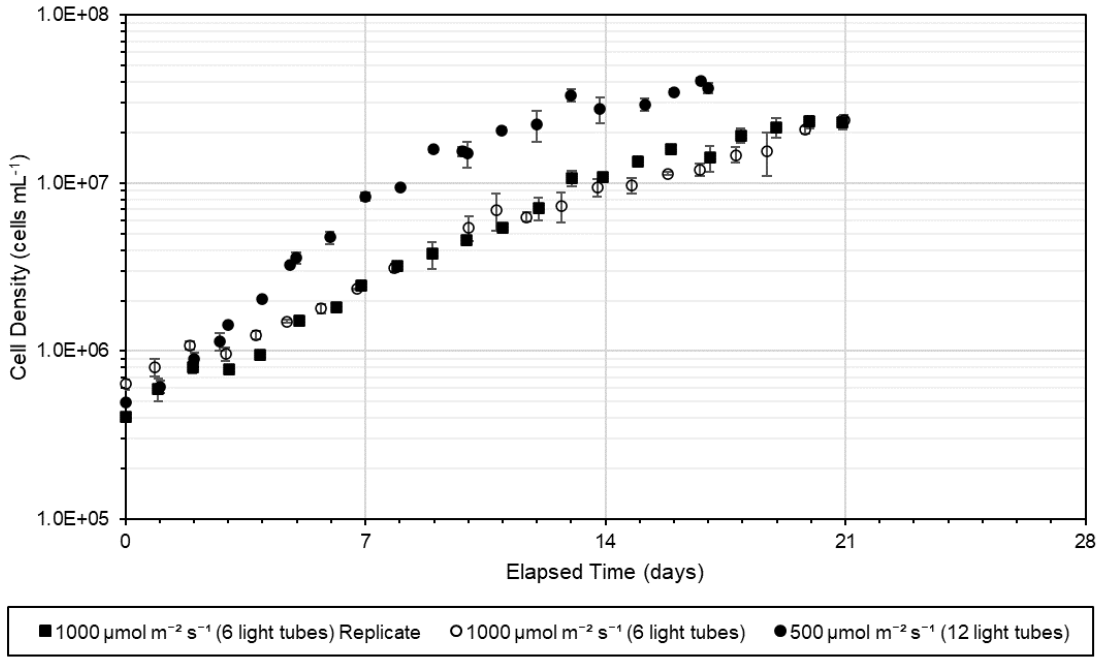

Figure 9.1 – Growth curves of replicate cultures in the tubular photobioreactor. Replicate of experiment in § 6.3.

The replicate cultures showed very similar results for the maximum specific growth rate and cell density. The maximum cell density in both cases was approximately 2.3×10^7 cells mL^{-1} with a typical error in cell counts of ± 10% based on the range of the cell counts in these studies. For the replicate study the maximum specific growth rate was determined to be 0.25 d^{-1} while it was found to be 0.24 d^{-1} in the original study. This gave an error in the specific growth rate of around ± 2%.

Some variability occurred with cell counts due to the sampling methods used and the inherent uncertainty of cell counting techniques. In shake flasks some settling of cells can occur before samples are taken and mixing may not be perfect prior to sampling. When sampling the photobioreactor the sampling port was flushed prior to taking the sample for cell counts; however, some carryover of settled cells in the sampling port may have occurred. Duplicate cell counts were taken on all occasions to mitigate errors in sampling and cell counting.

9.3 Optimal conditions for growth and photosynthesis

9.3.1 Light

The maximum growth rate achieved in the light conditions investigated in this study was in shake flasks at 500 µmol m^{-2} s^{-1} under constant illumination (24:0) This also produced the highest cell density of 1.0×10^8 cells mL^{-1}. Diurnal cycling decreased the maximum growth rate and cell densities achieved, as did lower light intensities. In the tubular photobioreactor, the maximum cell density of 8.1×10^7 cells mL^{-1} was achieved when light saturation was maintained through the culture up a to a maximum of 2872 µmol m^{-2} s^{-1}. Lower light intensities resulted in lower cell densities. However, maximum specific growth rates were higher under constant light intensity cultures with the highest growth rate achieved at 500 µmol m^{-2} s^{-1}. The maximum specific growth rate was higher in shake flasks and could not be replicated in the tubular photobioreactor. This was determined to be due to the light volume ratio in the tubular photobioreactor. The decrease in light volume ratio decreased the maximum specific growth rate and cell density of cultures. For oxygen evolution rate, warm white was the most efficient light colour compared to red, green, and blue based on the quantity of photons per cell required for light saturation. The light saturation value for photosynthesis with warm white light was 1.5×10^{10} photons $cell^{-1}$ s^{-1}. This result was proposed to be due to the broader distribution of light wavelengths produced by the warm white LEDs being able to be used more effectively by the microalga.

9.3.2 Nutrients

Carbon dioxide concentration was seen to influence both the fatty acid composition and growth of *Trachydiscus* sp. LCR-Awa-9-2. Growth was best at a concentration of 3% while EPA productivity was best at 10% CO_2. Low concentrations of CO_2 (such as air, 0.04%) resulted in carbon limitation of the culture as well as high pH, both of which limited the maximum cell density. Higher CO_2 concentrations inhibited growth and cells were unable to grow at 100% CO_2. It was determined that low pH was not a limiting factor for growth at high CO_2 concentrations and rather it was inhibition from CO_2 that limited growth. Cells were shown to acclimatise to higher CO_2 concentrations which was consistent with cells being reported to adapt their cellular structures to adapt to high CO_2 concentrations (Salih, 2011). While 10% CO_2 produced the highest EPA productivity, it was not significantly higher than what was achieved at 3% CO_2. As supplying additional CO_2 comes at a greater cost for microalgal cultures it is likely that 3% CO_2 would be the most economically viable operating point. However, tolerance of high CO_2 concentrations (up to 30%) shows that the use of waste CO_2 from sources such as flue gases may be able to be utilised to grow this microalga which is advantageous for reducing the cost of processes as well as providing carbon sequestration (Saifuddin *et al.*, 2015; Salih, 2011).

An increase in sodium chloride concentration decreased the maximum specific growth rate achieved and maximum cell density. Cells were able to grow at a sodium chloride concentration of 10 g L^{-1} but showed no growth at 35 g L^{-1}. This showed cells were unable to grow in seawater but could grow at moderate salinities. These results confirmed that freshwater media was a requirement for optimal growth of the microalga. One potential application of *Trachydiscus* sp. LCR-Awa-9-2 is as an aquaculture feed or supplement but as it unable to grow in seawater the microalga would need to be produced separately in freshwater in order to be fed to seawater-farmed seafood (Lavens & Sorgeloos, 1996). This would increase the complexity and cost of using *Trachydiscus* sp. LCR-Awa-9-2 as a saltwater aquaculture feed compared to a marine microalga such as *Nannochloropsis* sp. which is also used for this application (Stoyneva-Gärtner *et al.*, 2019). However, for freshwater aquaculture uses *Trachydiscus* sp. LCR-Awa-9-2 could be better suited than marine microalgae strains.

Z medium produced a similar maximum specific growth rate as BBMA medium, but the maximum cell density reached was lower. BBMA medium with Co and B

supplementation had little effect on maximum cell densities and specific growth rates. However, growth was stronger in the later exponential phase with Co supplemented media. Due to results from previous studies showing that Co was not required for growth (Alfiarty, 2018), it is likely that the result observed in this study was due to preferable lighting conditions in the incubator rather than nutrient effects. Measurement of the nitrate consumption rate showed that nitrate was consumed at a higher rate than was previously predicted by Alfiarty (2018) and so cultures were likely to be nitrate limited at lower cell densities than previously thought. However, supplementation of additional nitrate during semi-continuous culturing of the microalga in the tubular photobioreactor did not appear to increase the cell density or growth rate and so light limitation was deemed to be the limiting factor for growth.

Low pH did not significantly hinder the growth of bacterial and fungal contamination in mixotrophic cultures. Due to this, antibiotics and antifungal compounds would likely be necessary for large-scale mixotrophic cultivation of *Trachydiscus* sp. LCR-Awa-9-2. As the highest EPA productivities reported in literature for other microalgae were achieved with heterotrophic or mixotrophic growth (Table 2.5) further investigation is required to determine optimal conditions for EPA productivity for these culture approaches and options for controlling contamination.

9.3.3 Environmental conditions

Trachydiscus sp. LCR-Awa-9-2 cultures were able to grow at liquid velocities of 0.3, 0.6 and 1.2 m s^{-1} in the tubular photobioreactor; however, settling of cells was seen at 0.3 m s^{-1} and resulted in a much lower growth rate. Growth rates at 0.6 and 1.2 m s^{-1} were similar. The results from these experiments showed the cells were tolerant of the shear stresses experienced in tubular photobioreactor cultures which was important for any potential large-scale culturing.

Measurements of oxygen evolution rate showed that cells were tolerant of a wide range of pH values, from pH 3 to 7; however, oxygen evolution rates decreased at pH 2 and pH 8 and above. Measurements of the oxygen evolution rates at different temperatures showed that the maximum oxygen evolution rate was achieved at 20 °C and was similar at 25 °C as well. Oxygen evolution rates decreased below 20 °C and above 25 °C but cells continued to photosynthesise down to 5 °C and up to 40 °C. These results showed that the microalga was tolerant of a broad range of temperatures and pH values.

As these parameters are often not able to be finely controlled in large-scale cultures, tolerance of a wide range of conditions is a beneficial trait for microalgae to possess.

Trachydiscus sp. LCR-Awa-9-2 was able to semi-continuously cultured in the tubular photobioreactor in this study and did not form appreciable biofilms over the course of 35 days. The ability to be continuously cultured and lack of biofilm formation means that this microalga is well suited to commercial scale cultivation where continuous culturing is often used.

Overall, results from the environmental conditions tested indicate that *Trachydiscus* sp. LCR-Awa-9-2 was well suited to commercial cultivation. The results from this and other studies also provide data which can allow prediction of culture behaviour under the typical conditions that may be expected during large-scale cultivation.

9.4 Optimal conditions for EPA fraction and content

The highest EPA fraction achieved in this study was 46 ± 1 g/100 g fatty acids and the highest content was 6.1 ± 0.1 g/100 g dry biomass. These results were achieved growing in the tubular photobioreactor in BBMA medium harvested at a cell density of 2.6×10^7 cells mL^{-1}. The light intensity was 1500 µmol m^{-2} s^{-1} with warm white light. CO_2 was supplied at 3 vol% and the temperature of the culture was 25.0 ± 0.1 °C. At the time the biomass was harvested the culture was in the late exponential phase and still growing strongly at a growth rate of approximately 0.20 ± 0.02 d^{-1}.

The EPA fraction achieved under these conditions was higher than the maximums that had been achieved in previous studies of 38.3 g/100 g fatty acids (Tangestani, 2019) and 41.3 g/100 g fatty acids (Alfiarty, 2018). However, the EPA content of 8.7 g/100 g dry biomass achieved by Tangestani (2019) was not able to be achieved in this study. While a high EPA fraction is desirable as it indicates lower levels of other undesired fatty acids, the EPA content is normally the more important factor for EPA productivity alongside biomass productivity. High EPA fractions can be of use when high purity EPA is of interest and the overall quantity produced is less important. Higher EPA fractions can be advantageous for further purification processes and reduce the cost and quantity of by-products (Cohen, 1999). EPA fractions of other eustigmatophytes such as *Nannochloropsis* sp. have been reported up to 44 g/100 g total fatty acids and 49.3 g/100 g total fatty acids for *Monodus subterraneus* (Stoyneva-Gärtner *et al.*, 2019) and so the results

from this study for *Trachydiscus* sp. LCR-Awa-9-2 were consistent with other species in its class.

9.5 Optimal conditions for EPA productivity

The maximum sustainable EPA productivity that was able to be achieved in this study was 30 ± 2 mg L^{-1} d^{-1}. This was nearly two times higher than the highest productivity previously achieved of 15.6 mg L^{-1} d^{-1} in batch cultures (Tangestani, 2019). The higher productivity in this study was achieved primarily due to the use of semi-continuous culturing as previous work had focussed on batch cultures. The optimal conditions for EPA productivity in this study were achieved in the tubular photobioreactor using BBMA medium. The temperature was 25 °C and supplemental CO_2 was supplied at 3 vol%. Semi-continuous culturing was operated at a cell density of approximately 4.5×10^7 cells mL^{-1} and harvesting 15 L d^{-1}, or a dilution rate of 0.19 d^{-1}. In this study an initial dilution rate of 0.26 d^{-1} was used which gave an EPA productivity of 42 ± 2 mg L^{-1} d^{-1} but the culture began to wash out at this rate of harvesting and so this was not sustainable. A decreased dilution rate of 0.19 d^{-1} was able to be maintained at this cell density resulting in the above maximum maintainable EPA productivity.

In batch cultures the highest EPA productivity achieved was 16 ± 2 mg L^{-1} d^{-1} in shake flasks. This productivity was achieved with 10 vol% CO_2 in BBMA medium at a light intensity of 500 µmol m^{-2} s^{-1}. However, this result was not significantly higher than the next highest productivity achieved with 3 vol% CO_2 of 14 ± 1 mg L^{-1} d^{-1}. Both of these results were similar to the maximum productivities achieved by Tangestani (2019).

Compared to the EPA productivities of other microalgae that were reported in Table 2.5 the results from this study fell in the mid to high range of what has been achieved with other strains in photoautotrophic cultures. Results for *Trachydiscus minutus* showed an EPA productivity of up to 88 mg L^{-1} d^{-1} was possible (Rezanka *et al.*, 2010), but this was not achieved in a scalable culture system and so it is not expected that this could be replicated on a commercial scale. Lukavský (2012) showed that the EPA productivity was 20–30 mg L^{-1} d^{-1} for *Trachydiscus minutus* in pilot scale ponds which further indicated that the previous higher productivity reported may not be achievable in commercial scale reactors. However, these results still indicate that there could be potential for future improvement of the EPA productivity of *Trachydiscus* sp. LCR-Awa-9-2, particularly if the EPA content and growth rate could be increased during semi-continuous culturing.

EPA productivities of other microalgae such as *Monodus subterraneus* and *Phaeodactylum tricornutum* in photoautotrophic cultures at similar or larger scales to this study have been reported in the region of 50 to 60 mg L^{-1} d^{-1} (Table 2.5). However, it is feasible that through a combination of optimal culture conditions or two-stage culturing investigated in this and other studies (Alfiarty, 2018; Tangestani, 2019) that EPA productivities in this region may be possible with *Trachydiscus* sp. LCR-Awa-9-2. The EPA productivity reported for heterotrophic cultures of *Nitzschia laevis* was 175 mg L^{-1} d^{-1} (Rezanka *et al*., 2010) which shows the potential for far higher EPA productivities using heterotrophic culture strategies compared to photoautotrophic cultures. It is unlikely that the EPA productivities achieved by heterotrophic cultures would be achievable in photoautotrophic cultures, largely due to the limited biomass concentration achievable due to light limitations.

9.6 Potential limitations to further optimisation

9.6.1 Maximum achievable EPA content

One of the major limitations that was identified for the continued improvement of EPA productivity from *Trachydiscus* sp. LCR-Awa-9-2 was the physical limit of the quantity of EPA a single cell can contain. Mass spectrometry results from the degraded lipids from *Trachydiscus* sp. LCR-Awa-9-2 showed a large proportion of 20:5/20:5 species and so the majority of the lipids were likely to be EPA-saturated. Due to this, even if the EPA fraction could theoretically be increased to 100% in the EPA-containing lipids (i.e. converting species such as DG 20:5/16:1 to DG 20:5/20:5), the EPA productivity would not be expected to significantly increase. Additionally, cells require a mix of different proportions of fatty acids to maintain functionality and fluidity of their membranes (Gurr & Harwood, 1991) and so artificial alteration of the EPA content of membranes could hinder the ability of cells to function correctly. Further lipidomic studies are required to determine the potential limitations to improvements that could be made.

The other approach to increasing EPA content is increasing the total quantity of EPA containing lipids. EPA is primarily associated with thylakoid membranes in the chloroplast. Therefore, if the size of the chloroplast could be increased, and thus the quantity of lipids required for membranes, there would be potential to increase the EPA content of the cells. Electron microscopy that has been conducted of the cells showed that the thylakoid membranes were tightly packed (Tangestani, 2019) which indicated there may not be much scope for increasing the quantity of membranes further.

Trachydiscus sp. LCR-Awa-9-2 was shown to produce lipid storage bodies (Tangestani, 2019); however, these typically consist mainly of triacylglycerides (Cagliari *et al.*, 2011) which do not normally contain a high proportion of EPA in microalgae (Cohen, 1999). Based on the fatty acid results from TLC separations during the lipidomic investigations up to 20 g/100 g total EPA was located in the neutral lipids containing the triacylglycerides. As triacylglycerides can be readily accumulated in microalgae, they would be a useful mechanism to utilise for accumulation of EPA in the cells. The majority of EPA appeared to occur in MGDG lipids rather than triacylglycerides in wild-type cells and so genetic modification would likely need to be employed to promote the production of triacylglycerides containing high levels of EPA. This approach raises numerous issues, namely in the difficulty of modifying the relevant genes as well as producing cells which may be less tolerant of adverse culture conditions or may not be as productive. Genetic modification still has a negative connotation in the general public, and as one of the major applications of EPA from microalgae is the human health market this aspect could also be a barrier to this approach (Cardozo *et al.*, 2007).

The maximum EPA contents achieved in this study did not exceed those which had been previously achieved for this microalga, and it was expected that EPA contents significantly exceeding those which have already been achieved is unlikely. EPA contents for related strains of microalgae such as *Nannochloropsis gaditana* were also in the region of what have been achieved for this microalga (Camacho-Rodríguez *et al.*, 2014); however, results from *Trachydiscus minutus* of EPA contents up to 36 g/100 g dry biomass have been reported (Stoyneva-Gärtner *et al.*, 2019) indicating that further improvement may be possible.

9.6.2 Light limitations on photoautotrophic growth and economics of artificial lighting

The maximum cell density achievable was limited primarily by light. However, further increases to light intensity were unlikely to have a worthwhile impact on increasing EPA productivity by increased biomass production. One major limitation encountered in this study was the ability to remove excess heat from the reactor and so temperature control at high light intensities limited the light intensity that could be used. While a more powerful cooling system may be able to overcome this limitation, the operating cost of cultures would increase as the energy required to maintain the culture temperature increases. Even if sufficient cooling could be achieved and the cost of energy

was negligible, there were diminishing returns in the increase in cell density at higher light intensities (> 2000 µmol m^{-2} s^{-1}) and increasing the light intensity did not proportionally increase the cell density at this level (see Figure 6.5). Therefore, further increases in light intensity above those used in this study were unlikely to cause an appreciable increase in biomass concentration and thus EPA productivity.

On top of the cost of energy required for cooling the reactor, increasing the light intensity also requires greater energy input for production of artificial lighting. The maximum light intensity was also limited by the maximum output of the lighting apparatus. To increase light intensity further would require addition of a greater quantity of, or brighter, light sources. Once again, increasing the cost of the system. The combination of these factors showed that during photoautotrophic growth there are limited further gains to be achieved due to light limitations.

At the highest light intensities used in this study the power requirement was approximately 3 kW with an additional 0.5 kW required for the pump to recirculate the culture. The heat from the lights and pumping also needed to be removed from the system at an additional power requirement of around 1 kW, giving a total power requirement of around 4.5 kW. During an optimistic batch culture length of around 14 days this equates to an energy consumption of around 1500 kWh. A batch culture from this photobioreactor setup could produce around 19 g of EPA, resulting in an energy consumption of approximately 80 kWh g^{-1} for EPA. At a typical industrial electricity unit cost in New Zealand in 2019 of around \$0.15 kWh^{-1} (Ministry of Business Innovation and Employment, 2020) the energy cost alone per gram of EPA produced was found to be around \$12 (2019, NZD). For a continuous culture producing around 30 mg L^{-1} d^{-1} (2.28 g d^{-1}) the energy requirement was calculated to be around 47 kWh g^{-1} of EPA[ii] at a cost of approximately \$7 g^{-1} EPA (2019, NZD). As typical daily fish oil supplements retailed at the time of this study at prices of around \$0.07 per 1500 mg capsule containing around 270 mg of EPA (rough price of \$0.38 g^{-1} EPA, not accounting for other ingredients such as DHA) (Pharmacy Direct, 2020), it is clear that artificially illuminated cultures were unlikely to be economically viable to produce EPA for this market at current prices. Due

[ii] Calculation does not include the energy requirement during the batch stage of the culture required to reach the cell density required for continuous culturing.

to this, using sunlight was likely to be a necessity for a commercially viable process as well as increasing the scale of the photobioreactors used. Removing the lighting energy requirement could potentially reduce the energy cost per gram of EPA by 66%, provided that similar EPA productivities could be achieved.

9.7 Overall outcomes and contributions from this research

Prior to this work *Trachydiscus* sp. LCR-Awa-9-2 had not been grown on a scale larger than approximately one litre. This work showed that this microalga could be grown in a tubular photobioreactor at semi-pilot scale at a culture volume of 76 L. A tubular photobioreactor was built that was suitable to grow this microalga and the volumetric EPA productivity was able to be increased from the previously reported maximum of 15.6 mg L^{-1} d^{-1} to a maximum sustainable productivity of 30 ± 2 mg L^{-1} d^{-1}, a nearly 2-fold increase. Although the maximum cell densities achieved in shake flasks were not able to be achieved in the tubular photobioreactor, light was identified as the key limiting factor in reaching this goal. The dark volumes present in the tubular photobioreactor's bubble column and pump were one of the main limitations to achieving the maximum growth rate and cell density achieved in shake flasks.

Investigation of the lipidome of *Trachydiscus* sp. LCR-Awa-9-2 showed that the major EPA containing class was MGDG as it is in most other microalgae. Extraction of lipids directly from fresh biomass was required to prevent degradation of lipid extracts and further research is required to determine the implication of this on extraction of EPA. TLC separations of lipids from *Trachydiscus* sp. LCR-Awa-9-2 indicated the presence of an unconfirmed minor glycolipid class which was possibly monoglucosyl diacylglyceride (GlcDG). GlcDG is not normally produced by eukaryotic algae and so confirmation of the presence of this lipid class may indicate a gene transfer event from cyanobacteria.

Overall, the results from this study in conjunction with the work from Alfiarty (2018) and Tangestani (2019) showed that *Trachydiscus* sp. LCR-Awa-9-2 was a promising strain for large-scale production of EPA. The microalga's tolerance of conditions such as pH and light intensities that are likely to be encountered in large-scale photobioreactors showed that the microalga was well suited to large-scale culturing. However, the results from this study indicated that producing EPA by photoautotrophic culturing at the scale used in this study was unlikely to be commercially viable without further improvement. Many approaches can be used to improve the economics of microalgal cultures such as

economies of scale, production of other products of value from the biomass, heterotrophic or mixotrophic culturing, and reduction of energy requirements such as through the use of natural light. Further work into these areas may improve the economics of EPA production from this microalga and provide another source of EPA to meet the ever-increasing world demand for this product.

10 Future work

As discussed throughout this work, future research on this microalga could focus on many areas not yet explored by this or previous studies. In terms of continuing investigation into the commercial feasibility of EPA production from *Trachydiscus* sp. LCR-Awa-9-2, it is suggested that future work focusses on other commercially interesting metabolites from the microalga, as well as minimising the cost of biomass production and further investigation into increasing the EPA productivity.

As is the case with any product, any and all side products should be utilised when possible. In the case of microalgae many other products are produced by cells beyond EPA. Cells also produce protein, pigments, and other bioactive compounds, all of which can be high value products in their own right. As this and other studies have focussed primarily on EPA it is suggested that further work be conducted into these by-products and their potential as alternative revenue streams. During the lipidomic study conducted in this work it was discovered that the cells contained a wide variety of pigments such as carotenoids and chlorophyll *a* which can be used in applications such as health supplements and cosmetics (Stoyneva-Gärtner *et al.*, 2019). Further investigation into the contents of these pigments is suggested to determine their potential value. Producing a variety of products from *Trachydiscus* sp. LCR-Awa-9-2 could greatly improve the economics of any potential commercial culturing, especially if they are already extracted in the process used to extract the EPA.

To improve the EPA content further lipidomic studies could be conducted into the nature of the lipid species in the cells and their associated metabolism. As lipid extracts were able to be obtained without degradation full lipidomic analysis should be conducted on these extracts to elucidate the true lipidome of the microalga. Further work should also be conducted to determine the root cause of the degradation of the lipids and suitable extraction techniques for further studies and production of EPA. Genomic investigation of the cells could provide insight into the mechanisms of lipid production of the cells and identify bottlenecks to improving the EPA content. In other studies the EPA content was able to reach up to 8.7 g/100 g dry biomass for *Trachydiscus* sp. LCR-Awa-9-2 and so if this could be replicated in the tubular photobioreactor during semi-continuous culturing there is potential that the EPA productivity could be increased to around 60 mg L^{-1} d^{-1}. The

lipidomic and genomic studies suggested may be able to determine whether these conditions are possible to combine in order to maximise the EPA productivity.

Outdoor culturing is one of the common approaches to lower the cost of microalgal culturing. Both the operating and capital cost of microalgal bioprocesses can be reduced by outdoor culturing and the feasibility of growing *Trachydiscus* sp. LCR-Awa-9-2 outdoors would need to be investigated. Results from this study showed that the microalga could grow at high light intensities and under diurnal cycles and so there is promise that cultures would perform satisfactorily outdoors. Scale up of microalgae bioprocesses beyond the scale used in this study is a key requirement for commercial production (Borowitzka & Vonshak, 2017). In this study the cells were shown to be able to grow in a 76 L tubular photobioreactor which was more than 100 times the volume used in previous studies. This style of photobioreactor is able to be scaled up to volumes 10 to 20 times larger than what was used in this study and so further work should be conducted into the behaviour of the cultures at larger scale. Of key interest to study on larger scale is the effects of longer solar receiver residence times and the effects of dissolved oxygen accumulation and potential carbon starvation. It is suggested that an increase to a pilot scale reactor of around 300–500 L in volume would be suitable to study these effects before any further scale up.

The maximum cell density that can be achieved in microalgal cultures is one their main limitations compared to other microorganisms. In this study, light was the major limiting factor for photoautotrophic growth; however, further increases in light intensity is unlikely to improve the cell density achieved beyond what was achieved in this study. Changes to the light distribution in the tubular photobioreactor to improve the light volume ratio shows promise to improve the growth rate and cell density. One approach to overcome light limitation is to grow cells heterotrophically or mixotrophically. However, addition of organic carbon sources to the medium greatly increases the consequences of contamination from bacteria or fungi. In previous studies antifungals and antibiotics were used to control contamination; however, when using microalgae for human health applications or animal feeds the presence of antibiotics can be problematic either due to public perception or by difficulty of removal from the resulting biomass. There is also great concern around development of antibiotic resistant bacteria which can occur with continued use of antibiotics in non-essential settings (Davies & Davies, 2010). As *Trachydiscus* sp. LCR-Awa-9-2 was tolerant of low pH, culturing the microalga at low

pH was one approach that was tried to mitigate contamination. Unfortunately, this approach did not control bacterial growth in cultures. In order to further pursue growth of this microalga on organic carbon sources the control of contamination should be further investigated by producing purely axenic cultures and investigation of other factors which could inhibit the growth of contaminants such as high CO_2 concentrations or salinities.

The tubular photobioreactor constructed in this study could also be used to investigate the growth of other species of microalgae. As this style of photobioreactor is the most applicable for scale up of microalgae cultures it could be used to screen potential strains for suitability for large-scale culturing. Investigating the behaviour of other strains under conditions tested in this study such as the light to dark volume ratio could also provide insight into development of models for the behaviour of microalgal cultures in this style of photobioreactor.

References

Abiusi, F., Sampietro, G., Marturano, G., Biondi, N., Rodolfi, L., D'Ottavio, M., & Tredici, M. R. (2014). Growth, photosynthetic efficiency, and biochemical composition of Tetraselmis suecica F&M-M33 grown with LEDs of different colors. *Biotechnology and Bioengineering, 111*(5), 956-964.

Abu-Ghosh, S., Dubinsky, Z., Banet, G., & Iluz, D. (2018). Optimizing photon dose and frequency to enhance lipid productivity of thermophilic algae for biofuel production. *Bioresource Technology, 260*, 374-379.

Acién Fernández, F. G., Camacho, F. G., Pérez, J. A. S., Sevilla, J. M. F., & Grima, E. M. (1997). A model for light distribution and average solar irradiance inside outdoor tubular photobioreactors for the microalgal mass culture. *Biotechnology and Bioengineering, 55*(5), 701-714.

Acién Fernández, F. G., Fernández Sevilla, J. M., & Molina Grima, E. (2013). Photobioreactors for the production of microalgae. *Reviews in Environmental Science and Bio/Technology, 12*(2), 131-151.

Acién Fernández, F. G., Fernández Sevilla, J. M., & Sánchez Pérez, J. A. (2010). Photosynthetic microorganisms and valuable products. In J. B. Gálvez, S. M. Rodríguez, E. Delyannis, V. G. Belessiotis, S. C. Bhattacharya, & S. Kumar (Eds.), *Solar Energy Conversion and Photoenergy Systems: Thermal Systems and Desalination Plants* (Vol. 1). Paris, France: EOLSS Publications.

Acién Fernández, F. G., Fernández Sevilla, J. M., Sánchez Pérez, J. A., Molina Grima, E., & Chisti, Y. (2001). Airlift-driven external-loop tubular photobioreactors for outdoor production of microalgae: assessment of design and performance. *Chemical Engineering Science, 56*(8), 2721-2732.

Acién Fernández, F. G., Pérez, J. A. S., Sevilla, J. M. F., Camacho, F. G., & Grima, E. M. (2000). Modeling of eicosapentaenoic acid (EPA) production from Phaeodactylum tricornutum cultures in tubular photobioreactors. Effects of dilution rate, tube diameter, and solar irradiance. *Biotechnology and Bioengineering, 68*(2), 173-183.

Adarme-Vega, T. C., Lim, D. K. Y., Timmins, M., Vernen, F., Li, Y., & Schenk, P. M. (2012). Microalgal biofactories: a promising approach towards sustainable omega-3 fatty acid production. *Microbial Cell Factories, 11*(1), 96.

Akimoto, M., Shirai, A., Ohtaguchi, K., & Koide, K. (1998). Carbon dioxide fixation and polyunsaturated fatty acid production by the red alga porphyridium cruentum. *Applied Biochemistry and Biotechnology, 73*(2), 269-278.

Alexandrov, S. D., Iliev, I. I., & Petkov, G. D. (2014). Establishment of growth conditions for cultivation of the microalga *Trachydiscus minutus* at laboratory scale. *Pure and Applied Biology*(3(1)), 1-9.

Alfiarty, A. (2018). *Optimization of Culture Medium Performance for Growth of Microalga Trachydiscus sp. LCR-Awa9/2.* (Masters of Engineering Thesis), University of Canterbury.

Algatechnologies Ltd. (2017). Algatech. Retrieved from https://www.algatech.com/. Retrieved 15th December 2017.

Andersen, R. A. (2005). *Algal Culturing Techniques*. USA: Elsevier Academic Press.

Andersen, R. A., Brett, R. W., Potter, D., & Sexton, J. P. (1998). Phylogeny of the Eustigmatophyceae based upon 18S rDNA, with emphasis on Nannochloropsis. *Protist, 149*(1), 61-74.

Apel, A. C., Pfaffinger, C. E., Basedahl, N., Mittwollen, N., Göbel, J., Sauter, J., . . . Weuster-Botz, D. (2017). Open thin-layer cascade reactors for saline microalgae production

evaluated in a physically simulated Mediterranean summer climate. *Algal Research, 25*, 381-390.
Atkinson, B., & Mavituna, F. (1991). *Biochemical Engineering and Biotechnology Handbook* (2nd ed.): Stockton Press.
Awai, K., Ohta, H., & Sato, N. (2014). Oxygenic photosynthesis without galactolipids. *Proceedings of the National Academy of Sciences of the United States of America, 111*(37), 13571-13575.
Basso, S., Simionato, D., Gerotto, C., Segalla, A., Giacometti, G. M., & Morosinotto, T. (2014). Characterization of the photosynthetic apparatus of the Eustigmatophycean Nannochloropsis gaditana: Evidence of convergent evolution in the supramolecular organization of photosystem I. *Biochimica et Biophysica Acta (BBA) - Bioenergetics, 1837*(2), 306-314.
Batchelor, G. K. (1947). Kolmogoroff's theory of locally isotropic turbulence. *Mathematical Proceedings of the Cambridge Philosophical Society, 43*(4), 533-559.
Béchet, Q., Shilton, A., & Guieysse, B. (2013). Modeling the effects of light and temperature on algae growth: State of the art and critical assessment for productivity prediction during outdoor cultivation. *Biotechnology Advances, 31*(8), 1648-1663.
Becker, E. W. (1994). *Microalgae: Biotechnology and Microbiology*. Cambridge, Great Britain: Cambridge University Press.
Behkish, A., Men, Z., Inga, J. R., & Morsi, B. I. (2002). Mass transfer characteristics in a large-scale slurry bubble column reactor with organic liquid mixtures. *Chemical Engineering Science, 57*(16), 3307-3324.
Bekirogullari, M., Fragkopoulos, I. S., Pittman, J. K., & Theodoropoulos, C. (2017). Production of lipid-based fuels and chemicals from microalgae: An integrated experimental and model-based optimization study. *Algal Research, 23*(Supplement C), 78-87.
Bellou, S., Baeshen, M. N., Elazzazy, A. M., Aggeli, D., Sayegh, F., & Aggelis, G. (2014). Microalgal lipids biochemistry and biotechnological perspectives. *Biotechnology Advances, 32*(8), 1476-1493.
Bernard, O., & Rémond, B. (2012). Validation of a simple model accounting for light and temperature effect on microalgal growth. *Bioresource Technology, 123*(Supplement C), 520-527.
Berney, M., Weilenmann, H.-U., Ihssen, J., Bassin, C., & Egli, T. (2006). Specific Growth Rate Determines the Sensitivity of *Escherichia coli* to Thermal, UVA, and Solar Disinfection. *Applied and Environmental Microbiology, 72*(4), 2586.
Birmingham, B. C., Coleman, J. R., & Colman, B. (1982). Measurement of Photorespiration in Algae. *Plant Physiology, 69*(1), 259-262.
Bligh, E. G., & Dyer, W. J. (1959). A rapid method of total lipid extraction and purification. *Canadian Journal of Biochemistry and Physiology, 37*(8), 911-917.
Borowitzka, M. A. (2013). High-value products from microalgae—their development and commercialisation. *Journal of Applied Phycology, 25*(3), 743-756.
Borowitzka, M. A., & Vonshak, A. (2017). Scaling up microalgal cultures to commercial scale. *European Journal of Phycology, 52*(4), 407-418.
Bosma, R., de Vree, J. H., Slegers, P. M., Janssen, M., Wijffels, R. H., & Barbosa, M. J. (2014). Design and construction of the microalgal pilot facility AlgaePARC. *Algal Research, 6*, 160-169.
Botsford, L. W., Castilla, J. C., & Peterson, C. H. (1997). The Management of Fisheries and Marine Ecosystems. *Science, 277*(5325), 509-515.
Brindley Alías, C., García-Malea López, M. C., Acién Fernández, F. G., Fernandez Sevilla, J. M., García Sánchez, J. L., & Molina Grima, E. (2004). Influence of power supply

in the feasibility of Phaeodactylum tricornutum cultures. *Biotechnology and Bioengineering, 87*(6), 723-733.

Brindley, C., Acién Fernández, F. G., & Fernández-Sevilla, J. M. (2011). Analysis of light regime in continuous light distributions in photobioreactors. *Bioresource Technology, 102*(3), 3138-3148.

Brindley, C., Acién, F. G., & Fernández-Sevilla, J. M. (2010). The oxygen evolution methodology affects photosynthetic rate measurements of microalgae in well-defined light regimes. *Biotechnology and Bioengineering, 106*(2), 228-237.

British Standards Institution. (2011) *Fat and oil derivatives - Fatty Acid Methyl Esters (FAME) - Determination of ester and linolenic acid methyl ester contents (BS EN 14103:2011)*

Buono, S., Langellotti, A. L., Martello, A., Rinna, F., & Fogliano, V. (2014). Functional ingredients from microalgae. *Food & Function, 5*(8), 1669-1685.

Burlew, J. S. (1953). *Algal Culture: from Laboratory to Pilot Plant*. Washington D.C., USA: Carnegie Institution of Washington.

Burrows, A., Holman, J., Parsons, A., Pilling, G., & Price, G. (2009). *Chemistry³: Introducing Inorganic, Organic and Physical Chemistry* (1st ed.). Oxford, UK: OUP.

Bwapwa, J. K., Jaiyeola, A. T., & Chetty, R. (2017). Bioremediation of acid mine drainage using algae strains: A review. *South African Journal of Chemical Engineering, 24*, 62-70.

Cagliari, A., Margis, R., Dos, F., Maraschin, F., Andreia, Turchetto-Zolet, A. C., . . . Margis-Pinheiro, M. (2011). Biosynthesis of Triacylglycerols (TAGs) in plants and alga. *International Journal of Plant Biology, 2*(1), 40-52.

Cai, T., Park, S. Y., & Li, Y. (2013). Nutrient recovery from wastewater streams by microalgae: Status and prospects. *Renewable and Sustainable Energy Reviews, 19*, 360-369.

Cajka, T., & Fiehn, O. (2014). Comprehensive analysis of lipids in biological systems by liquid chromatography-mass spectrometry. *TrAC Trends in Analytical Chemistry, 61*(Supplement C), 192-206.

Camacho-Rodríguez, J., Cerón-García, M. C., Fernández-Sevilla, J. M., & Molina-Grima, E. (2015). The influence of culture conditions on biomass and high value product generation by Nannochloropsis gaditana in aquaculture. *Algal Research, 11*(Supplement C), 63-73.

Camacho-Rodríguez, J., González-Céspedes, A. M., Cerón-García, M. C., Fernández-Sevilla, J. M., Acién-Fernández, F. G., & Molina-Grima, E. (2014). A quantitative study of eicosapentaenoic acid (EPA) production by Nannochloropsis gaditana for aquaculture as a function of dilution rate, temperature and average irradiance. *Applied Microbiology and Biotechnology, 98*(6), 2429-2440.

Camacho, F. G., Grima, E. M., Mirón, A. S., Pascual, V. G., & Chisti, Y. (2001). Carboxymethyl cellulose protects algal cells against hydrodynamic stress. *Enzyme and Microbial Technology, 29*(10), 602-610.

Cañavate, J. P., Armada, I., Ríos, J. L., & Hachero-Cruzado, I. (2016). Exploring occurrence and molecular diversity of betaine lipids across taxonomy of marine microalgae. *Phytochemistry, 124*, 68-78.

Cao, Y., Cao, Y., & Zhao, M. (2012). Biotechnological production of eicosapentaenoic acid: From a metabolic engineering point of view. *Process Biochemistry, 47*(9), 1320-1326.

Cardozo, K. H. M., Guaratini, T., Barros, M. P., Falcão, V. R., Tonon, A. P., Lopes, N. P., . . . Pinto, E. (2007). Metabolites from algae with economical impact. *Comparative Biochemistry and Physiology Part C: Toxicology & Pharmacology, 146*(1), 60-78.

Carreau, J. P., & Dubacq, J. P. (1978). Adaptation of a macro-scale method to the micro-scale for fatty acid methyl transesterification of biological lipid extracts. *Journal of Chromatography A, 151*(3), 384-390.

Carvalho, A. P., Silva, S. O., Baptista, J. M., & Malcata, F. X. (2011). Light requirements in microalgal photobioreactors: an overview of biophotonic aspects. *Applied Microbiology and Biotechnology, 89*(5), 1275-1288.

Cavonius, L. R., Carlsson, N.-G., & Undeland, I. (2014). Quantification of total fatty acids in microalgae: comparison of extraction and transesterification methods. *Analytical and Bioanalytical Chemistry, 406*(28), 7313-7322.

Cepák, V., Přibyl, P., Kohoutková, J., & Kaštánek, P. (2014). Optimization of cultivation conditions for fatty acid composition and EPA production in the eustigmatophycean microalga Trachydiscus minutus. *Journal of Applied Phycology, 26*(1), 181-190.

Cerón García, M. C., Fernández Sevilla, J. M., Acién Fernández, F. G., Molina Grima, E., & García Camacho, F. (2000). Mixotrophic growth of Phaeodactylum tricornutum on glycerol: growth rate and fatty acid profile. *Journal of Applied Phycology, 12*(3), 239-248.

Chen, C.-Y., Chen, Y.-C., Huang, H.-C., Ho, S.-H., & Chang, J.-S. (2015). Enhancing the production of eicosapentaenoic acid (EPA) from Nannochloropsis oceanica CY2 using innovative photobioreactors with optimal light source arrangements. *Bioresource Technology, 191*(Supplement C), 407-413.

Chen, C.-Y., Chen, Y.-C., Huang, H.-C., Huang, C.-C., Lee, W.-L., & Chang, J.-S. (2013). Engineering strategies for enhancing the production of eicosapentaenoic acid (EPA) from an isolated microalga Nannochloropsis oceanica CY2. *Bioresource Technology, 147*(Supplement C), 160-167.

Chen, G.-Q., & Chen, F. (2006). Growing Phototrophic Cells without Light. *Biotechnology Letters, 28*(9), 607-616.

Chen, M., & Blankenship, R. E. (2011). Expanding the solar spectrum used by photosynthesis. *Trends in Plant Science, 16*(8), 427-431.

Cheng, W., Huang, J., & Chen, J. (2016). Computational fluid dynamics simulation of mixing characteristics and light regime in tubular photobioreactors with novel static mixers. *Journal of Chemical Technology and Biotechnology, 91*(2), 327-335.

Chini Zittelli, G., Lavista, F., Bastianini, A., Rodolfi, L., Vincenzini, M., & Tredici, M. R. (1999). Production of eicosapentaenoic acid by Nannochloropsis sp. cultures in outdoor tubular photobioreactors. *Journal of Biotechnology, 70*(1), 299-312.

Chisti, Y. (1998). Pneumatically Agitated Bioreactors in Industrial and Environmental Bioprocessing: Hydrodynamics, Hydraulics, and Transport Phenomena. *Applied Mechanics Reviews, 51*(1), 33-112.

Chisti, Y. (2006). Microalgae as Sustainable Cell Factories. *Environmental Engineering and Management Journal, 5*(3), 261-274.

Chisti, Y. (2007). Biodiesel from microalgae. *Biotechnology Advances, 25*(3), 294-306.

Chisti, Y. (2008). Biodiesel from microalgae beats bioethanol. *Trends in Biotechnology, 26*(3), 126-131.

Chisti, Y. (2016). Large-Scale Production of Algal Biomass: Raceway Ponds. In F. Bux & Y. Chisti (Eds.), *Algae Biotechnology: Products and Processes* (pp. 21-40). Switzerland: Springer International Publishing.

Chrismadha, T., & Borowitzka, M. A. (1994). Effect of cell density and irradiance on growth, proximate composition and eicosapentaenoic acid production of Phaeodactylum tricornutum grown in a tubular photobioreactor. *Journal of Applied Phycology, 6*(1), 67-74.

Christie, W. W. (1989). *Gas Chromatography and Lipids: a Practical Guide*. Ayr, Scotland: The Oily Press.

Christie, W. W. (1993). *Preparation of Lipid Extracts from Tissues* (Vol. 2). Dundee, Scotland: The Oily Press.

Christie, W. W. (2019). Thin-layer Chromatography of Lipids. Retrieved from https://lipidlibrary.aocs.org/lipid-analysis/selected-topics-in-the-analysis-of-lipids/thin-layer-chromatography-of-lipids. Retrieved October 2019.

Clementson, L. A., & Wojtasiewicz, B. (2019). Dataset on the absorption characteristics of extracted phytoplankton pigments. *Data in Brief, 24*, 103875.

Cohen, Z. (1994). Production potential of eicosapentaenoic acid by Monodus subterraneus. *Journal of the American Oil Chemists' Society, 71*(9), 941-945.

Cohen, Z. (Ed.) (1999). *Chemicals from Microalgae*. London: Taylor & Francis Ltd.

Concas, A., Lutzu, G. A., Locci, A., & Cao, G. (2013). Nannochloris eucaryotum growth: Kinetic analysis and use of 100% CO2. *Advances in environmental research, 2*(1), 19-33.

Converti, A., Casazza, A. A., Ortiz, E. Y., Perego, P., & Del Borghi, M. (2009). Effect of temperature and nitrogen concentration on the growth and lipid content of Nannochloropsis oculata and Chlorella vulgaris for biodiesel production. *Chemical Engineering and Processing: Process Intensification, 48*(6), 1146-1151.

Cooney, M., Young, G., & Nagle, N. (2009). Extraction of Bio-oils from Microalgae. *Separation & Purification Reviews, 38*, 291-325.

Cooper, V. C. (1996). *Microalgae: Microscopic Marvels*. Hamilton, N.Z: Riverside Books.

Cornish-Bowden, A. (2014). *Fundamentals of Enzyme Kinetics*. USA: Wiley.

Costache, T. A., Acién Fernández, F. G., Morales, M. M., Fernández-Sevilla, J. M., Stamatin, I., & Molina, E. (2013). Comprehensive model of microalgae photosynthesis rate as a function of culture conditions in photobioreactors. *Applied Microbiology and Biotechnology, 97*(17), 7627-7637.

da Costa, E., Silva, J., Mendonca, S. H., Abreu, M. H., & Domingues, M. R. (2016). Lipidomic Approaches towards Deciphering Glycolipids from Microalgae as a Reservoir of Bioactive Lipids. *Marine Drugs, 14*(5), 101.

Davies, J., & Davies, D. (2010). Origins and Evolution of Antibiotic Resistance. *Microbiology and Molecular Biology Reviews, 74*(3), 417.

de Nevers, N. (2005). *Fluid Mechanics for Chemical Engineers* (3rd ed.). Boston: McGraw-Hill Higher Education.

Deblois, C. P., Marchand, A., & Juneau, P. (2013). Comparison of Photoacclimation in Twelve Freshwater Photoautotrophs (Chlorophyte, Bacillaryophyte, Cryptophyte and Cyanophyte) Isolated from a Natural Community. *PLOS ONE, 8*(3), e57139.

Dembitsky, V. M. (1996). Betaine ether-linked glycerolipids: Chemistry and biology. *Progress in Lipid Research, 35*(1), 1-51.

Dermoun, D., Chaumont, D., Thebault, J.-M., & Dauta, A. (1992). Modelling of growth of Porphyridium cruentum in connection with two interdependent factors: Light and temperature. *Bioresource Technology, 42*(2), 113-117.

Dever, L. (2018). *Analysis of Lipids from Microalgae - ENCH495 Research Report*. Unpublished Honours Dissertation. University of Canterbury.

Dinsdale, A., & Moore, F. (1962). *Viscosity and its measurement*. London, U.K.: Chapman and Hall.

Doucha, J., & Lívanský, K. (2014). High Density Outdoor Microalgal Culture. In R. Bajpai, A. Prokop, & M. Zappi (Eds.), *Algal Biorefineries: Volume 1: Cultivation of Cells and Products* (pp. 147-173). Dordrecht: Springer Netherlands.

Dunstan, G. A., Volkman, J. K., Barrett, S. M., & Garland, C. D. (1993). Changes in the lipid composition and maximisation of the polyunsaturated fatty acid content of three microalgae grown in mass culture. *Journal of Applied Phycology, 5*(1), 71-83.

Eaton, A. D., Water Environment Federation, American Water Works Association, & American Public Health Association. (2005). *Standard Methods for the Examination of Water & Wastewater* (21st ed.). Washington, D. C: APHA-AWWA-WEF.

Ellis, R. J. (2010). Tackling unintelligent design. *Nature, 463*, 164.
Emerson, R., & Rabinowitch, E. (1960). Red Drop and Role of Auxiliary Pigments in Photosynthesis. *Plant Physiology, 35*(4), 477-485.
Fábregas, J., Otero, A., Maseda, A., & Domínguez, A. (2001). Two-stage cultures for the production of Astaxanthin from Haematococcus pluvialis. *Journal of Biotechnology, 89*(1), 65-71.
Fernandes, B. D., Mota, A., Teixeira, J. A., & Vicente, A. A. (2015). Continuous cultivation of photosynthetic microorganisms: Approaches, applications and future trends. *Biotechnology Advances, 33*(6), 1228-1245.
Fernández, I., Gabriel Acién, F., Berenguel, M., & Guzmán, J. L. (2014). First Principles Model of a Tubular Photobioreactor for Microalgal Production. *Industrial & Engineering Chemistry Research, 53*(27), 11121-11136.
Fernández Sevilla, J. M., Molina Grima, E., García Camacho, F., Acién Fernández, F. G., & Sánchez Pérez, J. A. (1998). Photolimitation and photoinhibition as factors determining optimal dilution rate to produce eicosapentaenoic acid from cultures of the microalga Isochrysis galbana. *Applied Microbiology and Biotechnology, 50*(2), 199-205.
Filali, R., Tebbani, S., Dumur, D., Isambert, A., Pareau, D., & Lopes, F. (2011). Growth modeling of the green microalga Chlorella vulgaris in an air-lift photobioreactor. *IFAC Proceedings Volumes, 44*(1), 10603-10608.
Finco, A. M., Goyzueta Mamani, L., De Carvalho, J., Pereira, G., Thomaz-Soccol, V., & Soccol, C. (2016). Technological trends and market perspectives for production of microbial oils rich in omega-3. *Critical Reviews in Biotechnology, 37*, 1-16.
Fu, W., Gudmundsson, O., Feist, A. M., Herjolfsson, G., Brynjolfsson, S., & Palsson, B. Ø. (2012). Maximizing biomass productivity and cell density of Chlorella vulgaris by using light-emitting diode-based photobioreactor. *Journal of Biotechnology, 161*(3), 242-249.
Gao, B., Huang, L., Wang, F., & Zhang, C. (2019). Trachydiscus guangdongensis sp. nov., a new member of Eustigmatophyceae (Stramenopiles) isolated from China: morphology, phylogeny, fatty acid profile, pigment, and cell wall composition. *Hydrobiologia, 835*(1), 37-47.
Gao, X., Wang, X., Li, H., Roje, S., Sablani, S. S., & Chen, S. (2017). Parameterization of a light distribution model for green cell growth of microalgae: Haematococcus pluvialis cultured under red LED lights. *Algal Research, 23*(Supplement C), 20-27.
García-Camacho, F., Sánchez-Mirón, A., Molina-Grima, E., Camacho-Rubio, F., & Merchuck, J. C. (2012). A mechanistic model of photosynthesis in microalgae including photoacclimation dynamics. *Journal of Theoretical Biology, 304*(Supplement C), 1-15.
García Camacho, F., Contreras Gómez, A., Acién Fernández, F. G., Fernández Sevilla, J., & Molina Grima, E. (1999). Use of concentric-tube airlift photobioreactors for microalgal outdoor mass cultures. *Enzyme and Microbial Technology, 24*(3), 164-172.
García, J. L., Vicente, M., & Galán, B. (2017). Microalgae, old sustainable food and fashion nutraceuticals. *Microbial Biotechnology, 10*(5), 1017-1024.
Gašparović, B., Kazazić, S. P., Cvitešić, A., Penezić, A., & Frka, S. (2015). Improved separation and analysis of glycolipids by Iatroscan thin-layer chromatography–flame ionization detection. *Journal of Chromatography A, 1409*, 259-267.
Gest, H. (1993). Photosynthetic and Quasi-Photosynthetic Bacteria. *Fems Microbiology Letters, 112*(1), 1-6.
Gest, H. (2002). History of the word photosynthesis and evolution of its definition. *Photosynthesis Research, 73*(1), 7-10.

Girard, J.-M., Roy, M.-L., Hafsa, M. B., Gagnon, J., Faucheux, N., Heitz, M., . . . Deschênes, J.-S. (2014). Mixotrophic cultivation of green microalgae Scenedesmus obliquus on cheese whey permeate for biodiesel production. *Algal Research, 5*, 241-248.

Glemser, M., Heining, M., Schmidt, J., Becker, A., Garbe, D., Buchholz, R., & Brück, T. (2016). Application of light-emitting diodes (LEDs) in cultivation of phototrophic microalgae: current state and perspectives. *Applied Microbiology and Biotechnology, 100*(3), 1077-1088.

Gopalakrishnan, K. (2015). *Isolation, characterisation and screening of New Zealand alpine algae for the production of secondary metabolites in photobioreactors.* (Ph.D. Thesis), Univeristy of Canterbury.

Gregory, J. (2005). *Particles in Water: Properties and Processes*. USA: CRC Press.

Grima, E. M., Perez, J. A. S., Camacho, F. G., Sanchez, J. L. G., & Alonso, D. L. (1993). n-3 PUFA productivity in chemostat cultures of microalgae. *Applied Microbiology and Biotechnology, 38*(5), 599-605.

Grima, E. M., Sevilla, J. M. F., Pérez, J. A. S., & Camacho, F. G. (1996). A study on simultaneous photolimitation and photoinhibition in dense microalgal cultures taking into account incident and averaged irradiances. *Journal of Biotechnology, 45*(1), 59-69.

Grobbelaar, J. U. (2012). Microalgae mass culture: the constraints of scaling-up. *Journal of Applied Phycology, 24*(3), 315-318.

Grubišić, M., Šantek, M. I., & Šantek, B. (2019). Potential of Microalgae for the Production of Different Biotechnological Products. *Chemical and Biochemical Engineering Quarterly, 33*(2), 161–181.

Guella, G., Frassanito, R., & Mancini, I. (2003). A new solution for an old problem: the regiochemical distribution of the acyl chains in galactolipids can be established by electrospray ionization tandem mass spectrometry. *Rapid Communications in Mass Spectrometry, 17*(17), 1982-1994.

Guiry, M. D. (2012). How Many Species of Algae are There? *Journal of Phycology, 48*(5), 1057-1063.

Gurr, M. I., & Harwood, J. L. (1991). *Lipid Biochemistry An Introduction* (4th ed.). Melbourne, Australia: Chapman and Hall.

Hall, D. O., Acién Fernández, F. G., Guerrero, E. C., Rao, K. K., & Grima, E. M. (2003). Outdoor helical tubular photobioreactors for microalgal production: Modeling of fluid-dynamics and mass transfer and assessment of biomass productivity. *Biotechnology and Bioengineering, 82*(1), 62-73.

Han, B.-P. (2002). A Mechanistic Model of Algal Photoinhibition Induced by Photodamage to Photosystem-II. *Journal of Theoretical Biology, 214*(4), 519-527.

He, L., Subramanian, V. R., & Tang, Y. J. (2012). Experimental analysis and model-based optimization of microalgae growth in photo-bioreactors using flue gas. *Biomass and Bioenergy, 41*, 131-138.

Heimann, K., & Huerlimann, R. (2015). Microalgal Classification: Major Classes and Genera of Commercial Microalgal Species. In *Handbook of Marine Microalgae* (pp. 25-41). Boston: Academic Press.

Henry, W. (1803). III. Experiments on the quantity of gases absorbed by water, at different temperatures, and under different pressures. *Philosophical Transactions of the Royal Society of London, 93*, 29-274.

Herrero, M., Vicente, M. J., Cifuentes, A., & Ibáñez, E. (2007). Characterization by high-performance liquid chromatography/electrospray ionization quadrupole time-of-flight mass spectrometry of the lipid fraction of Spirulina platensis pressurized ethanol extract. *Rapid Communications in Mass Spectrometry, 21*(11), 1729-1738.

Hine, R., & Martin, E. (Eds.). (2016) A Dictionary of Biology (7th ed.). Oxford, UK: Oxford University Press.
Holland, F., & Bragg, R. (2002). *Fluid Flow for Chemical Engineers* (2nd ed.). Oxford: Butterworth Heineman.
Hölzl, G., & Dörmann, P. (2019). Chloroplast Lipids and Their Biosynthesis. *Annual Review of Plant Biology, 70*(1), 51-81.
Hörtensteiner, S. (1999). Chlorophyll breakdown in higher plants and algae. *Cellular and Molecular Life Sciences CMLS, 56*(3), 330-347.
Hoshida, H., Ohira, T., Minematsu, A., Akada, R., & Nishizawa, Y. (2005). Accumulation of eicosapentaenoic acid in Nannochloropsis sp. in response to elevated CO2 concentrations. *Journal of Applied Phycology, 17*(1), 29-34.
Hsueh, H. T., Li, W. J., Chen, H. H., & Chu, H. (2009). Carbon bio-fixation by photosynthesis of Thermosynechococcus sp. CL-1 and Nannochloropsis oculta. *Journal of Photochemistry and Photobiology B: Biology, 95*(1), 33-39.
Hu, C., van Dommelen, J., van der Heijden, R., Spijksma, G., Reijmers, T. H., Wang, M., . . . Hankemeier, T. (2008). RPLC-Ion-Trap-FTMS Method for Lipid Profiling of Plasma: Method Validation and Application to p53 Mutant Mouse Model. *Journal of Proteome Research, 7*(11), 4982-4991.
Hu, Q., Hu, Z. Y., Cohen, Z., & Richmond, A. (1997). Enhancement of eicosapentaenoic acid (EPA) and gamma-linolenic acid (GLA) production by manipulating algal density of outdoor cultures of Monodus subterraneus (Eustigmatophyta) and Spirulina platensis (Cyanobacteria). *European Journal of Phycology, 32*(1), 81-86.
Ippoliti, D., Gómez, C., del Mar Morales-Amaral, M., Pistocchi, R., Fernández-Sevilla, J. M., & Acién, F. G. (2016). Modeling of photosynthesis and respiration rate for Isochrysis galbana (T-Iso) and its influence on the production of this strain. *Bioresource Technology, 203*, 71-79.
IUPAC-IUB Commission on Biochemical Nomenclature. (1977). The Nomenclature of Lipids. *European Journal of Biochemistry, 79*(1), 11-21.
Jamialahmadi, M., Zehtaban, M. R., Müller-Steinhagen, H., Sarrafi, A., & Smith, J. M. (2001). Study of Bubble Formation Under Constant Flow Conditions. *Chemical Engineering Research and Design, 79*(5), 523-532.
Jeffrey, S. W., Mantoura, R. F. C., Wright, S. W., International Council of Scientific Unions. Scientific Committee on Oceanic Research, & UNESCO. (1997). *Phytoplankton Pigments in Oceanography: Guidelines to Modern Methods*. Paris, France: UNESCO Publishing.
Johnsen, S. (2011). *The Optics of Life - A Biologist's Guide to Light in Nature*. Princeton, USA: Princeton University Press.
Kantarci, N., Borak, F., & Ulgen, K. O. (2005). Bubble column reactors. *Process Biochemistry, 40*(7), 2263-2283.
Kates, M. (1986). *Techniques of Lipidology: Isolation, Analysis, and Identification of Lipids* (2nd rev. ed. Vol. 3, pt. 2). Amsterdam, The Netherlands: Elsevier.
Kato, M., Kobayashi, Y., Torii, A., & Yamada, M. (2003). Betaine Lipids in Marine Algae. In N. Murata, M. Yamada, I. Nishida, H. Okuyama, J. Sekiya, & W. Hajime (Eds.), *Advanced Research on Plant Lipids: Proceedings of the 15th International Symposium on Plant Lipids* (pp. 19-22). Dordrecht: Springer Netherlands.
Katritzky, A. R., & Rees, C. W. (1984). *Comprehensive heterocyclic chemistry: the structure, reactions, synthesis, and uses of heterocyclic compounds* (1st ed.). Oxford, UK: Pergamon Press.
Ke, B. (2001). *Photosynthesis*. Dordrecht, The Netherlands: Kluwer Academic Publishers.
Ketheesan, B., & Nirmalakhandan, N. (2013). Modeling microalgal growth in an airlift-driven raceway reactor. *Bioresource Technology, 136*(Supplement C), 689-696.

Khozin-Goldberg, I., Didi-Cohen, S., Shayakhmetova, I., & Cohen, Z. (2002). Biosynthesis of eicosapentaenoic acid (EPA) in the freshwater eustigmatophyceae Monodus subterraneus (eustigmatophyceae). *Journal of Phycology, 38*(4), 745-756.

Kim, C. W., Sung, M.-G., Nam, K., Moon, M., Kwon, J.-H., & Yang, J.-W. (2014). Effect of monochromatic illumination on lipid accumulation of Nannochloropsis gaditana under continuous cultivation. *Bioresource Technology, 159*, 30-35.

Klimov, V. V. (2003). Discovery of pheophytin function in the photosynthetic energy conversion as the primary electron acceptor of Photosystem II. *Photosynthesis Research, 76*(1), 247-253.

Kris-Etherton, P. M., Harris, W. S., & Appel, L. J. (2002). Fish Consumption, Fish Oil, Omega-3 Fatty Acids, and Cardiovascular Disease. *Circulation, 106*(21), 2747-2757.

Kulkarni, A. V. (2010). Design of a Pipe/Ring Type of Sparger for a Bubble Column Reactor. *Chemical Engineering & Technology, 33*(6), 1015-1022.

Kulkarni, A. V., & Joshi, J. B. (2011). Design and selection of sparger for bubble column reactor. Part I: Performance of different spargers. *Chemical Engineering Research and Design, 89*(10), 1972-1985.

Lairon, D. (2009). Digestion and absorption of lipids. In D. J. McClements & E. A. Decker (Eds.), *Designing Functional Foods* (pp. 68-93). Cambridge, UK: Woodhead Publishing.

Larkum, A. W. D., Douglas, S. E., & Raven, J. A. (Eds.). (2003). *Photosynthesis in Algae* (Vol. 14). The Netherlands: Kluwer Academic Publishers.

Latowski, D., Kuczyńska, P., & Strzałka, K. (2011). Xanthophyll cycle – a mechanism protecting plants against oxidative stress. *Redox Report, 16*(2), 78-90.

Lavens, P., & Sorgeloos, P. (Eds.). (1996). *Manual on the Production and Use of Live Food for Aquaculture*. Rome, Italy: FAO.

Lee, E., Jalalizadeh, M., & Zhang, Q. (2015). Growth kinetic models for microalgae cultivation: A review. *Algal Research, 12*, 497-512.

Letunic, I., & Bork, P. (2019). Interactive Tree Of Life (iTOL) v4: recent updates and new developments. *Nucleic Acids Research, 47*(W1), W256-W259.

Leupold, M., Hindersin, S., Gust, G., Kerner, M., & Hanelt, D. (2013). Influence of mixing and shear stress on Chlorella vulgaris, Scenedesmus obliquus, and Chlamydomonas reinhardtii. *Journal of Applied Phycology, 25*(2), 485-495.

Li, S., Xu, J., Chen, J., Chen, J., Zhou, C., & Yan, X. (2014). The major lipid changes of some important diet microalgae during the entire growth phase. *Aquaculture, 428-429*(Supplement C), 104-110.

Li, S., Xu, J., Jiang, Y., Zhou, C., Yu, X., Zhong, Y., . . . Yan, X. (2015). Lipidomic analysis can distinguish between two morphologically similar strains of Nannochloropsis oceanica. *Journal of Phycology, 51*(2), 264-276.

Lo, S.-K., Tan, C.-P., Long, K., Yusoff, M. S. A., & Lai, O.-M. (2008). Diacylglycerol Oil—Properties, Processes and Products: A Review. *Food and Bioprocess Technology, 1*(3), 223.

López-Rosales, L., Sánchez-Mirón, A., García-Camacho, F., Place, A. R., Chisti, Y., & Molina-Grima, E. (2018). Pilot-scale outdoor photobioreactor culture of the marine dinoflagellate Karlodinium veneficum: Production of a karlotoxins-rich extract. *Bioresource Technology, 253*, 94-104.

López, M. C. G.-M., Sánchez, E. D. R., López, J. L. C., Fernández, F. G. A., Sevilla, J. M. F., Rivas, J., . . . Grima, E. M. (2006). Comparative analysis of the outdoor culture of Haematococcus pluvialis in tubular and bubble column photobioreactors. *Journal of Biotechnology, 123*(3), 329-342.

Lu, C., Rao, K., Hall, D., & Vonshak, A. (2001). Production of eicosapentaenoic acid (EPA) in Monodus subterraneus grown in a helical tubular photobioreactor as affected by cell density and light intensity. *Journal of Applied Phycology, 13*(6), 517-522.

Luangpipat, T. (2013). *Photobioreactor production of microalgae for potential fuel oils.* (Ph.D. Thesis), Massey University.

Lubián, L. M., Montero, O., Moreno-Garrido, I., Huertas, I. E., Sobrino, C., González-del Valle, M., & Parés, G. (2000). Nannochloropsis (Eustigmatophyceae) as source of commercially valuable pigments. *Journal of Applied Phycology, 12*(3), 249-255.

Lukavský, J. (2012). Trachydiscus minutus: A new algal EPA producer. In D. Krueger & H. Meyer (Eds.), *Algae: Ecology, Economic Uses and Environmental Impact* (pp. 77-104). New York, USA: Nova Publishers.

MacIntyre, H. L., Kana, T. M., Anning, T., & Geider, R. J. (2002). Photoacclimation of Photosynthesis Irradiance Response Curves and Photosynthetic Pigments in Microalgae and Cyanobacteria. *Journal of Phycology, 38*(1), 17-38.

Martin, G. J. O., Hill, D. R. A., Olmstead, I. L. D., Bergamin, A., Shears, M. J., Dias, D. A., . . . Callahan, D. L. (2014). Lipid Profile Remodeling in Response to Nitrogen Deprivation in the Microalgae Chlorella sp. (Trebouxiophyceae) and Nannochloropsis sp. (Eustigmatophyceae). *PLOS ONE, 9*(8).

Mata, T. M., Martins, A. A., & Caetano, N. S. (2010). Microalgae for biodiesel production and other applications: A review. *Renewable and Sustainable Energy Reviews, 14*(1), 217-232.

Mazumda, N. (2018). *'Algal blushing ': Characterization and optimization of culture conditions of a novel alpine Haematococcus species from New Zealand for astaxanthin production.* (Ph.D. Thesis), University of Canterbury.

McDonald, A. G., & Magande, H. L. (2012). Appendix C: Heat Exchanger Design. In A. G. McDonald & H. L. Magande (Eds.), *Introduction to Thermo-Fluids Systems Design* (pp. 373-382).

Meiser, A., Schmid-Staiger, U., & Trösch, W. (2004). Optimization of eicosapentaenoic acid production by Phaeodactylum tricornutumin the flat panel airlift (FPA) reactor. *Journal of Applied Phycology, 16*(3), 215-225.

Meng, Y., Jiang, J., Wang, H., Cao, X., Xue, S., Yang, Q., & Wang, W. (2015). The characteristics of TAG and EPA accumulation in Nannochloropsis oceanica IMET1 under different nitrogen supply regimes. *Bioresource Technology, 179*(Supplement C), 483-489.

Menon, K. R., Balan, R., & Suraishkumar, G. K. (2013). Stress induced lipid production in Chlorella vulgaris: Relationship with specific intracellular reactive species levels. *Biotechnology and Bioengineering, 110*(6), 1627-1636.

Michels, M. H. A., van der Goot, A. J., Norsker, N.-H., & Wijffels, R. H. (2010). Effects of shear stress on the microalgae Chaetoceros muelleri. *Bioprocess and Biosystems Engineering, 33*(8), 921-927.

Michels, M. H. A., van der Goot, A. J., Vermuë, M. H., & Wijffels, R. H. (2016). Cultivation of shear stress sensitive and tolerant microalgal species in a tubular photobioreactor equipped with a centrifugal pump. *Journal of Applied Phycology, 28*(1), 53-62.

Mikami, K., & Hosokawa, M. (2013). Biosynthetic pathway and health benefits of fucoxanthin, an algae-specific xanthophyll in brown seaweeds. *International journal of molecular sciences, 14*(7), 13763-13781.

Ministry of Business Innovation and Employment. (2020). Energy prices. Retrieved from https://www.mbie.govt.nz/building-and-energy/energy-and-natural-resources/energy-statistics-and-modelling/energy-statistics/energy-prices/. Retrieved 12th March 2020.

Mitra, M., Patidar, S. K., & Mishra, S. (2015). Integrated process of two stage cultivation of Nannochloropsis sp. for nutraceutically valuable eicosapentaenoic acid along with biodiesel. *Bioresource Technology, 193*(Supplement C), 363-369.

Mitsuhashi, S., Hosaka, K., Tomonaga, E., Muramatsu, H., & Tanishita, K. (1995). Effects of shear flow on photosynthesis in a dilute suspension of microalgae. *Applied Microbiology and Biotechnology, 42*(5), 744-749.

Mohsenpour, S. F., Richards, B., & Willoughby, N. (2012). Spectral conversion of light for enhanced microalgae growth rates and photosynthetic pigment production. *Bioresource Technology, 125*, 75-81.

Molina Grima, E., Acién Fernández, F. G., García Camacho, F., Camacho Rubio, F., & Chisti, Y. (2000). Scale-up of tubular photobioreactors. *Journal of Applied Phycology, 12*(3-5), 355-368.

Molina Grima, E., Acién Fernández, F. G., García Camacho, F., & Chisti, Y. (1999). Photobioreactors: light regime, mass transfer, and scaleup. *Journal of Biotechnology, 70*(1-3), 231-247.

Molina Grima, E., Camacho, F. G., Perez, J. A. S., Sevilla, J. M. F., Fernandez, F. G. A., & Gomez, A. C. (1994a). A Mathematical Model of Microalgal Growth in Light-Limited Chemostat Culture. *Journal of Chemical Technology and Biotechnology, 61*(2), 167-173.

Molina Grima, E., Fernández Sevilla, J. M., Acién Fernández, F. G., & Chisti, Y. (2001). Tubular photobioreactor design for algal cultures. *Journal of Biotechnology, 92*(2), 113-131.

Molina Grima, E., Fernández Sevilla, J. M., Acién Fernández, F. G., & Flickinger, M. C. (2009). Microalgae, Mass Culture Methods. In M. C. Flickinger (Ed.), *Encyclopedia of Industrial Biotechnology: Bioprocess, Bioseparation, and Cell Technology*: John Wiley & Sons, Inc.

Molina Grima, E., Sánchez Pérez, J. A., García Camacho, F., Fernández Sevilla, J. M., & Acién Fernández, F. G. (1994b). Effect of growth rate on the eicosapentaenoic acid and docosahexaenoic acid content of Isochrysis galbana in chemostat culture. *Applied Microbiology and Biotechnology, 41*(1), 23-27.

Molina Grima, E., Sánchez Pérez, J. A., García Camacho, F., Fernández Sevilla, J. M., Acién Fernández, F. G., & Urda Cardona, J. (1995). Biomass and icosapentaenoic acid productivities from an outdoor batch culture of Phaeodactylum tricornutum UTEX 640 in an airlift tubular photobioreactor. *Applied Microbiology and Biotechnology, 42*(5), 658-663.

Monod, J. (1949). The Growth of Bacterial Cultures. *Annual Review of Microbiology, 3*(1), 371-394.

Monroig, Ó., Tocher, D. R., & Navarro, J. C. (2013). Biosynthesis of Polyunsaturated Fatty Acids in Marine Invertebrates: Recent Advances in Molecular Mechanisms. *Marine Drugs, 11*(10), 3998-4018.

Moo-Young, M., & Blanch, H. W. (1981). Design of biochemical reactors mass transfer criteria for simple and complex systems. In *Reactors and Reactions* (pp. 1-69). Heidelberg, Germany: Springer.

Mook, W. (2000). Chemistry of carbonic acid in water. In International Atomic Energy Agency & United Nations Educational Scientific and Cultural Organization (Eds.), *Environmental Isotopes in the Hydrological Cycle: Principles and Applications* (pp. 143-165).

Mühlroth, A., Li, K., Røkke, G., Winge, P., Olsen, Y., Hohmann-Marriott, F. M., . . . Bones, M. A. (2013). Pathways of Lipid Metabolism in Marine Algae, Co-Expression Network, Bottlenecks and Candidate Genes for Enhanced Production of EPA and DHA in Species of Chromista. *Marine Drugs, 11*(11).

National Institute of Water and Atmospheric Research (NIWA). (2020a). Atmospheric Carbon Dioxide at Baring Head. Retrieved from https://niwa.co.nz/atmosphere/our-data/trace-gas-plots/carbon-dioxide. Retrieved 5th May 2020.

National Institute of Water and Atmospheric Research (NIWA). (2020b). Mean Daily Air Temperature (°C). Retrieved from https://niwa.co.nz/climate/information-and-resources/nz-temperature-record. Retrieved 5th May 2020.

Nguyen, H. M., Cuiné, S., Beyly-Adriano, A., Légeret, B., Billon, E., Auroy, P., . . . Li-Beisson, Y. (2013). The Green Microalga Chlamydomonas reinhardtii Has a Single ω-3 Fatty Acid Desaturase That Localizes to the Chloroplast and Impacts Both Plastidic and Extraplastidic Membrane Lipids. *Plant Physiology, 163*(2), 914-928.

Noeparvar, P. (2018). *Development of a Computational Framework for the Prediction of Free–Ion Activities, Ionic Equilibria and Solubility in Dairy Liquids.* (Ph.D. Thesis), University of Canterbury.

Norsker, N.-H., Barbosa, M. J., Vermuë, M. H., & Wijffels, R. H. (2011). Microalgal production — A close look at the economics. *Biotechnology Advances, 29*(1), 24-27.

O'Connor, K. C., Cowger, N. L., De Kee, D. C. R., & Schwarz, R. P. (2002). Prolonged shearing of insect cells in a couette bioreactor. *Enzyme and Microbial Technology, 31*(5), 600-608.

Olofsson, M., Lamela, T., Nilsson, E., Berge, J.-P., Pino, V. d., Uronen, P., & Legrand, C. (2014). Combined Effects of Nitrogen Concentration and Seasonal Changes on the Production of Lipids in Nannochloropsis oculata. *Marine Drugs, 12*(4), 1891-1910.

Olofsson, M., Lamela, T., Nilsson, E., Bergé, J. P., del Pino, V., Uronen, P., & Legrand, C. (2012). Seasonal Variation of Lipids and Fatty Acids of the Microalgae Nannochloropsis oculata Grown in Outdoor Large-Scale Photobioreactors. *Energies, 5*(5), 1577.

Otero, A., García, D., & Fábregas, J. (1997a). Factors controlling eicosapentaenoic acid production in semicontinuous cultures of marine microalgae. *Journal of Applied Phycology, 9*(5), 465-469.

Otero, A., García, D., Morales, E. D., Arán, J., & Fábregas, J. (1997b). Manipulation of the biochemical composition of the eicosapentaenoic acid-rich microalga Isochrysis galbana in semicontinuous cultures. *Biotechnology and Applied Biochemistry, 26*(3), 171-177.

Öztürk, S. S., Schumpe, A., & Deckwer, W. D. (1987). Organic liquids in a bubble column: Holdups and mass transfer coefficients. *AIChE Journal, 33*(9), 1473-1480.

Pal, D., Khozin-Goldberg, I., Cohen, Z., & Boussiba, S. (2011). The effect of light, salinity, and nitrogen availability on lipid production by Nannochloropsis sp. *Applied Microbiology and Biotechnology, 90*(4), 1429-1441.

Patil, L., & Kaliwal, B. (2017). Effect of CO2 Concentration on Growth and Biochemical Composition of Newly Isolated Indigenous Microalga Scenedesmus bajacalifornicus BBKLP-07. *Applied Biochemistry and Biotechnology, 182*(1), 335-348.

Pauly, D., Christensen, V., Guenette, S., Pitcher, T. J., & et al. (2002). Towards sustainability in world fisheries. *Nature, 418*(6898), 689-695.

Perez-Garcia, O., Escalante, F. M. E., de-Bashan, L. E., & Bashan, Y. (2011). Heterotrophic cultures of microalgae: Metabolism and potential products. *Water Research, 45*(1), 11-36.

Pharmacy Direct. (2020). Fish Oil (Omega-3). Retrieved from https://www.pharmacydirect.co.nz/Fish-Oil-(Omega-3)/. Retrieved 5th May 2020.

Posten, C. (2009). Design principles of photo-bioreactors for cultivation of microalgae. *Engineering in Life Sciences, 9*(3), 165-177.

Posten, C., & Walter, C. (Eds.). (2012). *Microalgal Biotechnology: Potential and Production*. Berlin, Germany: De Gruyter.

Prasad, R. (Ed.) (1996). *Manual on Membrane Lipids*. Germany: Springer.

Pulz, O. (2001). Photobioreactors: production systems for phototrophic microorganisms. *Applied Microbiology and Biotechnology, 57*(3), 287-293.

Qiao, H., Cong, C., Sun, C., Li, B., Wang, J., & Zhang, L. (2016). Effect of culture conditions on growth, fatty acid composition and DHA/EPA ratio of Phaeodactylum tricornutum. *Aquaculture, 452*, 311-317.

Quach, H. T., Steeper, R. L., & Griffin, G. W. (2004). An Improved Method for the Extraction and Thin-Layer Chromatography of Chlorophyll a and b from Spinach. *Journal of Chemical Education, 81*(3), 385.

Radakovits, R., Jinkerson, R. E., Darzins, A., & Posewitz, M. C. (2010). Genetic Engineering of Algae for Enhanced Biofuel Production. *Eukaryotic Cell, 9*(4), 486.

Ratledge, C. (1997). Microbial Lipids. In H. Kleinkauf & H. von Döhren (Eds.), *Biotechnology: Products of Secondary Metabolism* (2nd ed., Vol. 7, pp. 133-197). Weinheim, Germany: VCH.

Raven, J. A. (2011). The cost of photoinhibition. *Physiologia Plantarum, 142*(1), 87-104.

Raven, J. A., & Geider, R. J. (2003). Adaptation, Acclimation and Regulation in Algal Photosynthesis. In A. W. D. Larkum, S. E. Douglas, & J. A. Raven (Eds.), *Photosynthesis in Algae* (pp. 385-412). Dordrecht: Springer Netherlands.

Rebolloso Fuentes, M. M., García Sánchez, J. L., Fernández Sevilla, J. M., Acién Fernández, F. G., Sánchez Pérez, J. A., & Molina Grima, E. (1999). Outdoor continuous culture of Porphyridium cruentum in a tubular photobioreactor: quantitative analysis of the daily cyclic variation of culture parameters. *Journal of Biotechnology, 70*(1), 271-288.

Reece, J., Urry, L., Cain, M., Wasserman, S., Minorsky, P., & Jackson, R. (2010). *Campbell Biology* (9th ed.). USA: Pearson.

Reis, A., Gouveia, L., Veloso, V., Fernandes, H. L., Empis, J., & Novais, J. M. (1996). Eicosapentaenoic acid-rich biomass production by the microalga Phaeodactylum tricornutum in a continuous-flow reactor. *Bioresource Technology, 55*(1), 83-88.

Řezanka, T., Lukavský, J., Nedbalová, L., & Sigler, K. (2011). Effect of nitrogen and phosphorus starvation on the polyunsaturated triacylglycerol composition, including positional isomer distribution, in the alga Trachydiscus minutus. *Phytochemistry, 72*(18), 2342-2351.

Rezanka, T., Petrankova, M., Cepak, V., Pribyl, P., Sigler, K., & Cajthaml, T. (2010). Trachydiscus minutus, a new biotechnological source of eicosapentaenoic acid. *Folia Microbiologica, 55*(3), 265-269.

Richmond, A. (2008). *Handbook of Microalgal Culture: Biotechnology and Applied Phycology*. USA: Wiley.

Rocha, J. M. S., Garcia, J. E. C., & Henriques, M. H. F. (2003). Growth aspects of the marine microalga Nannochloropsis gaditana. *Biomolecular Engineering, 20*(4), 237-242.

Rodolfi, L., Biondi, N., Guccione, A., Bassi, N., D'Ottavio, M., Arganaraz, G., & Tredici, M. R. (2017). Oil and eicosapentaenoic acid production by the diatom Phaeodactylum tricornutum cultivated outdoors in Green Wall Panel (GWP®) reactors. *Biotechnology and Bioengineering, 114*(10), 2204-2210.

Rodolfi, L., Zittelli, G. C., Bassi, N., Padovani, G., Biondi, N., Bonini, G., & Tredici, M. R. (2009). Microalgae for oil: Strain selection, induction of lipid synthesis and outdoor mass cultivation in a low-cost photobioreactor. *Biotechnology and Bioengineering, 102*(1), 100-112.

Rodríguez, J. J. G., Mirón, A. S., Camacho, F. G., García, M. C. C., Belarbi, E. H., Chisti, Y., & Grima, E. M. (2009). Causes of shear sensitivity of the toxic dinoflagellate Protoceratium reticulatum. *Biotechnology Progress, 25*(3), 792-800.

Roels, J. A. (1983). *Energetics and kinetics in biotechnology*. USA: Elsevier Biomedical Press.

Roquette Klötze GmbH & Co. KG. (2017). Algomed. Retrieved from https://www.algomed.de/en/homepage/. Retrieved 15th December 2017.

Rousch, J. M., Bingham, S. E., & Sommerfeld, M. R. (2003). Changes in fatty acid profiles of thermo-intolerant and thermo-tolerant marine diatoms during temperature stress. *Journal of Experimental Marine Biology and Ecology, 295*(2), 145-156.

Rubio, F. C., Camacho, F. G., Sevilla, J. M. F., Chisti, Y., & Grima, E. M. (2003). A mechanistic model of photosynthesis in microalgae. *Biotechnology and Bioengineering, 81*(4), 459-473.

Saifuddin, N. M., Puvunathan, P., Aisswarya, K., & Juan, Y. P. (2015). Sequestration of High Carbon Dioxide Concentration for Induction of Lipids in Microalgae for Biodiesel Production. *Journal of Applied Sciences, 15*, 1045-1058.

Salih, F. (2011). Microalgae Tolerance to High Concentrations of Carbon Dioxide: A Review. *Journal of Environmental Protection, 2*(5), 648-654.

San Pedro, A., González-López, C. V., Acién, F. G., & Molina-Grima, E. (2015). Outdoor pilot production of Nannochloropsis gaditana: Influence of culture parameters and lipid production rates in raceway ponds. *Algal Research, 8*, 205-213.

Sánchez Mirón, A., Contreras Gómez, A., García Camacho, F., Molina Grima, E., & Chisti, Y. (1999). Comparative evaluation of compact photobioreactors for large-scale monoculture of microalgae. *Journal of Biotechnology, 70*(1), 249-270.

Sander, R. (2015). Compilation of Henry's law constants (version 4.0) for water as solvent. *Atmospheric Chemistry and Physics, 15*(8), 4399-4981.

Sarpal, A. S., Teixeira, C. M. L. L., Silva, P. R. M., da Costa Monteiro, T. V., da Silva, J. I., da Cunha, V. S., & Daroda, R. J. (2016). NMR techniques for determination of lipid content in microalgal biomass and their use in monitoring the cultivation with biodiesel potential. *Applied Microbiology and Biotechnology, 100*(5), 2471-2485.

Sato, N. (2015). Is Monoglucosyldiacylglycerol a Precursor to Monogalactosyldiacylglycerol in All Cyanobacteria? *Plant & cell physiology, 56*(10), 1890-1899.

Sato, T., Yamada, D., & Hirabayashi, S. (2010). Development of virtual photobioreactor for microalgae culture considering turbulent flow and flashing light effect. *Energy Conversion and Management, 51*(6), 1196-1201.

Scarsella, M., Torzillo, G., Cicci, A., Belotti, G., De Filippis, P., & Bravi, M. (2012). Mechanical stress tolerance of two microalgae. *Process Biochemistry, 47*(11), 1603-1611.

SCHOTT AG. (2016). *Tubular Glass Photobioreactors [Brochure]*. Germany: SCHOTT AG.

SCHOTT AG. (2017a). *Borosilicate Glass Properties [Brochure]*. Germany: SCHOTT AG.

SCHOTT AG. (2017b). Photobioreactor Tutorial [Video]. Retrieved from https://www.schott.com/tubing/english/photobioreactor/videos-tutorials.html. Retrieved 30th June 2017

Schubert, E. F. (2006). *Light-emitting diodes*. Cambridge: Cambridge University Press.

Schulze, P. S. C., Barreira, L. A., Pereira, H. G. C., Perales, J. A., & Varela, J. C. S. (2014). Light emitting diodes (LEDs) applied to microalgal production. *Trends in Biotechnology, 32*(8), 422-430.

Schulze, P. S. C., Guerra, R., Pereira, H., Schüler, L. M., & Varela, J. C. S. (2017). Flashing LEDs for Microalgal Production. *Trends in Biotechnology, 35*(11), 1088-1101.

Schulze, P. S. C., Pereira, H. G. C., Santos, T. F. C., Schueler, L., Guerra, R., Barreira, L. A., . . . Varela, J. C. S. (2016). Effect of light quality supplied by light emitting diodes

(LEDs) on growth and biochemical profiles of Nannochloropsis oculata and Tetraselmis chuii. *Algal Research, 16*, 387-398.

Serra-Maia, R., Bernard, O., Gonçalves, A., Bensalem, S., & Lopes, F. (2016). Influence of temperature on Chlorella vulgaris growth and mortality rates in a photobioreactor. *Algal Research, 18*, 352-359.

Serway, R., & Jewett, J. (2007). *Physics for Scientists and Engineers*. Australia: Cengage Learning.

Shannon, R. R., & Wyant, J. C. (1979). *Applied Optics and Optical Engineering* (Vol. 7). London, UK: Academic Press.

Sharma, K., & Schenk, P. M. (2015). Rapid induction of omega-3 fatty acids (EPA) in Nannochloropsis sp. by UV-C radiation. *Biotechnology and Bioengineering, 112*(6), 1243-1249.

Shene, C., Chisti, Y., Vergara, D., Burgos-Díaz, C., Rubilar, M., & Bustamante, M. (2016). Production of eicosapentaenoic acid by Nannochloropsis oculata: Effects of carbon dioxide and glycerol. *Journal of Biotechnology, 239*(Supplement C), 47-56.

Shimizu, K., Takada, S., Minekawa, K., & Kawase, Y. (2000). Phenomenological model for bubble column reactors: prediction of gas hold-ups and volumetric mass transfer coefficients. *Chemical Engineering Journal, 78*(1), 21-28.

Shiran, D., Khozin, I., Heimer, Y. M., & Cohen, Z. (1996). Biosynthesis of eicosapentaenoic acid in the microalga Porphyridium cruentum. I: The use of externally supplied fatty acids. *Lipids, 31*(12), 1277-1282.

Siegenthaler, P. A., & Murata, N. (1998). *Lipids in photosynthesis: structure, function, and genetics* (Vol. 6). Dordrecht, The Netherlands: Kluwer Academic Publishers.

Silva, C., Soliman, E., Cameron, G., Fabiano, L. A., & Seider, W. D. (2014). Commercial-Scale Biodiesel Production from Algae. *Industrial & Engineering Chemistry Research, 53*(13), 5311-5324.

Simionato, D., Basso, S., Giacometti, G. M., & Morosinotto, T. (2013). Optimization of light use efficiency for biofuel production in algae. *Biophysical Chemistry, 182*(Supplement C), 71-78.

Simopoulos, A. P. (1991). Omega-3 fatty acids in health and disease and in growth and development. *The American Journal of Clinical Nutrition, 54*(3), 438-463.

Simopoulos, A. P. (2002). Omega-3 Fatty Acids in Inflammation and Autoimmune Diseases. *Journal of the American College of Nutrition, 21*(6), 495-505.

Skillman, J. B. (2008). Quantum yield variation across the three pathways of photosynthesis: not yet out of the dark. *Journal of Experimental Botany, 59*(7), 1647-1661.

Sobczuk, T. M., Camacho, F. G., Rubio, F. C., Acién Fernández, F. G., & Grima, E. M. (2000). Carbon dioxide uptake efficiency by outdoor microalgal cultures in tubular airlift photobioreactors. *Biotechnology and Bioengineering, 67*(4), 465-475.

Spolaore, P., Joannis-Cassan, C., Duran, E., & Isambert, A. (2006). Commercial applications of microalgae. *Journal of Bioscience and Bioengineering, 101*(2), 87-96.

Stoyneva-Gärtner, M., Uzunov, B., Gärtner, G., Borisova, C., Draganova, P., Radkova, M., . . . Atanassov, I. (2019). Current bioeconomical interest in stramenopilic Eustigmatophyceae: a review. *Biotechnology & Biotechnological Equipment*, 1-13.

Su, C.-H., Chien, L.-J., Gomes, J., Lin, Y.-S., Yu, Y.-K., Liou, J.-S., & Syu, R.-J. (2011). Factors affecting lipid accumulation by Nannochloropsis oculata in a two-stage cultivation process. *Journal of Applied Phycology, 23*(5), 903-908.

Su, X., Xu, J., Yan, X., Zhao, P., Chen, J., Zhou, C., . . . Li, S. (2013). Lipidomic changes during different growth stages of Nitzschia closterium f. minutissima. *Metabolomics, 9*(2), 300-310.

Sukenik, A., & Carmeli, Y. (1990). Lipid synthesis and fatty acid composition in Nannochloropsis sp. (eustigmatophyceae) grown in a light-dark cycle. *Journal of Phycology, 26*(3), 463-469.

Sukenik, A., Carmeli, Y., & Berner, T. (1989). Regulation of fatty acid composition by irradiance level in the eustigmatophyte Nannochloropsis sp. *Journal of Phycology, 25*(4), 686-692.

Sukenik, A., Levy, R. S., Levy, Y., Falkowski, P. G., & Dubinsky, Z. (1991). Optimizing algal biomass production in an outdoor pond: a simulation model. *Journal of Applied Phycology, 3*(3), 191-201.

Taiz, L., & Zeiger, E. (1991). *Plant physiology*. Redwood City, USA: Benjamin Cummings Publishing Co.

Takache, H., Pruvost, J., & Marec, H. (2015). Investigation of light/dark cycles effects on the photosynthetic growth of Chlamydomonas reinhardtii in conditions representative of photobioreactor cultivation. *Algal Research, 8*(Supplement C), 192-204.

Talbot, P., Gortares, M. P., Lencki, R. W., & de la Noüe, J. (2004). Absorption of CO2 in algal mass culture systems: A different characterization approach. *Biotechnology and Bioengineering, 37*(9), 834-842.

Tangestani, M. (2019). *Improvement of Eicosapentaenoic acid (EPA) Production by the Alga Trachydiscus sp. in Concentric Airlift Photobioreactors.* (Ph.D. Thesis), University of Canterbury.

Theodoridis, G. A., Gika, H. G., Want, E. J., & Wilson, I. D. (2012). Liquid chromatography–mass spectrometry based global metabolite profiling: A review. *Analytica Chimica Acta, 711*, 7-16.

Thermo Fisher Scientific Inc. (2007). *Dissolved Oxygen Probe User Guide (Rev. A)*. USA: Thermo Fisher Scientific Inc.

Thom, R. (2015). *Production of the Omega-3 Fatty Acid, Eicosapentaenoic Acid (EPA), in Airlift Photobioreactors from the Algal Species Trachydiscus sp. "awarua"*. (Unpublished BE(Hons) Dissertation), University of Canterbury.

Tiago Toscano, S., Zhang, L., Ariöz, C., Wieslander, Å., & Norling, B. (2014). Subcellular Localization of Monoglucosyldiacylglycerol Synthase in Synechocystis sp. PCC6803 and Its Unique Regulation by Lipid Environment. *PLOS ONE, 9*(2).

Tocher, R. D., Betancor, B. M., Sprague, M., Olsen, E. R., & Napier, A. J. (2019). Omega-3 Long-Chain Polyunsaturated Fatty Acids, EPA and DHA: Bridging the Gap between Supply and Demand. *Nutrients, 11*(1).

Tredici, M. R., Zittelli, G. C., & Rodolfi, L. (2013). Photobioreactors. In M. C. Flickinger (Ed.), *Upstream Industrial Biotechnology: Equipment, Process Design, Sensing, Control and cGMP Operations* (1st ed., Vol. 2). Somerset, United States: John Wiley & Sons Incorporated.

Tsuzuki, M., Ohnuma, E., Sato, N., Takaku, T., & Kawaguchi, A. (1990). Effects of CO2 Concentration during Growth on Fatty Acid Composition in Microalgae. *Plant Physiology, 93*(3), 851-856.

Uttaro, A. D. (2006). Biosynthesis of polyunsaturated fatty acids in lower eukaryotes. *IUBMB Life, 58*(10), 563-571.

van't Riet, K., & Tramper, J. (1991). *Basic bioreactor design*. New York, USA: CRC Press.

van Oorschot, J. L. P. (1955). *Conversion of Light Energy in Algal Culture*. Wageningen, The Netherlands: Veenman & Zonen.

Vandanjon, L., Rossignol, N., Jaouen, P., Robert, J. M., & Quéméneur, F. (1999). Effects of shear on two microalgae species. Contribution of pumps and valves in tangential flow filtration systems. *Biotechnology and Bioengineering, 63*(1), 1-9.

Vardar-Sukan, F. (1998). Foaming: Consequences, prevention and destruction. *Biotechnology Advances, 16*(5), 913-948.
Volkman, J. K., Brown, M. R., Dunstan, G. A., & Jeffrey, S. W. (1993). The biochemical composition of marine microalgae from the class eustigmatophyceae. *Journal of Phycology, 29*(1), 69-78.
Wada, H., & Murata, N. (2009). *Lipids in Photosynthesis: Essential and Regulatory Functions* (Vol. 30). Dordrecht, The Netherlands: Springer.
Waltz, E. (2009). Biotech's green gold? *Nature Biotechnology, 27*(1), 15-18.
Wang, Z., & Benning, C. (2011). Arabidopsis thaliana Polar Glycerolipid Profiling by Thin Layer Chromatography (TLC) Coupled with Gas-Liquid Chromatography (GLC). *JoVE*(49), e2518.
Ward, O. P., & Singh, A. (2005). Omega-3/6 fatty acids: Alternative sources of production. *Process Biochemistry, 40*(12), 3627-3652.
Wei, L., El Hajjami, M., Shen, C., You, W., Lu, Y., Li, J., . . . Xu, J. (2019). Transcriptomic and proteomic responses to very low CO2 suggest multiple carbon concentrating mechanisms in Nannochloropsis oceanica. *Biotechnology for Biofuels, 12*(1), 168.
Wen, Z.-Y., & Chen, F. (2001). A perfusion–cell bleeding culture strategy for enhancing the productivity of eicosapentaenoic acid by Nitzschia laevis. *Applied Microbiology and Biotechnology, 57*(3), 316-322.
Wenk, M. R. (2005). The emerging field of lipidomics. *Nature Reviews. Drug Discovery, 4*(7), 594-610.
Wilkes, J. O., & Bike, S. G. (1999). *Fluid mechanics for chemical engineers*. Upper Saddle River, N.J: Prentice Hall PTR.
Wishkerman, A., & Wishkerman, E. (2017). Application note: A novel low-cost open-source LED system for microalgae cultivation. *Computers and Electronics in Agriculture, 132*, 56-62.
Wu, X., & Merchuk, J. C. (2002). Simulation of algae growth in a bench-scale bubble column reactor. *Biotechnology and Bioengineering, 80*(2), 156-168.
Wu, Y.-H., Li, X., Yu, Y., Hu, H.-Y., Zhang, T.-Y., & Li, F.-M. (2013). An integrated microalgal growth model and its application to optimize the biomass production of Scenedesmus sp. LX1 in open pond under the nutrient level of domestic secondary effluent. *Bioresource Technology, 144*, 445-451.
Xia, M. (2019). *Analysis of Lipids from Microalgae - ENCH495 Research Report.* (Unpublished BE(Hons) Dissertation), University of Canterbury.
Xia, M. (2020). *Analysis of Lipids from Microalgae Research Method*. Unpublished research report. University of Canterbury.
Xu, Y., & Boeing, W. J. (2014). Modeling maximum lipid productivity of microalgae: Review and next step. *Renewable and Sustainable Energy Reviews, 32*, 29-39.
Yang, A. (2011). Modeling and Evaluation of CO2 Supply and Utilization in Algal Ponds. *Industrial & Engineering Chemistry Research, 50*(19), 11181-11192.
Yap, C. Y., & Chen, F. (2001). Polyunsaturated Fatty Acids: Biological Significance, Biosynthesis, and Production by Microalgae and Microalgae-Like Organisms. In F. Chen & Y. Jiang (Eds.), *Algae and their Biotechnological Potential: Proceedings of the 4th Asia-Pacific Conference on Algal Biotechnology, 3–6 July 2000 in Hong Kong* (pp. 1-32). Dordrecht: Springer Netherlands.
Yongmanitchai, W., & Ward, O. P. (1991). Growth of and omega-3 fatty acid production by Phaeodactylum tricornutum under different culture conditions. *Applied and Environmental Microbiology, 57*(2), 419-425.
Yongmanitchai, W., & Ward, O. P. (1992). Growth and eicosapentaenoic acid production by Phaeodactylum tricornutum in batch and continuous culture systems. *Journal of the American Oil Chemists Society, 69*(6), 584-590.

Yun, Y. S., & Park, J. M. (2003). Kinetic modeling of the light-dependent photosynthetic activity of the green microalga Chlorella vulgaris. *Biotechnology and Bioengineering, 83*(3), 303-311.

Zagorevskii, D. V., Nasrullah, M. J., Raghunadh, V., & Benicewicz, B. C. (2006). The effect of tetrahydrofuran as solvent on matrix-assisted laser desorption/ionization and electrospray ionization mass spectra of functional polystyrenes. *Rapid Communications in Mass Spectrometry, 20*(2), 178-180.

Zeriouh, O., Reinoso-Moreno, J. V., Lopez-Rosales, L., Ceron-Garcia, M. D., Sanchez-Miron, A., Garcia-Camacho, F., & Molina-Grima, E. (2017). Biofouling in photobioreactors for marine microalgae. *Critical Reviews in Biotechnology, 37*(8), 1006-1023.

Zhao, Y.-Y., Wu, S.-P., Liu, S., Zhang, Y., & Lin, R.-C. (2014). Ultra-performance liquid chromatography–mass spectrometry as a sensitive and powerful technology in lipidomic applications. *Chemico-Biological Interactions, 220*(Supplement C), 181-192.

Zou, N., Zhang, C. W., Cohen, Z., & Richmond, A. (2000). Production of cell mass and eicosapentaenoic acid (EPA) in ultrahigh cell density cultures of Nannochloropsis sp. (Eustigmatophyceae). *European Journal of Phycology, 35*(2), 127-133.

Appendix A. Nomenclature

Abbreviations

ADP	Adenosine diphosphate
ATP	Adenosine triphosphate
BBM	Bold's basal medium
BBMA	Bold's basal modified Awarua (medium)
CAD	Charged aerosol detector
CoA	Coenzyme A
DG	Diacylglyceride
DGCC	Diacylglyceryl-carboxyhydroxymethylcholine
DGDG	Digalactosyl diacylglyceride
DGTA	Diacylglyceryl-hydroxymethyl-N,N,N-trimethyl-beta-alanine
DGTS	Diacylgyceryl-N-trimethylhomoserine
DO_2	Dissolved oxygen (also DO)
DPG	Diphosphatidylglycerol
EDTA	Ethylenediaminetetraacetic acid
ESI	Electrospray ionisation
FAME	Fatty acid methyl ester
Fd	Ferredoxin
FID	Flame ionisation detection/detector
GC	Gas chromatography
GlcDG	Monoglucosyl diacylglyceride
HPLC	High-pressure (or high-performance) liquid chromatography
ID	Internal diameter
LED	Light-emitting diode
MGDG	Monogalactosyl diacylglyceride
MS	Mass spectrometry
NADP+	Nicotinamide adenine dinucleotide phosphate
NADPH	Reduced form of nicotinamide adenine dinucleotide phosphate
NZD	New Zealand dollars
OD	Outside diameter
Pc	Plastocyanin
PC	Phosphatidylcholine
PE	Phosphatidylethanolamine
PG	Phosphatidylglycerol
Pi	Inorganic phosphate
PI	Phosphatidylinositol
PMMA	Poly(methyl methacrylate); acrylic
ppm	Parts per million
Pq	Plastoquinone
PS	Phosphatidylserine
psi	Pounds per square inch (lb in^{-2})
PTFE	Poly(tetrafluoroethene); Teflon
PVC	Poly vinyl chloride
PWM	Pulse width modulation
rcf	Relative centrifugal force
RGBWW	Red, green, blue, warm white
RO	Reverse osmosis
rpm	Revolutions per minute
sccm	Standard cubic centimetres per minute
slpm	Standard litres per minute
SQDG	Sulphoquinovosyl diacylglyceride
TFA	Total fatty acids (expressed as free fatty acids)

Fatty acid glossary

Shorthand	Trivial Name	IUPAC Name	Acronym
8:0	Caprylic acid	Octanoic acid	
10:0	Capric acid	Decanoic acid	
12:0	Lauric acid	Dodecanoic acid	
14:0	Myristic acid	Tetradecanoic acid	
16:0	Palmitic acid	Hexadecanoic acid	
18:0	Stearic acid	Octadecanoic acid	SA
20:0	Arachidic acid	Eicosanoic acid	
22:0	Behenic acid	Docosanoic acid	
24:0	Lignoceric acid	Tetracosanoic acid	
14:1 n-5	Myristoleic acid	(9Z)-tetradec-9-enoic acid	
16:1 n-7	Palmitoleic acid	(9Z)-hexadec-9-enoic acid	
16:1 n-10	Sapienic acid	(Z)-6-hexadecenoic acid	
18:1 n-9	Oleic acid	(9Z)-octadec-9-enoic acid	OA
18:2 n-6	Linoleic acid	(9Z,12Z)-octadeca-9,12-dienoic acid	LA
18:3 n-3	α-linolenic acid	(9Z,12Z,15Z)-octadeca-9,12,15-trienoic acid	ALA
18:3 n-6	γ-linolenic acid	All-cis-6,9,12-octadecatrienoic acid	GLA
18:4 n-3	Stearidonic acid	(6Z,9Z,12Z,15Z)-6,9,12,15-octadecatetraenoic acid	SDA
20:2 n-6	Eicosadienoic acid	(11Z,14Z)-icosadienoic acid	EDA
20:3 n-3	Eicosatrienoic acid	(11Z,14Z,17Z)-icosa-11,14,17-trienoic acid	ETrA
20:3 n-6	Dihomo-γ-linolenic acid	(8Z,11Z,14Z)-icosa-8,11,14-trienoic acid	DGLA
20:4 n-3	Eicosatetraenoic acid	(5E,8E,11E,14E)-icosa-5,8,11,14-tetraenoic acid	ETA
20:4 n-6	Arachidonic acid	(5Z,8Z,11Z,14Z)-5,8,11,14-eicosatetraenoic acid	AA
20:5 n-3	Eicosapentaenoic acid	(5Z,8Z,11Z,14Z,17Z)-5,8,11,14,17-eicosapentaenoic acid	EPA
22:1 n-9	Erucic acid	(Z)-docos-13-enoic acid	
22:6 n-3	Docosahexaenoic acid	(4Z,7Z,10Z,13Z,16Z,19Z)-docosa-4,7,10,13,16,19-hexaenoic acid	DHA

Variables

Symbol	Description	Value	Units	Equation first used in
A	Area	-	m^2	(4.39)
a, b, c, n	Experimentally determined parameters	-	Varies	(2.8) - (2.11)
a, b, c	Fitting parameters	-	-	(2.22)
$A_{220\,nm}$	Absorbance at 220 nm	-	-	(3.4)
$A_{275\,nm}$	Absorbance at 275 nm	-	-	(3.4)
$A_{CS,G}$	Gas cross-sectional area	-	m^2	(4.1)
A_{CS}	Cross-sectional area	-	m^2	(2.26)
A_{rad}	Contact area of radiation	-	m^{-2}	(2.31)
$A_{transfer}$	Area for heat transfer	-	m^2	(2.31)
Bd_o	Orifice Bond number	-	-	(4.20)
c	Speed of light in a vacuum	3.00×10^8	$m\ s^{-1}$	(2.1)
Cf	Fanning friction factor	-	-	(4.41)
$C^*_{H^+}$	Equilibrium concentration of H^+	-	$mol\ L^{-1}$	(2.3)
C_{CO_2}	CO_2 concentration	-	$mol\ L^{-1}$	(2.14)
$C^*_{CO_2}$	Equilibrium concentration of dissolved CO_2	-	$mol\ L^{-1}$	(2.3)
$C^*_{CO_3^{2-}}$	Equilibrium concentration of CO_3^{2-}	-	$mol\ L^{-1}$	(2.5)
C_{DIC}	Total dissolved inorganic carbon concentration	-	$mol\ L^{-1}$	(2.3)
C_G	Concentration of gas	-	$mol\ L^{-1}$	(2.29)
C^*_G	Equilibrium concentration of gas	-	$mol\ L^{-1}$	(2.29)
$C^*_{HCO_3^-}$	Equilibrium concentration of HCO_3^-	-	$mol\ L^{-1}$	(2.4)
$C_{NO_3^-,0}$	Initial nitrate concentration	-	$mg\ L^{-1}$	(7.1)
$C_{NO_3^-}$	Nitrate concentration	-	$mg\ L^{-1}$	(3.4)
C_N	Nitrogen source concentration	-	$mol\ L^{-1}$	(2.13)
C_S	Substrate concentration	-	$mol\ L^{-1}$	(2.12)
C_b	Biomass concentration	-	$g\ L^{-1}$	(2.20)
$\Delta C_{biomass}$	Change in biomass concentration	-	$g\ L^{-1}$	(7.1)
$C_{cell,max}$	Maximum cell density	-	$cells\ mL^{-1}$	-
C_{cell}	Cell concentration	-	$cells\ mL^{-1}$	(3.1)
c_p	Specific heat capacity	-	$J\ kg^{-1}\ K^{-1}$	(2.31)
D	Dilution rate	-	d^{-1}	-
$\mathcal{D}_{AB}$	Diffusivity of A in B	-	$m^2\ s^{-1}$	(4.29)
$\mathcal{D}_{il}$	Diffusion coefficient of gas in liquid phase	-	$m^2\ s^{-1}$	(4.26)
d_{BC}	Bubble column diameter	-	m	-

Symbol	Description	Value	Units	Equation first used in
d_L	Impeller diameter	-	m	(4.46)
d_b	Bubble diameter	-	m	(4.4)
d_f	Dilution factor	-	-	(3.1)
d_o	Orifice diameter	-	m	(4.14)
d_p	Particle diameter	-	m	(2.27)
d_{pipe}	Pipe diameter	-	m	(2.32)
d_t	Tube diameter	-	m	(8.1)
$\frac{dv}{dx}$	Velocity gradient (v, velocity; x, distance)	-	s^{-1}	(2.6)
D_T	Bubble column diameter	-	m	(4.30)
E_a	Activation energy	-	J mol^{-1}	(2.17)
$E_a{}'$	Activation energy for protein denaturation	-	J mol^{-1}	(2.17)
E_λ	Energy of a photon with wavelength λ	-	J $photon^{-1}$	(2.1)
f_{pump}	Pump frequency	-	Hz	(4.47)
Fr	Froude number	-	-	(4.20)
G	Global radiation	-	W m^{-2}	(2.31)
g	Acceleration due to gravity	9.81	m s^{-2}	(4.7)
Ga	Galileo number	-	-	(4.20)
G_1	Morton number	-	-	(4.12)
G_2	Variable for bubble rise velocity	-	-	(4.13)
$\Delta H_{vaporisation}$	Heat of vaporisation	-	J kg^{-1}	(2.31)
h	Planck constant	6.63×10^{-34}	J s	(2.1)
h_{BC}	Bubble column height	-	m	-
H_G	Henry's constant	-	Varies	(2.30)
H_L	Static liquid height	-	m	(4.24)
I_0	Incident light intensity	-	µmol m^{-2} s^{-1}	-
I_{all}	Light intensity of all light colours combined	-	µmol m^{-2} s^{-1}	(3.5)
I_{av}	Average light intensity	-	µmol m^{-2} s^{-1}	-
I_{blue}	Blue light intensity	-	µmol m^{-2} s^{-1}	(3.8)
I_{cell}	Cell specific photon flux	-	µmol $cell^{-1}$ s^{-1}	-
I_{green}	Green light intensity	-	µmol m^{-2} s^{-1}	(3.7)
I_i	Inhibition light intensity	-	µmol m^{-2} s^{-1}	(2.11)
I_{max}	Maximum light intensity	-	µmol m^{-2} s^{-1}	-
I_{opt}	Optimal light intensity	-	µmol m^{-2} s^{-1}	(2.13)
I_{red}	Red light intensity	-	µmol m^{-2} s^{-1}	(3.6)
I_{total}	Total photon flux	-	µmol m^{-3} s^{-1}	-
I_{white}	White light intensity	-	µmol m^{-2} s^{-1}	(3.9)
I_{wm}	External irradiance	-	µmol $m^{-2}s^{-1}$	(2.23)
k	Boltzmann constant	1.38×10^{-23}	J K^{-1}	(2.17)
k_1	Strain specific parameter	-	Varies	(2.25)
k_2	Strain specific parameter	-	Varies	(2.25)

Symbol	Description	Value	Units	Equation first used in
$k_L a$	Overall mass transfer coefficient (k_L, liquid side mass transfer coefficient; a, interfacial area)	-	s^{-1}	(2.29)
K	Dimensionless constant	-	-	(2.17)
K_1	Equilibrium constant for reaction of CO_2 to HCO_3^-	4.47×10^{-7}	mol L^{-1}	(2.3)
K_1	Correlation dimension	-	-	(4.34)
K_2	Equilibrium constant for reaction of HCO_3^- to CO_3^{2-}	4.69×10^{-11}	mol L^{-1}	(2.3)
K_2	Correlation dimension	-	-	(4.35)
K_{CO_2}	CO_2 saturation constant	-	mol L^{-1}	(2.14)
K_I	Irradiance saturation constant	-	μmol m^{-2} s^{-1}	(2.8)
K_N	Nitrogen saturation constant	-	mol L^{-1}	(2.13)
K_S	Substrate saturation constant	-	mol L^{-1}	(2.12)
K_a	Biomass extinction coefficient	-	L g^{-1} m^{-1}	(2.24)
l_{eddy}	Length of microeddy	-	m	(4.43)
L_I	Optical path length	-	m	(2.26)
L_S	Sparger length	-	m	(4.24)
L_{SR}	Solar receiver length	-	m	(4.36)
L_{pipe}	Pipe length	-	m	(2.34)
m	Mass	-	kg	-
$m_{culture}$	Mass of culture	-	kg	(2.31)
$\dot{m}_{evaporated}$	Rate of mass loss by evaporation	-	kg s^{-1}	(2.31)
n_i	Number of cells in square 'i'	-	cells	(3.1)
N_0	Initial population density	-	mL^{-1}	(3.3)
N_P	Number concentration of particles	-	m^{-3}	(2.26)
N_{max}	Maximum population density	-	mL^{-1}	(3.3)
N_{pump}	Pump speed	-	min^{-1}	(4.45)
N_t	Population density at time 't'	-	mL^{-1}	(3.3)
P	Photosynthesis rate	-	Varies	-
P_T	Total pressure	-	Pa	(2.30)
P_{pump}	Pumping power	-	W	(2.34)
q	Heat	-	W	(4.39)
q_P	Rate of product formation in biomass	-	g g^{-1} d^{-1}	(2.20)
Q	Nutrient cell quota	-	g 100 g^{-1}	(2.13)
Q_F	Fluid flow rate	-	m^3 s^{-1}	(2.33)
Q_G	Gas volumetric flow rate	-	m^3 s^{-1}	(4.2)
Q_L	Liquid volumetric flow rate	-	m^3 s^{-1}	(4.3)
Q_{min}	Minimum cell quota for algal existence of nutrient	-	g 100 g^{-1}	(2.13)
Q_{sc}	Scattering coefficient	-	-	(2.27)

Symbol	Description	Value	Units	Equation first used in
r_P	Rate of product formation	-	$g\ L^{-1}\ d^{-1}$	(2.20)
r_{be}	Bubble radius	-	m	(4.7)
Re_L	Local Reynolds number	-	-	(4.45)
Re_{bubble}	Bubble Reynolds number	-	-	(4.4)
Re_o	Orifice Reynolds number	-	-	(4.15)
Re_{pipe}	Reynolds number for pipes	-	-	(2.32)
R_{O_2}	Rate of oxygen evolution	-	Varies	(4.36)
t	Time	-	s	(2.31)
t_R	Residence time	-	s	(4.37)
T	Temperature	-	℃	-
ΔT	Temperature difference	-	℃	(4.39)
T_{max}	Maximum temperature	-	℃	(2.19)
T_{min}	Minimum temperature	-	℃	(2.19)
T_{out}	Temperature of environment	-	℃	(2.31)
U	Overall heat transfer coefficient	-	$W\ m^{-2}\ K^{-1}$	(2.31)
$u_{G,V}$	Void superficial gas velocity	-	$m\ s^{-1}$	(4.2)
$u_{L,SR,avg}$	Average liquid velocity in the solar receiver	-	$m\ s^{-1}$	(4.47)
$u_{L,SR}$	Liquid velocity in the solar receiver	-	$m\ s^{-1}$	(4.36)
$u_{L,V}$	Void liquid superficial velocity	-	$m\ s^{-1}$	(4.3)
u_L	Liquid velocity		$m\ s^{-1}$	(2.32)
u_{cw}	Critical weep velocity	-	$m\ s^{-1}$	(4.24)
$u_{superficial}$	Superficial velocity	-	$m\ s^{-1}$	(2.33)
u_t	Terminal rise velocity	-	$m\ s^{-1}$	(4.4)
v_L	Liquid point velocity	-	$m\ s^{-1}$	(4.8)
V_G	Gas volume	-	m^3	-
V_L	Liquid volume	-	m^3	-
V_{PWM}	PWM value	0 - 255	-	(3.5)
x	Distance	-	m	(2.24)
Δx_o	Orifice hole spacing	-	m	(4.24)
y_G	Gas mole fraction	-	-	(2.30)
Y_N	Rate of nitrate consumption	-	$mg\ g^{-1}$	(7.1)
$Y_{P/X}$	Ratio of product formation to biomass formation	-	$g_P\ g_b^{-1}$	(2.21)
z	Charge	-	C	-
α	Void fraction	-	-	(4.1)
$\dot{\gamma}$	Shear rate	-	s^{-1}	(2.6)
δ	Boundary layer thickness	-	m	(8.1)
ε_G	Gas hold-up	-	-	(4.27)
η_G	Gas viscosity	-	Pa s	(4.19)
η_{eff}	Effective viscosity	-	Pa s	(4.35)
η_l	Liquid viscosity	-	Pa s	(2.6)

Symbol	Description	Value	Units	Equation first used in
λ	Wavelength	-	nm	(2.1)
μ	Specific growth rate	-	d^{-1}	-
μ_{max}	Maximum specific growth rate	-	d^{-1}	(2.7)
ξ	Energy dissipation per unit mass	-	J kg^{-1}	(4.43)
ρ_G	Gas density	-	kg m^{-3}	(4.7)
ρ_L	Liquid density	-	kg m^{-3}	(2.32)
τ_0	Wall shear stress	-	Pa	(4.41)
τ_{pump}	Shear stress at tip of pump impeller	-	Pa	(4.45)
σ	Surface tension		N m^{-1}	(4.9)
τ	Shear stress	-	N m^{-2}	(2.6)

Appendix B. Summary of HPLC methods in published microalgae lipidomic studies

Table B.1 below contains a summary of HPLC methods for some lipidomic studies of microalgae that were considered as starting points for the development of the HPLC method in this study.

Table B.1 - Summary of liquid chromatography methods for separation of lipids from microalgae.

Column Specifications	Sample Dry Weight	Mobile phases	Conditions	Reference
C_8 (2.1 × 100 mm, 1.7 µm)	50 mg	A: water:acetonitrile (1:2, v/v) B: acetonitrile:isopropyl alcohol:tetrahydrofuran (1:1:1, v/v) 0.01% lithium acetate and 0.1% formic acid as electrolyte.	$V_{injection} = 3$ µL $T_{column} = 40$ ℃ $T_{sample} =$ ℃ $Q_{column} = 200$ µL min^{-1} (1:4 effluent split) Mobile phase B from 0 to 50% in 15 minutes, to 80% in 30 min held for 2 min, returned to 0 in 2 min, equilibrated 11 min.	Li *et al.* (2014)
C_8 (2.1 × 100 mm, 1.7 µm)	15 mg	A: water:acetonitrile (1:2, v/v) B: acetonitrile:isopropyl alcohol: tetrahydrofuran (1:1:1, v/v) 0.01% lithium acetate and 15 mM formic acid as electrolyte for ESI positive. 15 mM ammonium hydroxide for ESI negative.	$V_{injection} = 3$ µL $T_{column} = 40$ ℃ $T_{sample} =$ ℃ $Q_{column} = \sim 200$ µL min^{-1} (1:4 effluent split) Mobile phase B from 0 to 50% in 15 minutes, to 80% in 30 min held for 2 min, returned to 0 in 2 min, equilibrated 11 min.	Li *et al.* (2015)
RP amide column (50 mm × 2.1 mm, 2.7 µm)	n.d.	A: water:methanol:tetrahydrofuran (50:20:30, v/v) with 10 mM ammonium formate. B: water:methanol:tetrahydrofuran (5:20:75, v/v) with 10 mM ammonium formate.	$V_{injection} =$ n. d. $T_{column} = 35$ ℃ $T_{sample} =$ n. d. $Q_{column} = 0.2$ mL min^{-1} Mobile phase: 100% A to 0% A linearly over 10 minutes, 1 minute hold at 0% A, re-equilibration at 100% A for 4 minutes.	Martin *et al.* (2014)

Table B.1 - Summary of liquid chromatography methods for separation of lipids from microalgae.

Column Specifications	Sample Dry Weight	Mobile phases	Conditions	Reference
C_{18} (2.1 × 150 mm, 2.6 µm)	n.d.	A: acetonitrile:water (60:40v/v) with 10mM ammonium formate. B: isopropanol:acetonitrile (90:10, v/v) with 10 mM ammonium formate and 0.1% formic acid (v/v).	$V_{injection} =$ n. d. $T_{column} = 45$ ℃ $T_{sample} =$ 7 ℃ $Q_{column} = 300$ µL min^{-1} The elution was performed with a gradient of 30 min; during 0-1.5 min isocratic elution with 32% B; from 1.5 to 4 min increase to 45% B, from 4 to 5 min increase to 52% B, from 5 to 8 min to 58% B, from 8 to 11 min to 66% B, from 11 to 14 min to 70% B, from 14 to 18 min to 75% B, from 18 to 21 min to 97% B, during 21 to 25 min 97% B is maintained; from 25-25.1 min solvent B was decreased to 32% and then maintained for another 4.9 min for column re-equilibration (as per Hu *et al.* (2008)).	Nguyen *et al.* (2013)
C_8 (2.1 × 100 mm, 1.7 µm)	n.d. (500 mL of culture)	A: water B: acetonitrile:methanol:isopropyl alcohol (56.5:28.5:15, v/v) 0.05 µM sodium formate and 0.1 % formic acid were added to the mobile phase as electrolyte.	$V_{injection} = 1.0$ µL $T_{column} =$ n. d. $T_{sample} = 8$ ℃ $Q_{column} = 0.25$ mL min^{-1} Mobile phase gradient (min/%B): 0/5, 8/70, 20/90, 28/95, 42/95, 43/100, 46/100.	Su *et al.* (2013)

Table B.1 - Summary of liquid chromatography methods for separation of lipids from microalgae.

Column Specifications	Sample Dry Weight	Mobile phases	Conditions	Reference
C_{18} (4 × 250 mm, 5µm)	n.d.	A: water B: methanol Ammonium acetate added as electrolyte for ESI positive mode.	$V_{injection} = \text{n. d.}$ $T_{column} = \text{n. d.}$ $T_{sample} = \text{n. d.}$ $Q_{column} = 1\ \text{mL min}^{-1}$ Mobile phase gradient 95:5 to 100% CH_3OH.	Guella *et al.* (2003)
'Luna', not specified (2.1 × 150 mm, 5 µm)	2.0 g	ESI- A: 10mM ammonium bicarbonate ESI- B: acetonitrile ESI+ A: 0.5% formic acid in water (v/v) ESI+ B: 0.5% formic acid in acetonitrile (v/v)	$V_{injection} = \text{n. d.}$ $T_{column} = \text{n. d.}$ $T_{sample} = \text{n. d.}$ $Q_{column} = 200\ \mu\text{L min}^{-1}$ ESI-: 20% to 95% B in 20 minutes then held for 30 min. ESI+: 20% to 95% B in 20 minutes then held for 30 min.	Herrero *et al.* (2007)

Appendix C. Total ion chromatograms from LC-MS controls

Figure C.1 A shows the chromatogram for the sample solvent used of acetonitrile/isopropyl alcohol (1:1, v/v). Figure C.1 B is the chromatogram for the TLC plate control which consisted of an identical TLC plate prepared as for the lipid separations but without any lipid sample added. Figure C.1 C is the chromatogram for the TLC plate with Bligh and Dyer extraction control which was prepared identically to the lipid separations but without any lipid sample; however, a sample from a Bligh and Dyer extraction control was added to the plate (i.e. a Bligh and Dyer extraction conducted without any biomass present). These controls served to determine the presence of contaminants from solvent residues, the TLC plates, or residues from glass or plasticware.

(A)

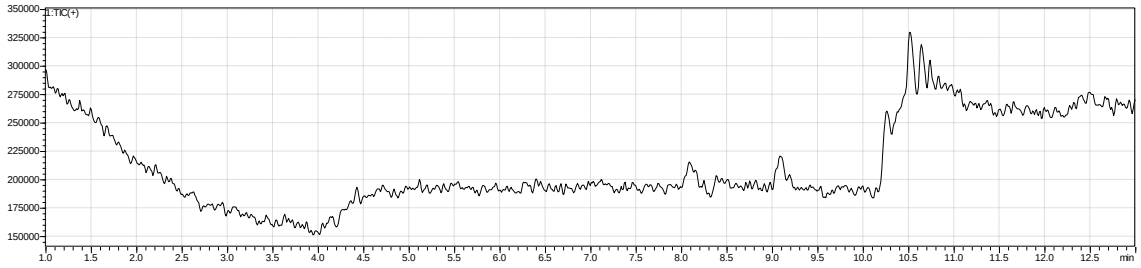

(B)

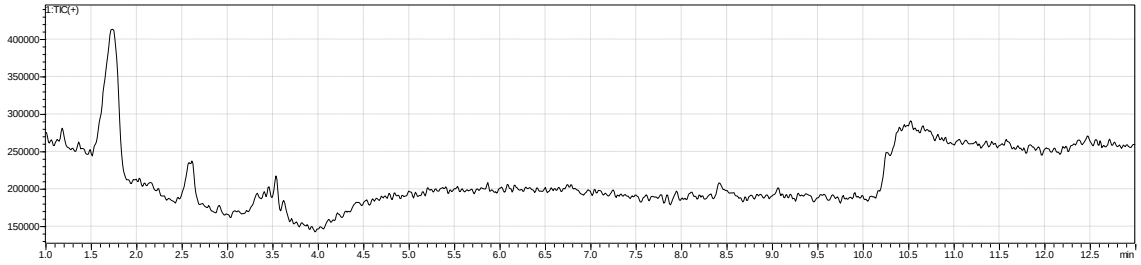

(C)

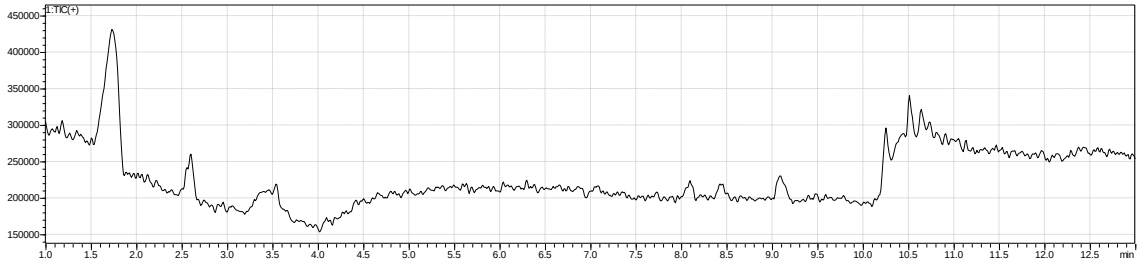

Figure C.1 - Total ion chromatograms for LC-MS of A) acetonitrile/isopropyl alcohol solvent control, B) TLC plate control, and C) TLC plate with Bligh and Dyer extraction control.

Appendix D. Fragmentation patterns of LC-MS peaks of *Chlorella vulgaris* MGDG lipid TLC spot

Figures D.1 to D.5 below contain the fragmentation mass spectra obtained from the lipidomic analysis of the MGDG lipids from *Chlorella vulgaris* in § 5.3.2. Each set of fragmentation patterns are from the peaks at the retention time noted in the figure caption.

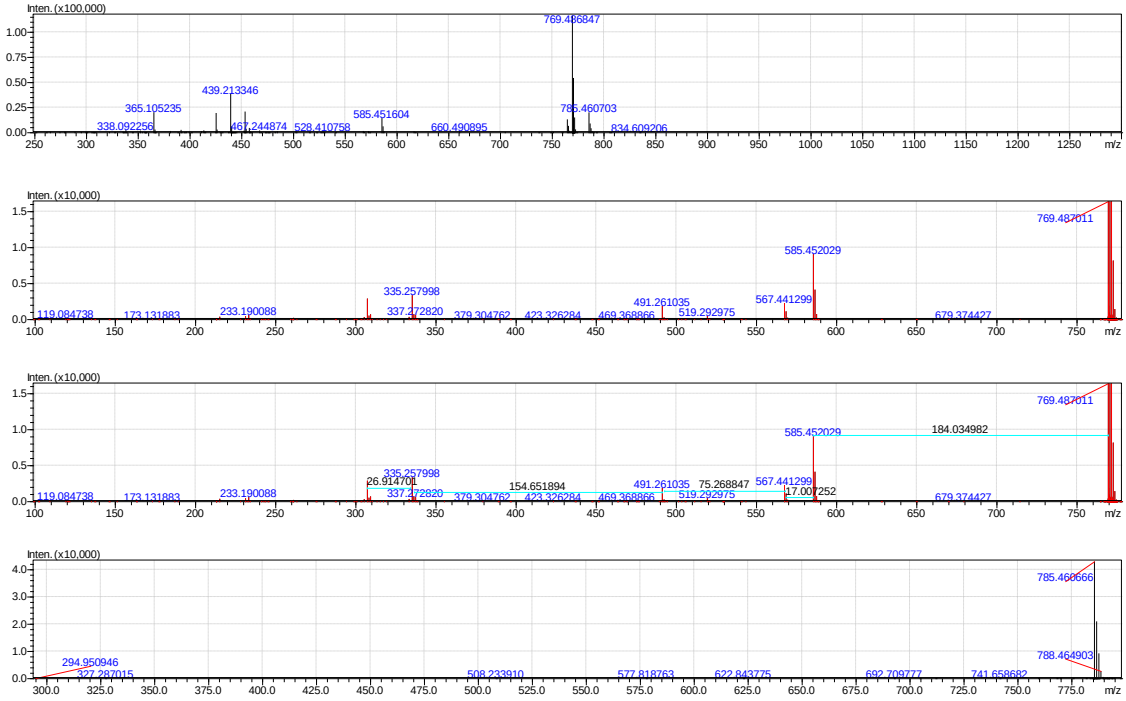

Figure D.1 – Fragmentation mass spectra for MGDG peak at 5.25 minutes.

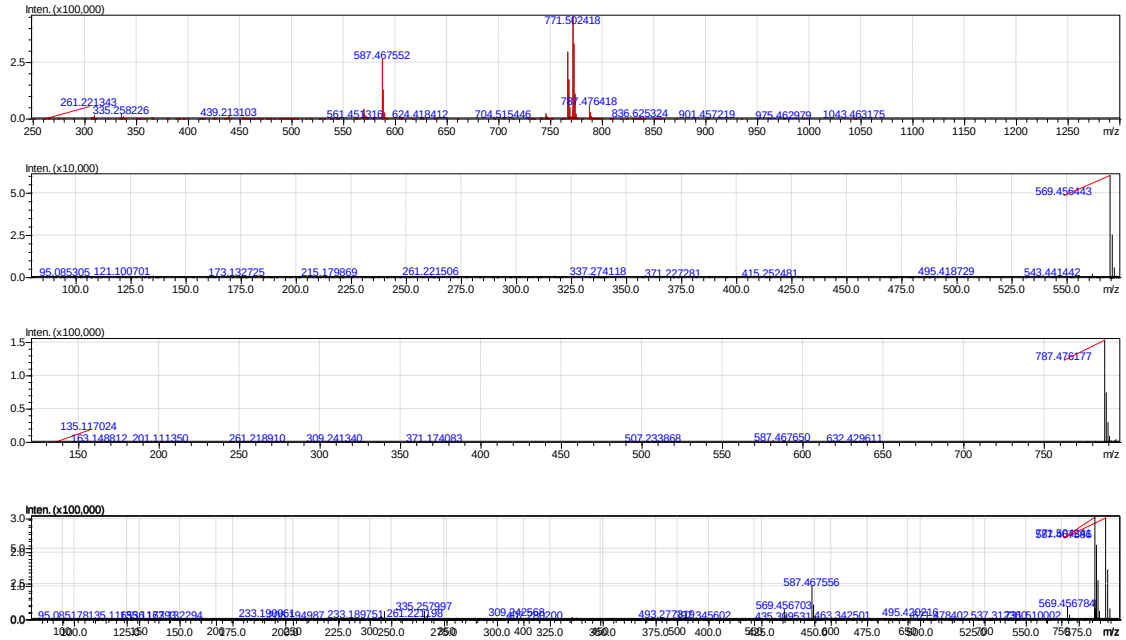

Figure D.2 – Fragmentation mass spectra from MGDG peak at 5.75 minutes.

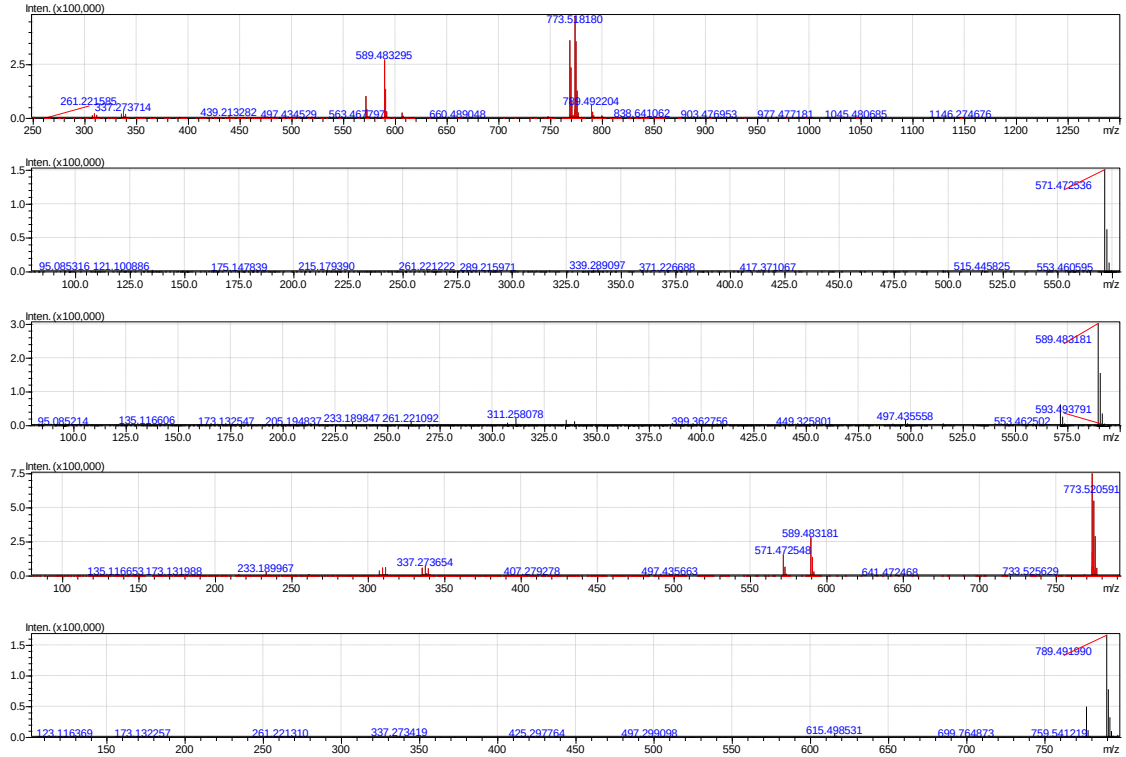

Figure D.3 – Fragmentation mass spectra for MGDG peak at 6.25 minutes.

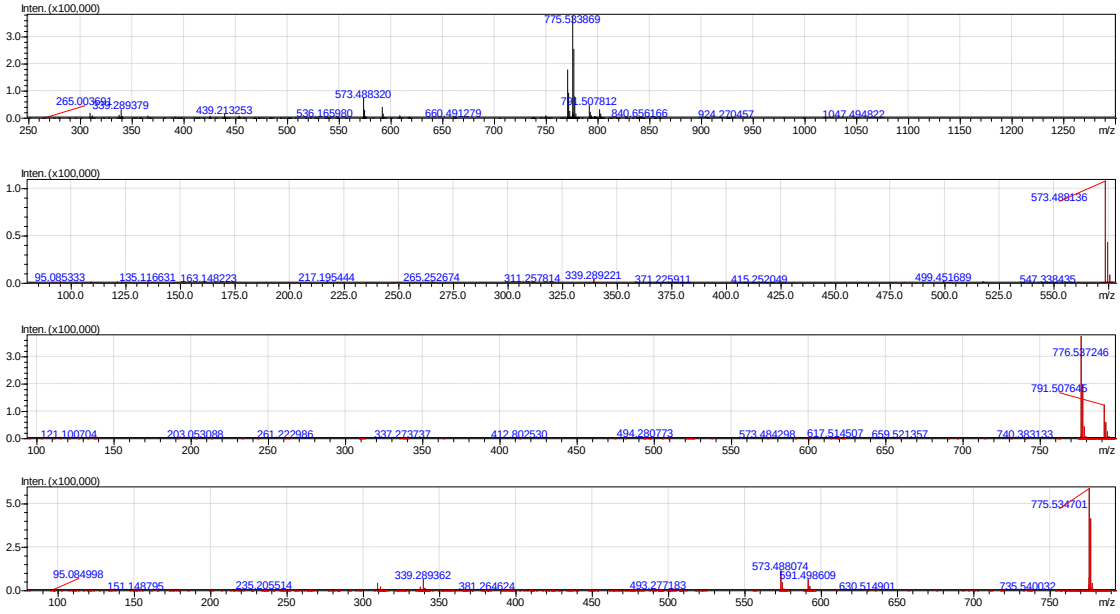

Figure D.4 – Fragmentation mass spectra from MGDG peak at 7.00 minutes.

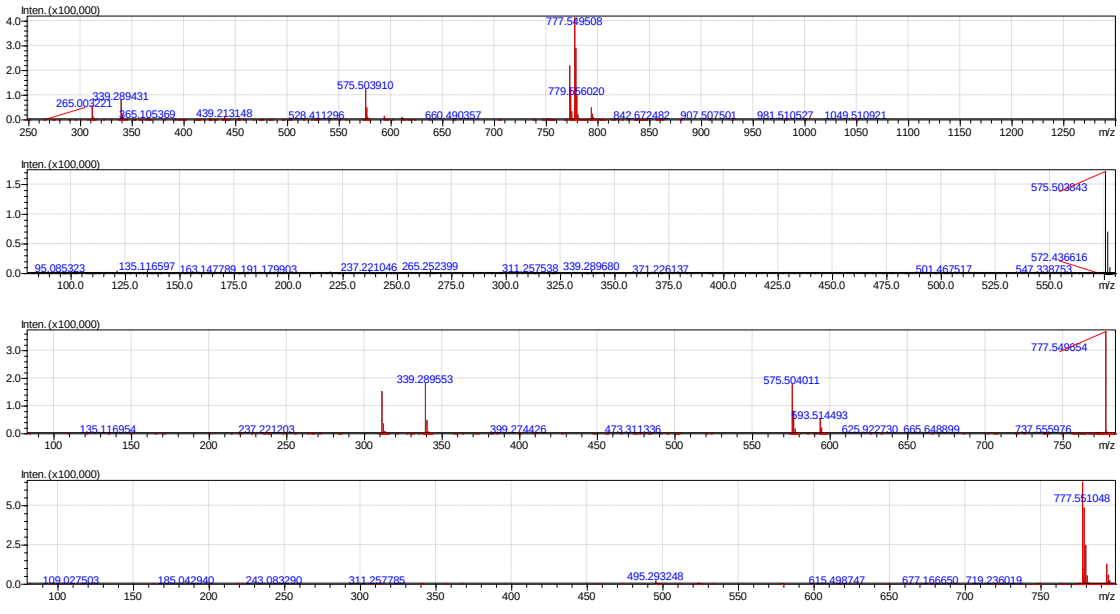

Figure D.5 – Fragmentation mass spectra of MGDG peak at 7.75 minutes.

Appendix E. Composition of commercial *Chlorella vulgaris* powder

Table E.1 – Stated composition of commercial Chlorella vulgaris powder.

	Average Quantity per 100 g
Energy	1729 kJ
Protein	70.0 g
-gluten	Nil
Fat, total	12.7 g
-saturated	1.2 g
Carbohydrate	Less than 1 g
-sugars	Nil
Dietary fibre	10.2 g
Sodium	69.4 mg
Chlorophyll	3.0 g

Appendix F. UV-Vis spectra of extracted pigments

Below in Figures F.1 to F.3 are the UV-Vis spectra of the extracted pigments that were isolated in § 6.4.4. All pigments were measured in 100% ethanol as the solvent.

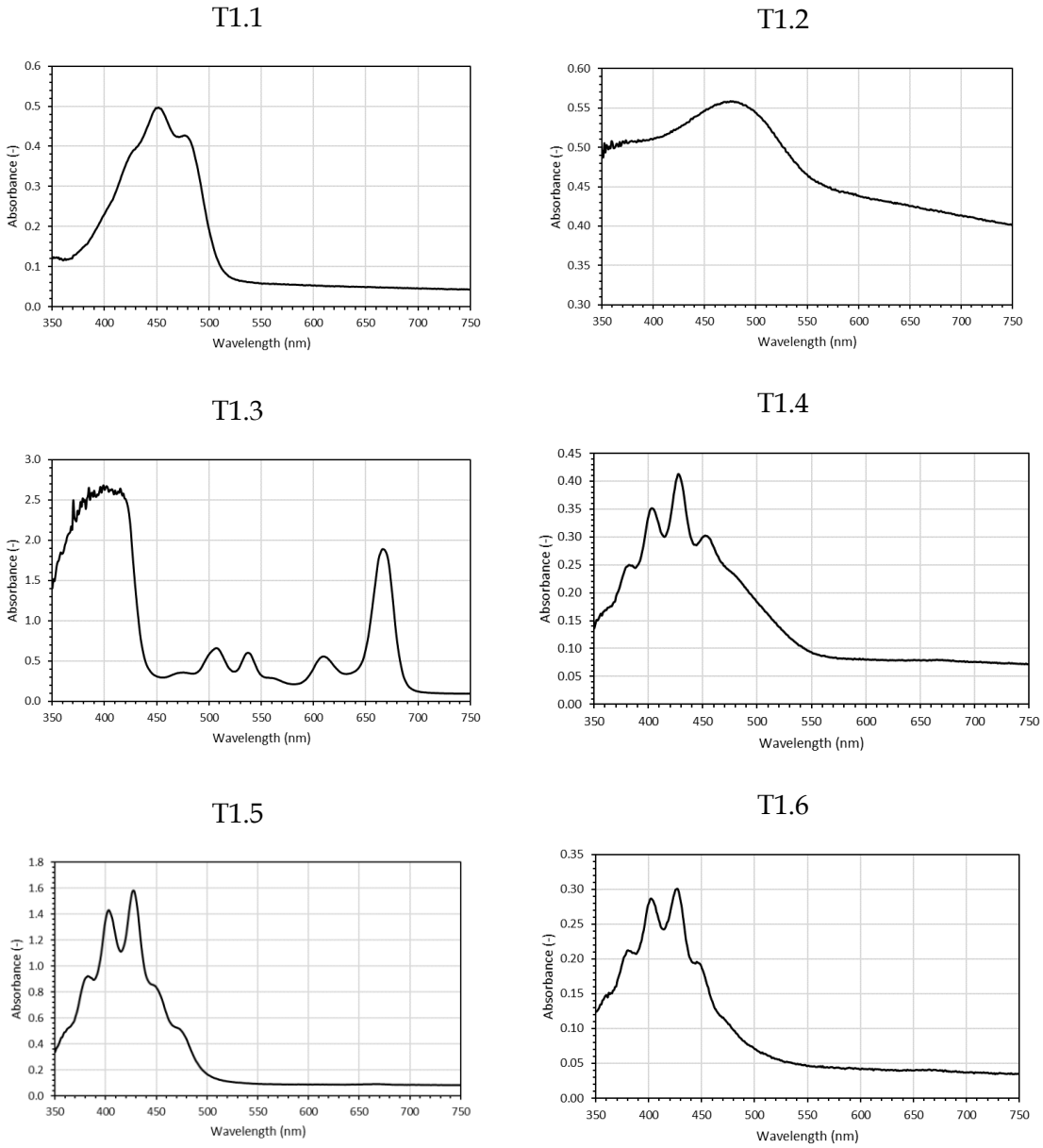

Figure F.1 – UV-vis absorbance spectra of pigments from Trachydiscus sp. LCR-Awa-9-2 in ethanol. Spot numbers are as labelled in Figure 6.16.

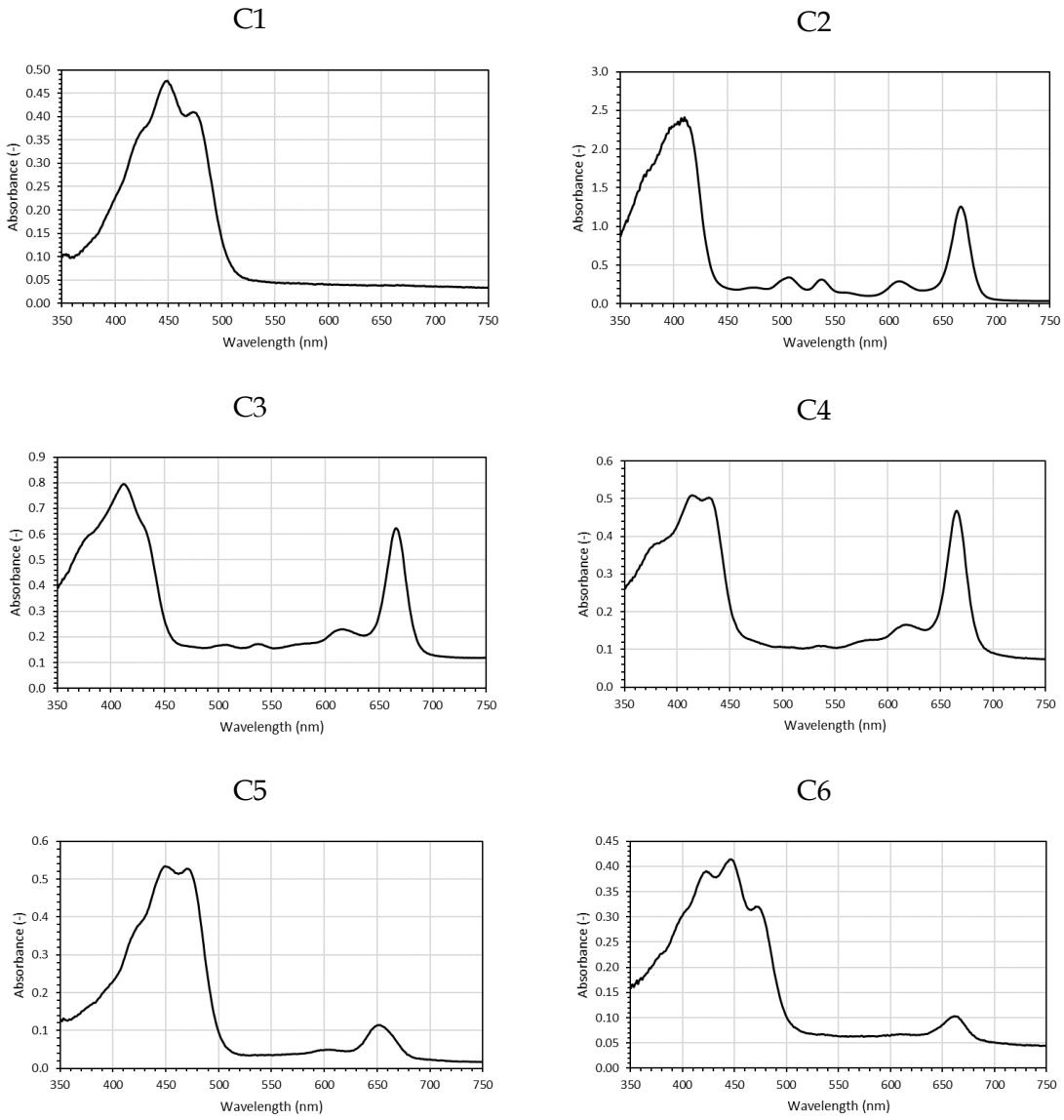

Figure F.2 – UV-vis absorbance spectra of pigments from Chlorella vulgaris in ethanol. Spot numbers are as labelled in Figure 6.16.

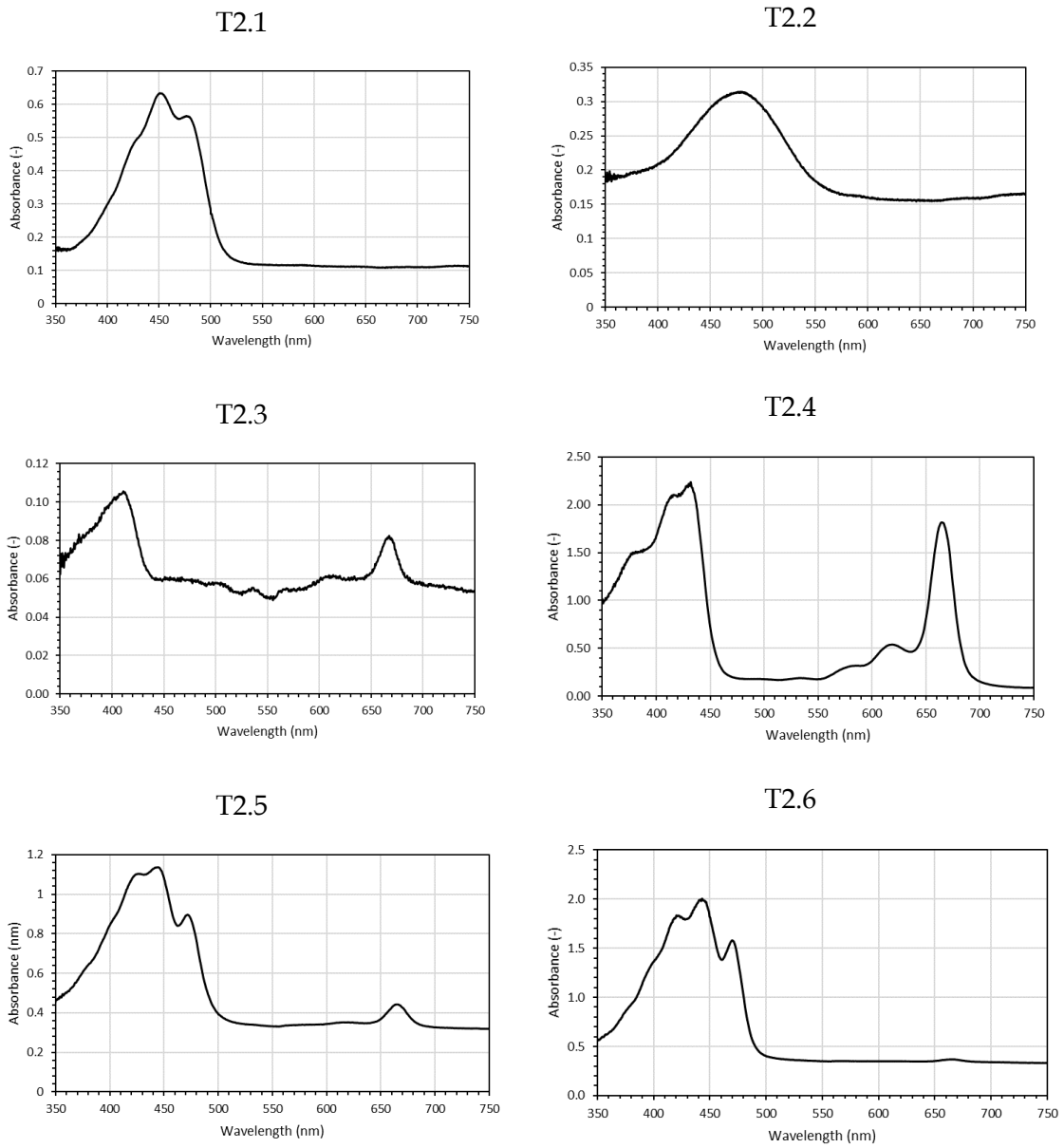

Figure F.3 – UV-vis absorbance spectra of pigments from Trachydiscus sp. LCR-Awa-9-2 in ethanol. Spot numbers are as labelled in Figure 6.17.